Seismic Assessment and Rehabilitation of existing RC Buildings not designed to withstand earthquakes

A thesis submitted for the degree of
Doctor of Philosophy

Giuseppe Occhipinti

Supervisor:
Prof.Ivo Caliò - University of Catania

Co-Supervisors:
Prof. Bassam Izzuddin - Imperial College of London
Prof. Lorenzo Macorini - Imperial College of London

Coordinator:
Prof. Massimo Cuomo - University of Catania

«Assessment and Mitigation of Urban and Territorial Risks»
XXIX Study Cycle

Department of Civil and Environmental Engineering
University of Catania

July,2017

Declaration

This submission is my own work. Any quotation from, or description of, the work of others is acknowledged herein by reference to the sources, whether published or unpublished.

Giuseppe Occhipinti
July 2017

Abstract

This thesis is focused on the seismic vulnerability assessment of existing multi-storey reinforced concrete buildings that were not designed to withstand earthquakes and on the identification of possible retrofitting strategies adoptable for their structural rehabilitation.
A typical ten-storey building has been identified as representative cases study of many similar buildings built in Catania (Sicily, south of ITALY) between the 60's and 80's before the introduction of a national seismic code in 1981. Since the building has been designed with reference to vertical loadings only it allowed the simple identification of further eight buildings characterised by different number of storeys, from nine to two, but maintaining the same plan layout.
Aiming at obtaining rigorous results and to validate the standard adopted procedures with those obtained by rigorous detailed simulations, the seismic assessment of the investigated buildings, before and after the proposed retrofitting measures, have been performed. For this purpose, advanced numerical models characterised by different modelling capabilities and computational demands have been implemented.
The seismic vulnerability assessments, consistent to the current European Code prescriptions, have been performed by using the research version of the computer code 3DMacro that allows performing nonlinear push-over analyses by considering the important contribution of the non-structural infill panels. The detailed nonlinear analyses have been performed by means of high fidelity realistic models implemented in the advanced nonlinear FEM software ADAPTIC that allows performing full nonlinear static and dynamic analyses accounting explicitly for material and geometric nonlinearity. Moreover, according to a powerful partition modelling strategy and the capabilities of the parallel calculus, ADAPTIC makes possible the implementation of mathematical model of structures with a huge amount of details. The interaction between concrete frames and non-structural unreinforced hollow brick masonry infills has been evaluated by means of a FEM ad hoc implementation of the planar discrete macro-element, already implemented in 3DMacro within a discrete element framework. The original non-trivial implementation of the discrete macro-element in the FEM code ADAPTIC represents a significant original contribution of the present thesis. The large displacements capabilities of the software ADAPTIC has also empowered a new original research investigation that relates the investigation of progressive collapse scenarios due to local failures

trigged by low, or moderate, earthquake actions on mid-rise weak reinforced concrete existing structures.
The thesis is divided into seven main chapters.
The first Chapter focuses the seismicity of the east coast of Sicily with major attention at the city of Catania. The second Chapter introduce the progressive collapse phenomena and it is preparatory to the investigation of the robustness of existing buildings designed for vertical loads only as possible consequence of moderate earthquake actions. The third Chapter investigates and discusses numerical simulations of an experimental test on progressive collapse of concrete frame structures already reported in literature. Several parametric analyses based on different nonlinear models have been performed with the aim of evaluating the influence of material parameters on the collapse response of typical reinforced concrete frames not designed to withstand earthquakes. In the fourth Chapter an original FEM implementation of a plane-discrete-macro-element is proposed aiming at modelling the non-structural infills in the nonlinear ADAPTIC models. The fifth Chapter describes the chosen case study and reports code-consistent parametric evaluations of seismic vulnerability of low- and mid-rise reinforced concrete buildings. The case study has been defined according to a simulated design that was based on the survey of existing residential buildings designed and built in Catania between the 60's and 80's and on the design code that the engineers adopted in those decades. In this preliminary evaluation, only push-over analyses have been performed with the computer code 3DMacro that empowers a reliable model of non-structural masonry panels. Starting from the definition and design of the case study ten-storey building, other eight structures have been obtained. Moreover, the results are expressed for different soil conditions according to the Italian 2008 technical code. Chapter sixth considers the seismic vulnerability evaluation of the ten storeys case-study by means of a realistic model implemented in ADAPTIC considering the ribbed slabs and the infilled masonry panels contributions. The detailed FEM implementation of the plane macro-element is adopted to model the non-structural walls. The non-linear dynamic response of the two models are compared and discussed underling the unreinforced clay walls contribution. The thorough vulnerability assessments have been performed according to nonlinear dynamic analyses considering both material and geometrical nonlinearities.
The possible retrofitting strategies of the ten-storey building are discussed in Chapter 7. The proposal is the results of the research project that has been financed by ANCE|Catania and developed by a research

team coordinated by Prof. I.Caliò and Prof. B.Izzuddin. The retrofitting strategy consists in an innovative structural perimetral steel skeleton made by a synergetic combination of centred braced frames and eccentric bracing system endowed with dissipative shear links. The proposed solution has been investigated by means of a high fidelity model implemented in the software ADAPTIC

The numerical results obtained from the high fidelity 3D nonlinear dynamic simulations showed a very poor seismic performance of the existing structure. The results of numerical simulations for the retrofitted structure confirm that the proposed solution significantly enhances the response under earthquake loading, allowing the structure to resist the design earthquake with only limited damage in the original RC beams and columns, highlighting the feasibility of retrofitting for this typical multi-storey RC building structure.

Keywords: Infill frame, Robustness, Seismic vulnerability, Existing RC buildings, Macroelement, High Fidelity Model.

.

Acknowledgments

I would like to express my sincere gratitude to my advisor Prof. Ivo Caliò for his priceless continuous support of my Ph.D. He guided and motivated me to get better results, not only for this thesis. I cannot fail to thanks him for his thorough review of the final manuscript. He profoundly supported me and acted as a mentor of immense knowledge.

I would like to express my special appreciation and thanks to Prof. Bassam A. Izzuddin for his immense support and his inestimable guideless. He gave me the opportunity to join his Computation Structural Mechanics group at Imperial College of London and let me to use ADAPTIC for my thesis.

My sincere thanks also goes to Prof. Lorenzo Macorini, he encouraged and motivated me. He had also a central role with its thorough reviews of articles and of the final manuscript of this thesis.

I am in debt with ANCE|Catania, the former president Nicola Colombrita and the president Giuseppe Piana. Under their guide, ANCE|Catania believed in the research, financed my scholarship and the related researches. No one of the results that have been achieved would have been obtained without their enlightened presidency.

I am also grateful to Ph.D. Francesco Cannizzaro for his stimulating observations on my results and to Ph.D. Davide Rapicavoli for his support in the definition of graphical user interface input/output facilities.

I would like to thank Ph.D. Carlos Escobar Del Pozo and Prof. Paulo Marcos Aguiar, good friends are rare but London gave me other two.

Finally, I reserve a special thanks to my family and my beloved Angela because no houses can be built on the sand no lives can be lived without true love.

Table of Contents

List of Tables

List of Figures

CHAPTER 1.
CATANIA'S SEISMIC HAZARD

The interest of the scientific community on the seismic assessment and the vulnerability of concrete frame structures grew exponentially after the introduction of the national seismic codes. In Italy, it happened in 1974 with the introduction of a seismic code for great part of the Italian territory. At the end of the 90's, several Italian university research groups were involved in a huge research project know as *Catania Project* focused on the assessment of the seismic risk of the city of Catania and more in general on the oriental area of Sicily. The Catania urban peculiarities and its high seismic risk, are well defined by the following words [1] "*The building process that take place in Italy after the World War II, and especially during the 50s and 60s, was characterised by concrete frame structures designed to resist only to gravity loads. Several Italian areas were defined prone regions after the latter period and, consequently, the study of those buildings is extremely interesting for the vulnerability assessment studies. From this point of view, the cold case Catania is hugely emblematic. The seismic assessment of the existing concrete frame buildings, which were designed to resist only to gravity loads, represents a highly relevant topic due to social and economic consequences, consistently with the huge number of similar building typologies in our Country […]"*

1.1 Background

The reinforced concrete frame buildings designed for vertical loads only are widespread in Italy and in a several Mediterranean countries. The thesis is focused on mid-rise buildings not designed to resist to earthquake loadings. A typical building that is representative of many similar structures built in Catania between the 60s and 80s, is considered as case study. Although it is assumed as a representative Catania middle-rise building, the obtained results can be extended to many similar buildings of different areas in the world that have been recently recognised seismic prone regions.

The structures that were built without seismic design methods are characterised by several structural weaknesses. In addition a natural degrade of the structural materials usually affects reinforced concrete structures in few years. These structural deficiencies affect and increase the seismic vulnerability and, consequently, the seismic risk. Furthermore, the seismic risk is a function of hazard, vulnerability and exposure in a specific area. Their meanings are explained below.

Seismic risk. It is defined as potential economic, social and environmental consequence of hazardous events that may be occur in a determinate area in a specific period.

Seismic hazard. It is the probability that an earthquake occurs in a geographic area, within a specific time span, and a ground motion intensity exceeding a threshold.

Seismic Vulnerability. It defines the condition resulting from physical, construction processes, geometric and material properties of a structure and environmental factors or processes that increase its susceptibility to the impact of a hazard.

Exposure. It indicates the elements that are affected by natural disasters (e.g. people and property).

Summarising, "risk" defines the expected value of losses (deaths, injuries, property, etc.) that a hazardous event may cause.

Disaster Risk = function (Hazard, Exposure, Vulnerability)

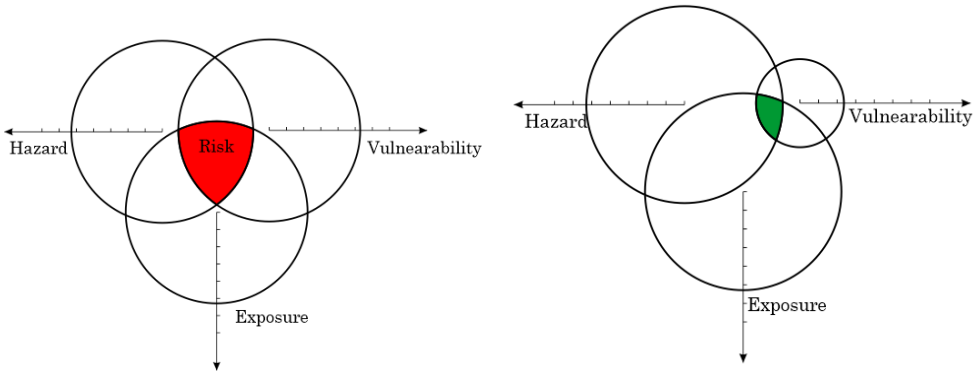

Figure 1.1 Graphical representation of the Risk function.

From an engineering point of view, the Figure 1.1 depicts the conventional and adopted strategy to reduce the Seismic Risk. The reduction of seismic vulnerability of existing structures not designed to withstand earthquakes decreases the Seismic Risk.

Several Mediterranean and European regions have been only recently defined seismic prone areas. Figure 1.2 visualises the previously described meanings of "hazard" and "exposure" comparing two meaningful maps. The first map (Figure 1.2.a) depicts the density of habitants in the European countries estimated in 2011. The latter map (Figure 1.2.b) reports the peak ground acceleration with the exceedance probability of 10% in a period of 50 years and the cold colours indicate comparatively low hazard areas (PGA$\leq$ 0.1g), yellow and orange indicate moderate-hazard values (0.1g). The comparison of the two colour maps underlines the strategic necessity of accurate evaluation of seismic vulnerability of existing buildings. In fact, by comparing the two images the higher level of population density are spread on the same areas with the higher expected peak ground accelerations.

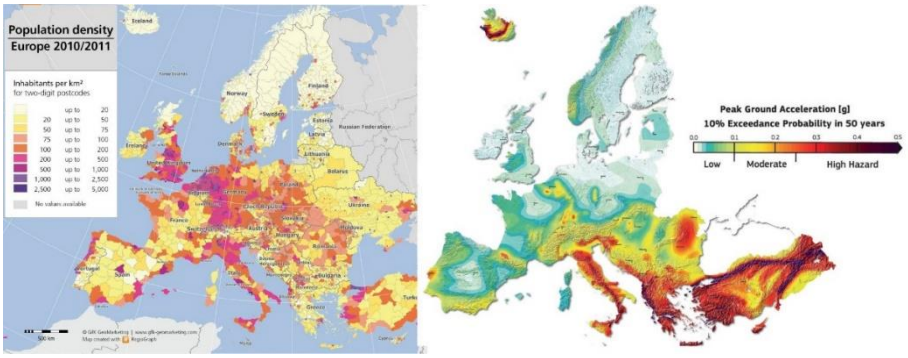

a *b*

Figure 1.2 (Colour) a) European population density 2010/2011, b)European Seismic Hazard Map (ESHM13) displaying the 10% exceedance probability in 50 years for peak ground acceleration (PGA) in units of gravity (g).

Even though it can be seemed irrational, several European cities with millenarian history are placed along the darker area of the hazard map. Cities like as Istanbul, Athens, and Tirana have an extremely high seismic hazard. On the other hand, the surrounding lands around these cities are characterised by a relative low population density. In this scenario, the Italian peninsula has a higher seismic risk. In fact, the population density map shows smaller cities but bigger areas characterised by the same density. Large areas, such as the Sicilian eastern cost, appear affected by unneglectable values of inhabitants per km^2 (200-500) and a high seismic hazard value (0.3-0.4g). Looking at Figure 1.3 and Figure 1.4, the high seismic risk of Sicily can be understand.

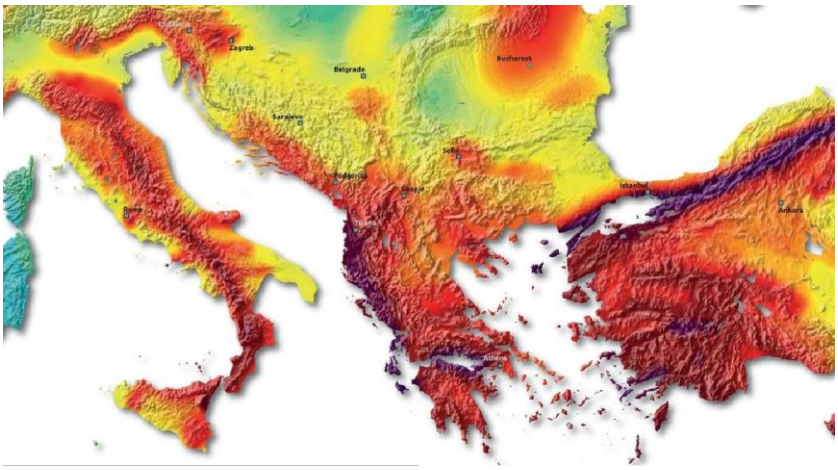

Figure 1.3 (Colour) Detail of the Seismic Hazard map of Europe.

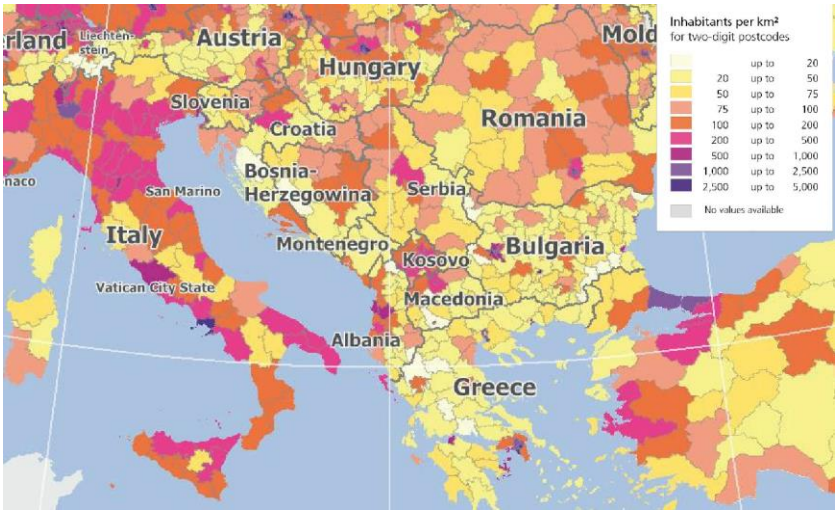

Figure 1.4 (Colour) Detail of the population density map

Furthermore, the inadequacy and vulnerability of the existing buildings in that area make Sicily one of the European regions characterised by high seismic risk and one of the higher in the all over the World. Lastly, aiming to underline this extremely dangerous condition, the Figure 1.5 compares the civil victims during the World War II and those of earthquakes in the XX century in Italy. The victims died immediately in building collapses of few days later due to the severe injuries.

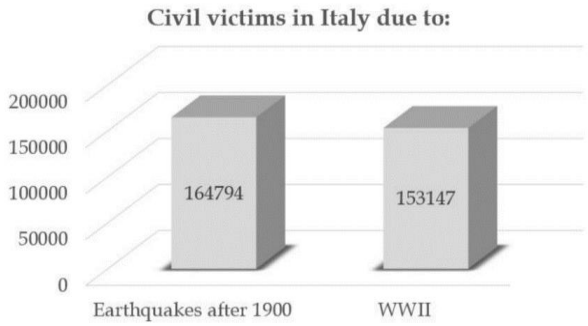

Figure 1.5 Civil victims in the XX century in Italy due to earthquakes or global war.

1.2 Seismic Hazard in Italy and Seismic Code evolution

Even though the seismic hazard of the Italian peninsula was seriously argued since the last decades of the 1800 by the academic researchers, Ferdinando IV Borbone of Kingdom of the Two Sicilies issued the first European Seismic Prescription in 1785. After the devastating earthquake that stroke the southern part of Italy on 5th February 1783, he issued a construction regulation that imposed an innovative construction technique, the "*casa baraccata*" (Figure 1.6). The construction method, which involved wooden frames and masonry infill panels, was applied in several towns and saved thousands life during the earthquakes of 1905 and 1908.

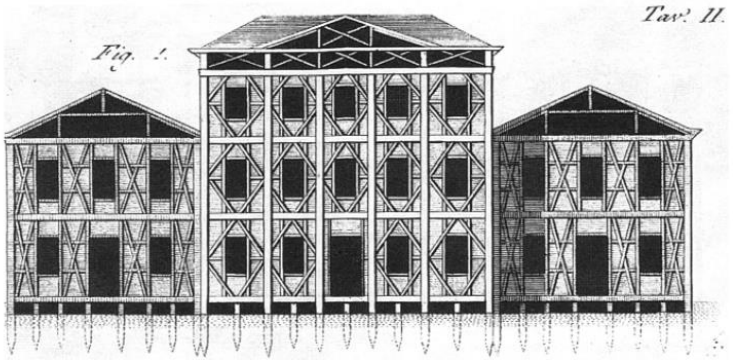

Figure 1.6 "Casa baraccata" (1783)

At the end of the 1800, the hazard map and the seismic classification were based on correlation between geological characteristics and historical earthquakes. In this way, Prof. Torquato Taramelli proposed a hazard map of the Italian peninsula in 1888, as Figure 1.7 shows. The map, the oldest in Italian seismology, described the seismic areas in terms of Mercalli scale effects. Taramelli worked for finding a correlation between the seismic areas and their geological properties, but he did not obtained evident correlations. On the other hand, it is notable that the map showed a seismic classification similar to the more modern hazard maps.

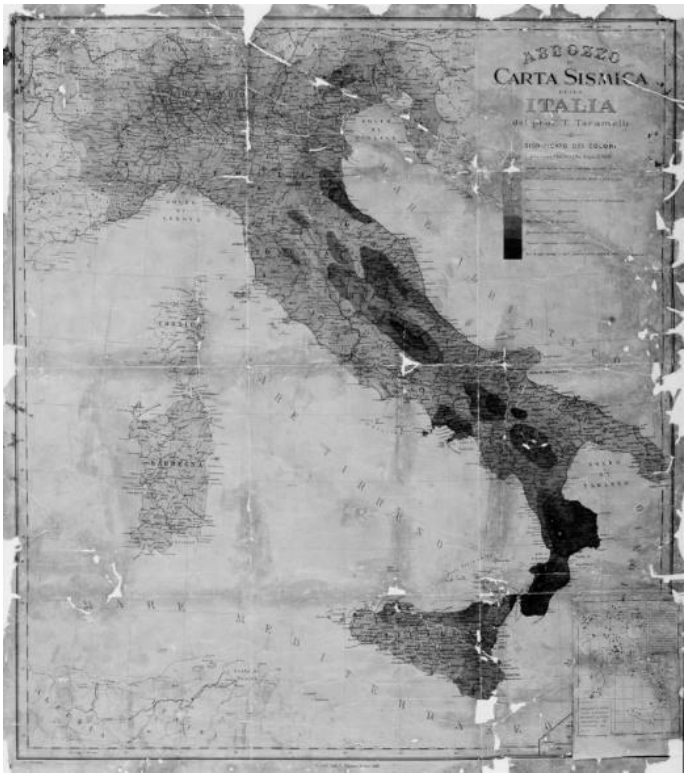

Figure 1.7 The first Italian Seismic Hazard Map. Prof. Torquato Taramelli, 1888

The first Italian Seismic Code that involved many peninsula areas was published in 1974 (law 64, 1974). The 1974 Building Code established the spectral horizontal design forces; but they were not explicitly related

to ground motion parameters. The local seismic coefficients were established according to some criteria and it was named "seismic classification".

Figure 1.8 "Progetto Finalizzato Geodinamica" CNR (1976-1981)

The 1984 seismic classification of the Italian territory, still in use in 1997 and until the 2002, derived from the results of research group called "*Progetto Finalizzato Geodinamica*" funded from 1976 until 1981 by CNR ((Italian) National Council of Research).

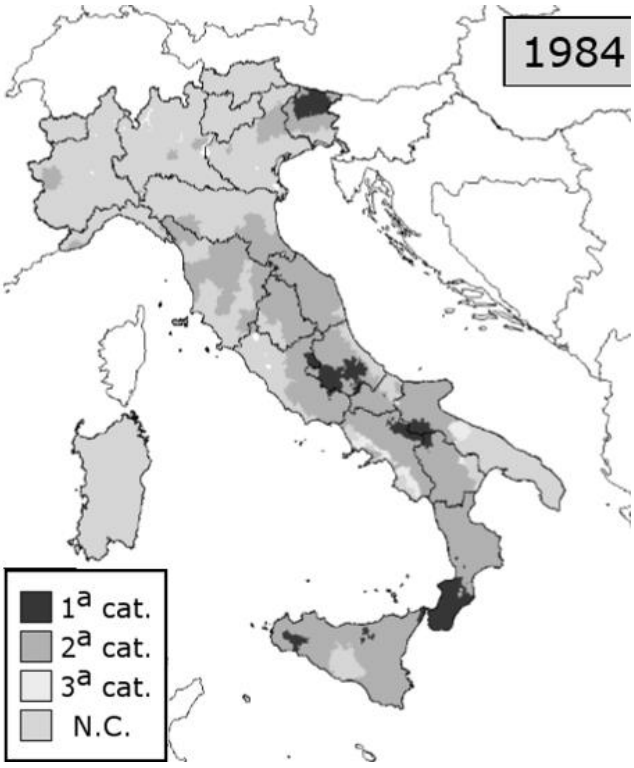

Figure 1.9 Italian hazard map in 1984 and seismic categories

Figure 1.9 shows the seismic classification of the Italian peninsula in 1984. According to the results of the before mentioned research group, the land was subdivided in four categories. The fourth category characterised the not prone areas. In that period, the Eastern Sicilian cost was catalogued as II seismic category.

After the Umbria-Marche earthquake in 1997, the Commission for the Major Risks established a working group charged of updating the seismic classification of the Italian territory. The parameters that have been adopted in that project were:

- Housner (1952; 1963) spectrum intensity
- H50 = 10% exc. probability in 50 years, 0.2-2 sec.
- H10 = 10% exc. probability in 10 years, 0.1-0.5 sec.
- Maximum observed intensity

Unfortunately, the results of the study were not adopted until the 2002.

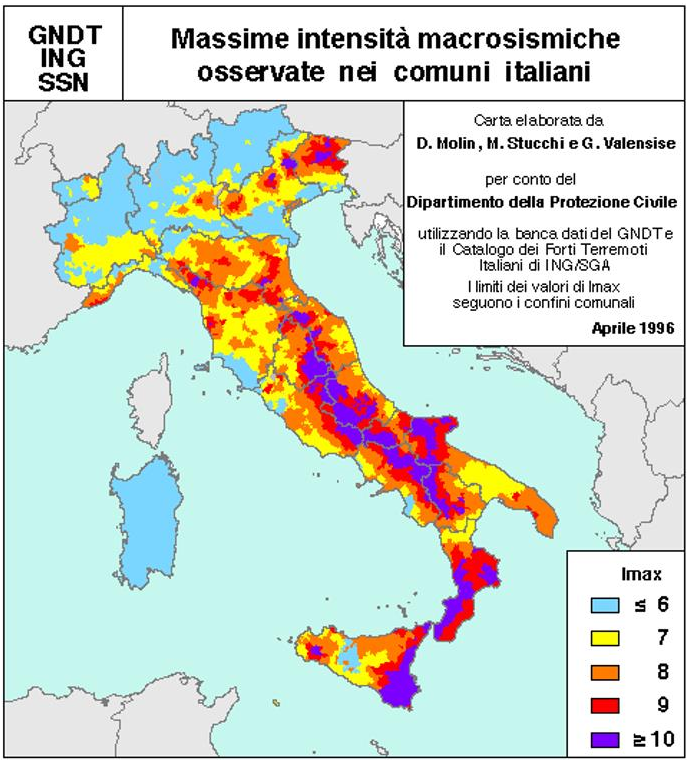

Figure 1.10 (Colour) Proposed Hazard map of Italy in 1996

In 2002 an earthquake struck Molise (a region in the mid of Italy) and an area that was not included in the seismic zonation was hit (Figure 1.11). Due to that evident lack in the seismic classification, the borders of each Italian seismic area were updated. After this event, the map of the "Proposta 98", read in terms of PGA, was adopted as the reference for the new seismic zonation.

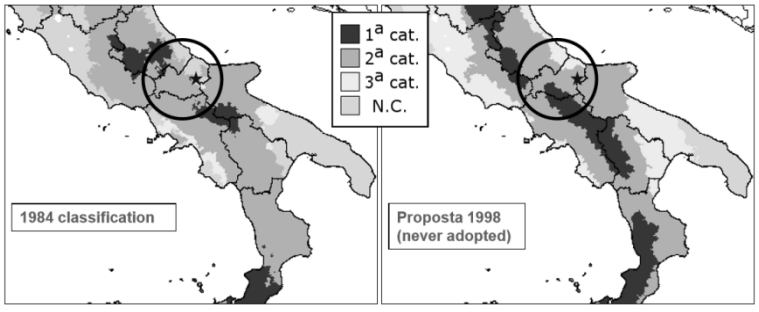

Figure 1.11 Comparison between the adopted map in 1997 (a) and the proposed map of the 1998. As the star shows the Molise earthquake struck a not classified area.

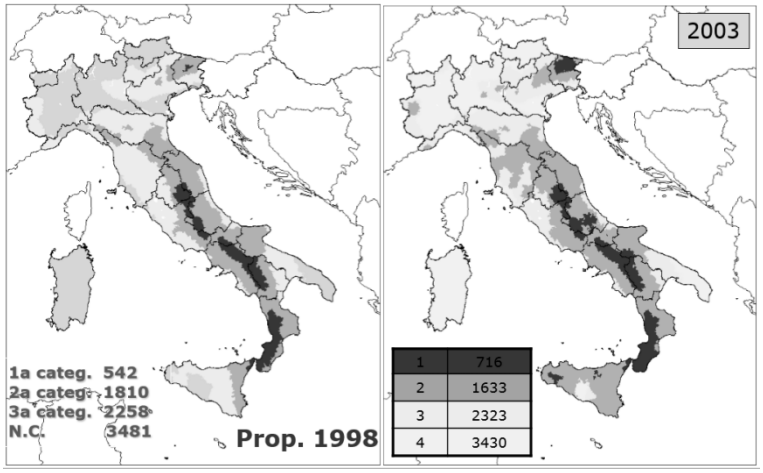

Figure 1.12 Map of 1998 ("Proposta 98") and the map of 2003 based on it.

Later, in 2003, PCM Ordinance 3274 required that a PGA map (10%, 50 years, hard ground) had to be compiled within 1 year (May 2004) according to the following, main criteria:

- To employ recent and widely used methods INGV initiative (started in July 2003)
- To employ updated input data (A new earthquake catalogue; a new seismogenic zonation; updated ground-motion attenuation relationships)
- To employ transparent procedures. Data and computing tool to be made available to public (zonesismiche.mi.ingv.it)
- Results to be checked through peer review : Review panel composed by: D. Giardini, F. Barberi, J. Bommer, M. Garcia-Fernandez, P. Gasparini, P.E. Pinto, D. Slejko

The Figure 1.13 shows the actual hazard map of the Italian peninsula. This map was the result of the mentioned revision and it was officially incorporated in the seismic code in 2008 and it use became mandatory.

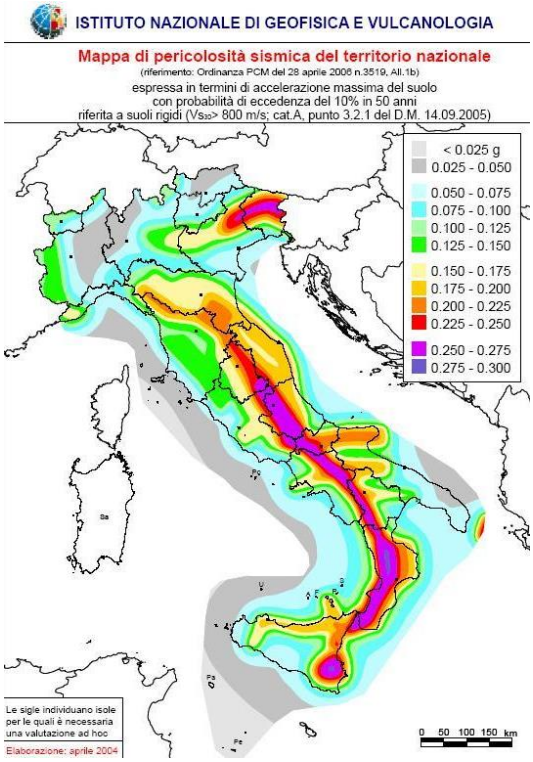

Figure 1.13 (Colour) Actual Hazard map of Italy. (April 2004)

1.3 Seismic Hazard in Sicily

The Sicily island, in south of Italy, is one of the Mediterranean area characterised by high seismic risk. Figure 1.14 shows Sicily and the main active faults that influence the seismicity of this area. The collision between the two continental plates (African and European) is the source of the seismic activity along the fault that goes though Sicily and Ionian Sea.

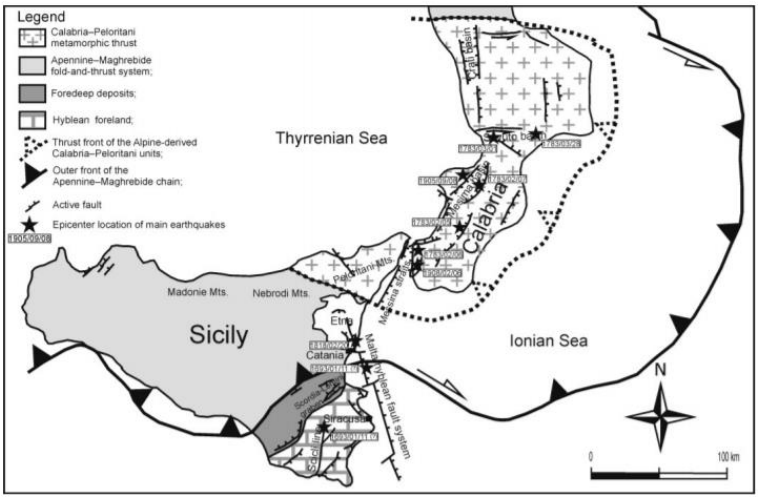

Figure 1.14 Tectonic framework of the study area with major structural domains of southern Italy and active faults identified through surface geological evidence

Eastern Sicily is delineated by the crossing of lithosphere structures that give rise to the origin of Mt. Etna and by the presence of the Malta Hyblean fault system that goes down to the Sicilian coast towards the Ionian Sea. The definition of seismic sources in eastern Sicily is a quite debated problem due to the lack of clear evidence of surface faulting and to the few high-magnitude instrumental earthquakes. For example, the location, size and kinematics of the January 11, 1693 earthquake (MW= 7.4, [2]) is particularly uncertain and debated in literature. Some authors locate the source inland, whereas others locate it offshore. The inland source models are based on geologic, geomorphologic and macro seismic intensity analyses. On the other hand, the models that adopt an offshore source are mainly based on results of seismic prospecting at sea

and on tsunami modelling which suggests either the rupture of a segment of the NNW-SSE Malta fault escarpment [3, 4, 5]; or the rupture of a locked subduction fault plane [6]. Recently, some authors associated the 1693 earthquake to the Sicilian basal thrust, to which they associated the 1818 Catania event (MW = 6.2, Working Group CPTI, 2004) as well [7].

In eastern Sicily, in addition to the seismicity related to these regional sized tectonic structures, there is an intense seismic activity due to the Etna volcano. It is characterized by low magnitude events and shallow hypocentres that produce destructive effects only at local scale [8].

Figure 1.15 Tectonic sketch and Epicentral map of the regional earthquakes.

1.4 Historical seismic events in Catania

The seismic activity in the Catania area is particularly high, as testified by the historical earthquakes. The main earthquakes that hit Catania occurred in 1169, 1542, 1693 and 1818 while the more recent, although moderate, occurred in 1990.

The main Catania urban changes have been determined by natural catastrophes such as volcano eruptions and massive earthquakes. Historical Etnean lava flows invaded and partially covered the ancient city of Catania many times (e.g., 683 BC, 252 AC) and several seismic events stroke the city in the millennia.

Basing on several researches on the Catania seismic history [9, 10, 11, 12], a short overview is proposed below.

4th February 1169

On the 4th February 1169, a heavy earthquake stroke the Sicily at 7:00 am on the eve of the feast of St. Agatha of Sicily. It had an estimated magnitude between 6.4 and 7.3 and an estimated maximum perceived intensity of X (Extreme) on the Mercalli intensity scale [9]. Catania was deeply damaged. The earthquake triggered a tsunami as well. Overall, 15,000 people died during the earthquake and they were almost the 65% of the entire population [9].

10th December 1542

This event caused several damages in the Ionian coast, but the seismic waves were felt through the whole island. The main shock was followed by a seismic period that started *die ultimo mesis novembris* (the last day of November) and continued for 40 days. Catania was severely damaged. Churches, monasteries and buildings completely or partially collapsed. Many structures were severely hit. A whole quarter in the western part of the city ruined.

8th March 1669

In the 1669, a devastating Etna eruption changed the town planning. The lava flowed in the western sector of the ancient town, destroyed part of it and its volume was able to fill up the moat of Ursino Castle.

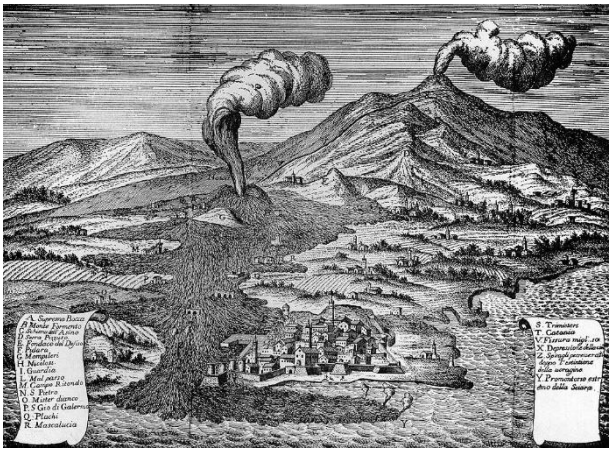

Figure 1.16 Ancient figuration of the 1669 eruption

9th and 11th January 1693

This was the most destructive event that the Italian country knew [13]. The 1693 Sicily earthquake struck parts of southern Italy near Sicily, Calabria and Malta on January 11th at around 9 pm local time. This earthquake was preceded by a damaging foreshock on January 9th. The main shock had an estimated magnitude of 7.4 on the moment magnitude scale, the most powerful in Italian history, and a maximum intensity of XI (Extreme) on the Mercalli intensity scale, destroying at least 70 towns and cities, seriously affecting an area of 5,600 square kilometres and causing the death of about 60,000 people. A tsunami happened and it destroyed several villages by the sea on the Ionian Sea and in the Straits of Messina. Almost two thirds of the entire population of Catania died (between 12 and 16 thousand victims over a population of 18-20 thousand people). The rebuilding process converged in a new and homogeneous Baroque style. The towns and villages of southeastern Sicily, particularly in the Val di Noto, were rebuilt in this new and elegant architectural style, described as "the culmination and final flowering of Baroque art in Europe". [13]

The old urban planning was replaced by a newest characterized by larger main roads cut off of squares, with a kind of anti-seismic aim.

Figure 1.17 The 1693 Earthquake in an ancient picture.

20th February 1818

The earthquake damaged several buildings in Catania did not caused victims. The buildings had internal collapses and widespread damages.

11th January 1848

The earthquake of the 1848 was the last serious seismic event that struck Catania. Nobody died in that event and there were few minor collapses of ornamental stones of façade parts.

The city of Catania grew hugely in the 19th century. At the end of the 20th century, between the 1960s and 70s, Catania, and Italy in general, knew its maximum urban expansion. This was the decade of the huge residential blocks, according to the contemporary architectural and urban philosophies.

Catania landscape started to be marked by mid-rise buildings, designed only for gravity loads and founded on rocks or soft soils as in some areas over the rubble of the 1963 earthquake that are generally characterised by an amplification of the seismic signals.

1.5 Definition of the seismic inputs

Aiming at performing seismic assessment of the different structural models under investigation by means of nonlinear dynamic analyses, the selection of suitable seismic inputs (accelerograms) is required. These could be obtained by considering the outcomes of numerous research works already performed for the Catania area or the oriental Sicily [14] or through a further seismological survey. However, the need to provide code-consistent seismic assessments as well as to investigate seismic retrofitting solutions to be applied in current practice led the choice towards the definition of simulated accelerograms compatible with the current design spectrum.

The literature divides the accelerograms in three main groups [15]. The first type consist of artificial spectrum-compatible accelerograms. Usually, they are obtained by procedures that generate power spectra density function from the smoothed response spectrum, and sinusoidal signals are then derived having random phase angles and amplitudes. The sinusoidal motions are then summed, and an iterative procedure can

be invoked to improve the match with the target response spectrum, by calculating the ratio between the target and actual response ordinates at selected frequencies. The power spectral density function is then adjusted by the square of this ratio and a new motion is generated. The second type consists of synthetic accelerograms generated from seismological source models and accounting for path and site effects. Finally, the third type involves the use of real recorded accelerograms. This last strategy is becoming more promising due to the increasing number of real records available by means of web-facilities and software [16] and web-databanks [17, 18, 19, 20, 21], making the use of real accelerograms a relatively straightforward and effective task [22].

Currently, the Italian national code and the European code allow defining seismic accelerations based on a spectral shape-based match. The artificial or adjusted inputs are individually compared to the elastic design spectrum, while the real recorded accelerograms are compared in terms of average values. In the latter respect, the Italian Seismic Code [23, 24] allows the use of real accelerograms, and imposes that these have to be compatible with the target spectrum in a specific range of vibration periods. Furthermore, the Italian Seismic Code states that the spectrum compatibility has to be achieved by the average real spectrum with the ξ =5% damping elastic response spectrum in the interval of 0.15s-2s and no less than the variance of 10% (Figure 1.18).

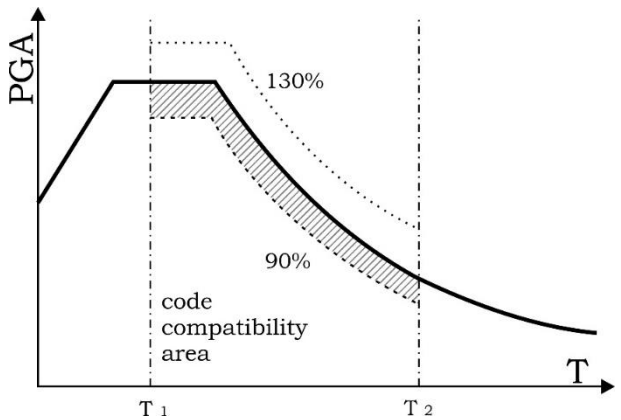

Figure 1.18 Spectrum compatibility area in the Italian Seismic code

In this research, a set of seven accelerograms, in their three components, has been used and the match with the target spectrum has been achieved by means of a linear scaling iterative procedure. The choice is consistent to the Italian Code and Eurocode prescriptions that allow considering the mean structural response from the nonlinear dynamic analysis if at least seven sets of accelerograms are selected.

The accelerograms have been defined by means of the software REXEL v3.5 [16]. It automatically provides the identification of the recorded accelerograms and verifies the spectrum compatibility. All the three components for each accelerograms have been considered, and the spectrum compatibility has been satisfied for the planar and vertical target spectrum.

Looking at the definition of the seven accelerograms, the disaggregation of the seismic hazard has been performed. This procedure allows identifying the parameters that influence the seismic hazard of a specific site. By means of the disaggregation, the modal values of Magnitude (M) and epicentral distance (R) can be defined. Their combination defines the probability of exceedance a related PGA in the defined return time (Tr).

Specifying the M and R intervals equal to 6-7 and 10-30 km, respectively, assigning a compatibility tolerance with respect to the average spectrum of 10% lower and 30% upper in the period range 0.15–2 sec the software returns the combinations of accelerograms shown in Figure 1.20 and Figure 1.21.

The target spectrum is defined by the values in Table 1-1.

Table 1-1 Target Spectrum

Lon. [°]:	Lat. [°]:	Site class:	Top. cat.:	Vn:	CU:	SL:
15.105	37.516	D	T1	50 years	II	SLC

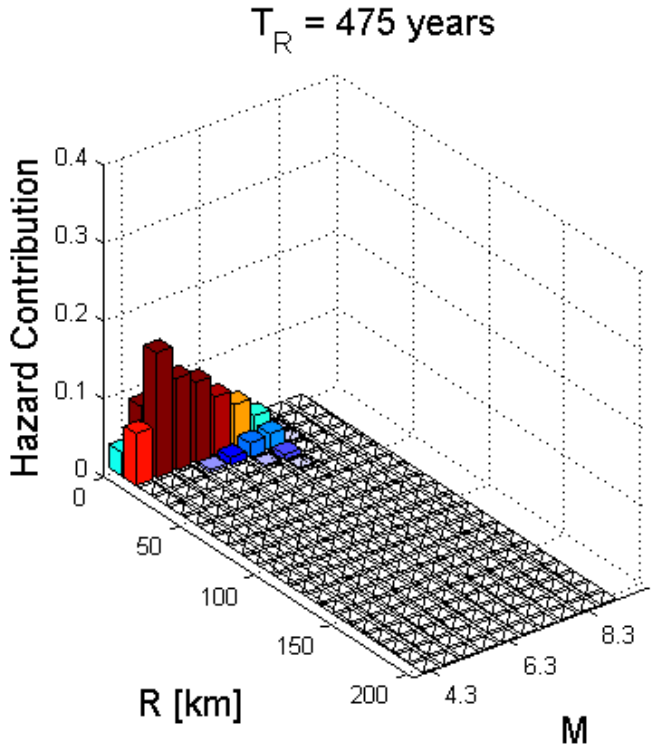

Figure 1.19 (Colour) Disaggregation in terms of Magnitude and Epicentral Distance for a Return Time of 475 year related to a Vt of 50 years and a soil type D (SLC. Soil D. Category T1)

Table 1-2 Main characteristics of the seven adopted records

Waveform ID	Earthquake ID	Station ID	Earthquake Name	Date	Mw	Fault Mechanism	Epicentral Distance [km]	EC8 Site class
343	142	SMTC	Christchurch	2011_February_21	6.2	reverse	16.52	C*
388	149	PPHS	Christchurch	2011_June_13	6	reverse	13.44	C*
421	46	CLT	Irpinia	1980_November_23	6.9	normal	18.85	B
391	149	SMTC	Christchurch	2011_June_13	6	reverse	14.86	C*
340	142	PPHS	Christchurch	2011_February_21	6.2	reverse	14.38	C*
444	89	EMO	Imperial Valley	1979_October_15	6.5	strike-slip	19.33	C
431	77	AI_137_DIN	Dinar	1995_October_01	6.4	normal	0.47	C
mean:					6,314		13,97857143	

Waveform ID	PGA_X [m/s^2]	PGA_Y [m/s^2]	PGV_X [m/s]	PGV_Y [m/s]	ID_X	ID_Y	Np_X	Np_Y
343	17.791	13.823	0.32596	0.22313	44.116	84.186	0.82095	0.88607
388	13.114	12.408	0.16771	0.18485	91.643	10.614	10.666	0.90819
421	17.177	1.55	0.29058	0.26018	170.711	164.311	0.91751	0.74678
391	0.8071	0.91367	0.10986	0.15112	116.701	87.824	11.438	0.79114
340	20.909	19.239	0.36407	0.46143	78.201	63.566	0.97392	0.98503
444	2.904	30.761	0.90421	0.71742	25.661	24.267	0.83861	11.843
431	32.125	27.292	0.44387	0.29856	89.025	126.863	0.81449	0.95534
mean:	1,974672144	1,830847524	0,372324283	0,328098736	8,800817951	9,387963884	0,939417673	0,922402656

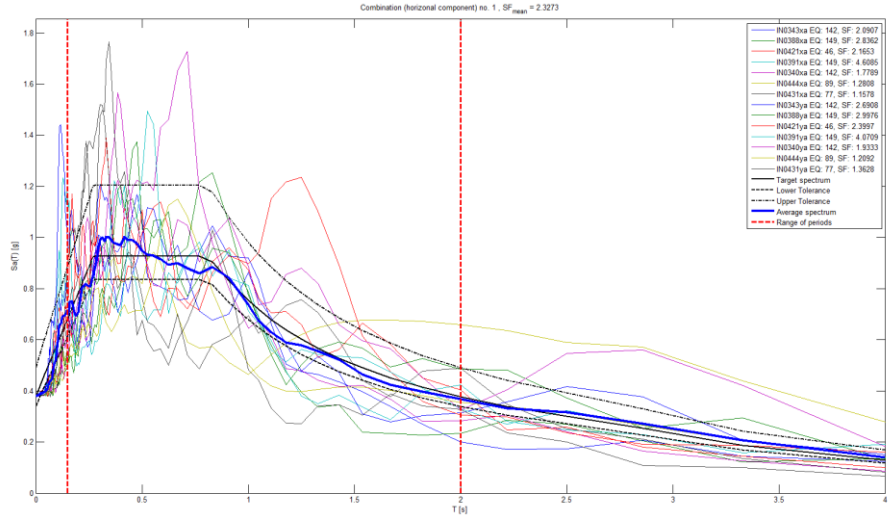

Figure 1.20 (Colour) Planar spectrum compatibility

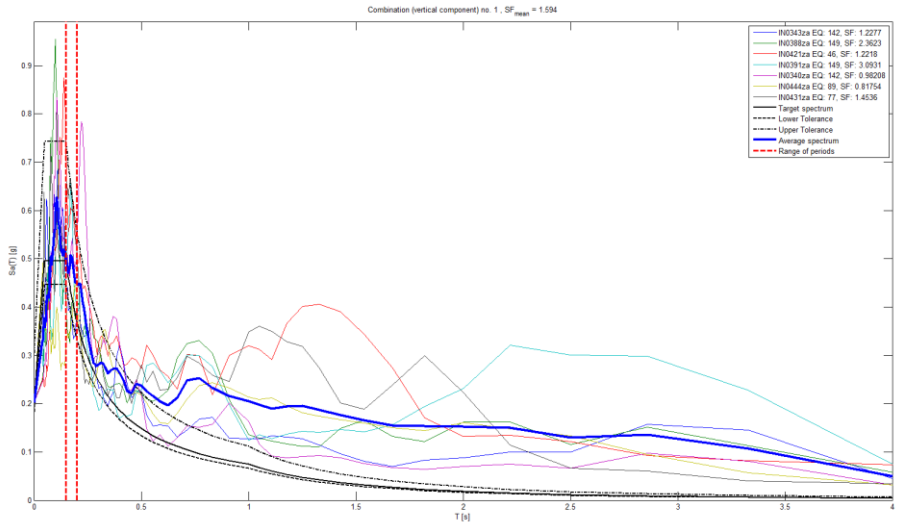

Figure 1.21 (Colour) Vertical spectrum compatibility

Finally, the accelerograms have been handled and their duration has been uniformly set to 25 seconds aiming to obtain a similar computational time effort. The length of each accelerograms has been reduced and an exponential decay has been applied on the last 8 seconds. Lastly, the spectrum compatibility has been checked again. The process has been handled through an iterative procedure through a numerical routine. In Figure 1.22 a flowchart of the adopted strategy for the

accelerograms identification is reported. Figure 1.23 shows the spectrum compatibility of the obtained accelerograms in terms of planar and vertical components. Finally, Figure 1.23 depicts the three components of the obtained accelerograms.

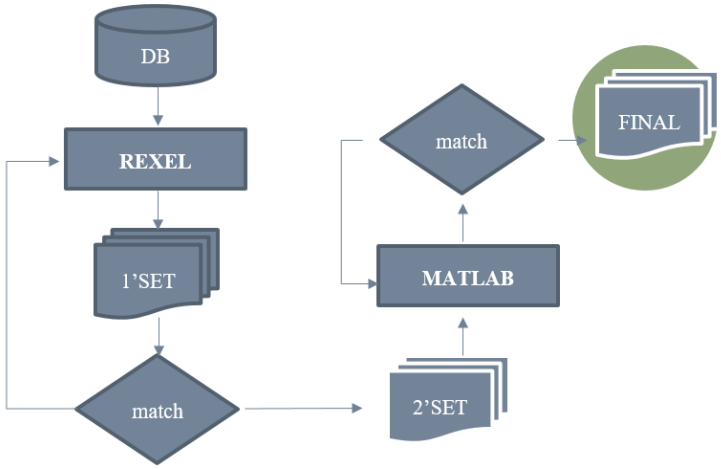

Figure 1.22 (Colour) Flowchart of the procedure for defining the accelerograms

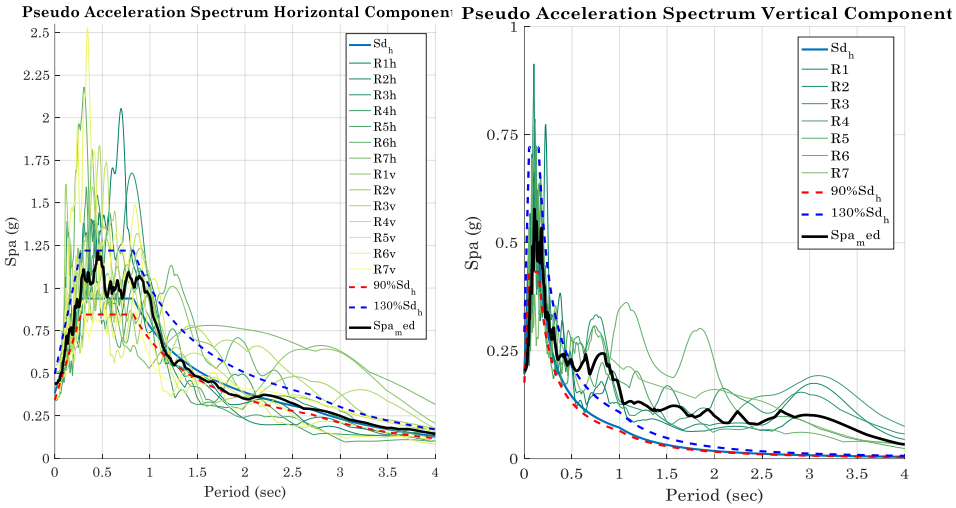

Figure 1.23 (Colour) Planar and vertical spectrum compatibility

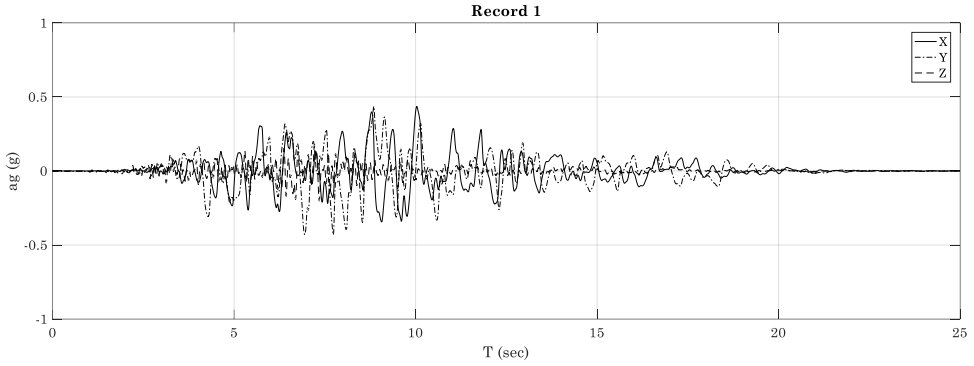
Record 1
X
Y
Z
ag (g)
T (sec)

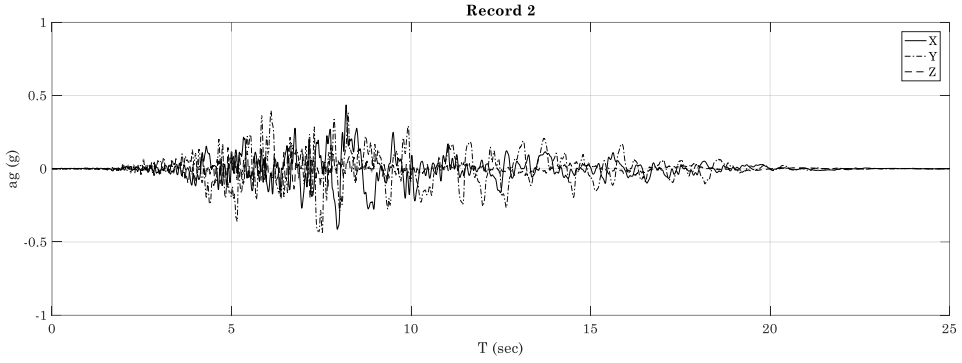
Record 2
X
Y
Z
ag (g)
T (sec)

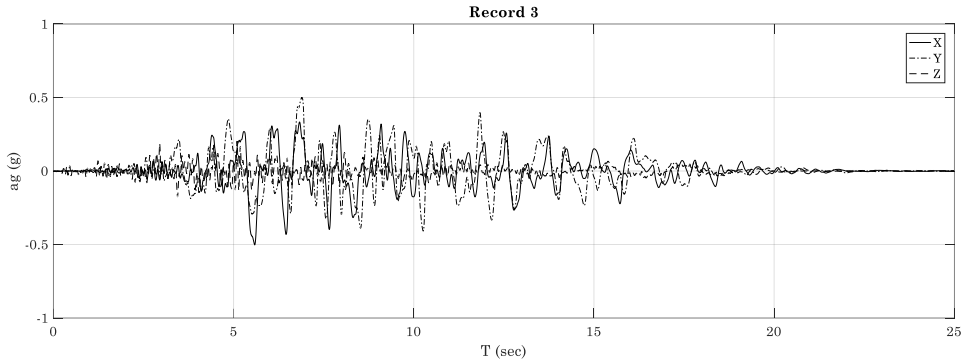
Record 3
X
Y
Z
ag (g)
T (sec)

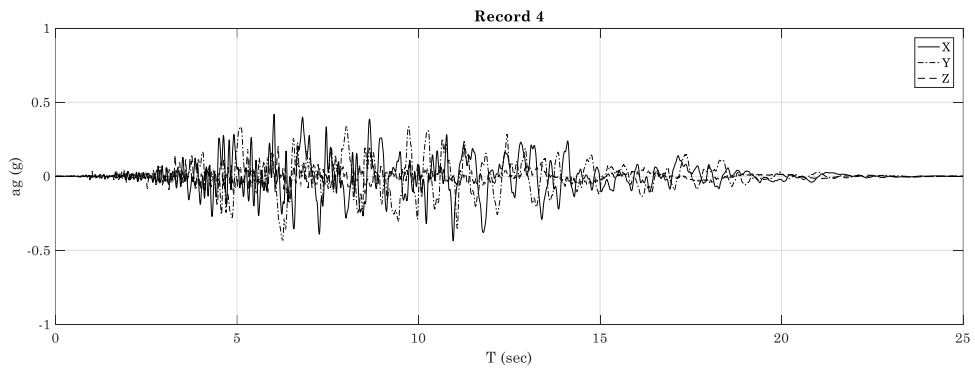
Record 4
X
Y
Z
ag (g)
T (sec)

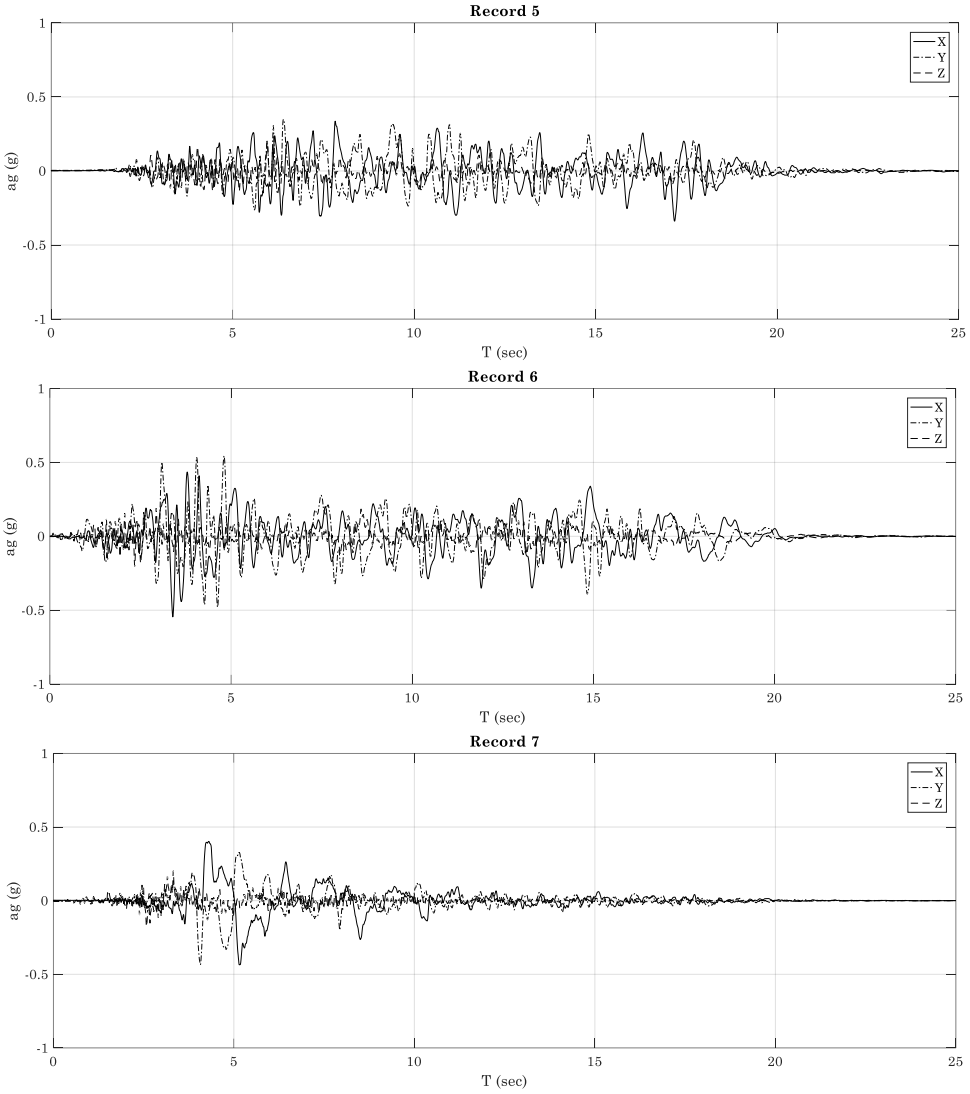

Figure 1.24 Seven accelerograms and their three components

CHAPTER 2. INTRODUCTION TO THE PROGRESSIVE COLLAPSE AND ROBUSTNESS ASSESSMENT

The present Chapter introduces the Progressive Collapse and the concept of Robustness with reference to multi-storey buildings. The Section aims to describe progressive collapse mechanisms due to typical damage scenarios in frame structures. According to different approaches, the assessment of a structure in a column loss scenario is discussed and different methodologies are described and commented. Since a unique assessment procedure does not exist, the *overload factor* [25] and the *simplified dynamic assessment* [26, 27] are assumed as representative of three different assessment strategies. Since *simplified dynamic assessment*, developed by professor B.A. Izzuddin at the Imperial College of London, has been adopted in the subsequent investigations it is accurately described.

2.1 Introduction to Progressive Collapse and Robusteness

The last decades have seen significant growth of scientific interest on the response of structures subjected to local damage eventually leading to progressive collapse (Figure 2.1). The attention was influenced by numerous partial or global structural failures occurred in the recent past and trigged by accidents or malicious acts. Some of the results obtained in previous studies have been incorporated in current standards [28, 29, 30, 31] providing specific robustness design prescriptions for new buildings.

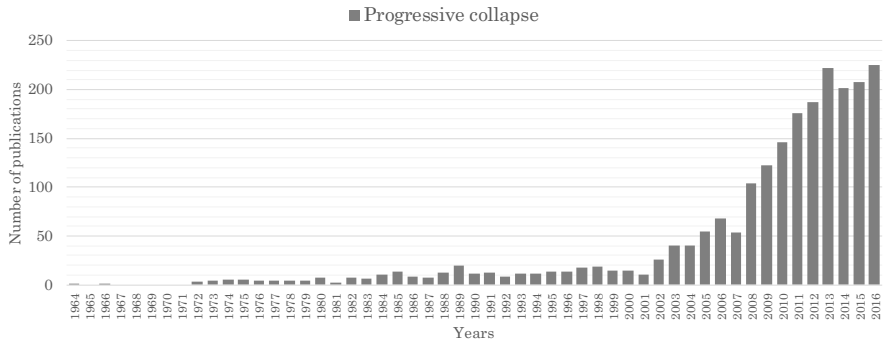

Figure 2.1 Growth of number of publications between 1964 and 2016 (scopus.com)

Thus far, not all the design codes incorporate specific prescription in order to assess the influence of local damage on the global behaviour of the overall structure with the aim to avoid that a local damage can lead to a disproportional collapse. So far, a unique and shared definition of the progressive collapse nomenclature has not been still produced. Due to this reason, two main concepts that define the phenomena and the structural attitude of withstanding local collapses have slightly different definitions. Storessek [32] attempted to coin a satisfactory definitions for *Collapse Resistance* and *Structural Robustness*, covering the several definitions that he found in codes and researches.

He defined:

Collapse Resistance the structural insensitivity to accidental (and rare) circumstances (extreme loading events), which are low probability events and unforeseeable incidents.

Structural Robustness the insensitivity to local failure, where "insensitivity" and "local failure" are to be quantified by the design objectives that are parts of the design criteria.

2.1.1 Design strategies against progressive collapse

The design codes adopted specific design strategies for new buildings to withstand disproportional collapses due to local failures. The design prescription are generally defined as *Bridging*, *Tie* and *Segmentation Method*.

The *Bridging Method*, usually called Alternative Load Path [33], aims to describe the structure in the damaged configuration. In new structures, the absence of bearing elements returns an alternative structural scheme in which the other elements have to be able to withstand forces redistribution. The capacity to resist global collapse in case of heavy local damages has to be verified in new structures according to several design codes [30, 31, 29].

The *Tie Method* is an indirect design method based on the capacity of prescribed structural elements to redistribute the forces during the collapse and contain its extension to the entire building. Figure 2.2 shows a scheme of this method. The ultimate version of the "Alternate Path Analysis & Design Guideline for Progressive Collapse Resistance" (GSA) [33] exclude the tie strategy even though it is still present in the "Design of Buildings to Resist Progressive Collapse" Unified Facilities Criteria (DOD-UFC) [31].

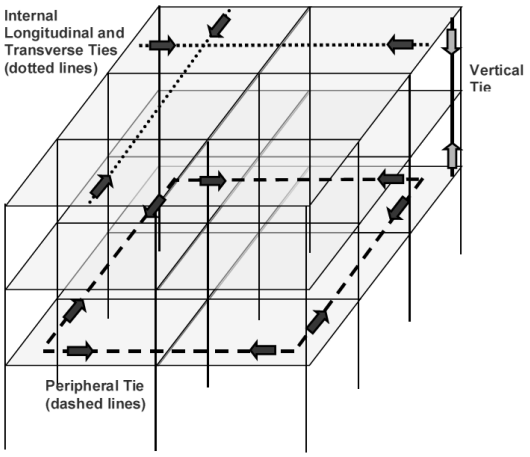

Figure 2.2 Tie Forces in a Frame Structure

Lastly*, Segmentation* is an alternative design strategy. The presence of weak elements within the structures can arrest the propagation of the collapse. It can be explicitly adopted in the design process or intrinsically present in existing structure designed under gravity loads only for instance. The absence of seismic detailing does not guarantee the continuity of reinforcement steel bars. On one hand this type of structures do not have resource to resist local collapses, on the other hand, the reinforcement local discontinuities can arrest disproportional collapses, causing partial collapse of the structure.

2.2 Review of prominent progressive collapses

As the Figure 2.1 shows, the last two decades saw the growing of interests on progressive collapse. Few strategic or relevant buildings suffered of progressive collapse, trigged by accidental or malicious events in the modern era. However, some of these events started the research interest in progressive collapse with the aim to identify the mechanisms that the structural elements develop during a local collapse and identify strengthening solution and appropriate design approaches. Few famous very important progressive collapse events had a flywheel effect on the scientific research that was also supported by governments.

In 1968, the Ronan Point Tower, placed in Canning Town near London, England, went through a disproportional collapse (Figure 2.3) due to an accidental gas explosion [34]. The building was a 22-storey residential block made by precast panels joined each one other without framed structure. The accidental event, trigged by a gas blast at the 18th floor at the southern corner, caused the collapse of the superior levels due to the leak of connection between the panels and the floor slabs. The construction technology defined the collapse of the floors but, at the same time, avoided the collapse propagation thanks to the segmentation that had a key role in the collapse mechanism. After this tragedy, the United Kingdom design code made mandatory structural details and design process to avoid disproportional collapse [35] in the new designed buildings.

Four people died in the failure.

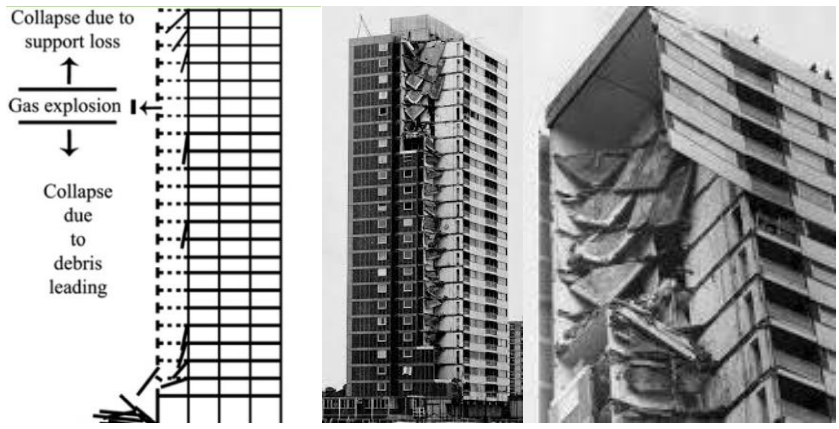

a) *b)* *c)*

Figure 2.3 Ronan Point Building a) scheme of the collapse b) global view c) details

In 1995, the Alfred P. Murrah Federal Building in Oklahoma City (Oklahoma) partially collapsed after the terroristic attack trigged by a truck-bomb, Figure 2.4. The truck blasted near the building severely damaging three columns. The collapse of the external columns changed the loading path within the concrete 3D structure and led to the collapse of the superior floors as Figure 2.4 shows. The damage extension was interrupted by the absence of continuity in the reinforcement bars in the floor slabs. As in the previous example, the segmentation of the structure strongly reduced the diffusion of the progressive collapse. On the other hand, the continuity of reinforcements may have increased the structural robustness and, potentially, avoided the collapse [36].

One-hundred-sixty-eight people died in the Alfred P. Murrah Federal Building collapse.

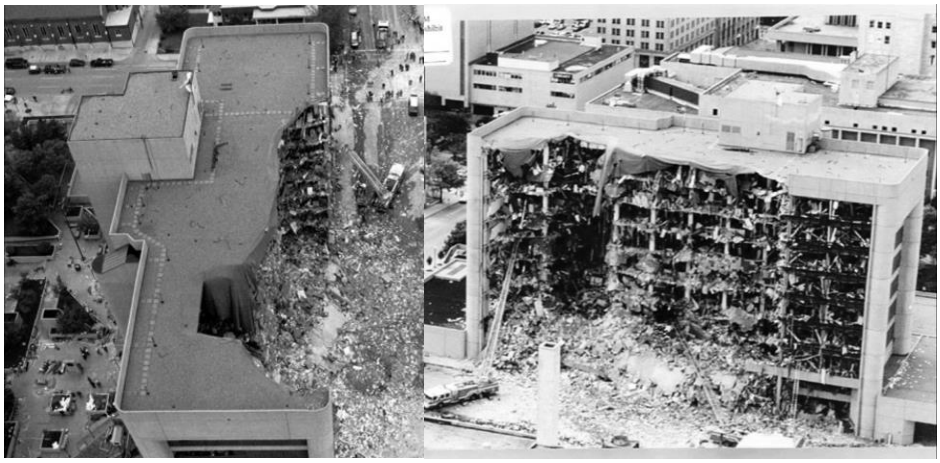

a) *b)*

Figure 2.4 Murrah Federal Office Building [1995] a) helicopter view, b) frontal view

In 2001, the World Trade Center in Manhattan, New York, was struck by a terroristic attack [37, 38]. Two airplanes hit the two twin towers that collapsed vertically. Although the collapse was trigged by a rare event,

it defined an immediate media, social and political interests and consequently a growing of interest on progressive collapse phenomena and robustness assessments criteria. This is congruent Figure 2.1 shows.

Two thousand and seven hundred fifty two people died in the event.

Figure 2.5 Collapse of the World Trade Center NY City [2001]

2.3 Behaviour of the structures under collapse

In order to resist to progressive collapse, a structure has to possess the capacity to redistribute the loads to other structural elements after the loss of a primary structural component, heavy damage can be accepted, but further collapse have to be avoided. Besides flexural action (bending in beams), resisting mechanisms include:

Vierendeel action;

Compressive arch;

Catenary effects;

Contribute of non-structural elements (infill walls).

In case of column loss, the forces, determined by the collapse of an intermediate column, may be not accommodate. The bending moments at the end of the beams, corresponding to the failed column, reverse sign and the reinforcement layout becomes not consistent with the internal force path. The comparison of Figure 2.6 and Figure 2.7 clarifies this concept. The star indicates the collapsed element in Figure 2.6.

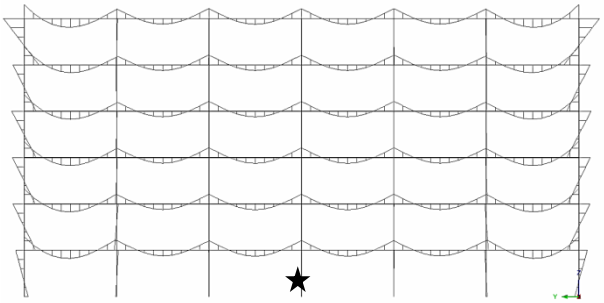

Figure 2.6 Static bending moments (My) in a framed structure [39]

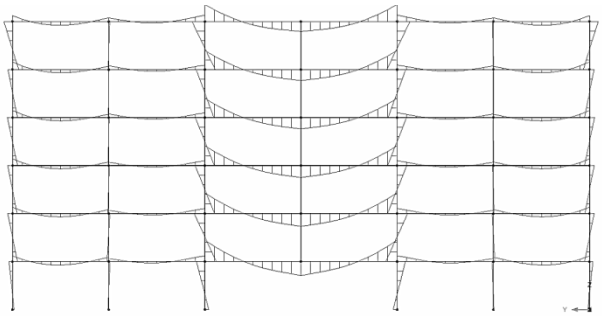

Figure 2.7 Collapse bending moments (My) in a framed structure [39]

With the term *Vierendeel (frame) action* is intended the resistance that is guaranteed by moment beam-column connections. This post-failure action was identified during experimental tests carried out on existing buildings. In 2008, M. Sasami conducted a real scale progressive collapse assessment on the Hotel San Diego building in San Diego, California [40]. The collapse was trigged by the loss of exterior columns, caused by a simultaneous explosion.

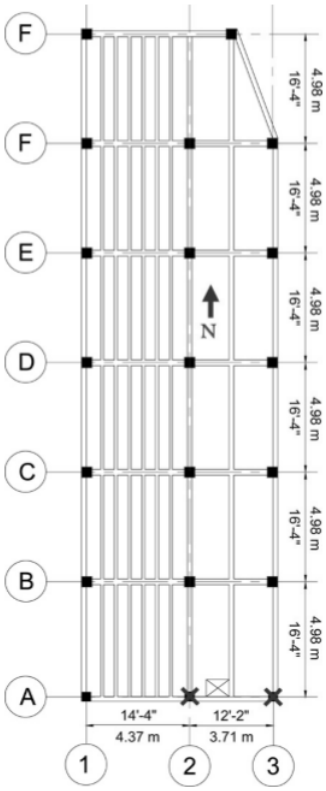

Figure 2.8 Plan of San Diego Hotel and blew up columns (crosses) [60]

Based on experimental data, the bidirectional Vierendeel action was identified as a major mechanism in the loads redistribution. Also the non-structural masonry walls influences the behaviour of the peripheral frames. In that case, the contributes of Vierendeel effects and infill walls increased the structural robustness of the building avoiding the global collapse.

The *Compressive arch action* is a resistance mechanism that increases the collapse resistance of concrete beams. This action depends on the beams geometry and it can be described as a strut mechanism. The Figure 2.9 and Figure 2.10 show the numerical simulation of an experimental test [41] that simulated a column loss scenario in a concrete frame structure and underline the compressed area in the concrete beam. The numerical simulation, developed during the first year of this research,

has been performed by means of plane stress and bar elements within a nonlinear finite elements software [39].

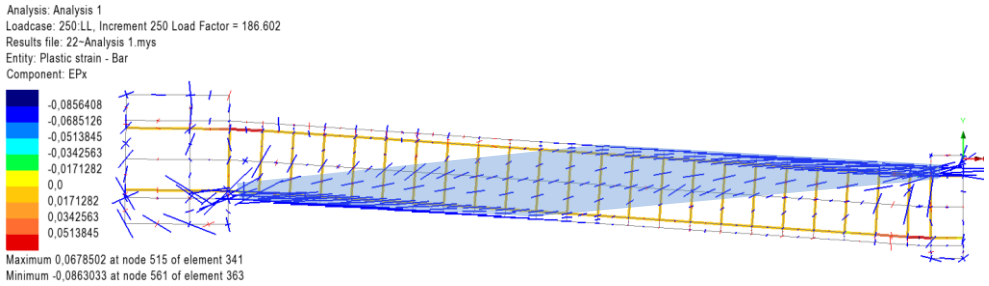

Figure 2.9 (Colour) Direction of principal stresses and Plastic strain of the bars and compressed area.

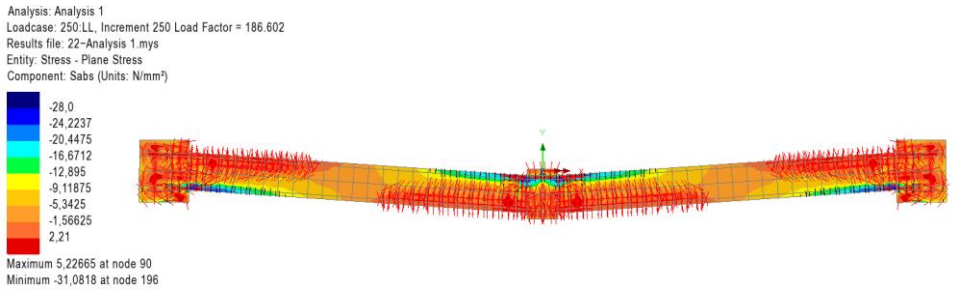

Figure 2.10 (Colour) Principal Tensions Map

An experimental campaign [42] has demonstrated that the arch effect increases the beam collapse capacity of 1.53÷2.63 times more than the flexural capacity.

The *catenary effect* defines the capacity of transferring vertical loads throughout tensile forces along the beam. In reinforced concrete frame structures this contribute becomes significant after a deflection of around 10% of the span length [43]. Even though this is a large deflection for a floor, the catenary action may prevent the complete failure of the structure directly affected by the column loss. In order to supply this type of action the continuity of reinforcement bars along the entire beam is needed. Furthermore, the steel area has to be sufficient to avoid plastic collapse of the bar and the anchorage of the bars has to avoid bond slip effects. Some authors [44] have demonstrated that even if the longitudinal bars are interrupted along the beam, which is typical of

building designed for vertical loads only, a catenary effect can be still established if the stirrups are able to transfer the tensile forces from the upper (negative bending moments reinforcements) to the lower (positive bending moments reinforcements) bars, Figure 2.11.

The ability of the beams to express catenary action in presence of discontinuities in longitudinal reinforcement bars depends on several factors such as stirrups size, spacing and details.

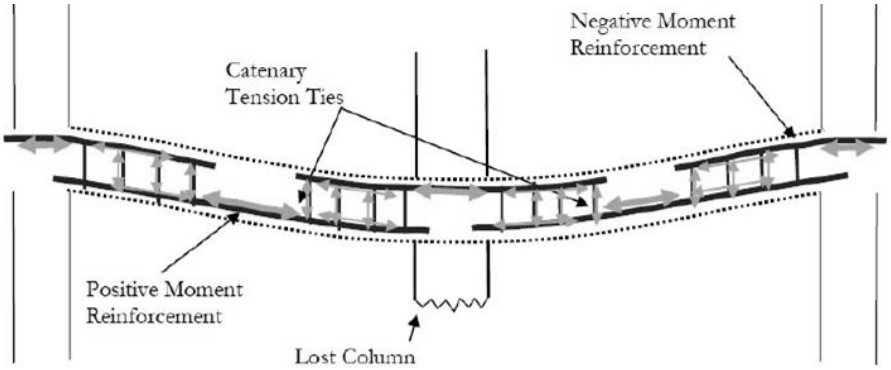

Figure 2.11 Tensile forces transferring through stirrups [44]

2.4 Introduction to the assessment strategy

When a multi-storey building is subjected to a sudden column loss, the structural behaviour is dynamic, typically characterised by significant geometric and material nonlinearities. In the robustness assessment procedures generally, two main assumptions are adopted. Firstly, especially in steel frame buildings, it is assumed that a column loss leads to a significant concentration of deformations in the beam-column connections and a typical triangular failure shape can be considered. Secondly, it is assumed that the columns that are not directly affected by the collapse are able to support the additional loading increments.

The most rigorous approach for evaluating the behaviour of a structure subjected to a column loss is the non linear dynamic analysis accounting for geometric and constitutive non linearity. However, the need to provide practical engineering strategy for assessing robustness

of buildings motivated many researches to propose efficient although simplified approaches.

Different approaches have been engaged by research groups aiming at reduce the computational effort of nonlinear dynamic analyses and maintain an accurate assessment of structural robustness. Some authors suggested a hybrid use of static nonlinear push down and dynamic nonlinear analysis [45]. Others proposed non-linear static push down method in order to define structural robustness [25].

Khandelwal and El Tawil [25] proposed a metric procedure of robustness based on pushdown nonlinear analyses and incremental analyses. The authors introduced the so-called static Overload Factor as the ratio between the failure load and the gravity loads evaluated in the appropriate load combination (Eq. 1).

$$OF = \frac{F_{failure}}{P_{gravity}} \qquad \textit{Eq. 1}$$

Other university research groups have engaged nonlinear dynamic and vertical pushdown analyses for defining the most critical damage sequence. In this light, the robustness metric has been defined as the minimum ratio of number of columns that can be removed without induce a global collapse [45]. The authors proposed the method that they defined Local Robustness Evaluation, and investigated several collapse scenario looking for the shorter sequence of column removing.

Even though those methods have been applied, a larger consensus has been growing on a more reliable robustness metric based on the ultimate capacity of a damaged structural system and a consequent energy-based interpretation of the nonlinear static pushdown analyses that accounts for the structural dynamic behaviour. This simplified and still accurate method has been developed at Imperial College of London [26] by prof. B.A. Izzuddin and it is discussed in the following Section.

2.4.1 Simplified dynamic assessment

The simplified method requires nonlinear static push down analyses to obtain a capacity curve while the dynamic effects are evaluated in a simplified, yet accurate, manner. This *Simplified dynamic assessment,* proposed by B.A. Izzuddin [26], was validated with numerical benchmarks [27] such as the multi-storey building depicted in Figure 2.12.

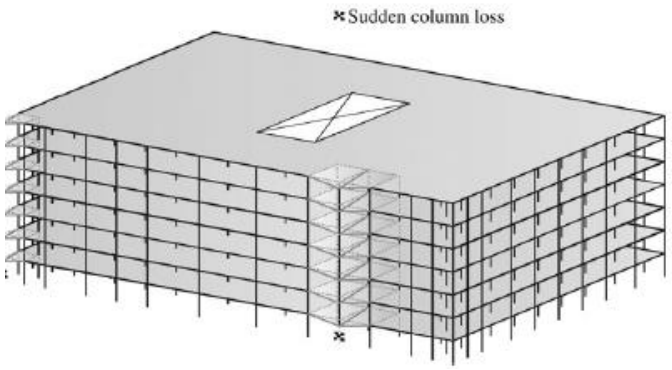

Figure 2.12 Sketch of the steel frame building [27]

In the present work, the *Simplified dynamic assessment* has been applied to concrete frame structures with particular reference to buildings not designed to resist to earthquakes.

The simplified dynamic assessment is based on main three steps:

Nonlinear static response of the damaged structure under gravity loading (push-down analysis);

Simplified dynamic assessment to establish the maximum dynamic response under sudden column loss;

Ductility assessment.

The versatility of the original framework represents its main goal, in fact it may be applied at overall structural levels Figure 2.13 or, accepting few initial hypotheses, to single sub-system or sub-structural levels. The simplified method is defined by the following hypotheses:

Appropriate boundary condition to represent the interaction with the surrounding structures defines a multi-level model simplification, Figure 2.13.a.

The surrounding columns can resist the redistributed load, Figure 2.13.b.

In addition the structure can be divided in sub structural levels and the robustness capacity of each structural element can be combined with the others if:

The properties in each floors in term of structure typology, loads distribution and material properties are identical and, consequently, theaxial force in the column immediately above the lost column is negligible. The structure may be reduced to the study of a single floor, Figure 2.13.c.

The planar effect within the floor slab can be ignored. The structure may be reduced to single beam subjected to an appropriate proportion of the gravity load, Figure 2.13.d.

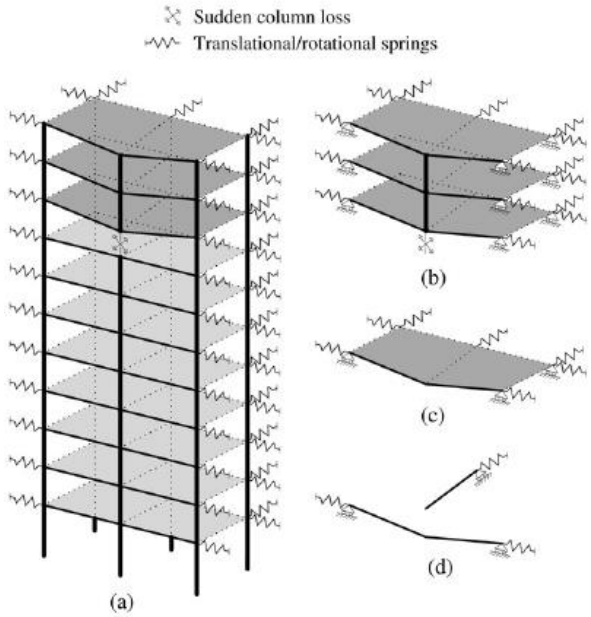

Figure 2.13 Sub structural levels for progressive collapse assessment

The dynamic response in the sudden column loss is similar to the instantaneous application of the gravity loads (P_0). The maximum dynamic response can be estimated from a static nonlinear push down analysis under amplified gravity load ($P=\lambda P_0$) [26].The Figure 2.14 explains the mentioned principle.

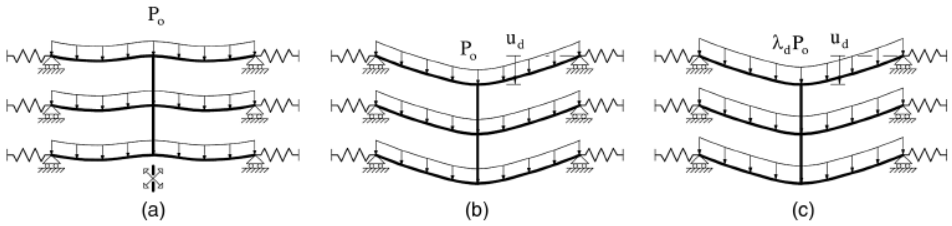

Figure 2.14 Sudden column event with gravity load Po [26]: (a) actual event; (b) step load dynamic idealization; (c) static analysis using amplification factor λd

Differently from steel beams, the existing concrete beams in framed structures, designed only for gravity loads, are usually affected by non-continuous reinforcement detailing. The collapse shape depends from these discontinuities and the typical triangular collapse deformation, characterising the steel frame structures,may not be respected.

The Figure 2.15.b depicts the deformed configuration in the catenary effect of a concrete frame structure in which the reinforcement bars layout is affected by heavy discontinuity as some experimental studies highlighted [46]. Furthermore, the Figure 2.15.a depicts an alternative collapse behaviour in which the plastic hinges are placed at the beams ends [44].

According to the above consideration, in steel or steel-concrete frame buildings, column loss usually causes significant concentration of deformations at the beam-column connections or at end of the beams and determinates a bi-linear shape deformation mode that involves the beams as shown in Figure 2.15a. On the other hand, in case of RC frames, the not uniform steel reinforcement longitudinal layout in beams determinates a different collapse, as depicted in Figure 2.15b.

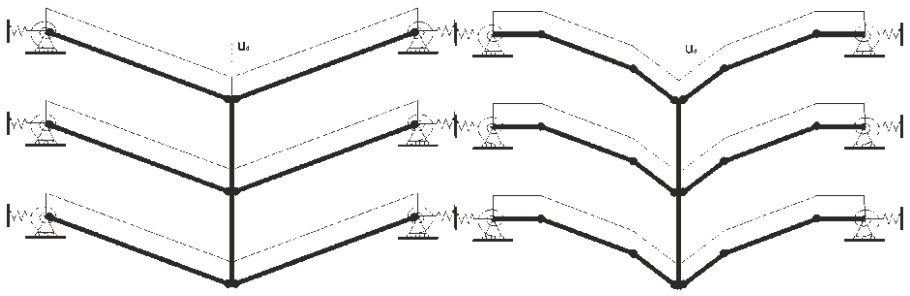

(a) *(b)*

Figure 2.15 Collapse modes due to column loss in steel (a) and RC (b) frames

In order to obtain accurate numerical simulations, a detailed modelling of the nonlinear static response is considered that has engaged advanced nonlinear finite elements. Different levels of sophistication may be applied and the structural behaviour of all the structural and not structural elements can be analysed.

Based on the assumption that the dynamic response may be obtained by the instantaneous load application on the damaged structure, the maximum dynamic response is achieved when the work done by the gravity loads becomes identical to the energy absorbed by the entire structure.

This assumption interprets the static nonlinear response obtained for incremental vertical loads.

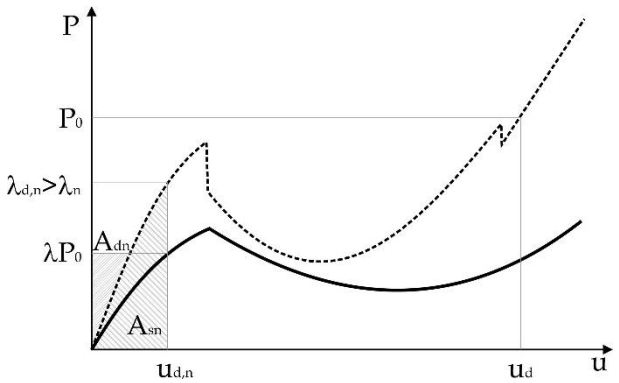

Figure 2.16 Qualitative representation of the B.Izzuddin's energetic approach.

The Figure 2.16 depicts with a black dot line the static nonlinear response of SDoF system due to a PushDown Analysis and, with a bold continuous curve, its pseudo-static interpretation. For each step, the equivalence of the external work and the internal energy is satisfied. This equivalence is always reached when the two areas, A_{sn} and A_{dn} are equal. Hence, the level of applied gravity load, which leads to a specific maximum dynamic displacement, is obtained from:

$$W_n = U_n \qquad \textit{Eq. 2}$$

$$W_n = \alpha \lambda_n P_0 u_{d,n} \qquad \textit{Eq. 3}$$

$$U_n = \int_0^{u_{d,n}} \alpha P du_s \qquad \textit{Eq. 4}$$

$$P_n = \lambda_n P_0 = \frac{1}{u_{d,n}} \int_0^{u_{d,n}} P du_s \qquad \textit{Eq. 5}$$

For each static step:

P_n is obtained by the Eq. 5 and it represents the applied gravity load;

u_{dn} is the correspondent maximum dynamic displacement;

P_0 represents the total gravity load.

The maximum dynamic displacement can be related to the ductility limits. As the original framework pointed out, the dynamic demand has to be related to the ductility and shear capacity of the beam sections.

2.5 International Standards

Several national design standards implement rules and indication in agreement with design or assessment of progressive collapse. All the design standards have the purpose of reducing the potential for progressive collapse in new or existing buildings. The Figure 2.17 summarises the years in which some renowned collapses happened and the years in which national regulations have been released. As the diagram shows, the last collapse event makes grow the number of design codes in the last two decades.

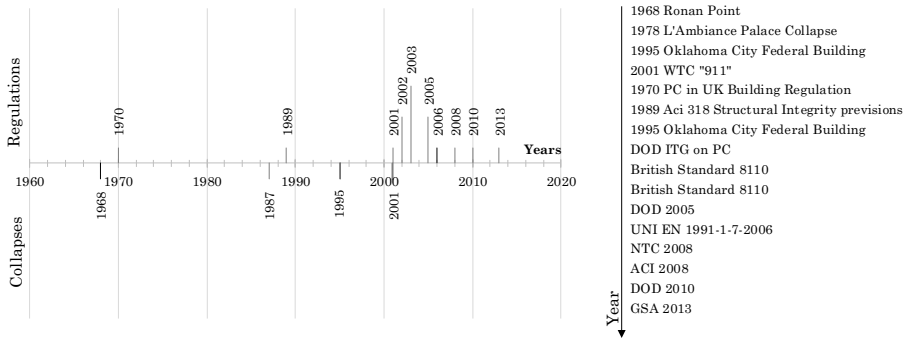

Figure 2.17 Timeline of collapse event and national regulation [47]

2.5.1 GSA

The General Service Administration (GSA) in 2013 [33] produced a sophisticated design regulation aiming to preserve federal buildings from progressive collapse. The regulation is oriented in terms of Alternative Load Path and a flexible risk-based approach. The requirements are driven by the security needs of the Federal tenant(s) and where implemented measures are commensurate with the level of risk. The application of these guidelines depends on the required level of protection, determinated by Facility Security Level (FSL) or facility-specific risk assessment.

This approach can be defined by the following flowchart:

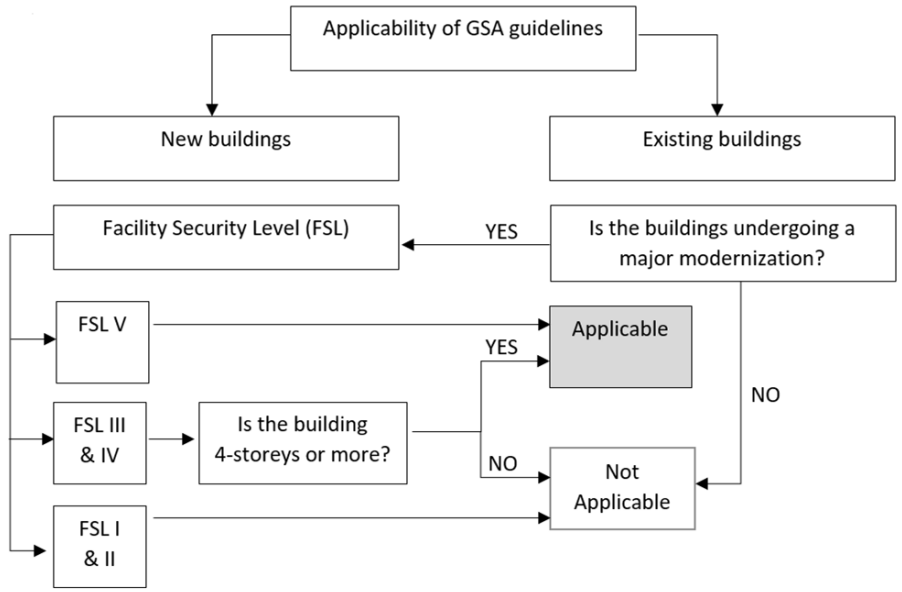

Figure 2.18 Applicability flowchart [33].

The guidelines have an accurate Section on the load distribution and collapse scenarios according to the linear, nonlinear, static or dynamic analysis. The Figure 2.19 shows two suggested collapse scenarios and the structural area involved in the progressive collapse phenomena. The load combination is incremented only on the grey area. All the elements out of the grey pattern are supposed not to be subjected to incremental load path.

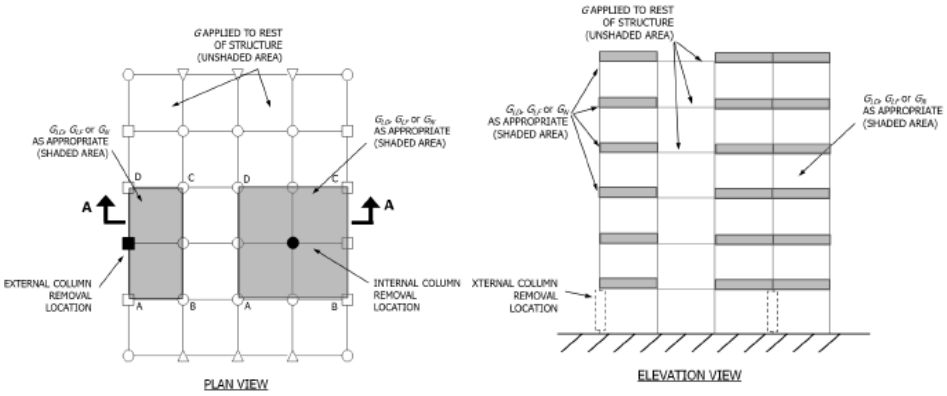

Figure 2.19 Load Locations for External and Internal Column Removal

The Table 2-1 summarises the load combinations in static and dynamic nonlinear analysis in which:

G_N is the increased gravity load

D is the dead load including façade loads

L is the live load including live load reduction

S is the snow load

Ω_N is the dynamic increase factor for calculating deformation-controlled and force-controlled actions for nonlinear static analysis. The code gives appropriate values for evaluating the Ω_N value.

Table 2-1 Loads and Analyses

GSA		
Non Linear Static Analyses	Increased Gravity Loads for Floor Areas Above Removed Column	$G_N = \Omega_N \left[1.2D + \left(0.5Lor 0.2S\right)\right]$
	Gravity Loads for Floor Areas Away from Removed Column	$G = \left[1.2D + \left(0.5Lor 0.2S\right)\right]$
Non Linear Dynamic Analyses	Gravity Loads for Entire Structure	$G_{ND} = \left[1.2D + \left(0.5Lor 0.2S\right)\right]$

2.5.2 DOD-UFC

The UFC 4-023-03 – *Design of buildings to resist progressive collapse* [31], in 2013, represent another dependable design guideline with the same purpose of the previously discussed guideline. The code concerns column loss scenarios and it is based on UFC 4-010-01 – *DoD Minimum antiterrorism standards for buildings* [30], that explicitly concerns progressive collapse assessment and design against malicious events. Due to this last point, the UFC 4-023-03 considers additional collapse scenarios that involves column in superiors floors, as Figure 2.20 shows.

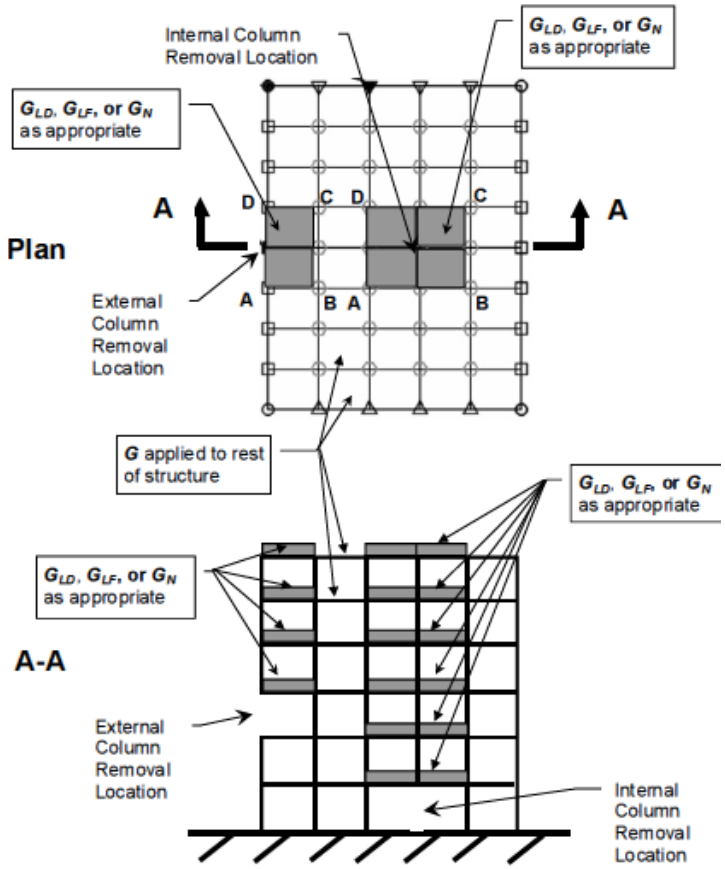

Figure 2.20 Loads and Load Locations for External and Internal Column [31]

2.5.3 UNI EN 1991-1-7-2006 1-7

The European Code [29] considers explicitly the robustness assessment with the purpose of mitigate progressive collapse. Even if the Robustness and Collapse Resistance (Figure 2.21) are mentioned and the strategy to mitigate or avoid them are defined, the guideline does not argue on load conditions, analysis methodologies, numerical models and collapse scenarios.

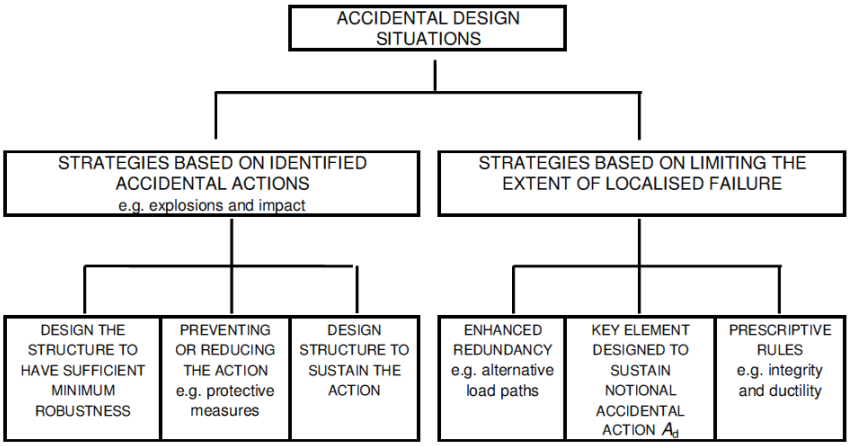

Figure 2.21 Strategies for Accidental Design Situations

More details can be found in the Annex A: Design for consequences of localised failure in buildings from an unspecified cause [29]. As the code explains, the scope is to give rules for designing buildings to withstand localised failure and prevent them from disproportionate collapse.

May be of interest to note that the code defines the necessity of a "*surviving period*" after the accident. Furthermore, the guidelines defines this *minimum period* as the period in which the building has to guarantee the safe evacuation and rescue of all the occupants from the building. In addition, longer periods have to be guarantee for buildings used for handling hazardous materials, provision of essential services, or for national security reasons.

It is notable that the Annex A defines an admissible local failure extension. It has to be evaluated in agreement with the type of building and it is recommended equal to 15% of the floor or 100 m^2 in each of two adjacent storeys, as the Figure 2.22 schematises.

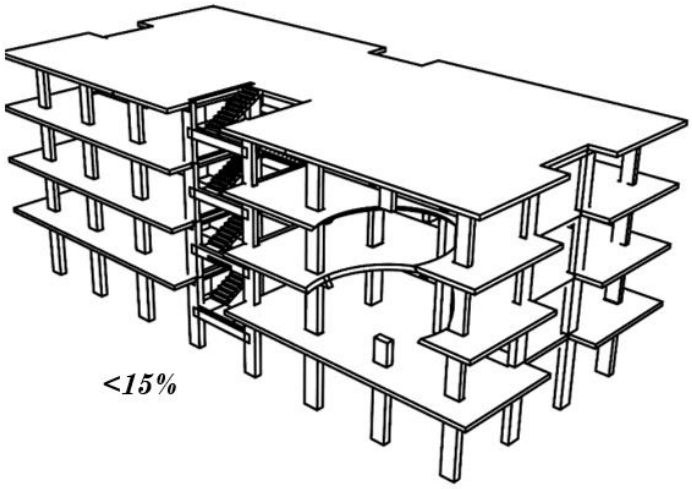

Figure 2.22 Recommended limit of admissible damage

2.5.4 NTC08

The Italian National Design Code [23] does not contain explicit design rules for new or existing buildings to withstand disproportional collapse as consequence of local failure.

On the other hand, the Section 2.1 of the NTC08 imposes that the building have to guarantee robustness to "exceptional loads" and that the damages due to disproportional collapse have to be take into account.

Furthermore, a specific load combination is defined for evaluating the structural response under unusual loads:

$$A_d + G_1 + G_2 + P + \Psi_{21} Q_{k1} + \Psi_{22} Q_{k2} + ... \qquad \textit{Eq. 6}$$

It may be concluded that, according to NTC08, the structural desinger is responsible in case of dispropotional collapse events but, on the other hand, the Italian building code does not currently provide prescription rules or guidelines.

CHAPTER 3.
NUMERICAL MODELS FOR PROGRESSIVE COLLAPSE ASSESSMENT

This Chapter presents and discusses the results of numerical simulations carried out to study the response of reinforced concrete (RC) frame buildings subjected to column loss. An advanced modelling strategy is developed and validated against physical tests [15]. A comprehensive parametric study has been conducted utilising different nonlinear models with the aim of evaluating the influence of the critical material parameters on the response up to collapse of typical reinforced concrete frames not designed to resist earthquake loading. Once the numerical model has been correctly calibrated based upon the experimental results, a full scale multi-storey building has been analysed assuming a column loss scenario to explore the contribution of the structural components in the 3D frame structure which are not considered in the experimental tests on the planar frame specimen. A comparison with the results obtained by simplified dynamic assessment proposed by B.A.Izzudin [26, 27] has been performed.

3.1 Introduction

Thus far most of research on progressive collapse assessment and mitigation has focused on steel or steel-concrete buildings, while limited experimental and numerical research has been devoted to the analysis of reinforced concrete (RC) multi-storey framed structures subjected to column loss [48, 49, 50, 51, 52, 44]. Moreover, only a few studies were aimed at investigating the progressive collapse behaviour of RC buildings designed according to old standards without allowing for earthquake loading [53, 46, 54, 45] which represent a substantial part of existing multi-storey structures in earthquake prone regions. In 2011, Stinger et al. [55] carried out an extensive experimental programme to study behaviour up to collapse of reduced-scale low-ductility two-storey RC frames subjected to prescribed vertical displacements at central column location. The experimental set-up was designed to represent the loss of a ground floor column of typical RC frames. RC frames with different geometrical and reinforcement characteristics were tested to shed some light on the physical behaviour of these structures under column loss, while providing substantial experimental data for the validation of nonlinear numerical descriptions.

In this research, accurate numerical models for detailed nonlinear analysis of existing RC frame buildings have been developed and used to investigate the robustness of realistic RC frame structures designed to resist vertical loading only. Firstly, the proposed numerical descriptions have been validated against the experimental results obtained by Stinger et al. [55]. Subsequently, a parametric study has been conducted investigating the influence of critical material parameters, boundary conditions and number of storeys on the response up to collapse of the analysed frames subjected to column loss. Nonlinear static simulations have been performed, while the effects due to the dynamic nature of progressive collapse have been accounted for using the ductility-centred robustness assessment framework developed at the Imperial College of London [26, 27]. Potential failure due to brittle mechanisms which are not directly represented by the employed numerical models (e.g. shear failure of RC beams and columns) has been investigated by performing

a back analysis of the numerical results. The results obtained in the extensive numerical investigation provides critical information towards a more detailed understanding of the robustness of typical RC framed structures.

3.2 Experimental tests and literature review

Experimental tests carried out on RC frame structures to investigate the response under column loss scenarios considered reduced scale or full scale specimens of different sizes including i) limited sub-structure specimens (LSS), ii) extended sub-structure specimens (ESS) and ii) whole building specimens (WB).

Most of previous work considered reduced scale LSS specimens [56, 49, 50, 55, 44] which were subjected to static, or dynamic push down loading on single or twin beams [57, 44]. Only a few experimental tests [52, 51] were performed on larger specimens allowing for the contribution of additional structural elements (ESS) such as RC columns and floor slabs. In tests on ESS specimens not only the beams, but also the columns and the slabs were subjected to vertical loading. Thus the results of these tests provide critical information on the physical behaviour of relatively large structural systems under column loss scenario including the contribution of the RC beam-column joints (e.g. Vierendeel action), columns and floors.

Only in rare cases progressive collapse tests were performed on full-scale specimens [40] allowing for the influence of 3D frames and non-structural components (e.g. masonry infill). Clearly these tests are very expensive and technically challenging.

Nonetheless, most of previous physical experiments considered RC elements with a regular reinforcement layout and a uniform distribution of longitudinal bars which guarantees the development of an effective catenary action when the beams are subjected to substantial vertical displacements induced by the loss of a column. On the other hand, Orton [44] showed experimentally that also RC beams with discontinuous longitudinal reinforcement can develop substantial catenary action

thanks to the stirrups which can transfer large tensile forces from the bottom to the top longitudinal bars.

In 2011, Stinger [46] carried out an extensive experimental programme on the collapse behaviour of RC frame structures under column loss condition. Three frames, with different geometrical and reinforcement details, were tested. In the experimental campaign, the influence of reinforcement discontinuity and masonry infill were investigated. As matter of fact, the masonry panels that have been considered were not full height and they were similar to masonry parapets, hence they did not influence the structural robustness. The specimens were similar to the frames of a real building which was previously subjected to column loss trigged by a gas blast at the first floor.

More recently, an experimental programme on three four-bay, two-storey planar frames was conducted [50, 49]. The tests involved bared frames and infilled frames with and without openings. The results showed that masonry infill provides a critical contributing to progressive collapse arrest, enhancing robustness. In general, such contribution can be represented only by using a realistic description of masonry infill, including its interaction with the frame components.

3.3 RC specimen designed to resist vertical but not earthquake loading

The experimental results mentioned before [15] on RC frames designed to resist gravity loading and subjected to column loss are considered here and used to validate advanced numerical descriptions. These physical tests were conducted on framed structures which resemble the main frames of typical existing RC buildings located in seismic areas but designed without allowing for earthquake loading, as most of old RC buildings in Italy.

A specific experimental specimen is analysed [46]. It corresponds to a two-storey frame representing the two initial levels of the main RC frame of an existing six-storey office building with 6 by 3 bays 7.30 m

center to center spacing and 3.65 m inter-storey height (Figure 3.1). The specimen was designed according to the 1971 ACI 318 Building Code [58].

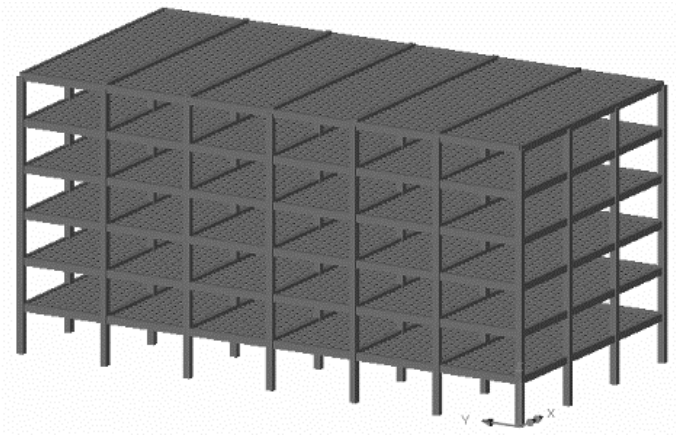

Figure 3.1 3D Numerical Model in LUSAS

Table 3-1 reports the main materials parameters of concrete and steel reinforcement used for constructing the specimen.

Table 3-1 Material Properties

	E MPa	fcm MPa	fym MPa	fum MPa
Concrete C28/35	28500	27.58		
ReBar Column	91011		415	650
ReBar Beam	120658		600	650

The reinforcement of the RC beams is characterised by a lack of longitudinal steel bars in the compressed zones in accordance with the design code [58] (Figure 4.2) which is a typical characteristic in existing buildings not designed to resist seismic loading. Clearly, this specific reinforcement layout may influence the ability of the beams to develop substantial arch and catenary actions redistributing the vertical loads due to column loss to the adjacent undamaged columns.

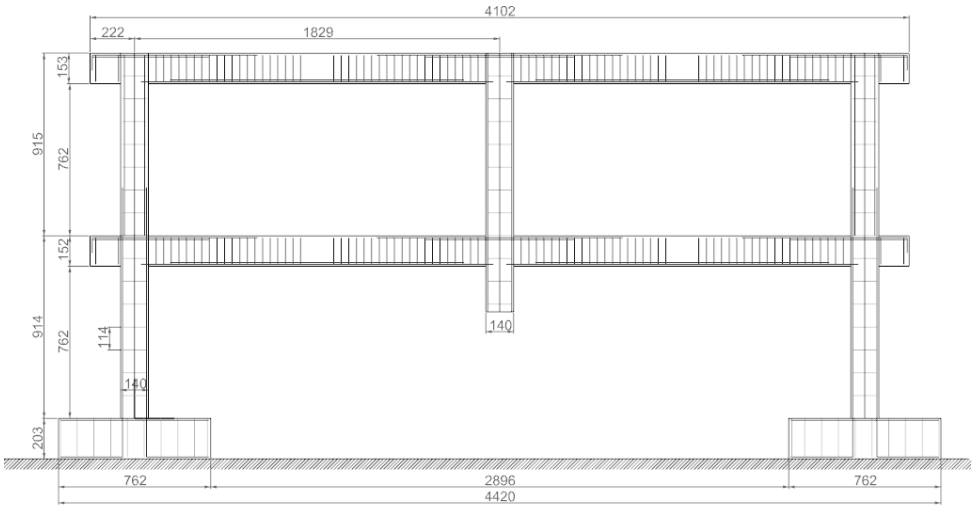

Figure 3.2 Two-storey RC frame specimen with beams with discontinuous longitudinal reinforcement

The experimental results showed that the analysed frame with deficient details guarantees a certain level of robustness. Arch and catenary actions developed in the beams, where the stirrups compensated the lack of continuity of the longitudinal bars transferring tensile forces from the bottom to the top bars. The specimen collapse was due to the failure of the beams which developed when the stirrups close to the mid column failed in tension. This mechanism is shown in Figure 3.3 and highlighted by a black marker. The physical response of the specimen is shown in Figure 4.4, where the vertical displacement that was recorder underneath the centre column of the frame is plotted against the applied vertical force. The experimental curve shows a sudden decrease of resistance and the extinction of the catenary effect at a vertical displacement of about 360 mm due to the tearing out of the stirrups close to the mid-column.

Figure 3.3 Tearing out of the stirrups is evident in the second level beam. [46]

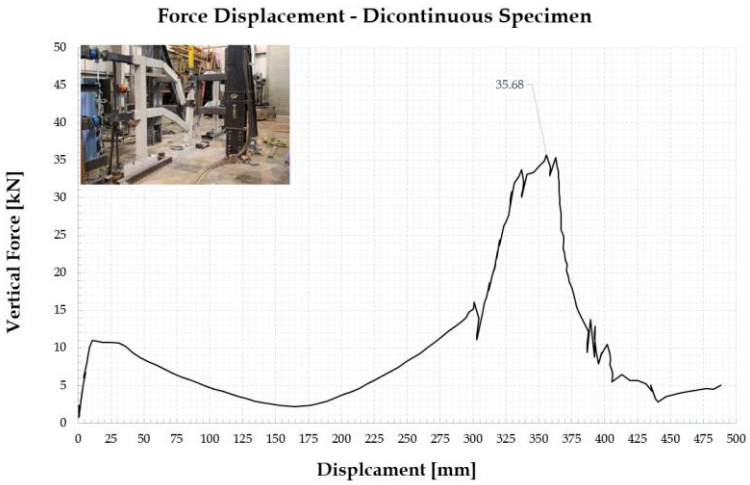

Figure 3.4 Experimental responses of the RC frame subjected to column loss.

3.4 The numerical models

To investigate the response up to collapse of the RC frame described in the previous section, numerical models have been developed in ADAPTIC, an advanced finite element program for nonlinear analysis of structures under extreme loading [59]. In the numerical descriptions,

RC beams and columns are represented by cubic beam-column elements allowing for material and geometrical nonlinearity. More specifically, mechanical nonlinearity is accounted for through a detailed fibre distributed plasticity discretization using realistic nonlinear constitutive relationships for concrete and steel reinforcement [60, 61], while large displacement contribution is taken into account through an efficient co-rotational formulation [62].

Figure 3.5 shows the FE model of the analysed RC frame, where a set of 2D beam elements are used to represent each physical RC beam and column, accurately describing the variation of longitudinal steel reinforcement along each RC member.

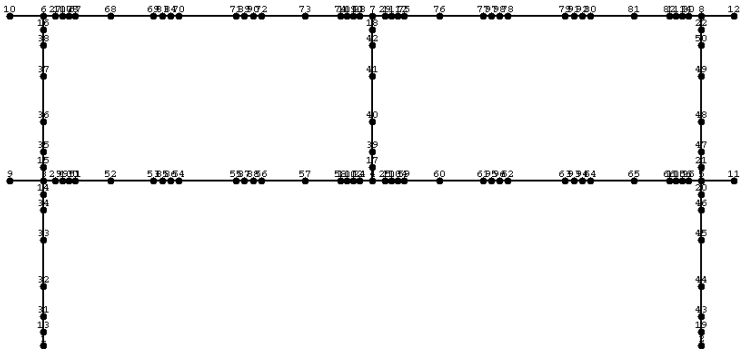

Figure 3.5 Numerical model in ADAPTIC.

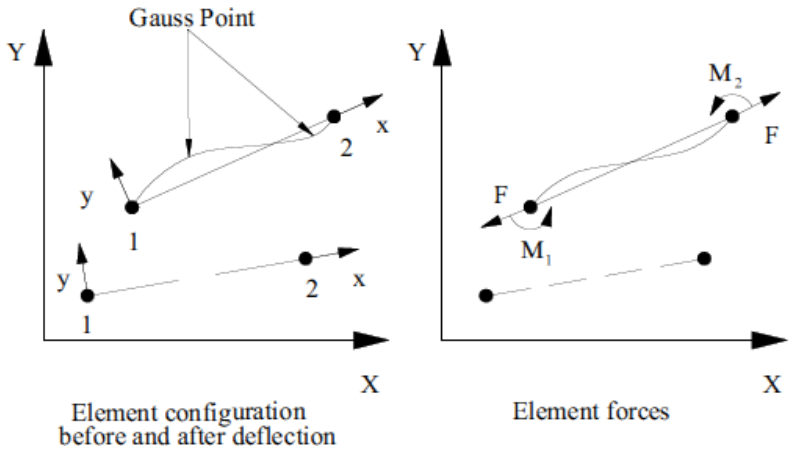

Figure 3.6 Local reference system and element forces for cbp2 element.

The *cbp2* 2D beam-column elements (Figure 3.6) in the ADAPTIC library [63] are adopted. The numerical integration along the element length is performed over two Gauss points where a number of monitoring points (section fibre discretization) are adopted to calculate stress resultants for the RC beam-column sections at Gauss point locations. As shown in Figure 3.7, in the numerical description each physical beam and column is represented using 17 and 6 *cbp2* elements, respectively. Importantly, the adopted discretisation takes into account the specific longitudinal reinforcement characteristics of the RC members and a finer mesh is used where substantial plastic deformations (e.g. plastic hinges) are expected to develop.

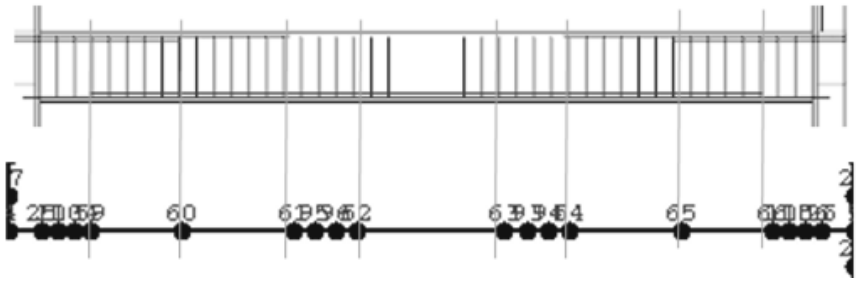

Figure 3.7 Longitudinal reinforcement bars and FEM discretization

The *rccs* (Figure 3.8a) and *rcts* (Figure 3.8b) RC sections in the ADAPTIC library have been used to represent columns and beams cross sections respectively.

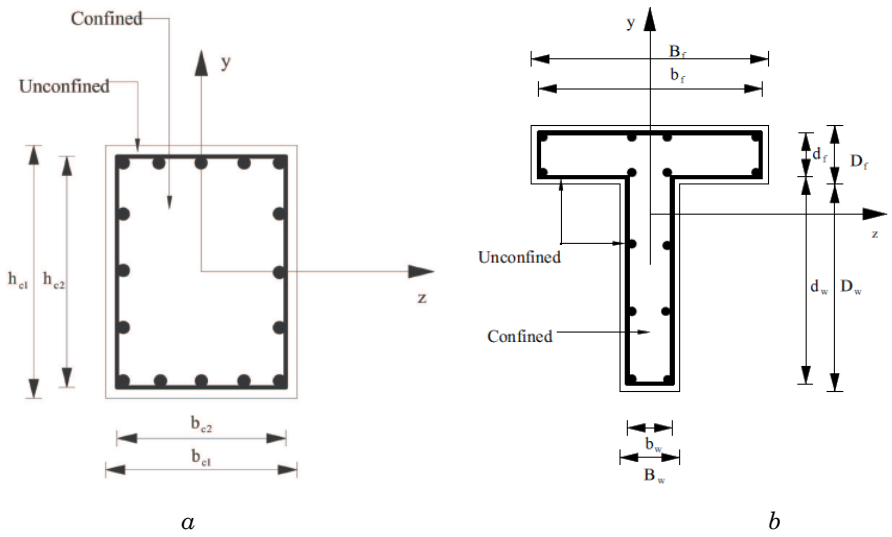

Figure 3.8 ADAPTIC fibre section types adopted in the finite element model: a)RCCS; b) RCTS. [63]

The multi-linear concrete model *con1* has been considered to model concrete (Figure 3.9). The model material parameters, shown in Table 3-2, have been calibrated considering the monotonic stress-strain relationship proposed by Kent & Park [60] as extended by Scott, Park and Priestley [61]. This model is shown in Figure 3.10 and provides a simple description of the nonlinear behaviour of concrete in tension and compression.

Finally, an elastic-plastic model with kinematic hardening has been used for describing the steel reinforcement behaviour (Figure 3.11). The material parameters are based on the experimental curves obtained in tension tests [55] and are summarised in Table 3-4.

The experimental results showed no damage in the beam-to-column joints, thus rigid joints have been assumed in the numerical description for the frame. Lastly, to describe the horizontal lateral support conditions for the physical frame, which were introduced in the experimental set-up to allow for the interaction with the adjacent frame components of the realistic building structure represented in the test [15], 2D joint elements with uncoupled moment, axial, shear forces have were connected to the end nodes of the beams at the two floor levels. The *jel2* joint element in

ADAPTIC has been used which features 3 nodes, where nodes (1) and (2) are initially coincident and node (3) defines the local x-axis.

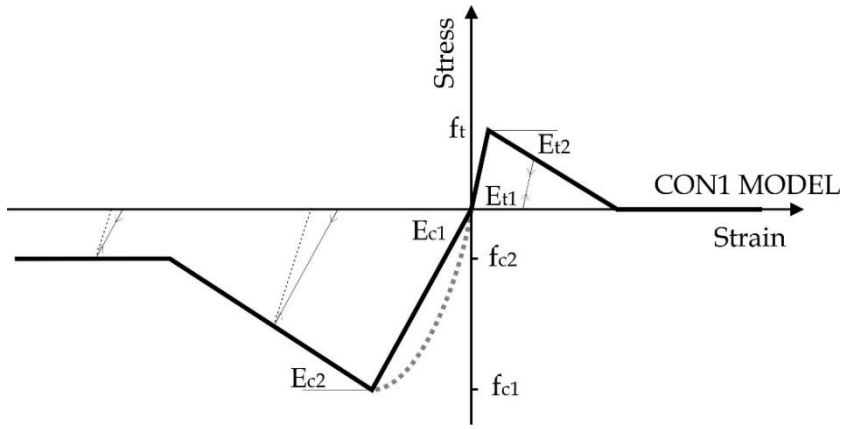

Figure 3.9: ADAPTIC CON1 model

Table 3-2 CON1 properties

Name	Model	Properties							
		Ec1 [MPa]	fc1 [MPa]	Ec2 [MPa]	Fc2 [MPa]	Et1 [MPa]	ft [MPa]	Et2 [MPa]	□
Conc	Con1	13665	27.83	-6582	5.56	13665	2.758	-6582	1
Conc_unc	Con1	13790	27.58	-6452	5. 52	13665	2.758	-6582	1
Conc1	Con1	13756	27.65	-6486	5. 52	13756	2.758	-6582	1

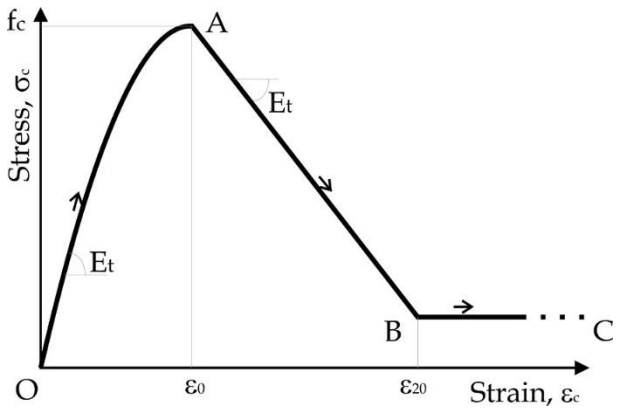

Figure 3.10 Modified Kent and Park [61].

Table 3-3 Modified Kent and Park [61].

Region	Strain	Stress	Tangent modulus
OA	$\varepsilon_c \le \varepsilon_0$	$f_c = Kf'_c\left[\frac{2\varepsilon_c}{\varepsilon_0} - \left(\frac{\varepsilon_c}{\varepsilon_0}\right)^2\right]$	$E_t = \frac{2Kf'_c}{\varepsilon_0}\left(1 - \frac{\varepsilon_c}{\varepsilon_0}\right)$
AB	$\varepsilon_0 \le \varepsilon_c \le \varepsilon_{20}$	$f_c = Kf'_c\left[1 - Z\left(\varepsilon_c - \varepsilon_0\right)\right]$	$E_t = -ZKf'_c$
BC	$\varepsilon_c \ge \varepsilon_{20}$	$f_c = 0.2Kf'_c$	$E_t = 0$

being:

ε_0 : concrete strain at the maximum concrete stress

ε_{20} : concrete strain at the 20% of the maximum compressive stress

K : factor that accounts for the strength increase due to the confinement

Z : strain-softening slope

f'_c : concrete compressive cylinder strength (unconfined peak compression), MPa;

f_{yh} : yield stress of the transverse reinforcement, MPa;

ρ_s : ratio of volume of the transverse reinforcements to the volume of concrete core measured to the outside of the stirrups;

$\rho_s = A_{str}L_{str} / A_{sez}s_h$

A_{str} : area of the stirrup

L_{str} : length of the stirrup

A_{sez} : area of the section measured as above defined

h' : width of the concrete core measured to the outside of stirrups

s_h : center to center spacing of stirrups or hoop set

and :

$$\varepsilon_0 = 0.002 \cdot \mathrm{K} \qquad K = 1 + \frac{\rho_s f_{yh}}{f'_c} \qquad Z = \frac{0.5}{\frac{3 + 0.29f'_c}{145f'_c - 1000} + 0.75\rho_s\sqrt{\frac{h'}{s_h}} - 0.002K}$$

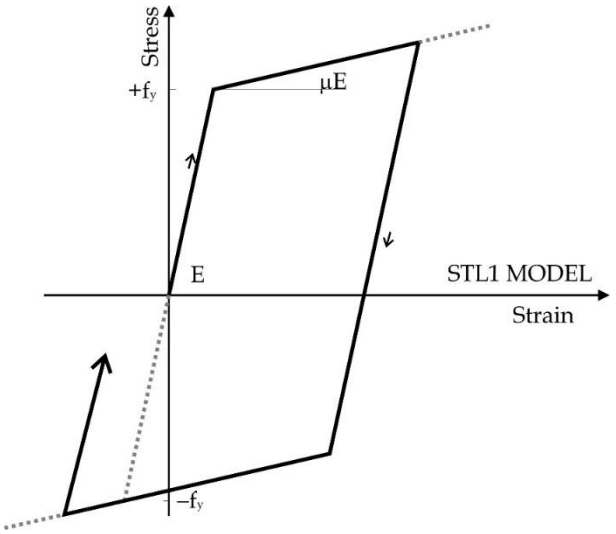

Figure 3.11 ADAPTIC STL1 model and model material parameters.

Table 3-4 SLT1 properties

Name	Model	Properties		
		E [MPa]	fy [MPa]	μ [–]
reb_beam	stl1	120658	600	0.006
reb_col	stl1	91010	430	0.02

The experimental results showed no damage in the beam-to-column joints, thus rigid joints have been assumed in the numerical description for the frame. Lastly, to describe the horizontal lateral support conditions for the physical frame, which were introduced in the experimental set-up to allow for the interaction with the adjacent frame components of the realistic building structure represented in the test [15], 2D joint elements with uncoupled moment, axial, shear forces have were connected to the end nodes of the beams at the two floor levels. The *jel2* joint element in ADAPTIC has been used which features 3 nodes, where nodes (1) and (2) are initially coincident and node (3) defines the local x-axis.

3.5 Parametric analysis and interpretation

Nonlinear push-down simulations have been conducted using the numerical frame model described in the previous section to investigate the response of the RC frame subjected to column loss. A parametric study has been carried out to analyse the influence of critical mechanical parameters and boundary conditions including (i)concrete compressive strength, (ii) softening modulus for concrete in tension, (iii) horizontal stiffness of the lateral supports, (iv) column base support characteristics.

In the following, the numerical results are presented and some figures are shown illustrating:

- **the nonlinear static vertical response** considering the variation of the vertical displacement at the control point placed at mid-column location against the total vertical reactions;
- **the nonlinear static horizontal reactions** considering the variation of the vertical displacement at the control point placed at mid-column against the horizontal reactions at the first floor lateral restrains.
- **the pseudostatic curve** transforming the static nonlinear curve into a pseudostatic response.

In all the figures, an arrow is used to indicate the variation in the response due to a positive increment of a specific parameter. Figure 3.12 depicts the influence of the concrete compressive strength f_c. Each curve represents the structural response for the same column loss scenario and loading distribution. The compressive strength values [MPa] considered in the numerical simulations are reported in Table 3.5

Table 3.5 Values of the compressive strength

11.03	16.58	22.064	27.58	33.0	38.61	44.13	49.64	55.16

Figure 3.12 shows a notable influence of concrete compressive strength on the vertical resistance. On the other hand, the discrepancy between the different numerical curves is almost negligible in Figure 3.12.b, where the horizontal restrain response curves are plotted.

Following the simplified dynamic assessment introduced in the previous chapter, Figure 3.12.c presents the pseudostatic interpretation of the static non-linear push down results [12]. The numerical curves confirm that the use of low compressive strength values leads to overestimating the actual pseudostatic capacity for small vertical displacements and more conservative pseudostatic capacity predictions for large displacements. Conversely, the use of concrete compressive strength values larger than the experimental value determines pseudostatic capacity curves with lower resistance for almost any vertical displacement.

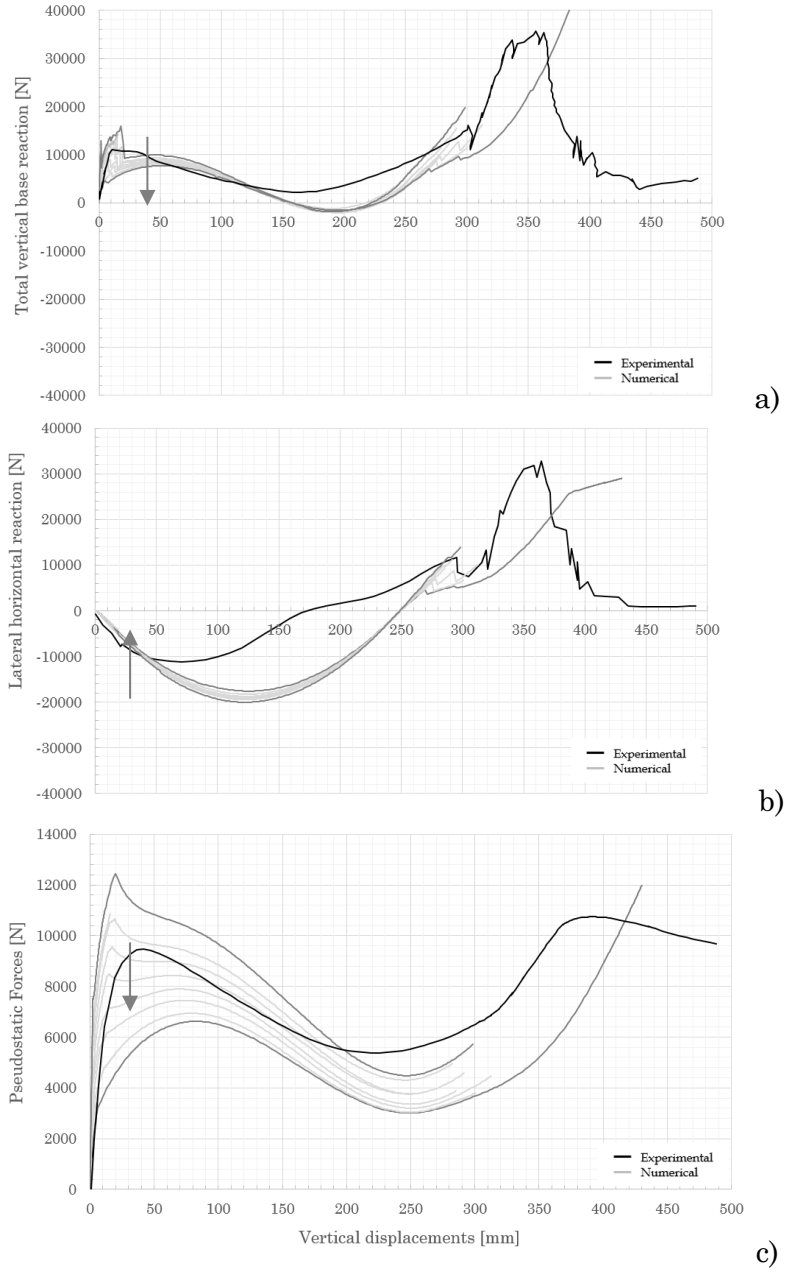

Figure 3.12 Influence of Compressive Strength fc in a) Static Responses, b) Horizontal reaction, c) Pseudostatic Assessment

Figure 3.13 compares the experimental curves against numerical curves with different softening moduli of concrete in tension (E_{t2}) for the adopted concrete model *con1* (Figure 3.9). It is worth noting that E_{t2} is linked with the fracture energy considered to represent fracture of concrete in tension. Accordingly, high facture energy is associated with increased $E_{t2.}$ The softening modulus values [MPa] used in the numerical simulations are summarised in Table 3.6.

Table 3.6 Variation of second tensile elastic modulus

6.58	65.82	658.2	1316.4	6582

Figure 3.13.a depicts the influence of E_{t2} on the vertical response. It can be seen that the fracture energy for concrete in tension plays a critical role on the frame behaviour up to collapse. As expected, the upper numerical curve features the largest E_{t2} value. In this case, higher vertical resistance is achieved for displacements up to about 170 mm, but the response for larger displacements which is governed by catenary action is only marginally influenced by E_{t2}. Numerical curves with low and intermediate softening moduli provide a better prediction of the physical static response for different levels of vertical displacement. Only a minor overestimation of the initial stiffness has been found which seems to be independent from concrete softening modulus in tension.

Figure 3.13.b illustrates the variation of the horizontal reactions at the beam ends by increasing the vertical displacement. It should be noted that lateral restrains have been modelled using elastic springs. In general, concrete fracture energy does not significantly influence the variation of lateral reactions forces, where all the numerical curves overestimate the actual response, but not the initial stiffness which is slightly underestimated.

Figure 3.13.c presents the pseudostatic curves. As for the static response in Figure 4.14a, the use of the largest fracture energy for concrete in tension induces a substantial over prediction of the pseudostatic capacity, while intermediate a low E_{t2} values lead to more realistic results closer to the experimental curve.

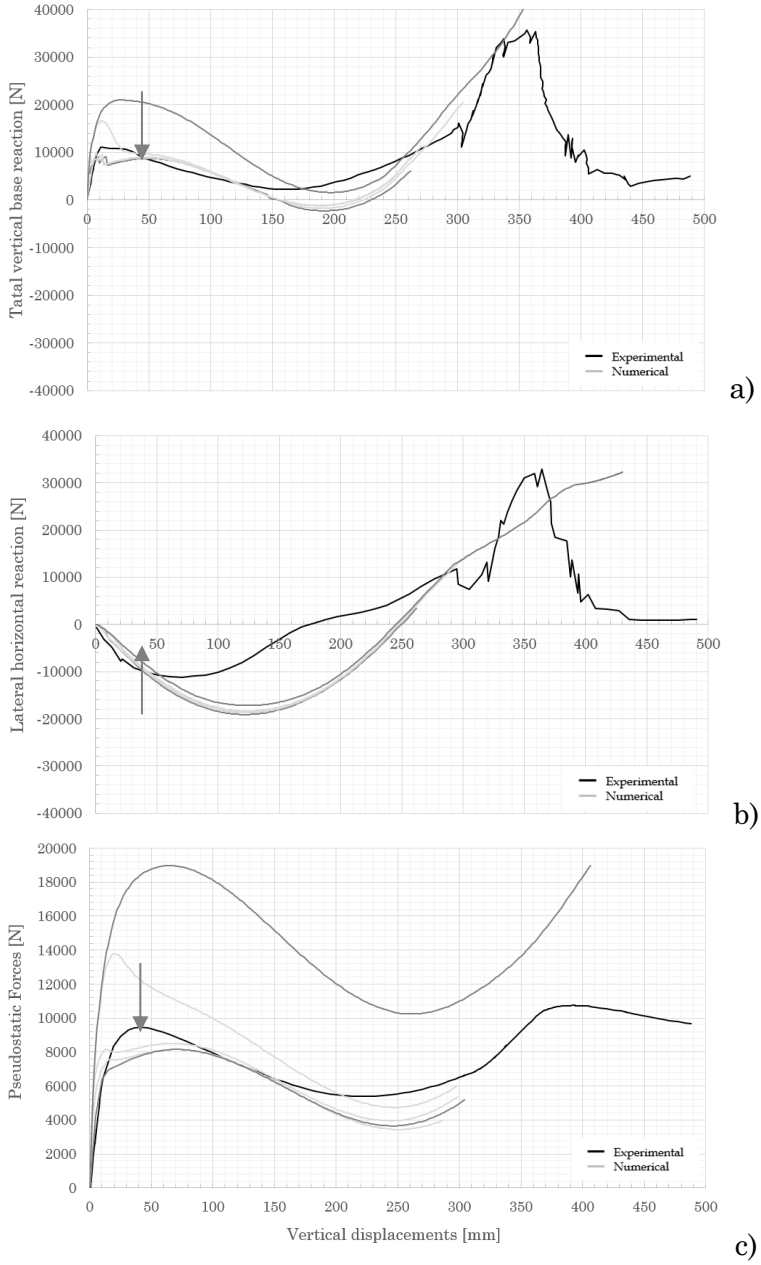

Figure 3.13 Influence of Second Tensile Elastic Modulus E_{t2} in a) Static Responses, b) Horizontal reaction, c) Pseudostatic Assessment

The results obtained by varying the stiffness of the lateral elastic restraints are summarised in Figure 3.14 Numerical simulations have been conducted adopting the horizontal stiffnesses [N/mm] reported in Table 3.7. These represent a range of stiffness values modelling the absence of restraints (0 stiffness) and the presence of stiff shear walls (largest stiffness value) restraining the analysed frame along the longitudinal direction.

Table 3.7 Values of the Lateral Restrains Stiffness

0	30	300	3000	30000	300000

Figure 3.14.a depicts the nonlinear static response in terms of vertical displacements versus vertical total reactions. As the figure illustrates, the increment of the lateral stiffness gives rise to an initial increment of the load capacity. Increased lateral stiffness reducing horizontal movement at floor level enhances the initial vertical resistance. If stiff structural elements such as concrete shear walls are placed on both sides of the frame structure, the frame resistance to progressive collapse is mainly associated with the axial capacity of the RC beams. The results confirm that the initial vertical resistance depends on the lateral confinement and, consequently, on the ultimate concrete compressive strength of the beams.

Figure 3.14.b shows the variation of horizontal lateral reactions at first floor level. The numerical curves follow trends similar to those observed for the vertical reactions. Moreover, the lateral stiffness values influence also the pseudostatic response as shown in Figure 3.14.c. Variations of the initial pseudostatic resistance from 70% up to 210% of the experimental have been found. This confirms that the use of unrealistic lateral stiffness values to present the contribution of the adjacent components of the RC frame may lead to very crude approximations of the physical response.

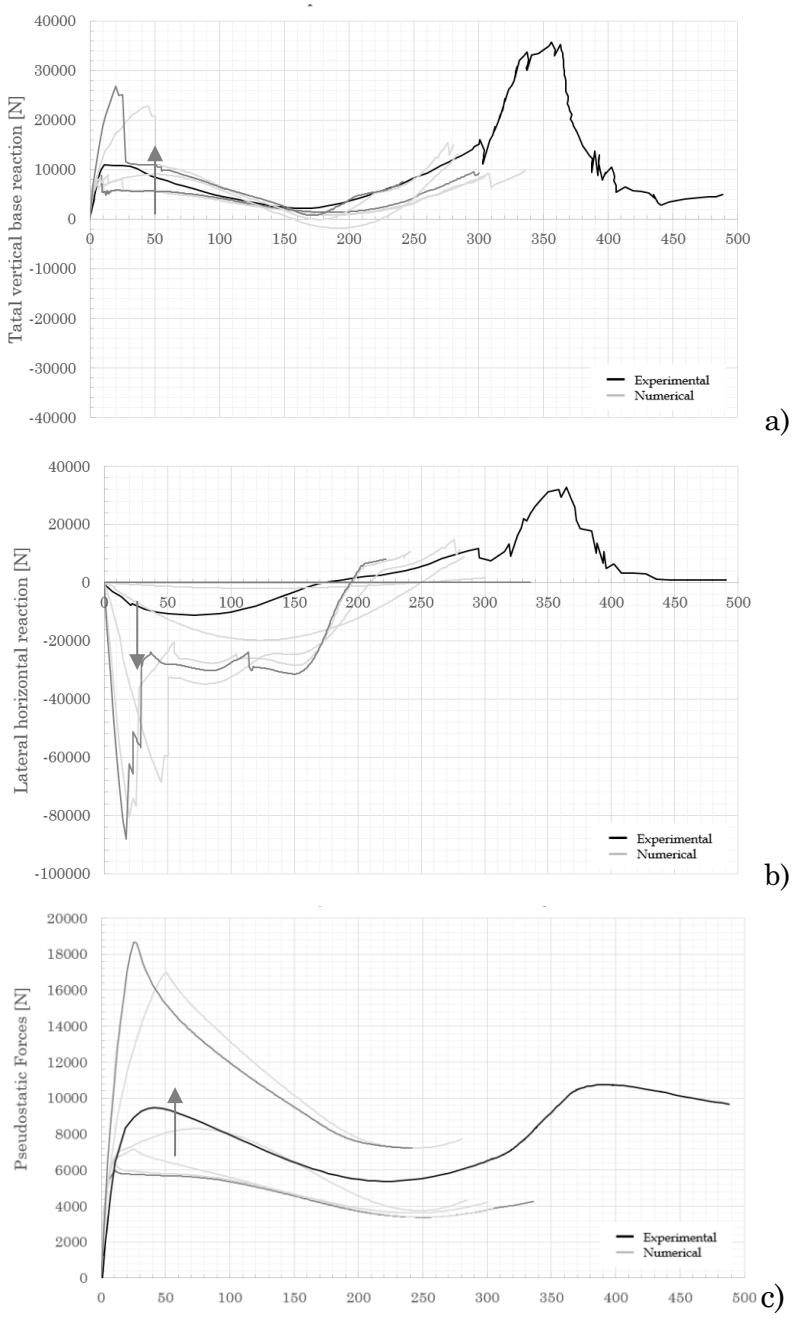

Figure 3.14 Influence of Lateral Restrains Stiffness in a) Static Responses, b) Horizontal reaction, c) Pseudostatic Assessment

The parametric study revealed that most of the analysed parameters have a remarkable influence on the vertical response (capacity curve), but the variation of some of them does not lead to a substantial change of the horizontal reactions. Additional numerical simulations have been carried out to identify the set of material parameters and boundary stiffness values which guarantee a good agreement with the experimental curves, as the black curve indicates in Figure 3.15. The results for the static response in term of vertical reactions are shown in Figure 3.15, whereas Figure 3.16 displays the pseudostatic curves. A very good agreement is achieved for vertical displacement up to around 180 mm. The transitory effects that develop after this point define an overestimation of the pseudostatic displacements in the catenary state. The numerical curve overestimates the catenary displacements found in the experimental test of more than 12%.

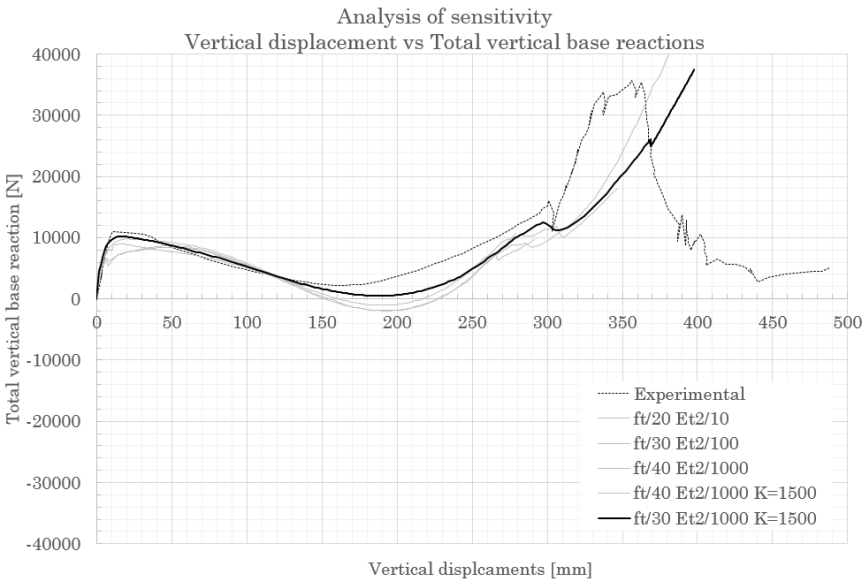

Figure 3.15 Best-fitting curve in nonlinear static response

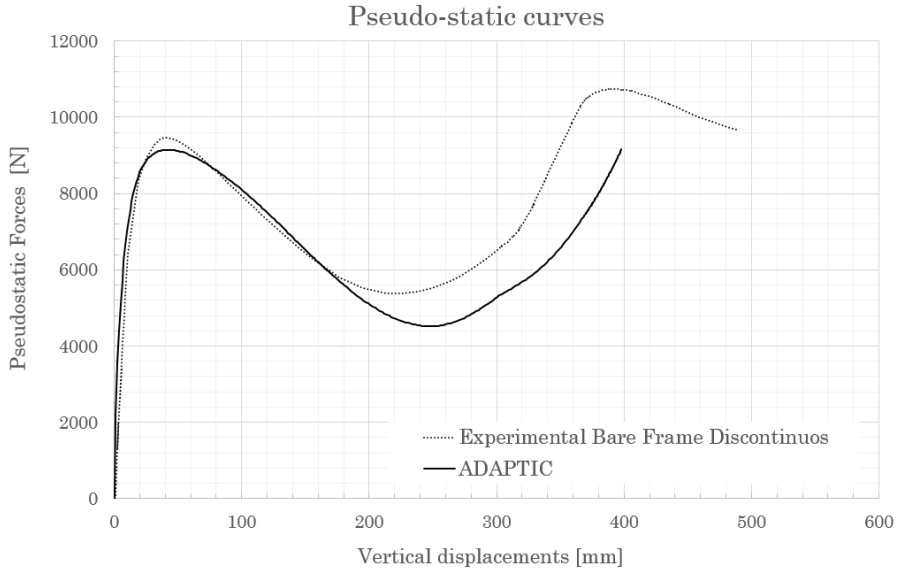

Figure 3.16 Best-fitting curve in the Pseudostatic response

The hinges position depends on the reinforcement layout. After a second resistance drop, the beam is able to support additional increments of load and vertical displacements up to collapse.

Figure 3.17 pictionary depict the generic nonlinear static push down response that can be recorded in column loss scenarios that affect framed reinforced concrete structures with not uniform reinforcement layouts.

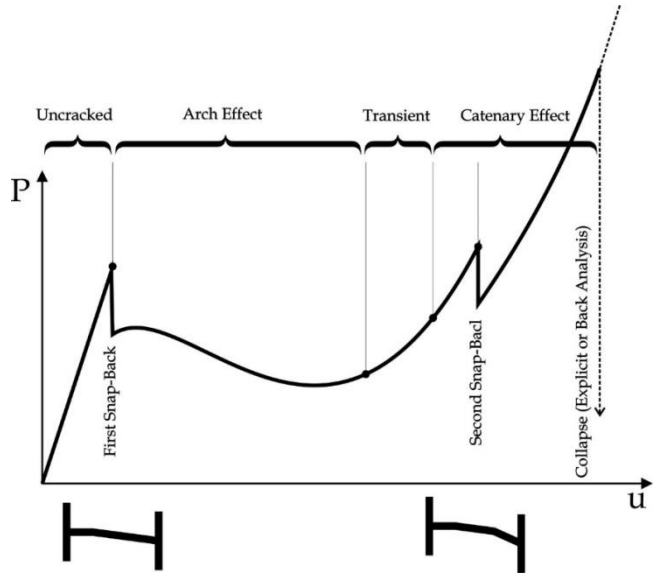

Figure 3.17 Schematic behaviour of a light reinforced concrete beam in a column loss event.

Figure 3.18 describes the correspondence between the experimental push down curve and the numerical response marking five principal points on the numerical push down curve. Point A indicates the elastic limit which is reached at the end of a quasi-elastic behaviour. The relationship between the applied force (in this case a push down concentrated force applied at the top of the mid-span column) and the vertical displacement is almost linear until when two external plastic hinges develop in the beams as shown in Figure 3.19.

Figure 3.18 Superimposing of the experimental response and the Adaptic response.

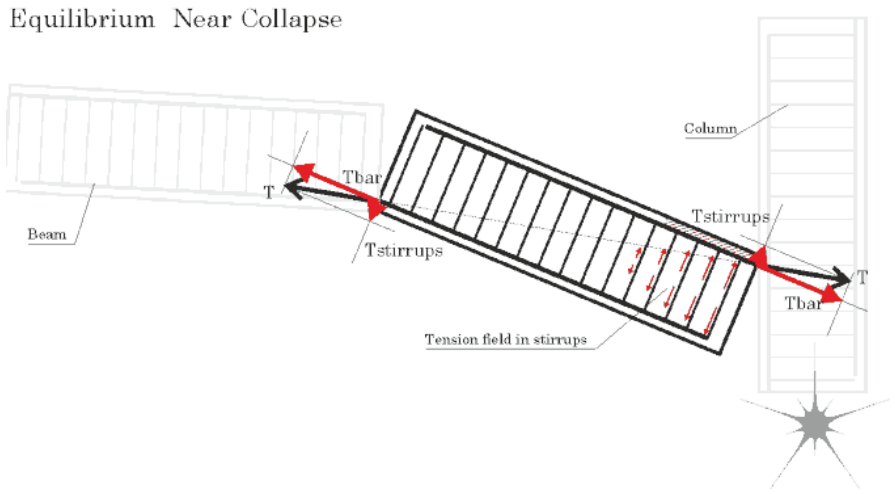

Figure 3.19 (Colour) Configuration of the concrete beam near the last peak value. The hatched area represents the concrete cover crushing.

Starting from point A up to the vertical displacement of about 188 mm (point B), a softening behaviour characterises the response when the arch effect develops. At the end of this stage, the FE model reaches a

vertical displacement larger than the displacement measured in the experimental test. During the transitory phase and the catenary action phase, the numerical model predicts the development of bending moments at an intermediate section along the beam at the first level approaching the plastic bending capacity of the beam cross section at that location. This leads to a fall in the vertical resistance at point B in Figure 4.19. The plastic hinge forms at the section where there is a discontinuity of longitudinal reinforcement (e.g. interruption of top reinforcement). The next marked point is C where plastic hinges form at the intermediate sections of the two top beams as for the beam at the fist level at point C. The numerical simulation terminates at point D because of convergence difficulties. The numerical model is not able represent the sudden decrease of resistance found in the experimental test at collapse which was due to the stirrups failure in tension at plastic hinge locations.

The numerical model in ADAPTIC with the calibrated model parameters provides an accurate representation of the experimental test.

Additional simulations have been performed to evaluate the influence of the physical components of the large frame of the analysed building which directly interact with the experimental frame providing lateral restraints. Thus, instead of introducing linear spring elements (e.g. joint elements in ADAPTIC) to allow for the actual horizontal restraints, additional frame components (e.g. beams and columns) have been explicitly modelled and connected to the two-span frame. More specifically, two additional models have been developed adding two or four spans to the original frame model.

Sections and elements are the same of the original model. The performance of the three models has been compared and the three nonlinear pushdown curves have been imposed to the experimental responce.

A first small difference can be noticed thought the arch effect phase in which the latter model reaches major.

After this phase, the three numerical curves have a good agreement each one other until the end of the transient phase and the rise of the pure catenary effects. A significant difference is recognisable between the

curves during the catenary phase due to the explicit geometric and mechanical nonlinearities of the additional spans. These differences may lay the following considerations:

- The number of bays influences the curves during the catenary phase due to the inelasticities raised through the analysis.
- Additional number of bays can amplify the arch effect, introducing a lateral stiffer restrain effect for the beams directly interested by collapse.
- The use of elastic restrains introduces evident and sensible approximation during the catenary effect.
- The experimental specimen showed an evident overestimation of the catenary stiffness and an underestimation of the arch effect contribute.

Since these considerations are supported by the numerical response, the presence of material nonlinearities in the whole concrete structure forces to estimate carefully the beam/column contributes that are not directly influenced by the collapse.

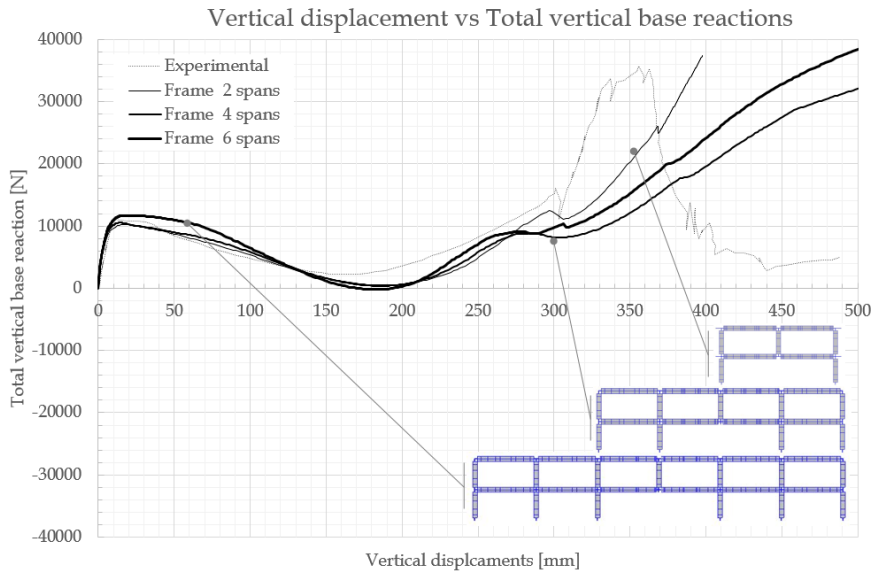

Figure 3.20 Static nonlinear response of three models.

3.6 Low-rise and mid-rise 2D bare frames

In the previous section, the framed models developed using ADAPTIC, have been validated against experimental results on a two-bay RC frame subjected to column loss. It was shown that the proposed numerical descriptions provide accurate representation of the frame response up to collapse, allowing for highly nonlinear phenomena including arch and catenary actions which are critical for a realistic evaluation of the frame ability to resist column loss preventing progressive collapse.

In the following, detailed frame models are employed to analyse the behaviour of multi-storey planar RC frame structures in the case of central column loss. The frame structures represent the external concrete frame of a prototype office building [55]. It is the six-storey frame structure presented in [46] and designed to resist gravity loading only. Table 3.8 summarises the geometrical characteristics of the cross sections of RC beams and columns.

Table 3.8 Geometry properties of the structural elements

Element name	Dimensions [mm]
Column	560x560
External Girders	305x610
Internal Girders	460x915
Joist	203x406
Slab	152

Figure 3.21, Figure 3.22 and Figure 3.23 present schematic views of the analysed prototype building. More specifically, Figure 3.21 shows a 3D axonometric view and indicating the analysed frame. Figure 3.22 depicts the structural plan indicating the floor slabs with ribs parallel to the longitudinal frame. Lastly, Figure 3.23 shows the main dimensions of the frame.

In the numerical models, the same material stress-strain relationships described in the previous section have been used with the mechanical properties for steel reinforcement reported in Table 3.9.

Table 3.9 SLT1 properties

Name	Model	Properties		
		E [MPa]	fy [MPa]	μ [–]
reb_beam	stl1	210000	413.69	0.006
reb_col	stl1	210000	413.69	0.02

Four different planar framed structures have been analysed allowing for the loss of the internal column. Figure 3.24 displays a schematic view of the frames. The four structures are characterised by a different number of storeys and have been modelled adopting the same FE discretisation (e.g. same number of beam-column element for each physical RC member) and same sections for beams and columns. As in the original case study analysed before, the RC columns feature uniform cross-section and longitudinal reinforcement along their height.

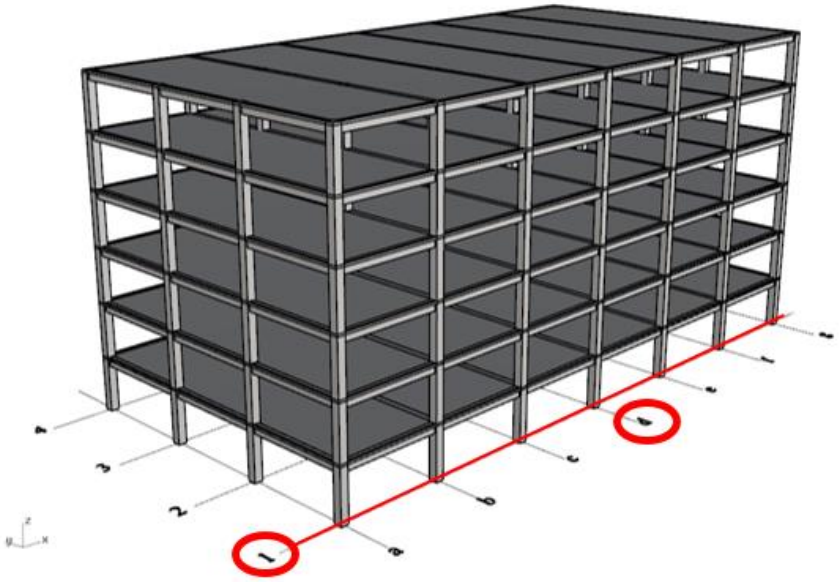

Figure 3.21 3D representation of the concrete frame building

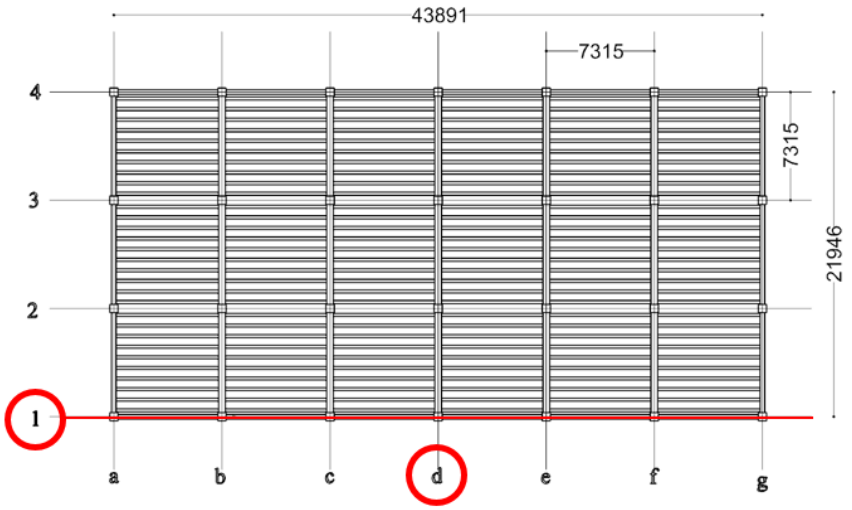

Figure 3.22 Plan view

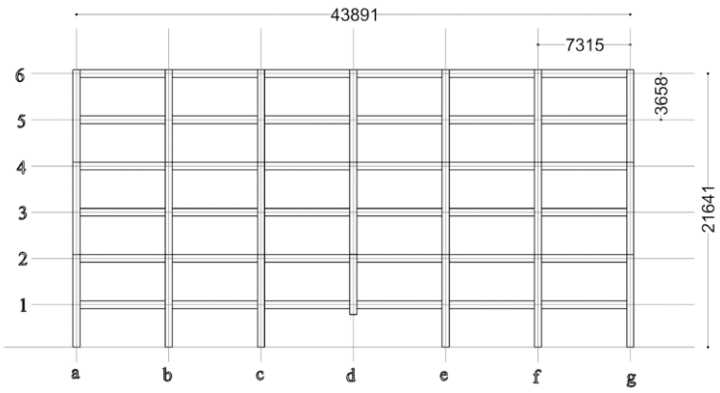

Figure 3.23 2D concrete bare frame, scale 1:1

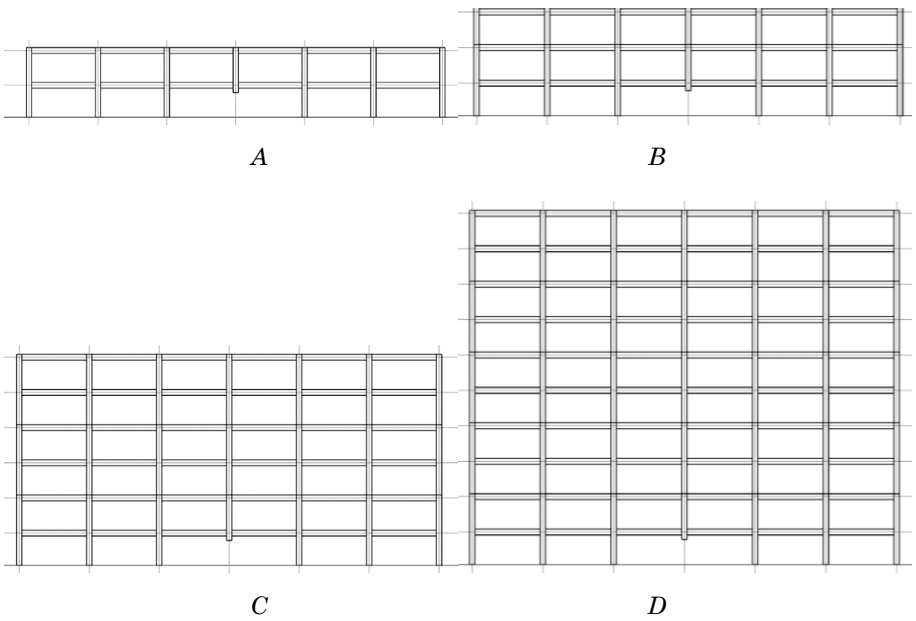

Figure 3.24 Model A: two floor, six bay frame; Model B: three store and six bay frame; Model C: six storey and six bay frame; Model D: ten storey and six bay frame

Static nonlinear push down analyses have been carried out applying vertical loads on the nodes of the columns above the column removed to represent column loss. No additional loads have been applied to the beams. The nodes at the base of the columns have been fully fixed. The contribution of the floor slabs is not taken into account in these initial simulations, but it is allowed for in the next section.

Figure 3.25 and Figure 3.26 show the response of the four frames in terms of static and pseudostatic load factors against the vertical displacement at central column, respectively. In both figures, the top curve represents the response of the two-floor frame and the lower one the response of the ten-floor frame, all the other curves lie in between. As shown in the figures, increasing the floors does not lead to an increment of the normalised load factor. Conversely, when the number of floors increases the load factor reduced in both static and pseudostatic cases. The load factors are expressed as the ratio between the applied vertical forces over the total vertical reaction before the column loss.

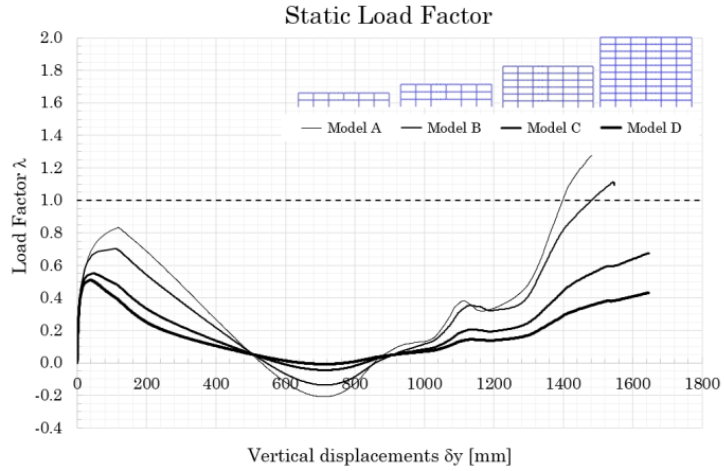

Figure 3.25 Static responses

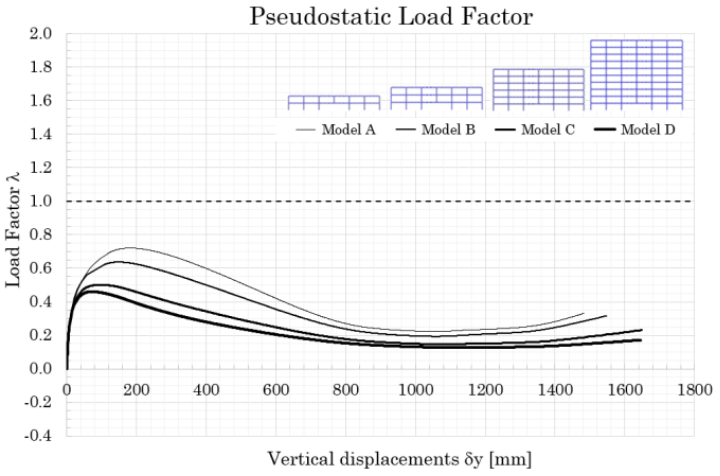

Figure 3.26 Pseudostatic responses

Figure 3.27 to Figure 3.30 describe the variation of the shear forces at the end of the beams directly affected by column loss by increasing the vertical displacement. It can be seen that shear forces in the beam at the first floor are much higher in the arching and catenary phases of the response. It is envisaged that this is due to the stiffening effect of the fixed supports at the column bases which does not affect the beams at the upper levels.

Figure 3.31 to Figure 3.34 show the variation of bending moment and shear force at the monitoring section shown in Figure 3.35. Similar curve for the internal forces at the first floor have been obtained for frames with different number of floors. On the other hand, the variation of internal forces at the monitoring section at the second floor depends on the number of floors above.

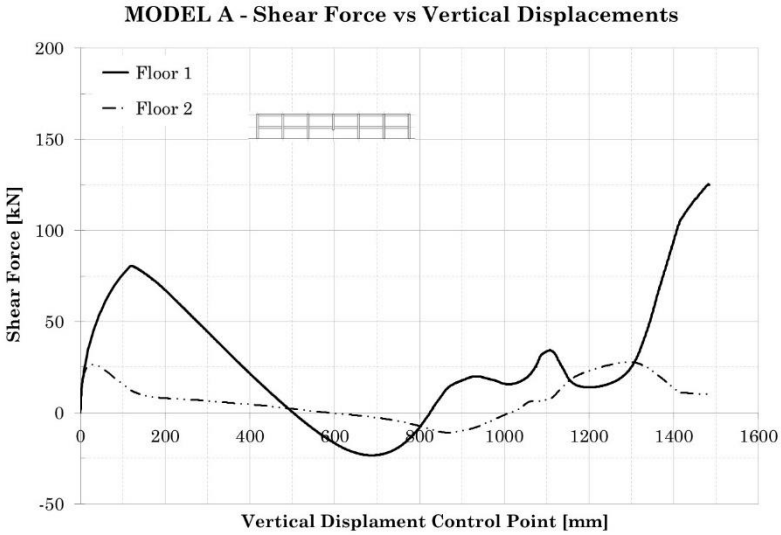

Figure 3.27 Diagrams of the shear forces variation in MODEL A

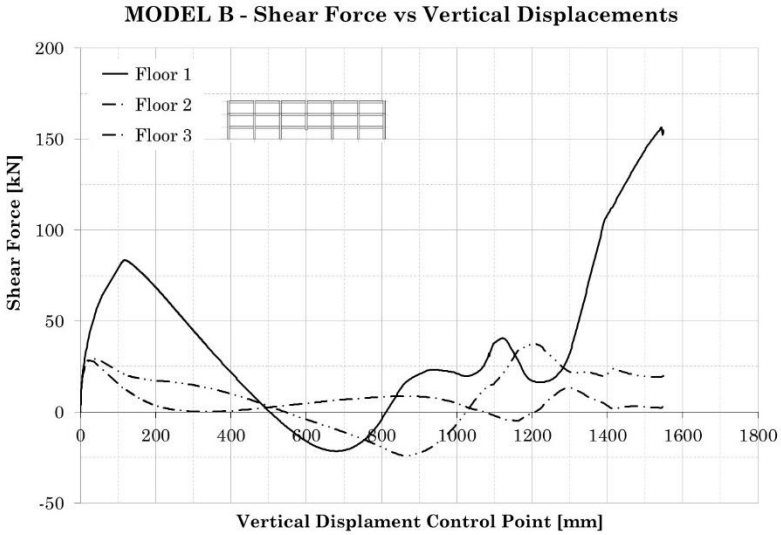

Figure 3.28 Diagrams of the shear forces variation in MODEL B

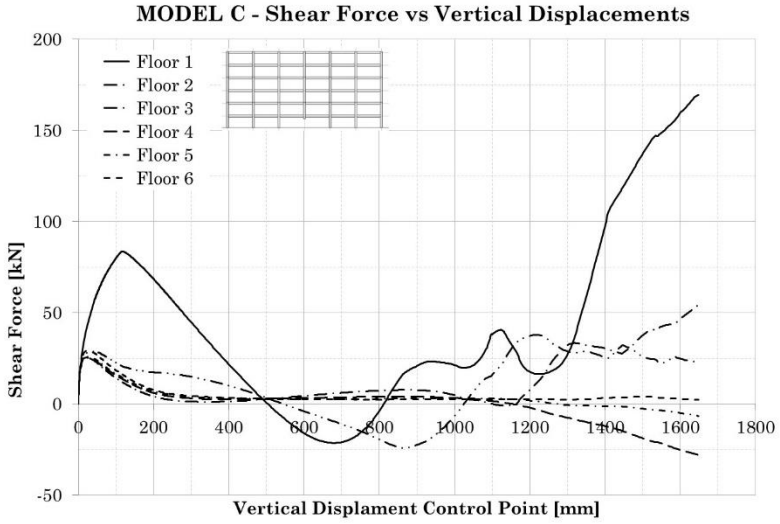

Figure 3.29 Diagrams of the shear forces variation in MODEL C

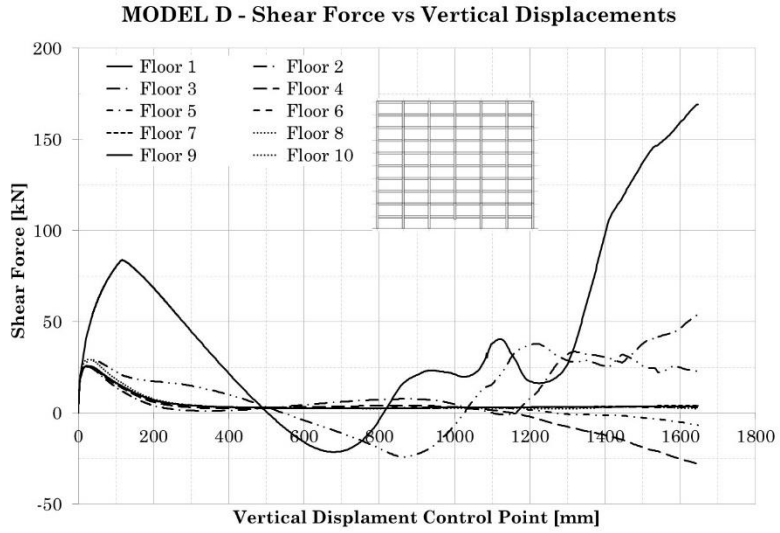

Figure 3.30 Diagrams of the shear forces variation in MODEL D

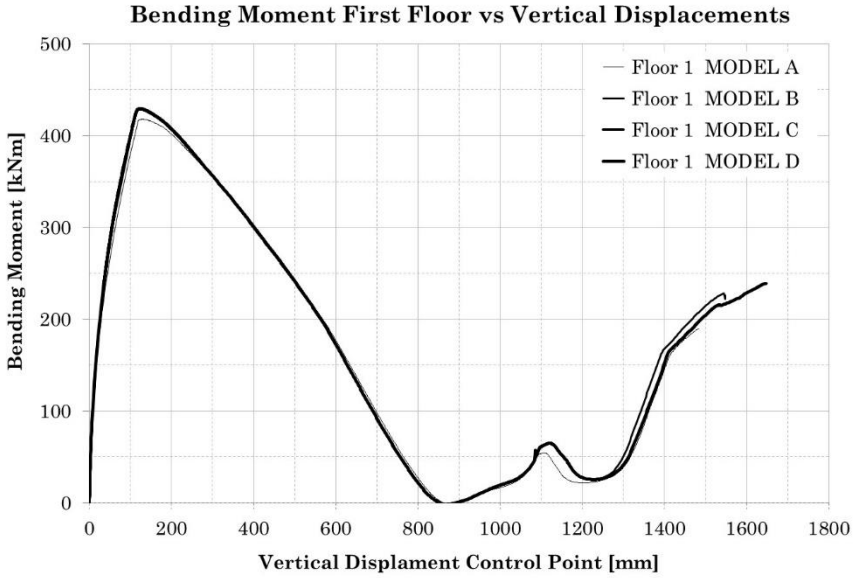

Figure 3.31 Comparison of the Bending Moments My in the first floor beam

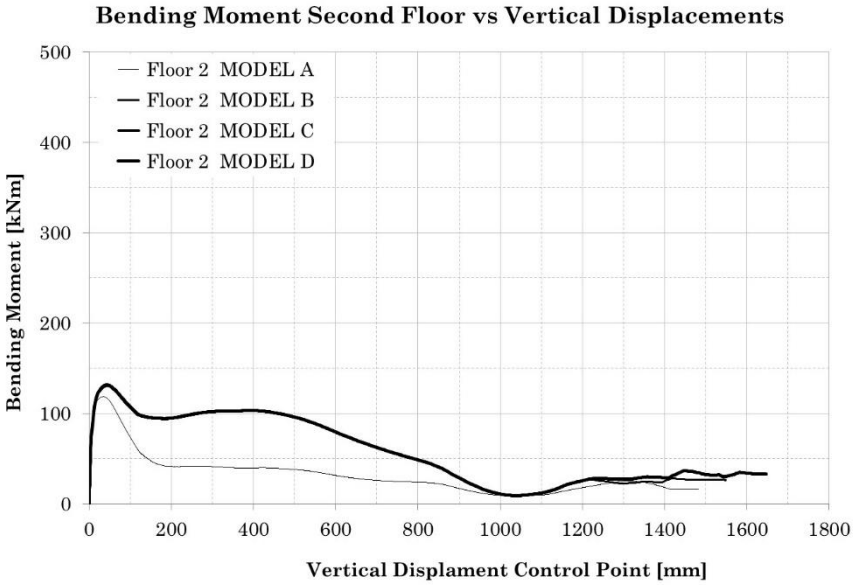

Figure 3.32 Comparison of Bending Moments My in the second floor beam

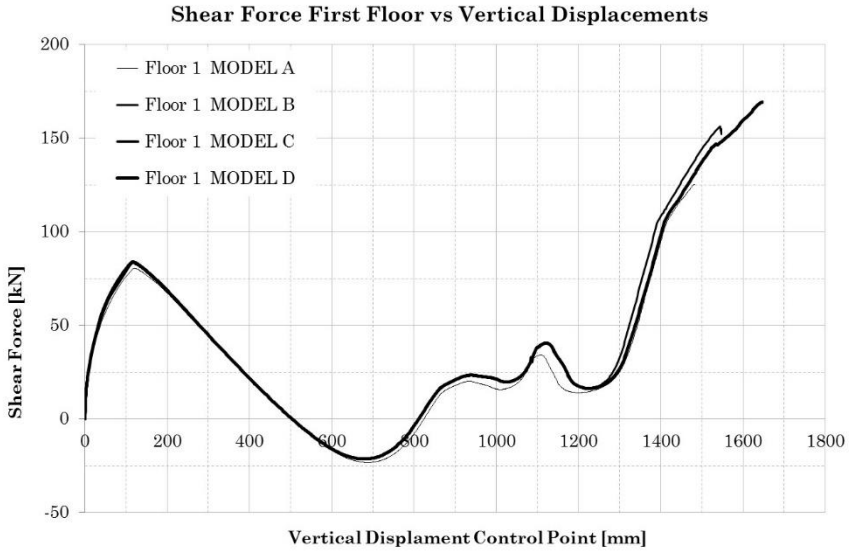

Figure 3.33 Comparison of Shear Forces Vz in the first floor beam

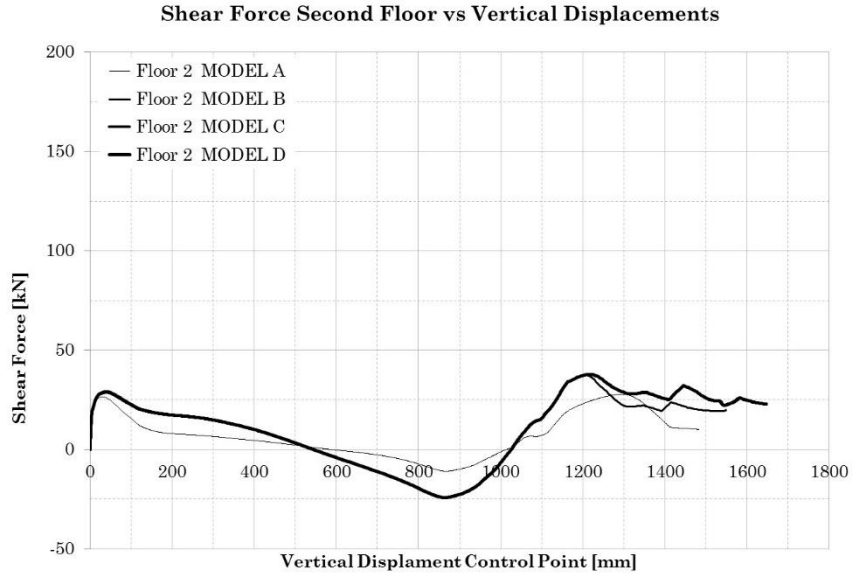

Figure 3.34 Comparison of Shear Forces Vz in the second floor beam

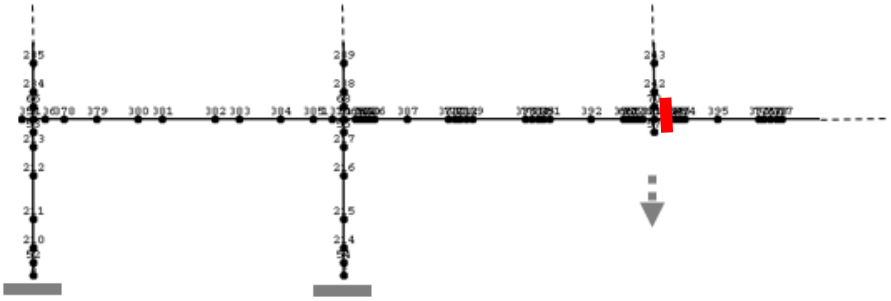

Figure 3.35 FE discretisation and monitored section (red)

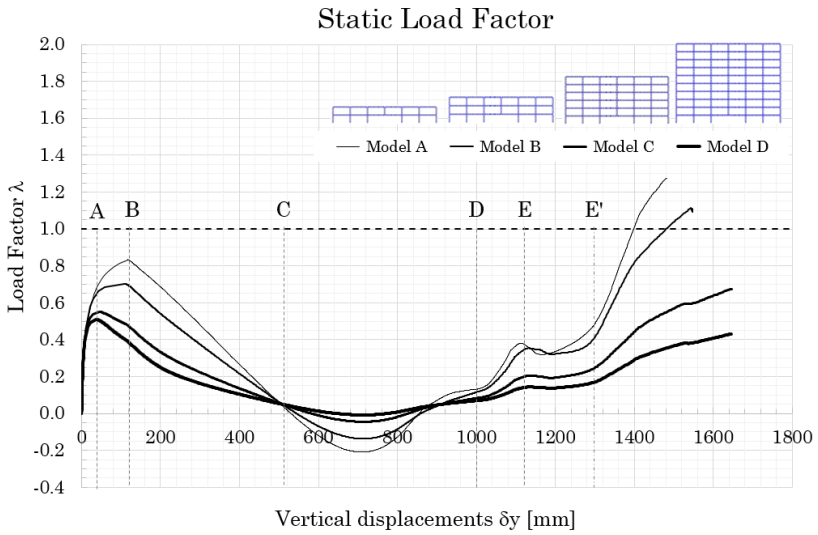

Figure 3.36 Push Down Curves and significant points

Finally, Figure 3.36 displays the four push down curves marking the main stages of the response. It can be observed that the pseudo-elastic branch ends (point A) at a vertical displacement level which depends on the number of floors and it included between 40 mm and 80 mm. The level of lateral restraint influences the vertical displacement at the first peak load (point B) and the slope of the first softening branch (B-C). Point D at a vertical displacement of about 1000 mm defines the end of the first transient part and the beginning of the catenary phase. Point E

defines the openings of the last pair of hinges and its associated vertical displacement and load depend on the reinforcement layout.

Figure 3.37 shows the deformed shape of the 10-storey frame at collapse. Failure mode of the first floor is influenced by the fixed column bases restrains facilitating the development of the arching actions in the beams at the first and partially second floors. In the figure below, black points indicate the position of plastic hinges position on half structure.

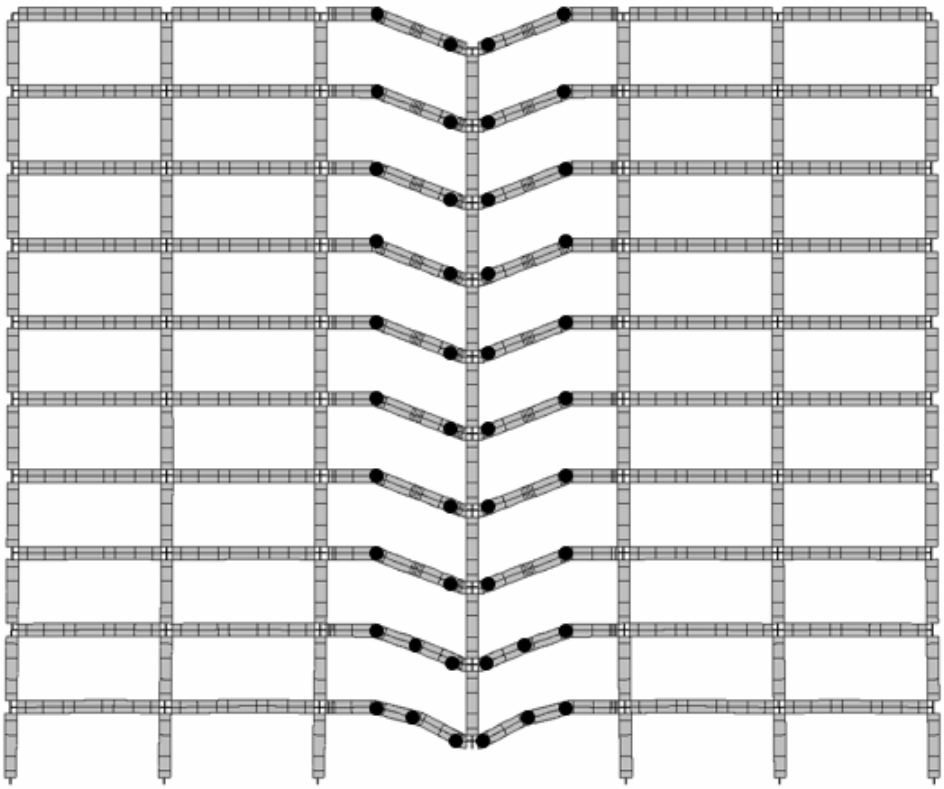

Figure 3.37 Collapse Shape after E point

3.7 Contribute of concrete slabs in a 3D model

Aiming to evaluate the contribute of concrete slab in terms of robustness, an high fidelity model has been developed on the base of the Stinger's building as the Figure 3.40 shows.

An accurate slab modelling has been adopted to take into account the interaction between concrete slabs, joists and beams. Elastic-plastic cubic beam-column elements [30] developed according to the distributed plasticity approach, for which the influence of large displacements is considered by using a co-rotational formulation [62], have been adopted in the modelling of concrete beams, columns and ribs. The generic RC cross-section is discretised into an opportune number of monitoring fibres (Figure 3.38) in which strains in concrete and steel reinforcement are determined and then used within specific material relationships to obtain the associated stresses. The specific material relationships have been discussed in §3.6. These laws allow for yielding and strain hardening of steel reinforcement, cracking in tension and crushing in compression of concrete and the specific hysteretic behaviour of the two materials.

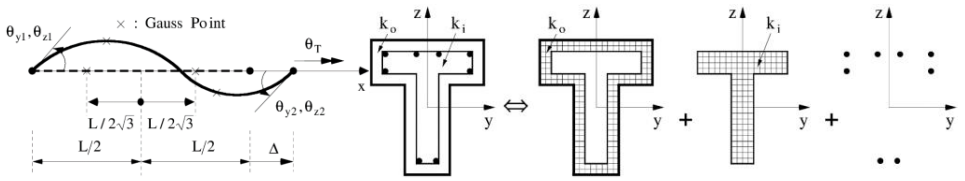

Figure 3.38 Sketch of the Fibre elements discretisation.

On the other hand, particular attention has been paid for representing the floor system that consists on one-way RC ribbed slabs. The system is depicted in Figure 3.39. Each floor rib has been modelled with a discrete number of 1D elastic-plastic beam-column elements that are rigidly connected to upper 2D slab elements representing for the top thin solid slab. The reinforced concrete ribs and the slabs have been connected by means of rigid links (lnks [63]).

The RC slab elements [64] consider material nonlinearity in both concrete and steel reinforcement, and account for both bending and membrane effects and geometric nonlinearity.

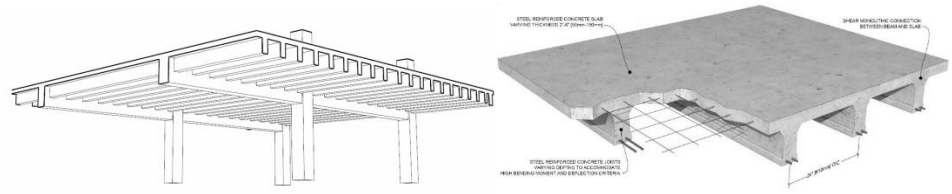

Figure 3.39 Detail of the one-way spanned ribbed slab

Figure 3.40 and Figure 3.41 depict the 3D high fidelity model and show the detail of the concrete slab modelling strategy, respectively.

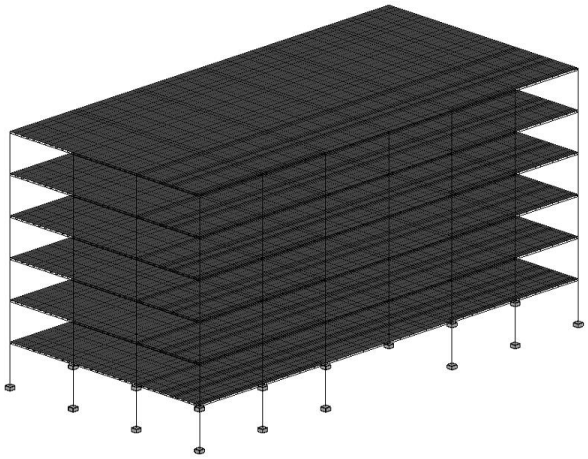

Figure 3.40 General view of the FEM 3D high fidelity model

Figure 3.41 Extruded view of the detail of concrete slabs system.

In agreement with the internal reinforcement layout, a more sophisticate subdivision has been employed for the elements on which the plastic hinges were expected. A realistic definition of the reinforcement bars layout allowed for an accurate section assignment shown in Figure 3.42.

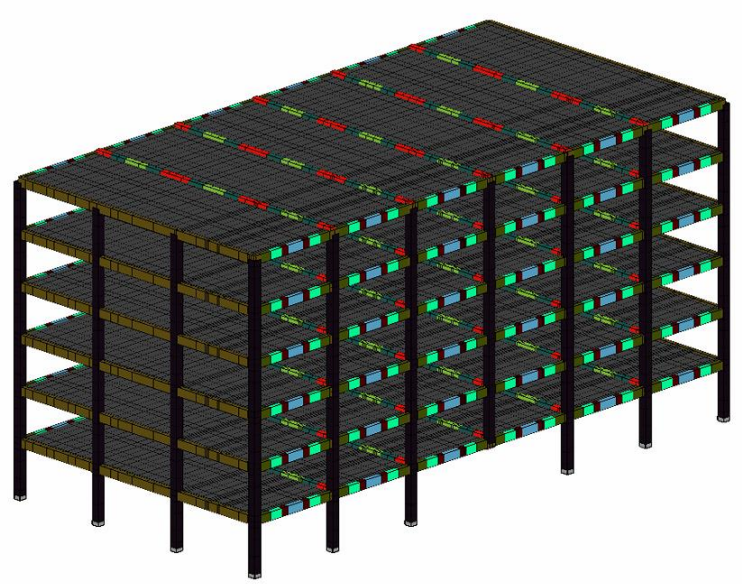

Figure 3.42 (Color) Assignment of sections in concrete frames

An intermediate floor has been extrapolated from the global and already discussed realistic model. The storey model aimed to evaluate separately the contribute of each element that composes the floor system. Base on that, three FEM models has been generated:

- Figure 3.43 shows the Model A that considers all the geometric elements that compose the floor slab system.
- Figure 3.44, shows the Model B that does not consider explicitly the slab contribute.
- Figure 3.45 shows the Model C that does not account explicitly for the slab and ribs contributes.

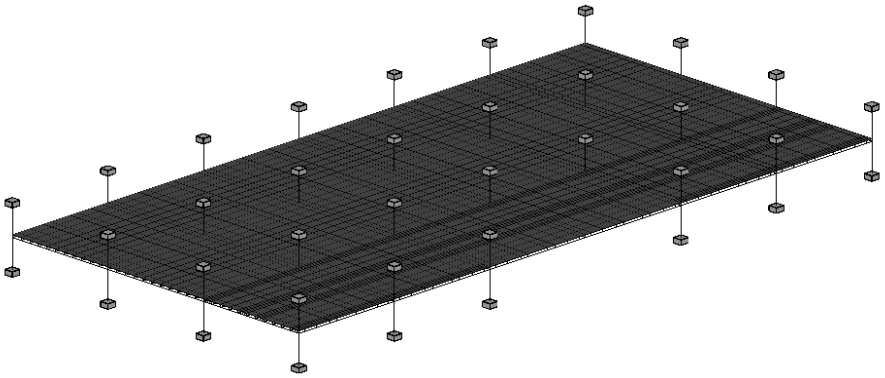

Figure 3.43 FEM Model of a generic high fidelity floor model. Model A

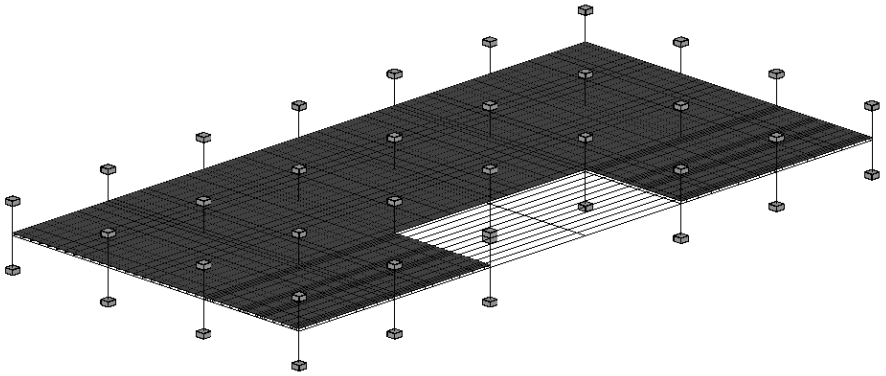

Figure 3.44 FEM Model of a generic high fidelity floor model without concrete slabs. Model B

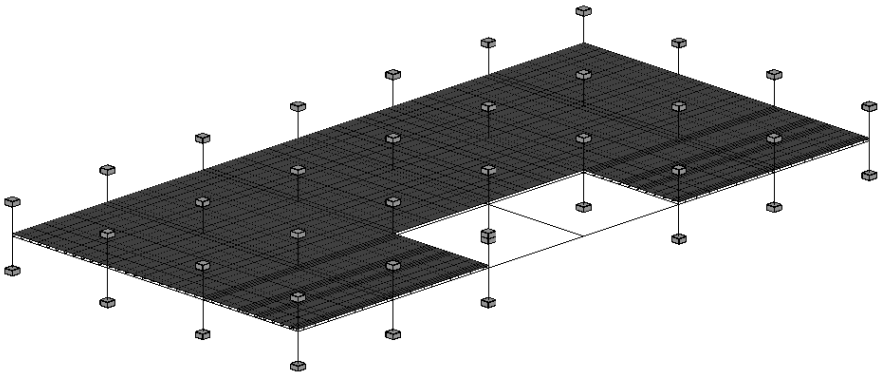

Figure 3.45 FEM Model of a generic high fidelity floor model without concrete slabs and ribs. Model C.

The three above presented models have been subjected to incremental vertical load analysis, namely PushDown Analysis, for evaluating the structural robustness of the slab system and the contribute of each component. Each model has been initially subjected to the specific load combination followed by on incremental concentrated load for a column loss simulation.

Figure 3.46 shows the deformed shape of the generic floor. The figure gives a visual information on influence of concrete slabs and joists on the collapse behaviour of the floor. The image depicts a V shape beam failure mode. Even though the accurate discretisation, consistent with the adopted in the planar cases, a different failure mode defines the floor collapse.

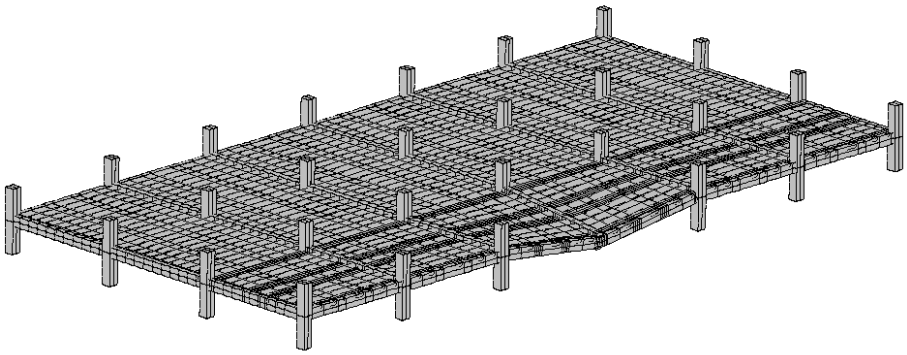

Figure 3.46 Deformed shape

The Figure 3.47 shows in a pictionary way the detail of the deformed shape of the peripheral frame. The Figure 3.47.a reproduces the obtained V shape in contrast with the Figure 3.47.b that reports the failure mechanism that has been observed in planar analyses that did not account explicitly for the slab contribute. The result let to consider that the concrete slab contribute may determinate the beams triangular shape (Figure 3.47).

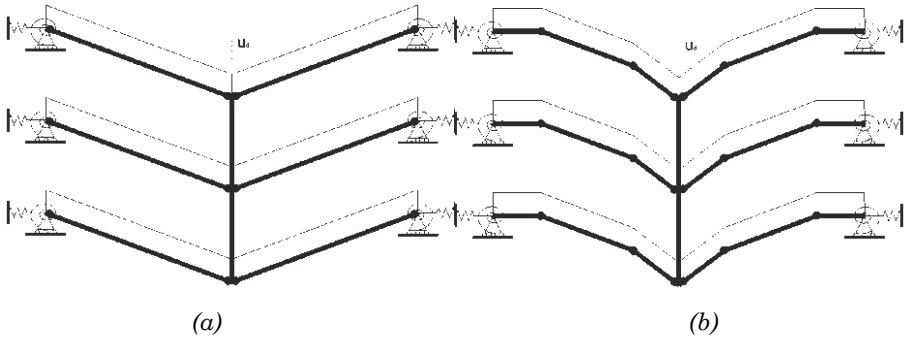

Figure 3.47 Typical deformation modes due to column loss in steel (a) and RC (b) frame structures.

Figure 3.48 depicts the response curve of the pushdown analyses on the generic floor. The curve is mainly characterised by two drops at the displacements values of 48 mm and 136 mm respectively.

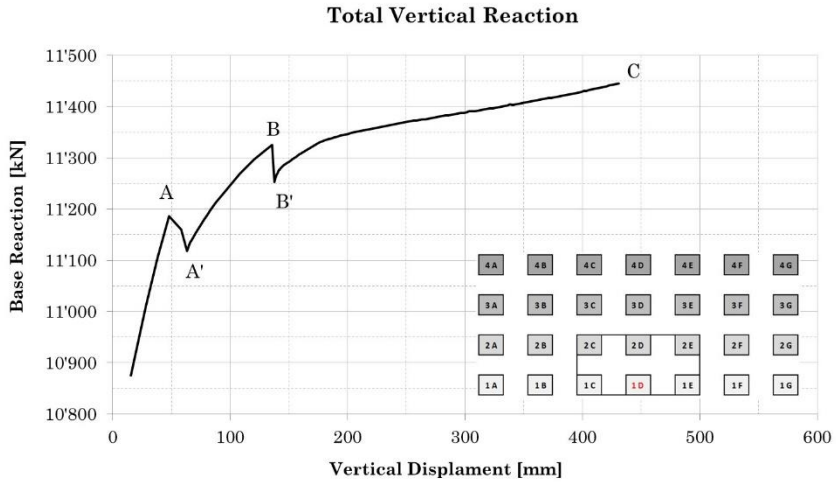

Figure 3.48 Push Down Curve Model A

According to the exposed results, the definition of the slabs contribute has been evaluated by comparing the response curve with the curves that have been obtained by means of Model B (Figure 3.44) and Model C (Figure 3.45) and summarised in Figure 3.49.

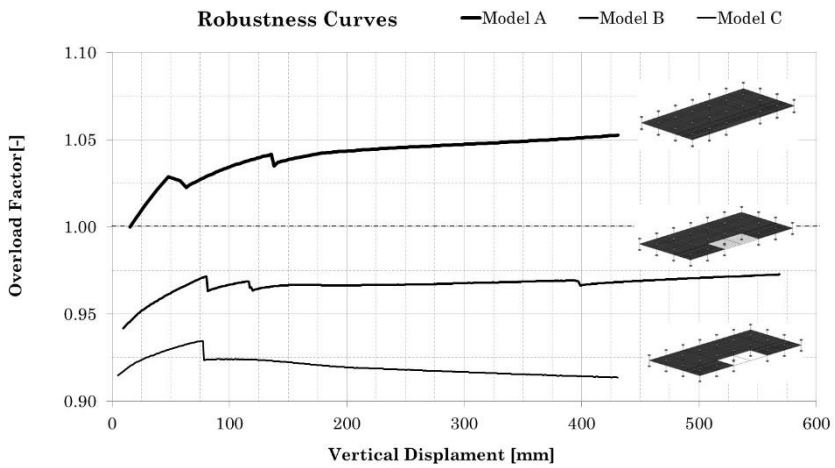

Figure 3.49 Push Down Curves of the three FEM floor models

The aim of the simplification has been to point out the contribute of different structural elements on the robustness of the generic floor.

The Figure 3.49 shows the three results in terms of normalised resistance forces. The nonlinear static reaction forces have been divided over the static reaction force of the not damaged structure. The diagram compares the three curves in which a similar behaviour can be identified. Initial and moderate resistance drops sign all the response curves. The drops in the static nonlinear response have been determinated by the failures in the principal beams elements. On the other hand, a sensible difference between the three curves and a huge contribute of the concrete slabs element in terms of resistance is recognisable. The concrete planar elements (thickness = 152mm) influence the concrete beams behaviour and increment the displacement capacity of the structure. The concrete joist contribute to the capacity and resistance too.

Lastly, the *simplified dynamic assessment* [26] that accounts for the dynamic effects in the column loss scenario confirms the capacity of the floor slab system to arrest the collapse and, potentially, preserve the structure from the failure. Figure 3.50 reports the assessment in terms of pseudostatic curve that reaches the Pesudostatic Overlad Factor of 1 at ~400mm.

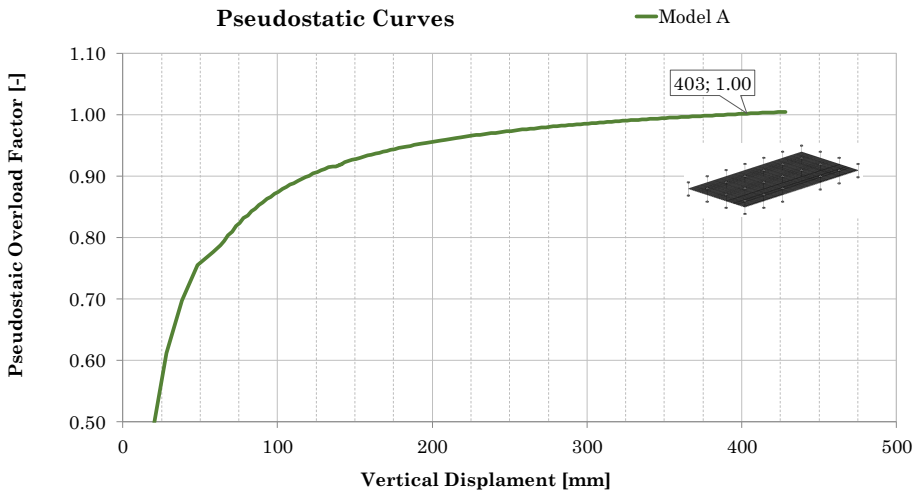

Figure 3.50 Pseudostatic Curve

It is worth noticing that even though the floor system avoid collapse, severe damages affect all the structural members. In detail, the slab shows cracks and crushes in the concrete slab and plastic behaviour of the planar reinforcement at the end of the analysis.

The Figure 3.51 and Figure 3.52 report the stress states on both concrete slab sides and directions. The tensile limit strength is exceeded in several elements (grey colour) and the ultimate compressive strength is exceeded too and influenced by the interaction with the concrete beams and joists.

The Figure 3.53 reports the stress state of the reinforcement bars for which the tensile yielding limit is exceeded in the joist direction (y direction). The plastic path is consistent with the plastic hinges that took place on the peripheral concrete beams.

The results demonstrate the necessity of accurate and realistic models for evaluating a reliable robustness metric.

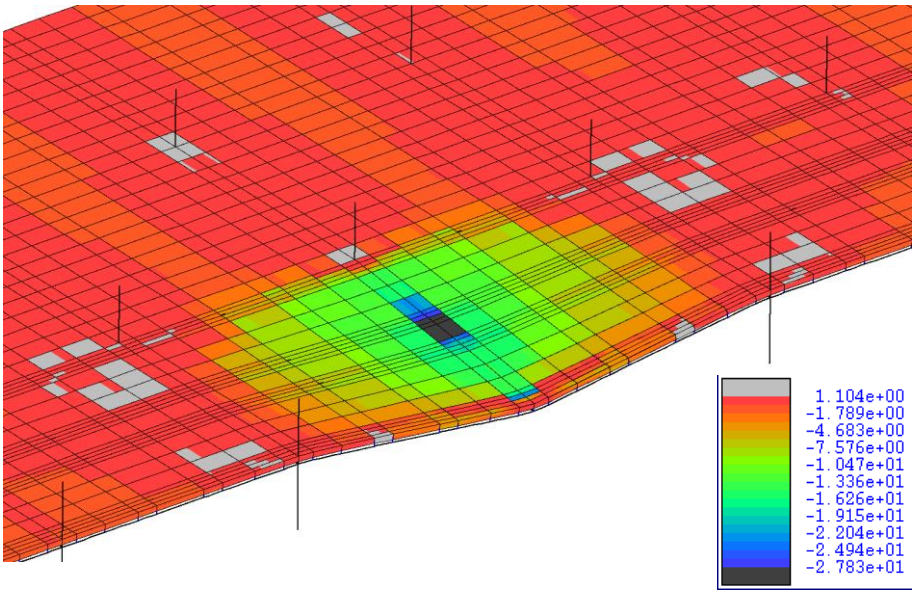

a

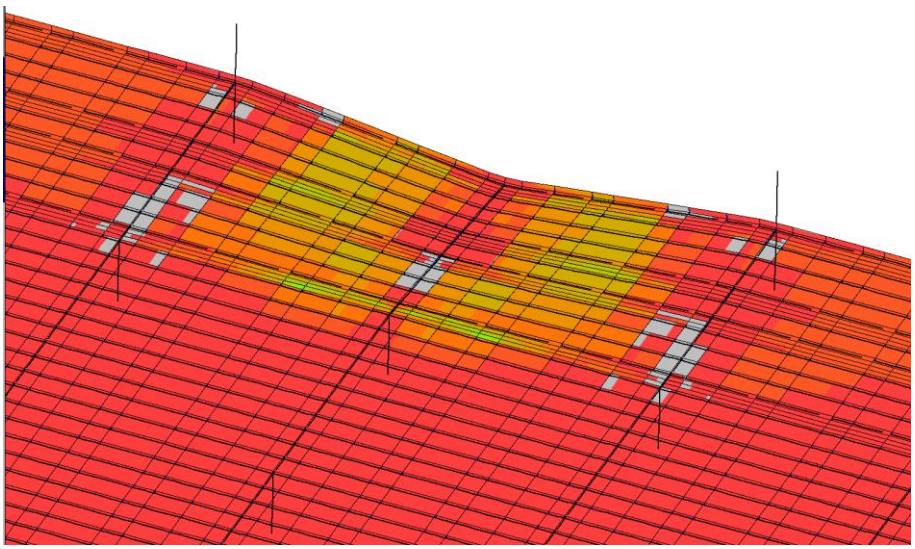

b

Figure 3.51 (Colour) Detail of Concrete slab stresses, σ_x [MPa], a) top, b) bottom

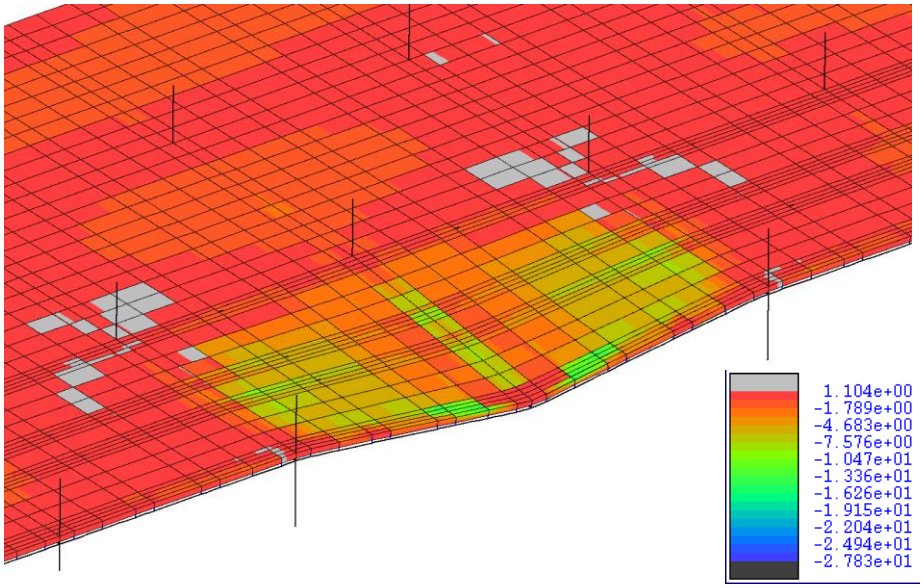

a

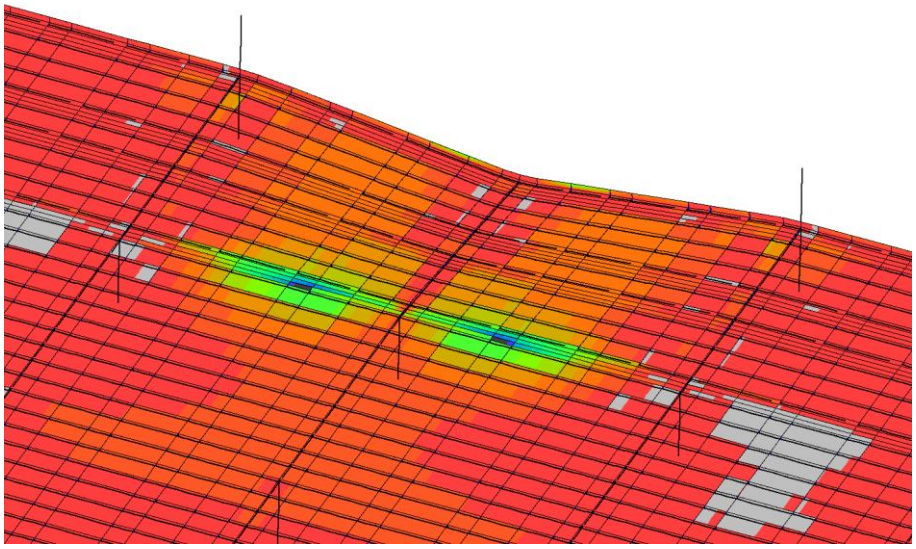

b

Figure 3.52 (Colour) Detail of Concrete slab stresses, σ_y [MPa] a) top, b) bottom

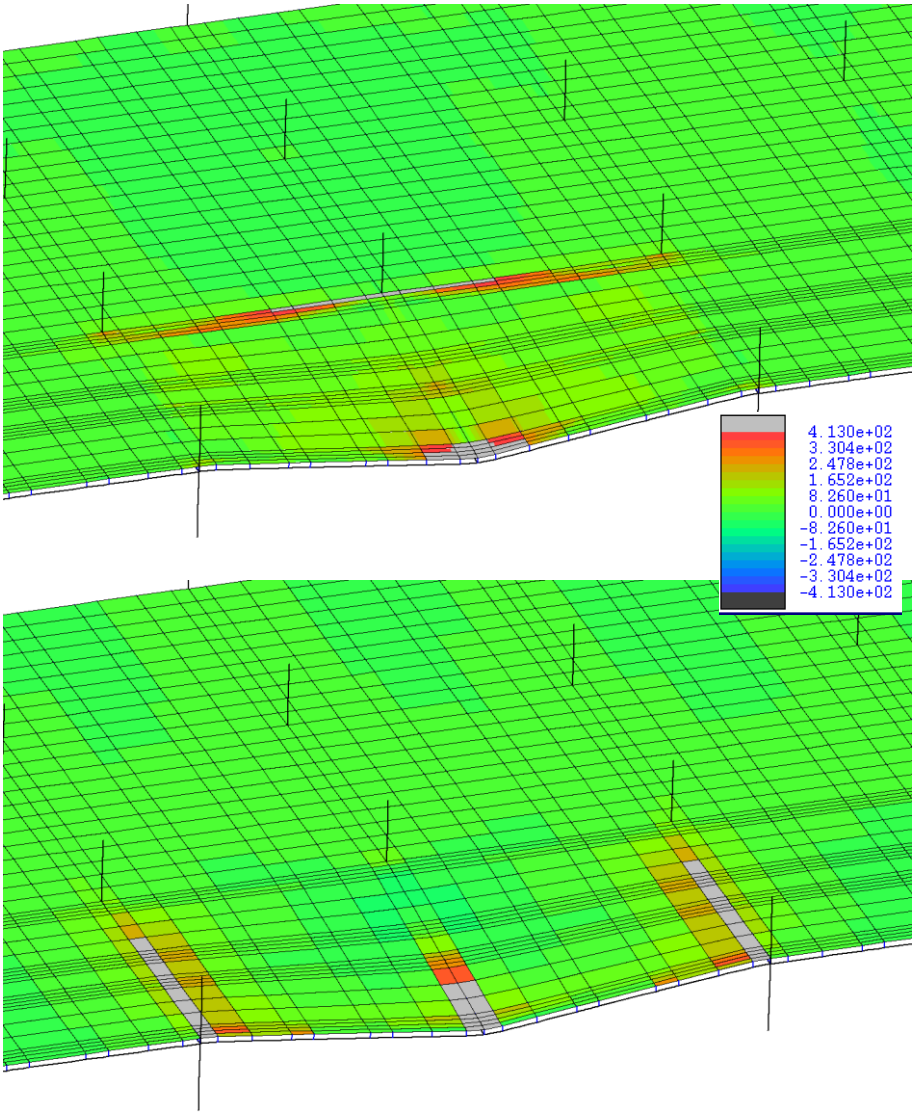

Figure 3.53 (Colour) Reinforcement tensile stresses, σ_x and σ_y [MPa]

CHAPTER 4.
INFLUENCE OF INFILLS ON COLLAPSE OF REINFORCED CONCRETE BUILDINGS

In order to obtain a high fidelity model of the structure, before and after its seismic retrofitting, a detailed representation of the non-structural infills is needed. To this aim, an original FEM implementation strategy of a recently proposed plane discrete macro-element [65], has been developed. The FEM macro-model has been implemented in the software ADAPTIC [63] and validated by several comparisons with the discrete element based software 3DMacro. The FEM implementation of the macro-element has been validated by means of some numerical comparisons with the results obtained by using the software 3DMacro.

4.1 Introduction

According to the literature [66], the most common type of failure in non-structural masonry infilled panels are:

Shear failure due to the debording of the mortar brick interfaces (shear friction failure), which can occur following a stepped cracking pattern or by horizontal sliding along a mortar joint

Diagonal tension failure of the masonry units, as a result of a combination of compressive and shear stresses in the masonry

Crushing of the masonry at the corner due to the high compressive stresses.

The analytical modelling of infilled frames is a complex task and it is still a key topic in computational research. The infill frame exhibits a highly nonlinear inelastic behaviour resulting from the interaction of unreinforced masonry panel and the surrounding frame [67].

The existing Reinforced Concrete buildings, not designed to resist to earthquake loadings, are usually characterised by low ductile RC frames, whose interaction with the unreinforced weak masonry infill walls may result in different failure mechanisms involving both the infills and the surrounding frames [68]. The seismic assessment of these structures has a huge importance from the standpoint of hazard mitigation and life safety.

From a numerical point of view, one of the biggest challenges in modelling infill frames is the continuously changing contact, during seismic events, between the infills and the surrounding frames.

Figure 4.1 reports some common in plane failure modes in a unreinforced masonry infill subjected to horizontal loadings [69].

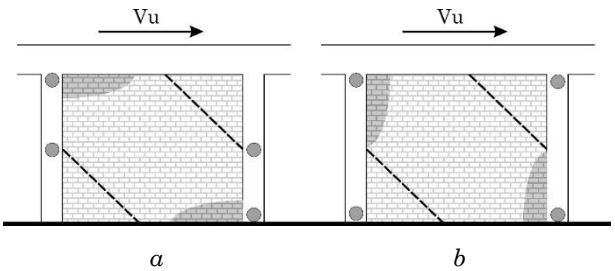

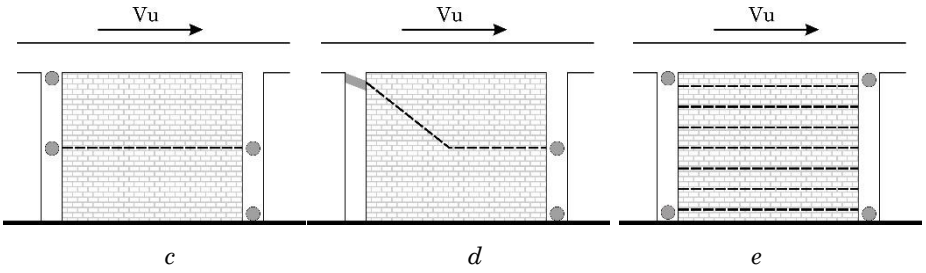

Figure 4.1 Failure modes for one storey single-bay infilled r.c. frames a) Corner crushing b) Compressed strut crushing c-d) Knee-braced e) Shear Sliding [69]

4.2 Literature review of infilled frame numerical modelling

An overview of the more reliable macro-element approaches for infilled frame is reported in the following sub Sections.

4.2.1 Single strut model

Currently, the most commonly used macromodel practical approach is the so called 'diagonal strut model', according to this approach the infilled masonry is represented by a diagonal bar under compression.

The first original work on the infill frame modelling solutions with the adoption of an equivalent strut was proposed by Polyakov [70] in 1956. Polyakov conduced analytical studies based on elastic theory. Later, in 1961 Holmes [71] proposed that the equivalent diagonal strut should have a width equal to 1/3 of the length of the panel. In a successive research, Stanford and Smith [72] refined the approach and started a series of test to investigate more precisely the width of equivalent strut, even though the single strut cannot describe properly the internal forces induced in the members of the frame since sharing information only at the nodes of the frame elements.

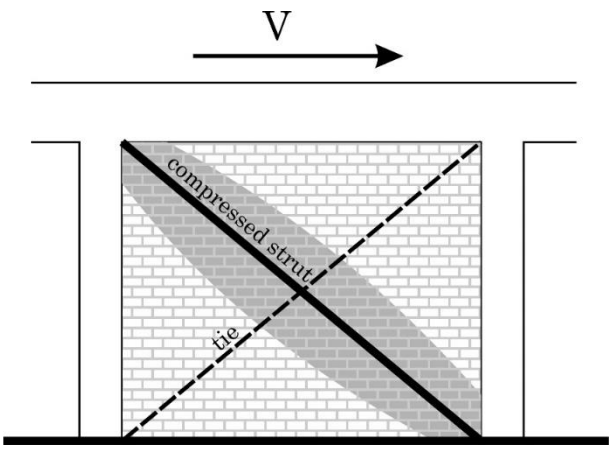

Figure 4.2 Single Strut Model Scheme

4.2.2 Multi Diagonal Struts Models

Since the last two decades some researchers pointed out that single strut models are inadequate to describe the interaction between panel and surrounding frames [73], and proposed alternative multi-strut models obtained as a combination of two or three struts (Figure 4.3).

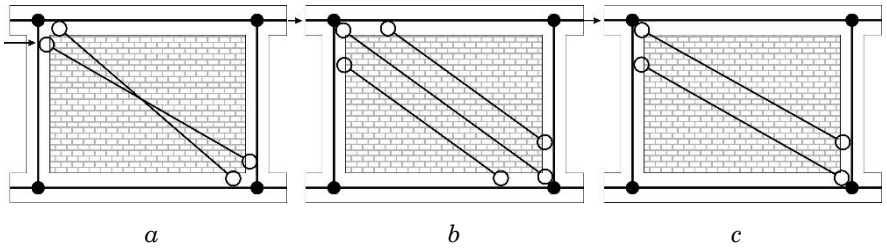

Figure 4.3 Few strut models: (a) Schimidt (b) Chrysostomou, (c) Crisafulli

All the proposed multiple strut models were not able to predict the shear sliding phenomena that occur in the infilled panel and within the interfaces. In this direction, Fiorato and Leuchars & Scrivener proposed a "knee braces frame" [74, 75]. The proposed model is reported in Figure 4.4.

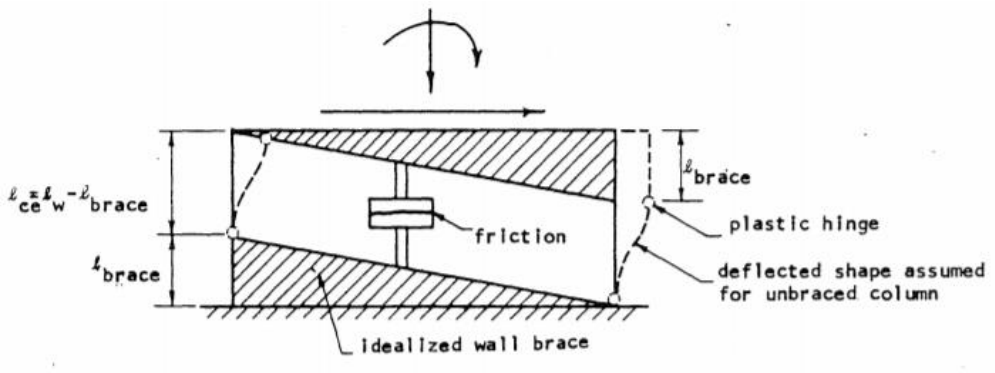

Figure 4.4 Knee Frame Model [74]

The Knee Frame Model allows to predict the increment of bending moment and shear force along the concrete column due to the interaction with the panel and the shear sliding response.

4.2.3 Crisafulli and Carr Model (2007)

Crisafulli and Carr [76] proposed a macroelement model that simulates both the truss and the shear behaviour mechanism Figure 4.5. However this model still neglects the interaction between the infill and the surrounding frame.

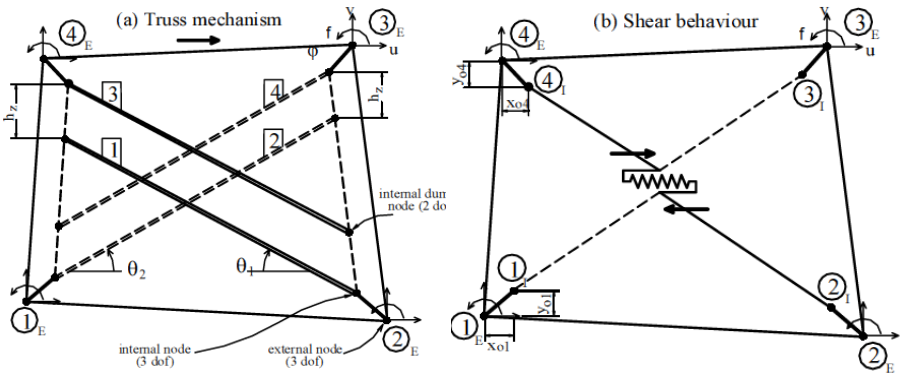

Figure 4.5 Crisafulli-Carr model [76]

The authors suggested to assume the stiffness of the shear spring k_s equal to a function of the total stiffness of the masonry strut

$$k_s = \gamma_s \frac{A_{ms} \; E_m}{d_m} \cos^2 \theta \qquad \textit{Eq. 7}$$

Where E_m is the tangent modulus of the masonry defined according to an adequate hysteretic model for masonry.

The authors considered a relationship between the equivalent strut area and the lateral displacement, expressed as the corresponding axial displacement. The Figure 4.6 shows this relationship and, according to the experimental results, the equivalent width of the strut decreases by about 20% to 50% due to cracking of the masonry panel.

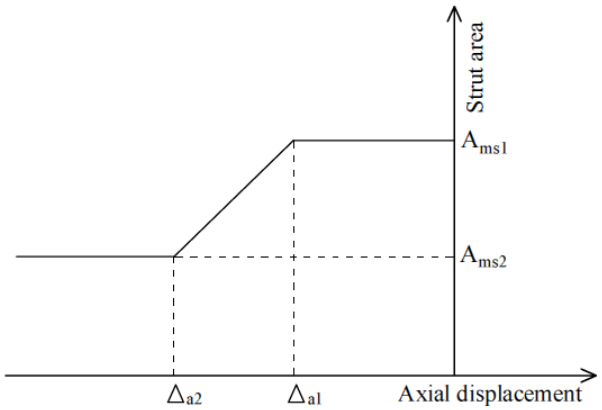

Figure 4.6 Variation of Area [76]

4.2.4 Hashemi and Mosalam – SAT Model (2007)

The SAT model proposed by Hashemi and Mosalam is made by eight compression-only struts model [77]. The Figure 4.7 shows a sketch of the macroelement and the only compression relationship that the authors assumed in the eight diagonal struts. From zero to peak stress the relationship is parabolic, while the post peak relationship is linear, own to a constant residual resistance.

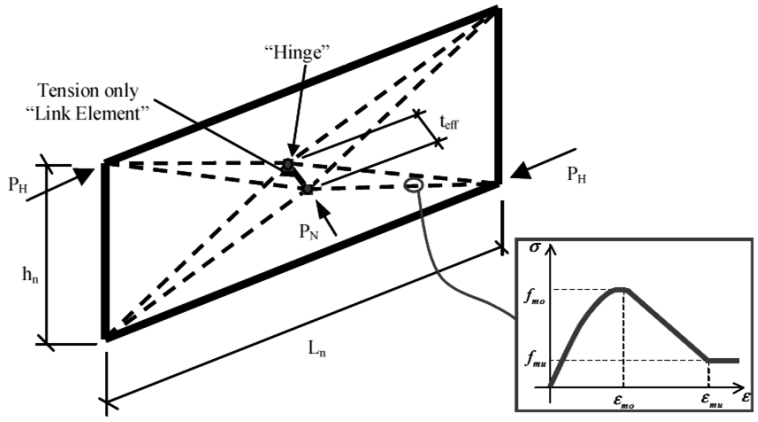

Figure 4.7 Strut and tie model (Hashemi and Mosalam 2007)

There are essentially two degrees of freedom in the SAT model: the In-Plane longitudinal deflection and the Out-Of-Plane transversal deflection.

As discussed in [77], the empirically expressions derived SAT model proposed by Hashemi and Mosalam exhibits some problematical behaviour under certain conditions. For instance, the In-Plane and Out-Of-Plane force path cannot violate the chosen interaction relationship. Additionally, the model may become unstable under combination of high IP displacement and high OOP loads.

4.2.5 Kadyesiewski and Mosalam Model (2009)

Kadysiewski and Mosalam developed a new model with fibre discretization. [78] for overstepping the SAT model issues.

The model consists of one diagonal member. The member is composed by two beam column elements, joined at the midpoint mode endowed with a concentraded mass, as the Figure 4.8 depicts.

The model assumes diagonal members with tensile and compression strengths. However, the single diagonal member approach does not provide a reliable distribution of forces in the surrounding frame. Furthermore, if the floor diaphragms are relatively stiff and strong, as is often the case, the authors assume tolerable the simplification and its consequences on the concrete elements.

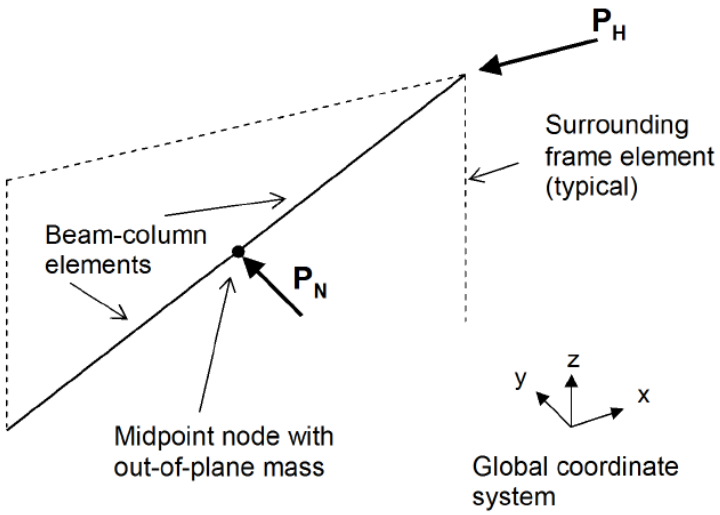

Figure 4.8 Strut and tie model (Kadyesiewski and Mosalam 2009)

The diagonal strut, according to Section 7.5 of FEMA 356 (FEMA 2000), defines the in-plane behaviour. The strut has the thickness equal to the panel and the width is given by Equation 7-14 in FEMA 356 (FEMA 2000).

The OOP strength of the URM infill wall is determined by means of the procedure in Section 7.5.3.2 of FEMA 356 (FEMA 2000).

The OOP capacity is based on arching action.

The authors also provided an interaction curve between in plane and out of plane capacities. The convex curve is depicted in Figure 4.9.

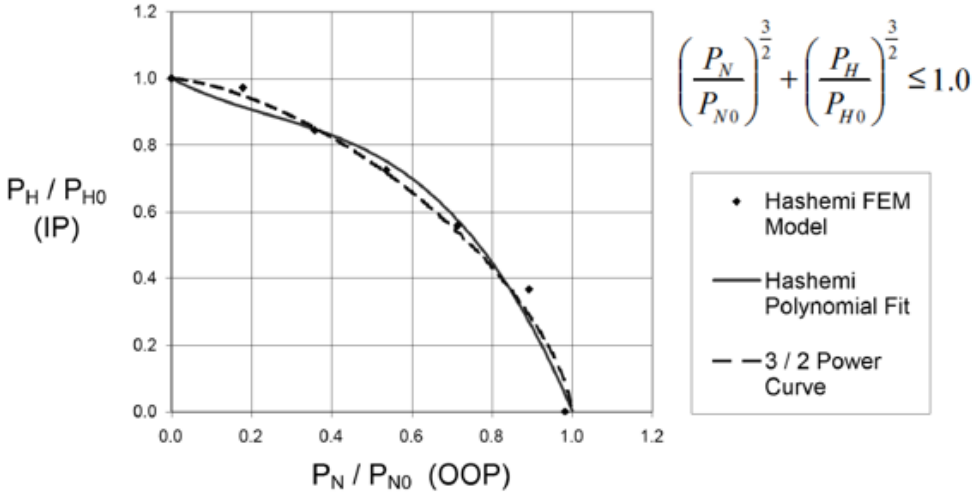

Figure 4.9 Interaction domain [78]

A more serious objection stems from the fact that the model IP axial and OOP moment strengths do not drop to zero when the CP limit state interaction curve is exceeded. In the actual structure, the collapse of an element is accompanied by an increase of load in neighbouring elements. If the objective of the analysis is a performance-based evaluation of an existing structure, the use of the proposed model may lead to unrealistically optimistic conclusions. To avoid the overestimation of robustness or seismic capacity the authors suggested to implement an automatic element removal procedure. The method was discussed and proposed by Mosalam in the 2008 [79].

4.2.6 Mohebkhah et al. MTS Model (2007)

In 2007 Mohebkhah et al. [80] proposed a Modified Three Struts (MTS) macroelement considering the presence of openings in the infill frames.

Firstly, a two dimensional discrete element model using the software UDEC was developed and validated against the available experimental data for non-linear static analysis of infilled steel frames subjected to in plane monotonic loadings.

Then, the model was implemented and adopted for evaluating the effects of different opening sizes on the lateral stiffness and collapse load.

4.2.7 Caliò et al. a two-dimensional MacroElement

A two dimensional macro-element model was proposed by Caliò et al. [65, 81, 82] and implemented in the computer software 3DMacro [83].

The basic element of the proposed approach has a simple mechanical scheme, Figure 4.10.

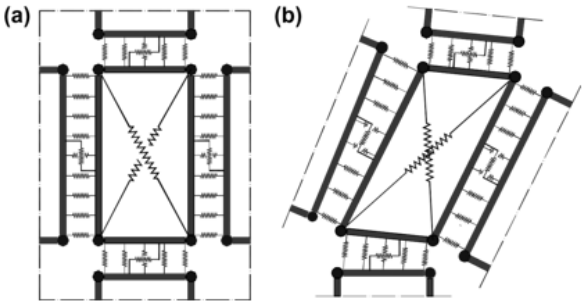

Figure 4.10 The basic macro-element: (a) undeformed configuration; and (b) deformed configuration.

It is represented by an articulated quadrilateral constituted by four rigid edges connected by four perfect hinges and two diagonal nonlinear springs. Each panel side can interact with other panels or elements or supports by means of a discrete distribution of nonlinear springs, also denoted as discrete interfaces. A discrete number of n nonlinear springs lie on the each edge orthogonally to the panel and a single parallel spring connect the edge to surrounding element and controls relative motion in the direction of the panel edge. In spite of its great simplicity, such a basic mechanical scheme is able to simulate the main in-plane failures of a portion of masonry wall subjected to horizontal and vertical loads. These well-known collapse mechanisms, namely flexural, diagonal shear and sliding shear failure, are represented in Figure 4.11. The schemes describe the typical crack patterns and the kinematics of masonry portion. Figure 4.12 shows how the macro-element can simulate the three

mentioned failure modes and how the damage indication in the nonlinear links can rule the collapse mechanisms.

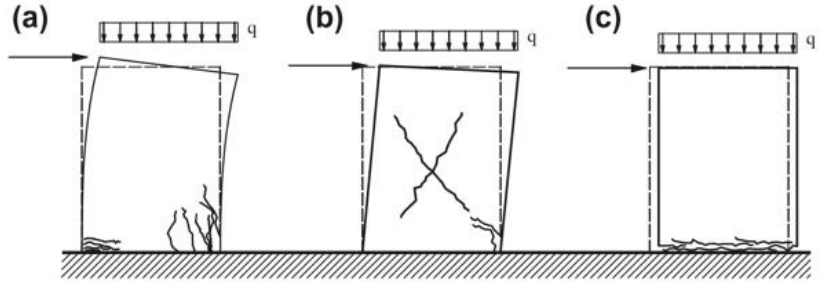

Figure 4.11 . Main in-plane failure mechanisms of a masonry portion: (a) flexural failure; (b) shear-diagonal failure; and (c) shear-sliding failure

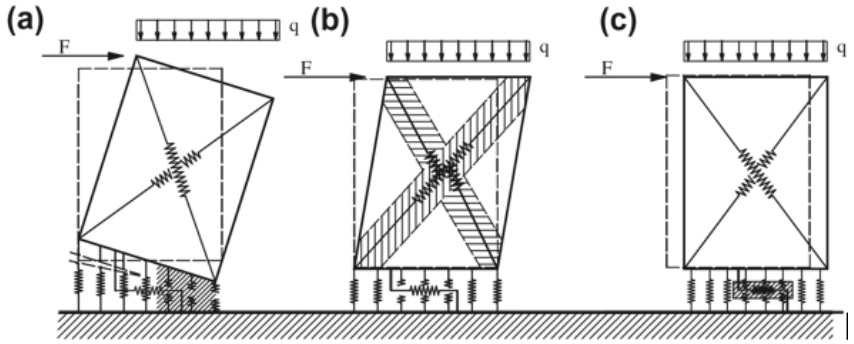

Figure 4.12 . Simulation of the main in-plane failure mechanisms of a masonry portion by means of the macro-element: (a) flexural failure; (b) shear-diagonal failure; and (c) shear sliding failure

According to this approach, the flexural failure mode (Figure 4.11a) is associated to the rocking of the masonry portion in its own plane. The loss of the bearing capacity is related to the progressive rupture of the panel in the tensile zone and/or to the crushing of the panel in the compressive zone. The axial and flexural deformability of the masonry panel is concentrated in the orthogonal nonlinear links according to a simple fibre model discretization, as is usually adopted for distributed plasticity beam element in reinforced concrete structures.

The diagonal-shear failure mode (Figure 4.11b) is associated to the loss of the bearing capacity of the masonry panel due to excessive shear and to the consequent formation of diagonal cracks along the directions of the principal compression stresses. Through the proposed discrete

element, this collapse mechanism can be governed by two diagonal nonlinear springs which simulate and predict the nonlinear shear response of the modelled masonry portion.

The sliding-shear failure mode is associated to the sliding of the masonry panel in its own plane (Figure 4.11c). In this case, the loss of the bearing capacity is associated to the cracks parallel to the bed joints. This failure mode, which generally occurs for low levels of vertical loads and/or low values of friction coefficients, is controlled by the longitudinal nonlinear springs on the interfaces.

4.3 An original FEM implementation of the MacroElement

The present sub-section discusses the implementation of the MacroElement that has been proposed by Caliò et al. [65, 81, 82]

The previous literature review has shown different proposed macroelement approaches. Most of them are based on Single or Multiple Struts approach. These strategies, as previously discussed, do not allow an accurate description of the complex interaction between the infill panel and the surrounding frame. Corners crush, bed mortar joints sliding and the interaction between the infill and the surrounding frame cannot be described by simplified strategies based on single or multiple struts. In this light the adoption of the plane element endowed with perimetral interfaces, proposed by Caliò et al., appears to be more accurate and suitable for being employed in high fidelity models of infilled frame structures. In addition this macroelement is characterised by a low computational cost and can be used for modelling entire buildings without leading to a dramatic increase of the degrees of freedom, typical of detailed nonlinear finite element modelling of infilled frame [84, 85, 86, 87].

Aiming at adopting the macro-element in the high-fidelity ADAPTIC models in this chapter an original low-cost FEM implementation of the macro-element for its representation in infilled frame structures is proposed. In the FEM implementation, the displacement field of the

macro-element is conveniently related to four internal degrees of freedom while the displacements at the perimetral interfaces are governed by cubic polynomial functions related to the displacements and rotations of eight external nodes at the macro-element corners, as reported in Figure 4.13.

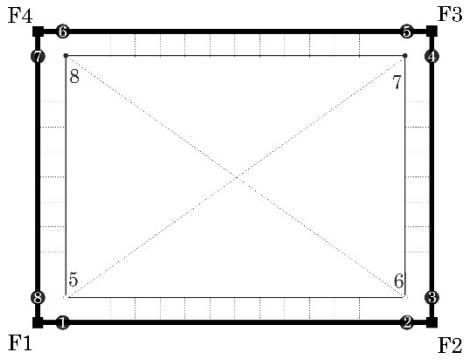

Figure 4.13 Proposed macroelement

4.3.1 The kinematics of the infilled macro-element

The proposed nonlinear plane discrete macro-element is defined according to an original approach that allows its implementation in any displacement based finite element code. The location and the corresponding orientation of the 24 degrees of freedoms of the 8-nodes and of 4 degrees of the quadrilateral are reported in Figure 4.14.

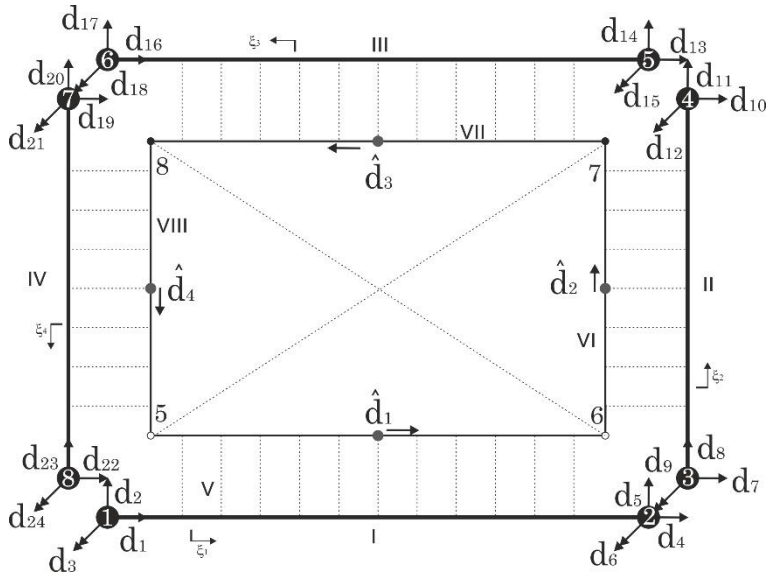

Figure 4.14 Location and the corresponding orientation of the degrees of freedom in the global system

For convenience, the 24 degrees of freedom associated to the 8 nodes are named as *external degrees of freedom* while the 4 degrees of freedom, related to the kinematics of the articulated quadrilateral, are identified as *internal degrees of freedom*.

The interface forces are related to the relative motion between the rigid edges of the quadrilateral and the displacement of the polynomial shape function (external edge displacement) associated to the external degrees of freedom, Figure 4.15.

The kinematics of the external edges of the element are described according to the following polynomial functions:

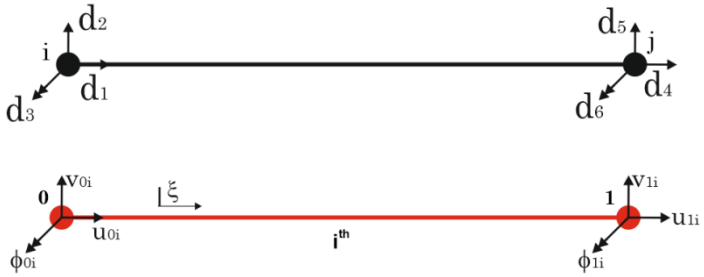

Figure 4.15 Relationship between local and global degrees of freedom in the external edges.

$$\begin{cases} N_1 = 1-\xi; \\ N_2 = 1-3\xi^2+2\xi^3; \\ N_3 = \xi-2\xi^2+\xi^3; \\ N_4 = \xi; \\ N_5 = 3\xi^2-\xi^3; \\ N_6 = -\xi+\xi^2 \end{cases} \qquad \textit{Eq. 8}$$

In the equations Eq. 8, ξ denotes the normalised abscissa, variable between 0 and 1, in the local reference system of the i^{th} external edge (i=1,2,3,4), as reported in Figure 4.15.

The local transverse displacement function $v_i(\xi)$ and local axial displacement function $u_i(\xi)$, of each external edge, can be expressed as a function of the auxiliary degrees of freedom of each external edge as follows:

$$\begin{Bmatrix} u_i(\xi) \\ v_i(\xi) \end{Bmatrix} = \begin{bmatrix} 1-\xi & 0 & 0 & \xi & 0 & 0 \\ 0 & 2\xi^3-3\xi^2+1 & \xi^3-2\xi^2+\xi & 0 & -2\xi^3+3\xi^2 & \xi^3-\xi^2 \end{bmatrix} \begin{Bmatrix} u_{oi} \\ v_{oi} \\ \varphi_{oi} \\ u_{1i} \\ u_{1i} \\ \varphi_{1i} \end{Bmatrix} \qquad \textit{Eq. 9}$$

The Eq. 9 can be expressed in compact notation as:

$$\underbrace{\{\mathbf{u}_i(\xi)\}}_{2x1} = \underbrace{[\mathbf{N}_L(\xi)]}_{2x6}\{\mathbf{u}_{Li}\}_{6x1} \qquad \textit{Eq. 10}$$

In the Eq. 10 $\mathbf{u}_{Li}$ is the local degrees of freedom of the i^{th}external edge that is directly related to the nodal degrees of freedom of the element. Collecting all the displacement functions, $u_i(\xi)$ $v_i(\xi)$ (i=1,2,3,4), in a single vector $\mathbf{u}(\xi)$, the expression which involves the displacements of the four external edges can be written in compact form as follows.

$$\underbrace{\{\mathbf{u}(\xi)\}}_{8x1} = \underbrace{[\mathbf{N}(\xi)]}_{8x24}\{\mathbf{u}_L\}_{24x1} \qquad \textit{Eq. 11}$$

The auxiliary local degrees of freedom of each edge can be related to the independent degrees of freedom of the edge's nodes by means of an afferent matrix, as the Eq. 12 depicts.

$$\underset{24x1}{\{\mathbf{u}_L\}} = \underset{24x24}{[\mathbf{A}]}\underset{24x1}{\{\mathbf{d}\}} \qquad \textit{Eq. 12}$$

being $\{\mathbf{d}\}$ the vector containing all the 24 degrees of freedom of the element nodes.

$[\mathbf{A}]$ is the afferent matrix and, in case of regular rectangular element, contains only 1,-1 and 0 values. This matrix can be expressed conveniently in a sub-matrix form as follows:

$$\underset{6x1}{\{\mathbf{u}_{Li}\}} = \underset{6x24}{[\mathbf{A}_i]}\underset{24x1}{\{\mathbf{d}\}} \qquad \textit{Eq. 13}$$

$\mathbf{A}_i$ is the sub-matrix and it is related to the i^{th}-side of the external quadrilateral.

Accordingly, having collected all the displacement functions $u_i(\xi)$ $v_i(\xi)$ (i=1...4) in a single vector $\{\mathbf{u}(\xi)\}$ (Eq. 10), the following expression is obtained.

$$\underbrace{\{\mathbf{u}(\xi)\}}_{8x1} = \underbrace{[\mathbf{N}(\xi)]}_{8x24}\underset{24x24}{[\mathbf{A}]}\underset{24x1}{\{\mathbf{d}\}} \qquad \textit{Eq. 14}$$

The kinematics of the rigid sides of the macroelement is related to linear shape function as expressed by Eq. 15.

$$\begin{Bmatrix} \hat{u}_i(\xi) \\ \hat{v}_i(\xi) \end{Bmatrix} = \begin{bmatrix} 1 & 0 & 0 \\ 0 & 1-\xi & \xi \end{bmatrix} \begin{Bmatrix} \hat{u}_{oi} \\ \hat{v}_{oi} \\ \hat{v}_{1i} \end{Bmatrix} \qquad \textit{Eq. 15}$$

where, ξ is the normalised abscissa associated to the i^{th} internal rigid edge and $\hat{v}_i(\xi)$ and $\hat{u}_i(\xi)$ are the local displacement functions.

The symbol $\hat{\square}$ identifies the quantities associated to the rigid articulated quadrilateral.

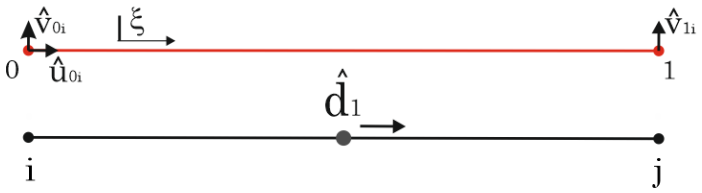

Figure 4.16 Relationship between local and global degrees of freedom in the internal edges.

$\hat{u}_{oi}$, $\hat{v}_{oi}$ and $\hat{v}_{1i}$ are the auxiliary local degrees of freedom of the i^{th} rigid internal edge, Figure 4.16. In compact notation eq. Eq. 15 becomes

$$\underbrace{\{\hat{\mathbf{u}}_i(\xi)\}}_{2x1} = \underbrace{\left[\hat{\mathbf{N}}_L(\xi)\right]}_{2x3} \{\hat{\mathbf{u}}_{Li}\}_{3x1} \qquad \textit{Eq. 16}$$

Eq. 16 can be extended to all the four rigid internal edges and it can be write as:

$$\underbrace{\{\hat{\mathbf{u}}(\xi)\}}_{8x1} = \underbrace{\left[\hat{\mathbf{N}}(\xi)\right]}_{8x12} \{\hat{\mathbf{u}}_L\}_{12x1} \qquad \textit{Eq. 17}$$

The total 12 local auxiliary degrees of freedom of the edges the quadrilateral are directly related to the independent additional degrees of freedom of the macro-element as the following equation shows.

$$\underset{12x1}{\left\{\hat{\mathbf{u}}_L\right\}} = \underset{12x4}{\left[\hat{\mathbf{A}}\right]}\underset{4x1}{\left\{\hat{\mathbf{d}}\right\}} \qquad \textit{Eq. 18}$$

Or, in "partition" fashion:

$$\underset{3x1}{\left\{\hat{\mathbf{u}}_{L_i}\right\}} = \underset{3x4}{\left[\hat{\mathbf{A}}_i\right]}\underset{4x1}{\left\{\hat{\mathbf{d}}\right\}} \qquad \textit{Eq. 19}$$

$\left[\hat{\mathbf{A}}_i\right]$ is the sub-matrix that is relative to the i^{th}-side of the rigid articulated quadrilateral.

$$\underbrace{\left\{\hat{\mathbf{u}}(\xi)\right\}}_{8x1} = \underbrace{\left[\hat{\mathbf{N}}(\xi)\right]}_{8x12}\underbrace{\left[\hat{\mathbf{A}}\right]\left\{\hat{\mathbf{d}}\right\}}_{\substack{12x4\ \ 4x1\\ 12x1}} \qquad \textit{Eq. 20}$$

It is worth noticing that, according to the adopted macro-element [81, 65] theory, the zero thickness interfaces incorporate the deformability of the infill panel. The masonry is considered as homogeneous but orthotropic.

Hence, the flexural and sliding kinematic depend on the interface relative displacements and the shear kinematic depends on the diagonal internal springs. All the nonlinearities are lumped in the Gauss point of the interfaces and in the diagonal springs.

The calibration procedure is based on a fibre approach and is discussed later in this Section.

The relative displacements in the interfaces are obtained by

$$\underbrace{\left\{\overline{\mathbf{u}}_{\text{int}}(\xi)\right\}}_{8x1} = \underbrace{\left\{\mathbf{u}(\xi)\right\}}_{8x1} - \underbrace{\left\{\hat{\mathbf{u}}(\xi)\right\}}_{8x1} = \underbrace{\left[\mathbf{N}(\xi)\right]}_{8x24}\underset{24x1}{\left\{\mathbf{u}_L\right\}} - \underbrace{\left\{\hat{\mathbf{N}}(\xi)\right\}}_{8x12}\underset{12x1}{\left\{\hat{\mathbf{u}}_L\right\}} \qquad \textit{Eq. 21}$$

Where the symbol $\overline{\square}$ identifies relative displacements. In view of Eq. 12 and Eq. 18, the Eq. 21 may be rewrite as:

$$\underbrace{\left\{\bar{\mathbf{u}}_{\text{int}}(\xi)\right\}}_{8x1} = \underbrace{\left[\mathbf{N}(\xi)\right]}_{8x24}\underbrace{[\mathbf{A}]}_{24x24}\underbrace{\{\mathbf{d}\}}_{24x1} - \underbrace{\left[\hat{\mathbf{N}}(\xi)\right]}_{8x12}\underbrace{\left[\hat{\mathbf{A}}\right]}_{12x4}\underbrace{\left\{\hat{\mathbf{d}}\right\}}_{4x1} \qquad \textit{Eq. 22}$$

By connecting vectors $\mathbf{d}$ and $\hat{\mathbf{d}}$ in the vector $\mathbf{d}_{tot}$ as follows:

$$\underbrace{\left\{\mathbf{d}_{tot}\right\}}_{28x1} = \underbrace{\begin{Bmatrix}\mathbf{d}\\ \hat{\mathbf{d}}\end{Bmatrix}}_{(24+4)x1} \qquad \textit{Eq. 23}$$

Eq. 22 can be written as:

$$\underbrace{\left\{\bar{\mathbf{u}}_{\text{int}}(\xi)\right\}}_{8x1} = \underbrace{\underbrace{\left[\mathbf{N}(\xi)\right]}_{8x24}\underbrace{[\mathbf{A}]}_{24x24}}_{8x24}\underbrace{\{\mathbf{d}\}}_{24x1} - \underbrace{\underbrace{\left[\hat{\mathbf{N}}(\xi)\right]}_{8x12}\underbrace{\left[\hat{\mathbf{A}}\right]}_{12x4}}_{8x4}\underbrace{\left\{\hat{\mathbf{d}}\right\}}_{4x1} \qquad \textit{Eq. 24}$$

$$\underbrace{\left\{\bar{\mathbf{u}}_{\text{int}}(\xi)\right\}}_{8x1} = \underbrace{\left[\underbrace{\underbrace{\left[\mathbf{N}(\xi)\right]}_{8x24}\underbrace{[\mathbf{A}]}_{24x24}}_{8x24} \;\middle|\; -\underbrace{\underbrace{\left[\hat{\mathbf{N}}(\xi)\right]}_{8x12}\underbrace{\left[\hat{\mathbf{A}}\right]}_{12x4}}_{8x4}\right]}_{28x1}\begin{Bmatrix}\mathbf{d}\\ \hat{\mathbf{d}}\end{Bmatrix} \qquad \textit{Eq. 25}$$

and, in compact form as:

$$\underbrace{\left\{\bar{\mathbf{u}}_{\text{int}}(\xi)\right\}}_{8x1} = \underbrace{\left[\mathbf{B}_{\text{int}}(\xi)\right]}_{8x28}\underbrace{\left\{\mathbf{d}_{tot}\right\}}_{28x1} \qquad \textit{Eq. 26}$$

where

$$\underbrace{\left[\mathbf{B}_{\text{int}}(\xi)\right]}_{8x28} = \left[\underbrace{\underbrace{\left[\mathbf{N}(\xi)\right]}_{8x24}\underbrace{[\mathbf{A}]}_{24x24}}_{8x24} \;\middle|\; -\underbrace{\underbrace{\left[\hat{\mathbf{N}}(\xi)\right]}_{8x12}\underbrace{\left[\hat{\mathbf{A}}\right]}_{12x4}}_{8x4}\right] \qquad \textit{Eq. 27}$$

The two diagonal nonlinear springs control the shear response. The two springs allow only axial strain according to linear shape function as the matrix $\left[\hat{\mathbf{N}}_{dL}\left(\xi\right)\right]$ depicts in the next equations.

$$\begin{Bmatrix}\hat{u}_{\mathrm{di}}\left(\xi\right)\\ \hat{v}_{di}\left(\xi\right)\end{Bmatrix}=\begin{bmatrix}1-\xi & 0 & \xi & 0\\ 0 & 1-\xi & 0 & \xi\end{bmatrix}\begin{Bmatrix}\hat{u}_{doi}\\ \hat{v}_{doi}\\ \hat{u}_{d1i}\\ \hat{v}_{d1i}\end{Bmatrix} \qquad \textit{Eq. 28}$$

$$\underbrace{\left\{\hat{\mathbf{u}}_{di}\left(\xi\right)\right\}}_{2x1}=\underbrace{\left[\hat{\mathbf{N}}_{dL}\left(\xi\right)\right]}_{2x4}\left\{\hat{\mathbf{u}}_{dLi}\right\}_{4x1} \qquad \textit{Eq. 29}$$

For each diagonal the local degree of freedom can be related to the additional four degree of freedom as the Eq. 30 shows:

$$\left\{\hat{\mathbf{u}}_{dL_i}\right\}_{4x1}=\left[\hat{\mathbf{A}}_{di}\right]_{4x4}\left\{\hat{\mathbf{d}}\right\}_{4x1} \qquad \textit{Eq. 30}$$

The previous equations can be write for both the diagonals as below:

$$\underbrace{\left\{\hat{\mathbf{u}}_{d}\left(\xi\right)\right\}}_{4x1}=\underbrace{\left[\hat{\mathbf{N}}_{d}\left(\xi\right)\right]}_{4x8}\left\{\hat{\mathbf{u}}_{dL}\right\}_{8x1} \qquad \textit{Eq. 31}$$

$$\left\{\hat{\mathbf{u}}_{dL}\right\}_{8x1}=\left[\hat{\mathbf{A}}_{d}\right]_{8x4}\left\{\hat{\mathbf{d}}\right\}_{4x1} \qquad \textit{Eq. 32}$$

$$\underbrace{\left\{\hat{\mathbf{u}}_{d}\left(\xi\right)\right\}}_{4x1}=\underbrace{\left[\hat{\mathbf{N}}_{d}\left(\xi\right)\right]}_{4x8}\left[\hat{\mathbf{A}}_{d}\right]_{8x4}\left\{\hat{\mathbf{d}}\right\}_{4x1} \qquad \textit{Eq. 33}$$

The two relative displacements of diagonals ends can be related to the internal degrees of freedom $\hat{\mathbf{d}}$. Assuming the direction of internal

degrees of freedom always oriented according to the local reference systems of the element the elongation of the diagonal can be written as:

$$\underset{2x1}{\begin{Bmatrix} \bar{u}_{d_1} \\ \bar{u}_{d_2} \end{Bmatrix}} = \underbrace{\begin{bmatrix} -c & s & -c & s \\ c & -s & c & -s \end{bmatrix}}_{2x4} \underset{4x1}{\begin{Bmatrix} \hat{d}_1 \\ \hat{d}_2 \\ \hat{d}_3 \\ \hat{d}_4 \end{Bmatrix}} \qquad \textit{Eq. 34}$$

Where, in case of small displacements:

$$c = \frac{H}{l_{diag}} \quad ; \quad s = \frac{B}{l_{diag}} \; and \qquad \textit{Eq. 35}$$
$$l_{diag} = \sqrt{B^2 + H^2}$$

Finally, the previous equations Eq. 34 can be associated to all the degrees of freedom:

$$\underset{2x1}{\left\{\bar{\mathbf{u}}_d\right\}} = \underset{2x4}{\left[\tilde{\mathbf{B}}_d\right]} \underset{4x1}{\left\{\hat{\mathbf{d}}\right\}} \qquad \textit{Eq. 36}$$

Global kinematic relationship

Lastly, the global expression in a compact fashion is expressed by the following formula:

$$\underbrace{\left\{\bar{\mathbf{u}}(\xi)\right\}}_{10x1} = \underbrace{\left[\mathbf{B}(\xi)\right]}_{10x28} \underset{28x1}{\left\{\mathbf{d}_{tot}\right\}} \qquad \textit{Eq. 37}$$

where

$$\underbrace{\left[\mathbf{B}(\xi)\right]}_{10x28} = \underbrace{\left[\begin{array}{c|c} \underbrace{\underbrace{\left[\mathbf{N}(\xi)\right]}_{8x24}\left[\mathbf{A}\right]}_{8x24} & -\underbrace{\underbrace{\left[\hat{\mathbf{N}}(\xi)\right]}_{8x12}\left[\hat{\mathbf{A}}\right]}_{8x4} \\ \hline \underbrace{\left[\mathbf{0}\right]}_{2x24} & \underbrace{\left[\tilde{\mathbf{B}}_d\right]}_{2x4} \end{array}\right]}_{10x28} = \underbrace{\left[\begin{array}{c} \underbrace{\left[\mathbf{B}_{\text{int}1}\right]}_{2x28} \\ \underbrace{\left[\mathbf{B}_{\text{int}2}\right]}_{2x28} \\ \underbrace{\left[\mathbf{B}_{\text{int}3}\right]}_{2x28} \\ \underbrace{\left[\mathbf{B}_{\text{int}4}\right]}_{2x28} \\ \underbrace{\left[\mathbf{B}_d\right]}_{2x28} \end{array}\right]}_{10x28}$$

Eq. 38

$$\underbrace{\left[\hat{\mathbf{A}}\right]}_{12x4} = \begin{bmatrix} 1 & . & . & -1 \\ . & 1 & . & . \\ . & 1 & . & . \\ -1 & . & . & . \\ . & . & 1 & . \\ . & . & 1 & . \\ . & -1 & . & . \\ . & . & . & 1 \\ . & . & . & 1 \\ . & . & -1 & . \\ 1 & . & . & . \end{bmatrix}$$

$$[\mathbf{A}]_{24x24} = \begin{bmatrix}
1 & . & . & . & . & . & . & . & . & . & . & . & . & . & . & . & . & . & . & . & . & . & . & . \\
. & 1 & . & . & . & . & . & . & . & . & . & . & . & . & . & . & . & . & . & . & . & . & . & . \\
. & . & 1 & . & . & . & . & . & . & . & . & . & . & . & . & . & . & . & . & . & . & . & . & . \\
. & . & . & 1 & . & . & . & . & . & . & . & . & . & . & . & . & . & . & . & . & . & . & . & . \\
. & . & . & 1 & . & . & . & . & . & . & . & . & . & . & . & . & . & . & . & . & . & . & . & . \\
. & . & . & 1 & . & . & . & . & . & . & . & . & . & . & . & . & . & . & . & . & . & . & . & . \\
. & . & . & . & 1 & . & . & . & . & . & . & . & . & . & . & . & . & . & . & . & . & . & . & . \\
. & . & -1 & . & . & . & . & . & . & . & . & . & . & . & . & . & . & . & . & . & . & . & . & . \\
. & . & . & 1 & . & . & . & . & . & . & . & . & . & . & . & . & . & . & . & . & . & . & . & . \\
. & . & . & . & 1 & . & . & . & . & . & . & . & . & . & . & . & . & . & . & . & . & . & . & . \\
. & . & . & -1 & . & . & . & . & . & . & . & . & . & . & . & . & . & . & . & . & . & . & . & . \\
. & . & . & . & 1 & . & . & . & . & . & . & . & . & . & . & . & . & . & . & . & . & . & . & . \\
. & . & . & . & . & 1 & . & . & . & . & . & . & . & . & . & . & . & . & . & . & . & . & . & . \\
. & . & . & . & . & -1 & . & . & . & . & . & . & . & . & . & . & . & . & . & . & . & . & . & . \\
. & . & . & . & . & 1 & . & . & . & . & . & . & . & . & . & . & . & . & . & . & . & . & . & . \\
. & . & . & . & . & . & -1 & . & . & . & . & . & . & . & . & . & . & . & . & . & . & . & . & . \\
. & . & . & . & . & . & . & 1 & . & . & . & . & . & . & . & . & . & . & . & . & . & . & . & . \\
. & . & . & . & . & . & . & -1 & . & . & . & . & . & . & . & . & . & . & . & . & . & . & . & . \\
. & . & . & . & . & . & . & . & 1 & . & . & . & . & . & . & . & . & . & . & . & . & . & . & . \\
. & . & . & . & . & . & . & . & -1 & . & . & . & . & . & . & . & . & . & . & . & . & . & . & . \\
. & . & . & . & . & . & . & . & . & 1 & . & . & . & . & . & . & . & . & . & . & . & . & . & . \\
. & . & . & . & . & . & . & . & . & -1 & . & . & . & . & . & . & . & . & . & . & . & . & . & . \\
. & . & . & . & . & . & . & . & . & . & 1 & . & . & . & . & . & . & . & . & . & . & . & . & . \\
. & . & . & . & . & . & . & . & . & . & -1 & . & . & . & . & . & . & . & . & . & . & . & . & . \\
. & . & . & . & . & . & . & . & . & . & . & 1 & . & . & . & . & . & . & . & . & . & . & . & . \\
. & . & . & . & . & . & . & . & . & . & . & -1 & . & . & . & . & . & . & . & . & . & . & . & . \\
. & . & . & . & . & . & . & . & . & . & . & . & 1 & . & . & . & . & . & . & . & . & . & . & . \\
. & . & . & . & . & . & . & . & . & . & . & . & -1 & . & . & . & . & . & . & . & . & . & . & . \\
. & . & . & . & . & . & . & . & . & . & . & . & . & 1 & . & . & . & . & . & . & . & . & . & . \\
. & . & . & . & . & . & . & . & . & . & . & . & . & -1 & . & . & . & . & . & . & . & . & . & . \\
. & . & . & . & . & . & . & . & . & . & . & . & . & . & 1 & . & . & . & . & . & . & . & . & . \\
. & . & . & . & . & . & . & . & . & . & . & . & . & . & -1 & . & . & . & . & . & . & . & . & . \\
. & . & . & . & . & . & . & . & . & . & . & . & . & . & . & 1 & . & . & . & . & . & . & . & . \\
. & . & . & . & . & . & . & . & . & . & . & . & . & . & . & -1 & . & . & . & . & . & . & . & . \\
. & . & . & . & . & . & . & . & . & . & . & . & . & . & . & . & 1 & . & . & . & . & . & . & . \\
. & . & . & . & . & . & . & . & . & . & . & . & . & . & . & . & -1 & . & . & . & . & . & . & . \\
. & . & . & . & . & . & . & . & . & . & . & . & . & . & . & . & . & 1 & . & . & . & . & . & . \\
. & . & . & . & . & . & . & . & . & . & . & . & . & . & . & . & . & -1 & . & . & . & . & . & . \\
. & . & . & . & . & . & . & . & . & . & . & . & . & . & . & . & . & . & 1 & . & . & . & . & . \\
. & . & . & . & . & . & . & . & . & . & . & . & . & . & . & . & . & . & -1 & . & . & . & . & . \\
. & . & . & . & . & . & . & . & . & . & . & . & . & . & . & . & . & . & . & 1 & . & . & . & . \\
. & . & . & . & . & . & . & . & . & . & . & . & . & . & . & . & . & . & . & -1 & . & . & . & . \\
. & . & . & . & . & . & . & . & . & . & . & . & . & . & . & . & . & . & . & . & 1 & . & . & . \\
. & . & . & . & . & . & . & . & . & . & . & . & . & . & . & . & . & . & . & . & -1 & . & . & . \\
. & . & . & . & . & . & . & . & . & . & . & . & . & . & . & . & . & . & . & . & . & 1 & . & . \\
. & . & . & . & . & . & . & . & . & . & . & . & . & . & . & . & . & . & . & . & . & -1 & . & . \\
. & . & . & . & . & . & . & . & . & . & . & . & . & . & . & . & . & . & . & . & . & . & 1 & . \\
. & . & . & . & . & . & . & . & . & . & . & . & . & . & . & . & . & . & . & . & . & . & -1 & . \\
. & . & . & . & . & . & . & . & . & . & . & . & . & . & . & . & . & . & . & . & . & . & . & 1
\end{bmatrix}$$

4.3.2 Mechanical response

It is worth noticing that, according to the adopted macro-element [81, 65] theory, the zero thickness interfaces incorporate the deformability of the infill panel assumed as an homogeneous orthotropic medium. The flexural and sliding kinematic is associated to the interface relative displacements controlled by the interface mechanical rersponse while the shear-diagonal deformability is related to the diagonal nonlinear links. All the nonlinearities are lumped in the Gauss point of the interfaces and in the diagonal nonlinear links.

In the implementation here adopted, the interfaces have been calibrated according to a uniform distribution of Gauss points as discussed later in this Section.

This formulation is intended to represent the nonlinear elastic response of the masonry infills by following a simplified approach based on an unsymmetric constitutive law for the mechanical representation of the interfaces.

The flexural behaviour is assumed independent by the shear forces hence, any uniaxial nonlinear constitutive law can be adopted for the stress-strain relationship in the interfaces orthogonal direction.

The interfaces sliding mechanism is here ruled by an elastoplastic behaviour whose limit is controlled according a constitutive law associated to the corresponding normal action.

The shear diagonal behaviour of the infilled panels, ruled by the shear deformation of the articulated quadrilateral, has been assumed independent from the average confinement strength on the panel, as better specified in the following.

It is worth noticing that in this simplified representation the infill deformation is partly associated to the pure shear deformation of the internal panel, described by the articulated quadrilateral, and partly concentrated to the interface relative displacements representing both the membrane infill deformability and the shear sliding behaviour [88].

Standard finite element technique is used to obtain the local nodal forces **F** and the local stiffness matrix **K** at the element level.

The expressions of the internal forces can be obtained, through the virtual work equality by integrating over the four interfaces and considering the further contribution of the shear deformation of the panel (Figure 4.13) as follows:

$$W_{vi} = \underbrace{\underbrace{\sum_{i=1}^{4} \left[\underbrace{\int_{A_{interface}} \sigma \cdot \delta\varepsilon dA}_{flexural\ contribute} + \underbrace{\int_{A_{interface}} \tau \cdot \delta\gamma dA}_{sliding\ contribute} \right]}_{on\ the\ interfaces} + \underbrace{\int_{V_{infill}} \tau_d \cdot \delta\gamma dA}_{shear\ contribute}}_{total\ internal\ work}$$

Eq. 39

By integrating over the thickness of the interfaces the internal work can be written as

$$\sum_{i=1}^{4} \underbrace{\ell_i \int_0^1 \left[f_{\text{int}v_i}(\xi)\delta\Delta v_i(\xi) + f_{\text{int}u_i}(\xi)\delta\Delta u_i(\xi) \right] d\xi}_{i^{th}\ interface} + \sum_{j=1}^{2} \underbrace{f_{d_j}\delta\Delta u_{d_j}}_{j^{th}\ diagonal}$$

Eq. 40

The distribution of forces for unit length, at the generic loading step, can be related to the tangent stiffness of the interfaces as follows:

$$\begin{aligned} f_{\text{int}v_i}(\xi) &= \Delta v_i(\xi) k_{\text{int}v_i} \\ f_{\text{int}u_i}(\xi) &= \Delta u_i(\xi) k_{\text{int}u_i} \end{aligned}$$

Eq. 41

Being $k_{\text{int}v_i}$ and $k_{\text{int}u_i}$ the components of the tangent stiffness matrix of the interfaces that in this simplified formulation are assumed to be independent.

Based on Eq. 41 the following expression can be written:

$$\sum_{i=1}^{4} \ell_i \int_0^1 \left[\Delta v_i(\xi) k_{\text{int}v_i} \delta\Delta v_i(\xi) + \Delta u_i(\xi) k_{\text{int}u_i} \delta\Delta u_i(\xi) \right] d\xi + \sum_{j=1}^{2} \Delta u_{d_j} k_{d_j} \delta\Delta u_{d_j}$$

Eq. 42

In view of Eq. 28 and Eq. 34, all the displacements can be expressed in terms of the nodal displacements $\mathbf{d}$ and $\hat{\mathbf{d}}$ and Eq. 42 becomes

$$\sum_{i=1}^{4} \ell_i \int_0^1 \left[\underset{1x24}{\mathbf{d}^T} \underbrace{\mathbf{N}_{\mathbf{A}_i}^T(\xi)}_{24x2} \underset{2x2}{\mathbf{k}_{\text{int}_i}} \underset{2x24}{\mathbf{N}_{\mathbf{A}_i}} \underset{24x1}{\delta\mathbf{d}} - \underset{1x4}{\hat{\mathbf{d}}^T} \underbrace{\hat{\mathbf{N}}_{\mathbf{A}_i}^T(\xi)}_{4x2} \underset{2x2}{\mathbf{k}_{\text{int}_i}} \underset{2x4}{\hat{\mathbf{N}}_{\mathbf{A}_i}} \underset{4x1}{\delta\hat{\mathbf{d}}} \right] d\xi + \underset{1x4}{\hat{\mathbf{d}}^T} \underset{4x2}{\mathbf{N}_D^T} \underset{2x2}{\mathbf{k}_d} \underset{2x4}{\mathbf{N}_D} \underset{4x1}{\delta\hat{\mathbf{d}}}$$

Eq. 43

That, in view of Eq. 38, can be written as:

$$\sum_{i=1}^{4} \ell_i \int_0^1 \left[\underset{1x28}{\mathbf{d}_{tot}^T} \underbrace{\mathbf{B}_{\text{int}i}^T(\xi)}_{28x2} \underset{2x2}{\mathbf{k}_{\text{int}_i}} \underbrace{\mathbf{B}_{\text{int}i}(\xi)}_{2x28} \underset{28x1}{\delta\mathbf{d}_{tot}} \right] d\xi + \underset{1x28}{\mathbf{d}_{tot}^T} \underset{28x2}{\mathbf{B}_d^T} \underset{2x2}{\mathbf{K}_d} \underset{2x28}{\mathbf{B}_d} \underset{28x1}{\delta\mathbf{d}_{tot}}$$

Eq. 44

The tangent stiffness matrix is.

$$\left[\mathbf{K}_{tot}\right] = \sum_{i=1}^{4} \left[\mathbf{K}_{\text{int}_i}\right] + \left[\mathbf{K}_{D_i}\right] \qquad \textit{Eq. 45}$$

Being:

$$\left[\mathbf{K}_{\text{int}_i}\right] = \ell_i \int_0^1 \left[\underbrace{\mathbf{B}_{\text{int}i}^T(\xi)}_{28x2} \underset{2x2}{\mathbf{k}_{\text{int}_i}} \underbrace{\mathbf{B}_{\text{int}i}(\xi)}_{2x28} \right] d\xi \qquad \textit{Eq. 46}$$

$$\underset{28x2}{\left[\mathbf{K}_{D_i}\right]} = \underset{28x2}{\mathbf{B}_d^T} \underset{2x2}{\mathbf{K}_d} \underset{2x28}{\mathbf{B}_d} \qquad \textit{Eq. 47}$$

4.4 Calibration procedures

The present Section illustrates the calibration process following the same approach adopted in the software 3DMacro [83] that has been to several scientific validations [81, 65] and adopted in several seismic assessments of real unreinforced masonry buildings.

The calibration of the macro-element follows a phenomenological approach in which the interfaces governs the membrane (axial/flexural) and shear-sliding behaviour while the diagonal links rules the internal shear deformability.

4.4.1 Axial/Flexural calibration

The flexural and axial failure are governed by the orthogonal reactions in the interfaces.

An appropriate cyclic material model has been adopted in ADAPTIC aiming to simulate the asymmetric tension-compression behaviour. Namely the STMD147 model, depicted in Figure 4.17, has been used.

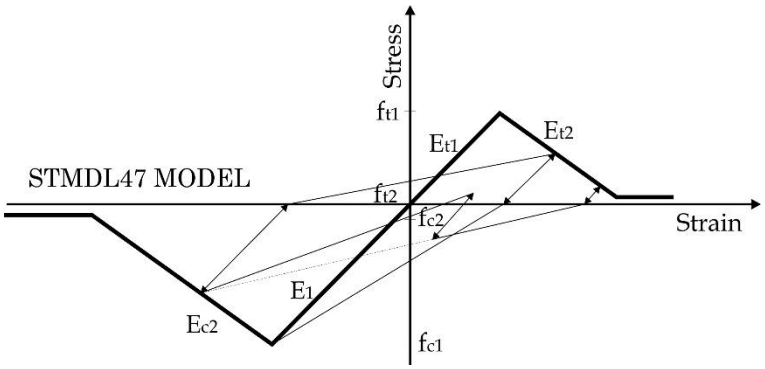

Figure 4.17 STMDL47 Cyclic material model

The following parameters have to be specified in the DAT file in terms of material characteristics.

E_1	Initial Tensile/Compression Tangent Modulus
f_{t1}	Tensile limit strength
E_{t2}	Tensile softening modulus (Based on fracture energy)
f_{c1}	Compressive limit strength

E_{c2} Compression softening modulus (Based on ductility)
f_{t2} Residual Tensile strength
f_{c2} Residual Compressive strength

In this thesis the calibration procedure have been based on the approach introduced by Caliò et al. [81, 65] for the discrete formulation of the plane macro-element. The orthogonal stress-strain relationship in each regular distribution of Gauss points on the interfaces simulates the axial stiffness and strength of the pertinent panel's fibre, as reported in Figure 4.18. According to this simplified fibre approach the panel in divided in several strips (fibres) according to the number of Gauss points and the calibration of the mechanical parameters of the material model is consistent to the adopted discretization.

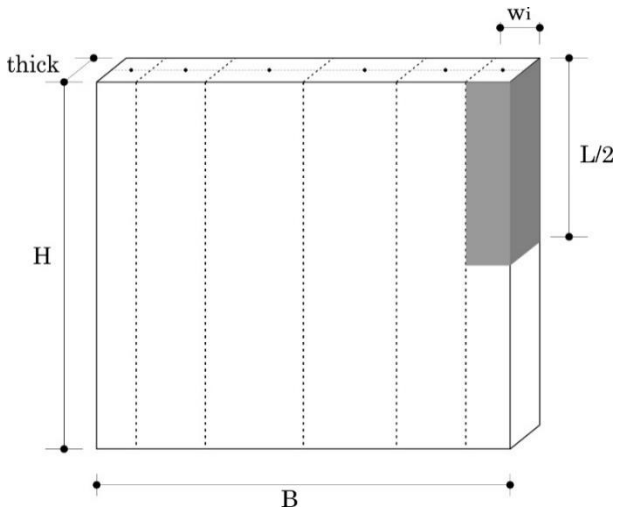

Figure 4.18 Schematic representation of the fibre discretisation

Figure 4.18 shows the fibre approach in case of vertical discretization. The calibration of the vertical interfaces, corresponding to horizontal fibres, follows the same strategy. It is worth noticing that the vertical and horizontal discretization may be different and they are considered independent.

In the follow the initial linear elastic stiffnesses and the limit forces corresponding to the each fibre are reported.

$$K_i = \frac{thick \cdot \omega_i \cdot E}{0.5 \cdot H} \qquad \textit{Eq. 48}$$

$$F_{t1_i} = thick \cdot \omega_i \cdot f_{t1} \qquad \textit{Eq. 49}$$

$$K_{t2_i} = \frac{thick \cdot \omega_i \cdot E_{t2}}{0.5 \cdot H} \qquad \textit{Eq. 50}$$

$$F_{c1_i} = thick \cdot \omega_i \cdot f_{c1} \qquad \textit{Eq. 51}$$

$$K_{c2_i} = \frac{thick \cdot \omega_i \cdot E_{c2}}{0.5 \cdot H} \qquad \textit{Eq. 52}$$

Being for each fibre:

thick	The panel thickness:
ω_i	The Gauss point weight times length of the corresponding edge;
H	The panel height;
E	The tangent elastic modulus, namely E1 and Et1 in Figure 4.17;
E_{c2}	Compression softening modulus (Based on ductility)
E_{t2}	Tensile softening modulus (Based on fracture energy)
K_i	The initial tangent fibre stiffness
$K_{t2\,i}$	The tensile softening fibre stiffness
$K_{c2\,i}$	The compressive softening fibre stiffness
$F_{t1\,i}$	The tensile limit force
$F_{c1\,i}$	The compressive limit force

4.4.2 Sliding Calibration

As before discussed, the interfaces simulate the shear-sliding failure mechanisms on all the four element edges. A Mohr-Coulomb cohesive constitutive law has been engaged and the cyclic stress-strain STL1 (Figure 4.19) model have been used. In particular, sliding occurs when

the force in the Gauss point reaches the limit value (plastic branch in the model).

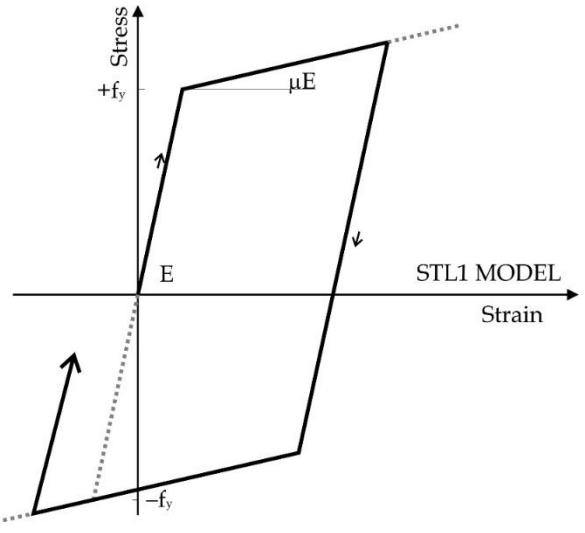

Figure 4.19: ADAPTIC STL1 model and model material parameters.

It is worth specifying that the following parameters have to be inserted in the DAT file in terms of material characteristics.

E_s	Sliding Elastic Modulus
c_s	Sliding Cohesion
μ_s	Sliding friction coefficient
E_{sm}	Sliding post peak modulus (μE in Figure 4.19)

The masonry mechanical behaviour is characterised by the cohesion (c_s) and the sliding friction coefficient (μ_s). The panel orthotropic behaviour is accounted, in a simplified way, by the independency of the vertical and horizontal material parameters, as before discussed for the orthogonal interface components. Furthermore, the limit of the sliding shear component is defined by:

$$\tau_{\lim i} = c_i + \mu_{si} \cdot f_{G0i} \qquad \textit{Eq. 53}$$

The subscript i is related to the vertical or horizontal interfaces and the i^{th} Gauss point. The Eq. 53 can be rewritten in terms of force by

multiplying c_i times the fibre cross section and the following equation is obtained:

$$T_{ui} = c_i \cdot thick \cdot \omega_i \cdot + \mu_{si} \cdot f_{G0i} \cdot thick \cdot \omega_i \qquad \textit{Eq. 54}$$

The value of $f_{G0i} \cdot thick \cdot \omega_i$ represents the average vertical force on the i^{th} fibre at the last converged step.

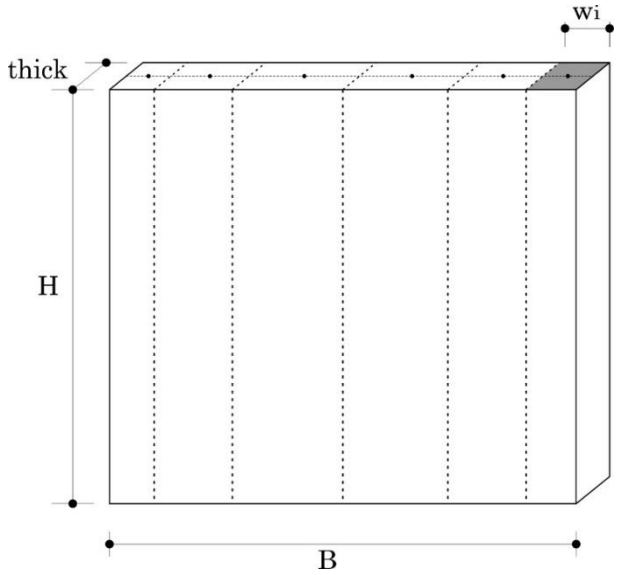

Figure 4.20 Representation of the fibre discretisation and sliding calibration

4.4.3 Shear diagonal behaviour

The inelastic model of the two internal diagonal "springs" controls the shear diagonal failure. A Mohr Coulomb law, characterised by specific parameters, has been adopted also for the shear diagonal response of the panel. The parameters that have to be defined in the DAT file are the following:

E_d	Shear Elastic Modulus (G)
c_d	Shear Cohesion (c)
μ_d	Shear Poisson's coefficient
E_{dm}	Shear Softening Modulus (Bases on fracture energy)

The calibration of the diagonal spring in the initial elastic range is obtained by engaging the elastic equivalence between the internal quadrilateral element and the homogenised masonry panel as proposed by Caliò et al. [81]. In this case, the following equation defines the displacement in the homogenous panel.

$$\delta = \frac{V}{G \cdot A_t} h \qquad \textit{Eq. 55}$$

As the Figure 4.21 shows, the Eq. 55 engages the pure shear force V, the homogenised elastic shear modulus G, the transversal section A_t and the panel height h. The horizontal (or vertical) displacement of the pure shear deformation is defined δ.

While the pure shear displacement in the macro-element representation is:

$$\delta = \frac{V}{2 \cdot \cos^2 \alpha \cdot K_{diag}} \qquad \textit{Eq. 56}$$

The Eq. 56 engages the initial elastic diagonal stiffness of each link K_{diag} and the angle between the diagonal and the vertical axes α all the other symbols have the abovementioned meaning . It is worth adding that α=arctan(b/h). By comparing the two values, the K_{diag} is obtained as:

$$K_{diag} = \frac{G \cdot A_t}{2 \cdot h \cdot \cos^2 \alpha} \qquad \textit{Eq. 57}$$

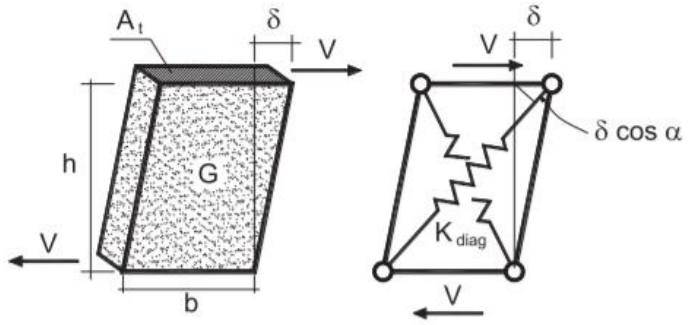

Figure 4.21 Homogenised equivalence for the shear springs calibration [65]

The ultimate displacement value of each diagonal spring can be derived by the knowledge of the mechanical material properties of the masonry by means of the adopted shear resistance criteria [65]. On the other hand, the shear displacement limit can be considered in terms of fracture energy. Due to this aim, the advanced material model STMD147 considers softening rules and a more reliable shear behaviour can be simulated.

The material model STMDL47, reported inFigure 4.22, has been adopted. The following assumptions have been introduced in the algorithm for considering a symmetric tension-compression behaviour of the two shear springs. The tensile and compressive elastic moduli E1 and Et1 have been considered equal each one other. The limit strength ft1has been considered equal to fc1. The residual values, ft2 and fc2, have been assumed equal to zero. The shear softening modulus is assume identical in tension and compression.

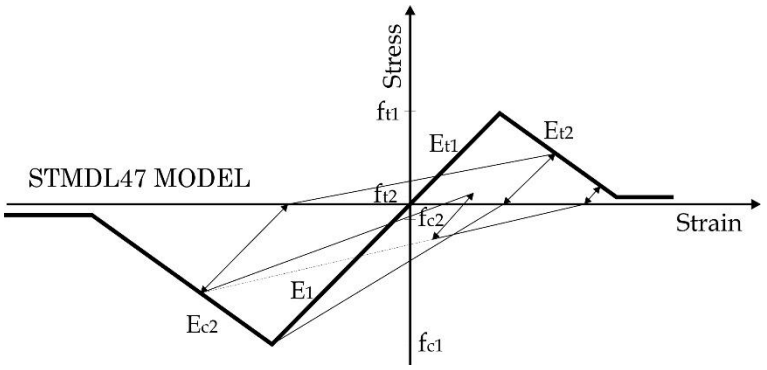

Figure 4.22 STMDL47 Cyclic material model

According to this model the defined mechanical properties are adapted as follows:

$$E_1 = E_{t1} = G \qquad \textit{Eq. 58}$$

$$f_{t1} = f_{c1} = f_{v0} = 0.5 \cdot (c_d + miu_d s_{dt}) \qquad \textit{Eq. 59}$$

$$f_{t2} = f_{c2} = 0 \qquad \textit{Eq. 60}$$

$$E_{t2} = E_{c2} = E_{dm} \qquad \textit{Eq. 61}$$

4.5 Reliability of the proposed Macro-Element

Numerical simulations of experimental tests in which in scale specimens have been adopted to simulate the seismic behaviour of infilled frame structures and column loss scenarios have achieved the dependability of the implemented macroelement. As authors noted in their researches [49], the pros and cons of infill walls on progressive collapse are not completely defined and clear very limited data are available for studying and investigating accurately the contribute of the brick clay infills walls. On the other hand, the proposed finite element represents a powerful tool to account for the infill frame contribute in the nonlinear analysis and particularly for seismic and progressive collapse responses of real structures.

As in the Section 3.2 has been documented, several experimental tests, for progressive collapse investigations, have been performed on scaled frame structures and only in rare cases on full-scale specimens. The number of experimental tests that considered concrete frames and unreinforced masonry walls is still negligible. A recent experimental campaign aimed to evaluate accurately the behaviour and the consequent contribute of infill frames in concrete frame structures was recentely conducted by Shaung Li in 2016 [49, 50]. This campaign was focused

on a one-third scaled specimen. The model was a two-storey, four-bay concrete frame structure and it aimed at investigating the response of a concrete frame structure in a column loss scenario in three different configurations: bare frame, full height infill walls and infill walls with openings. All the reinforced concrete frames had similar geometric and mechanical properties.

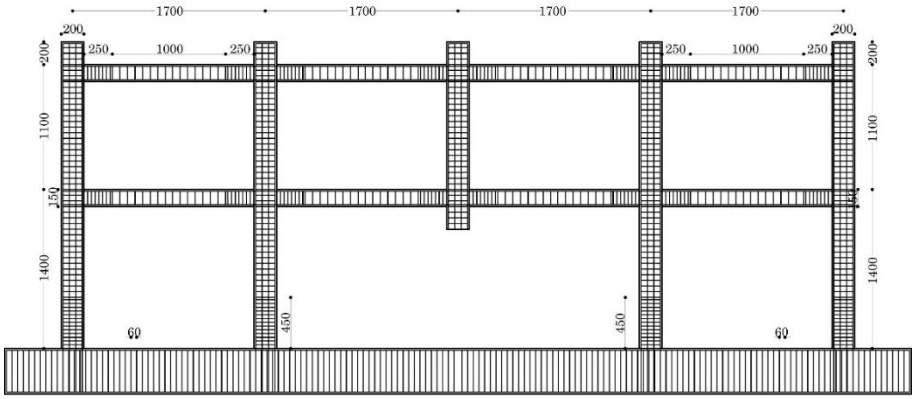

Figure 4.23 Bare Frame Model

The authors tested the bare frame structure firstly without infill panels. The bare frame had a comparison purpose. As the authors noticed, the frame experienced three main phases. Firstly, elastic behaviour defined the structural response under the incremental concentrated load. The elastic phase ended in the early stages and it was followed by a second branch dominated by arch effects. This phase ended at 204.5 mm when the beams of the two spans went in the catenary effect. During the two last phases several cracks formed near the beams end in which plastic hinges occurred. In agreement with the collapse shapes that have been discussed in the previous chapters, the uniform distribution of reinforcement bars led to plastic hinges at the ends of each involved beam (Figure 4.24).

The first reinforcement bar failure occurred at 317.1 mm.

Figure 4.24 (Colour) Collapse shape of the bare frame specimen [49]

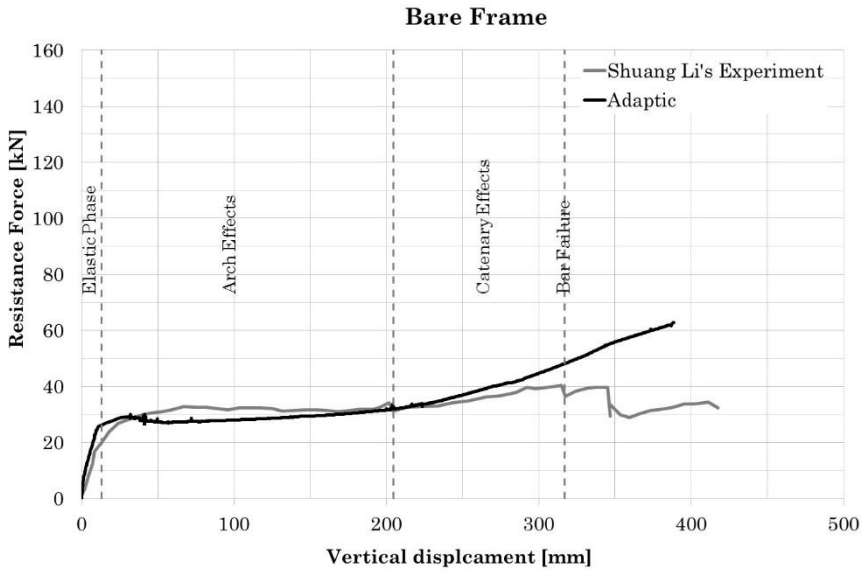

Figure 4.25 Bare Frame Response curve

Figure 4.25 shows the superposition of the experimental response and the numerical result here obtained. The numerical bare model has been developed for comparison and validation purposes. A very good agreement has been obtained by superimposing the two curves, as the figure shows. Three different branch have been noticed in the numerical model as well as in the experimental behaviour. On the other hand, a

minor difference has been noticed in the initial elastic phase. In this light, the experimental model curve has been affected by a more evident stiffness reduction probably due to imperfections. Lastly, the numerical model does not take explicitly into account fragile rapture and reinforcement failure and this determinates the absence of resistance drop.

The experimental campaign investigated also the collapse robustness of the bare frame filled with unreinforced masonry walls. The authors developed two specimens, with openings (Figure 4.26A) and without openings (Figure 4.26B).

For simplicity, the geometric properties of the two structural elements are summarised in a unique Figure 4.27.

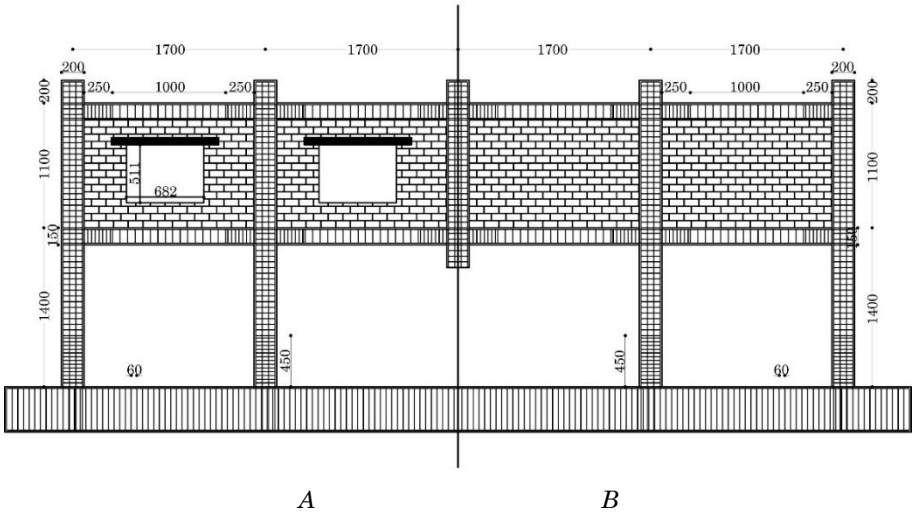

Figure 4.26 Infilled Frame Models synthetic description: left side, specimen with openings [50]; right side, specimen with full eight walls [49]

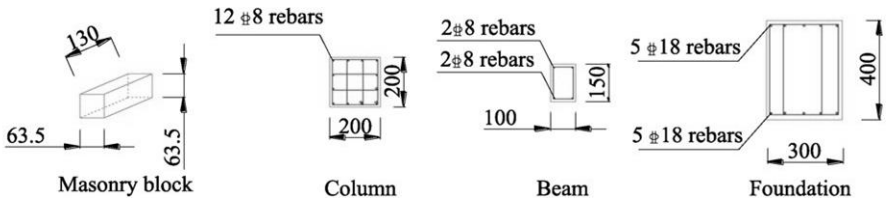

Figure 4.27 Structural cross-sections and bricks dimensions [49].

During the experimental test on the full-height infill frame, different crack pattern affected the two collapsed bays. Probably due to differences in the mechanical material properties, bricks layout and construction quality, the two patterns determinated an asymmetric structural response and two sudden resistance degrade. Figure 4.28 shows the experimental curves of bare and full-height infill frame. In the diagram, vertical lines underline the main failures. The major cracks developed at 20.3 mm and a continuous degrade affected the curve up to the displacement of 367.50 mm. The specimen noticed several sudden resistance falls due to masonry (20 mm), beams (90 mm) and bars (143.4 mm) failures.

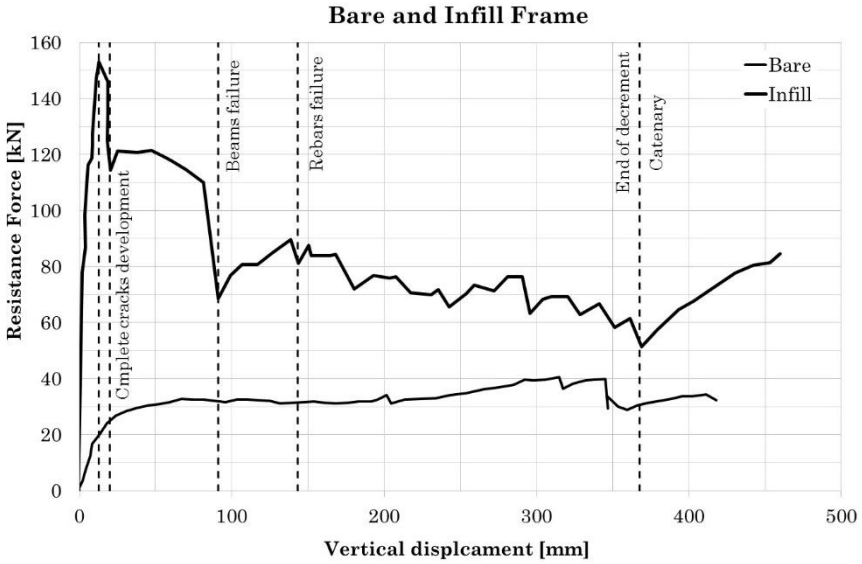

Figure 4.28 Full-height Infill Frame structural response

Different levels of sophistication has been engaged in terms of panel discretisation and parametric analyses have been performed aiming to investigate the model dependence from the principal parameters. Figure 4.29 schematises the numerical model and the macroelement discretization is represented. An *ad hoc* routine has been developed for introducing the macroelement with the sougtht discretisation.

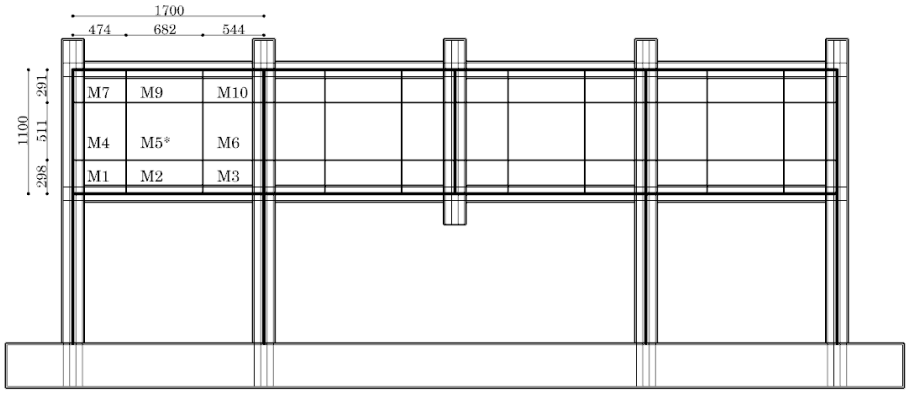

Figure 4.29 Scheme of the FEM model

4.5.1 Parametric analysis

Aiming at evaluating the influence of fundamental material parameters on the collapse behaviour of the specimens a sensitivity analysis with respect to some significative parameters has been performed. The parametric investigation has been focused on the material properties that have influenced the post peak behaviour or have defined an unrealistic ductile response.

Only the mechanical parameters of the masonry infills have been taken into account.

- Shear Softening Modulus (E_{dm})

The performed analyses had shown a great influence on the choice of the softening shear modulus of masonry infills, whose actual response is relatively fragile [89]. Three values of the softening shear modulus have been assumed as reported in Table 4-1, the first value corresponds to the almost perfect ductile response of the infill panels. Figure 4.30 shows the comparison between the numerical results and the experiments.

The values, expressed in MPa, are summarised in Table 4-1.

Table 4-1 Variation of softening shear modulus

E_{dm} [MPa]	E_{dm} [MPa]	E_{dm} [MPa]
0.01	50	100

As the figure depicts, the unlimited ductile case (dot curve) strongly overestimates the actual structural robustness leading to hardening behaviour. The other two considered cases show a good agreement with the experimental results as can better recognised form.

Figure 4.31 that reports in more details the three obtained curves around the peak value.

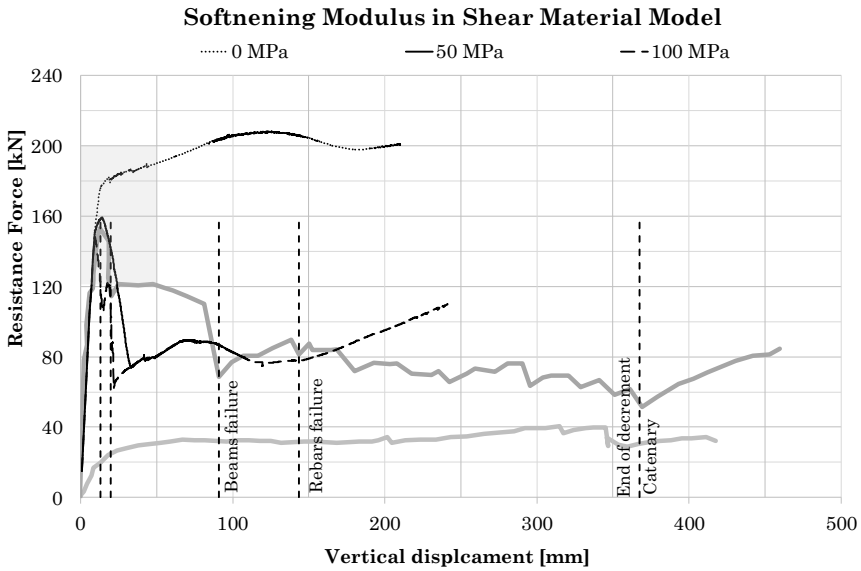

Figure 4.30 Influence of the Shear Model Softening Modulus

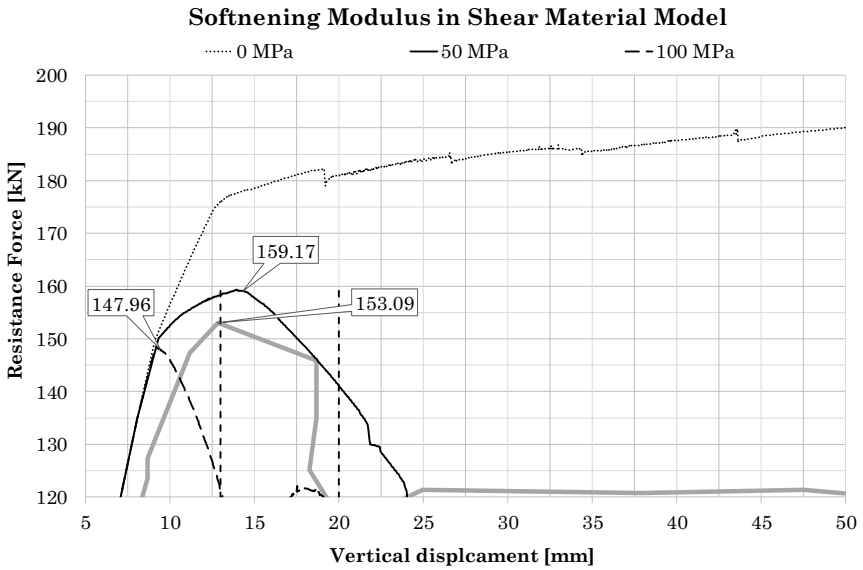

Figure 4.31 Detail of the diagram on the Influence of the Shear Model Softening Modulus

- Shear ultimate strength (f_{v0})

A further parameter that strongly influences the numerical response is the ultimate shear strength of the masonry infill panels.

Three very different values, as reported in Table 4-2, have been considered. The results are reported in Figure 4.32 and in more detail in Figure 4.33. It can be observed how the shear resistance of the infills strongly increases the peak resistance of the structure but leads to a post-peak fragile response.

Table 4-2 Variation of shear ultimate strength

f_{v0} [MPa]	f_{v0} [MPa]	f_{v0} [MPa]
1.00	5.00	100.00

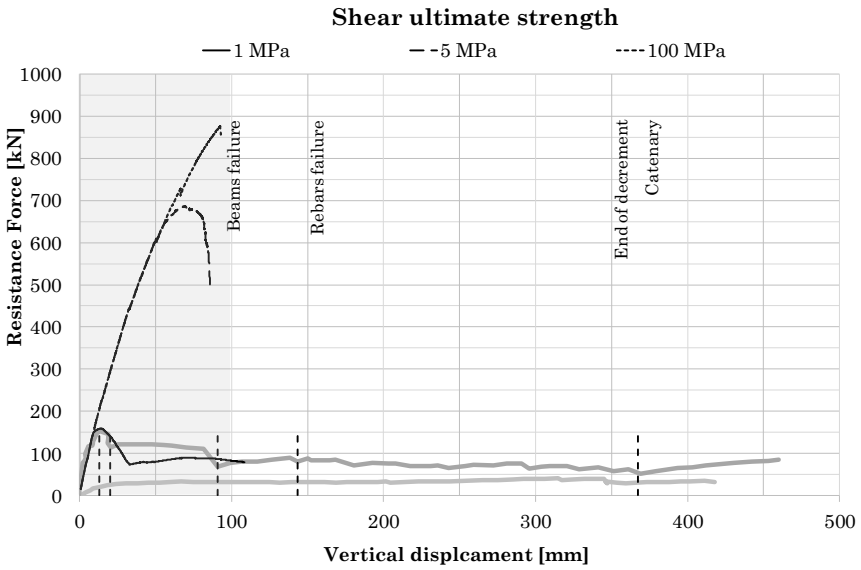

Figure 4.32 Influence of the Shear Ultimate Strength

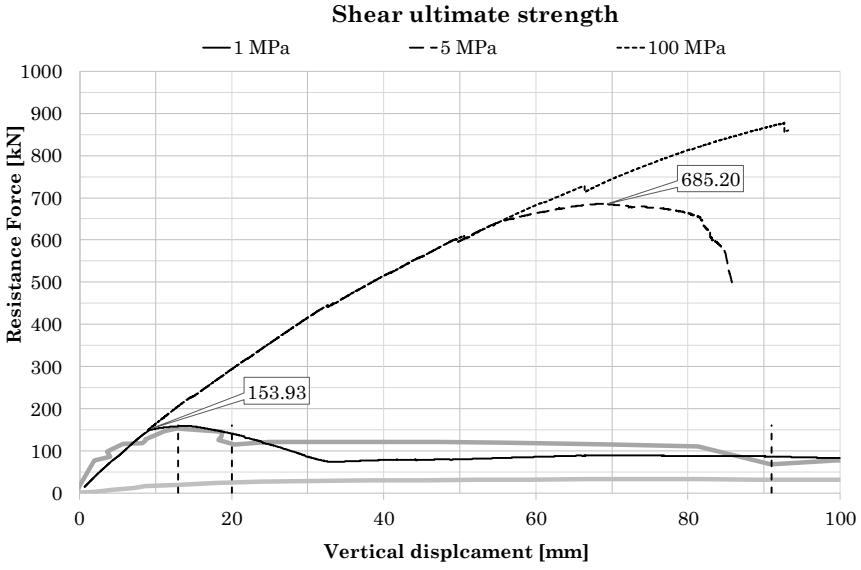

Figure 4.33 Detail of the diagram on the Influence of the Shear Ultimate Strength

- Tensile Softening modulus of the axial/flexural infill panel interfaces

In this sub-paragraph the influence of the tensile softening modulus of the masonry infill interfacesis investigated. Three values, as reported in Table 4-3 have been considered ranging from the fragile to the ductile behaviour.

Table 4-3 Variation of tensile softening modulus

E_{t2} [MPa]	E_{t2} [MPa]	E_{t2} [MPa]
6	600	6000

As the Figure 4.34 shows, minor differences have been obtained. Figure 4.35 details the numerical curves in the early stages, up to the displacement of 50 mm. This figure shows a detail of the curve around the peak value and only post peak minor differences are notable. It is worth noticing that the tensile strength is 0.6MPa and, as the figures shows, a higher value of fracture energy do not substantially modify the collapse response but, on the other hand, give more stability to the convergence.

The values, expressed in MPa, are summarised in Table 4-3.

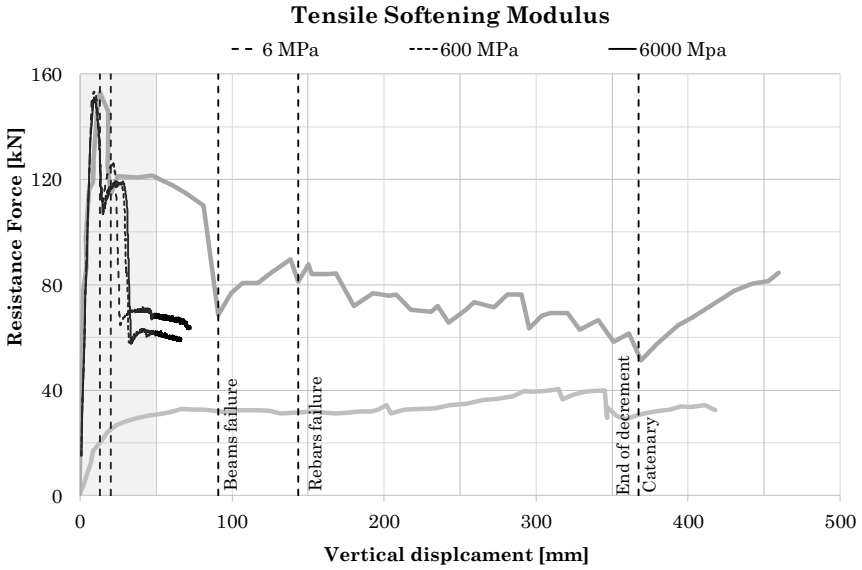

Figure 4.34 Influence of Tensile Softening Modulus

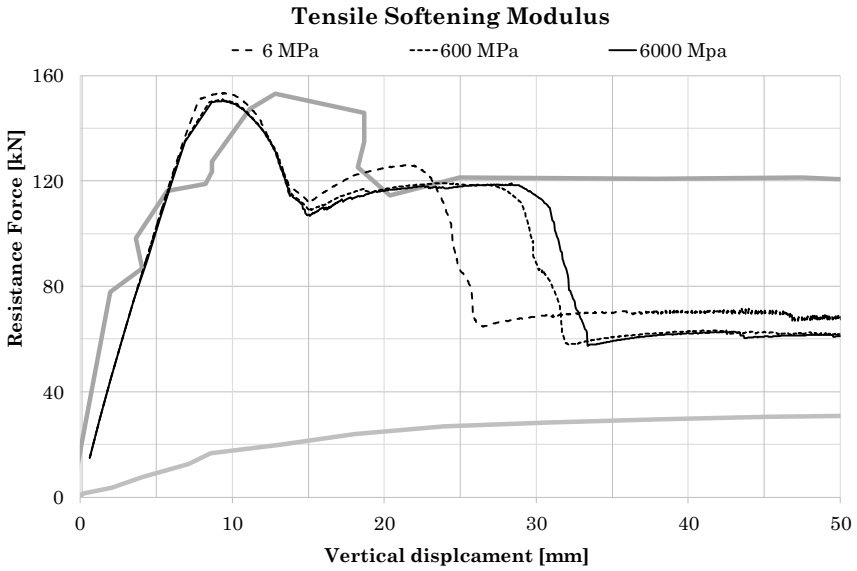

Figure 4.35 Detail of the Influence of Tensile Softening Modulus

- Sliding Shear Strength of the masonry panel

This sub-section exposes the influence of the sliding shear strength ultimate value in the masonry interfaces. The Table 4-4 contains the values that have been considered. It is worth noticing that the specimen did not show sliding failures in the masonry-concrete frame interfaces. On the other hand, sliding failures may occur in the internal mortar bed horizontal bed joints. Due to that, the sliding shear strength can influence the collapse behaviour as the Figure 4.36 depicts.

Table 4-4 Variation of sliding shear strength

τ_{lim} [Mpa]	τ_{lim} [Mpa]	τ_{lim} [Mpa]
1	2	10

Figure 4.36 shows the structural response for each of the sliding shear strengths that have been reported and more in detail in Figure 4.37. The peak values are not affected by the analysed parameter. The value of 10MPa that represents an almost elastic behaviour of the sliding interfaces does not affect the initial peak but improve convergence.

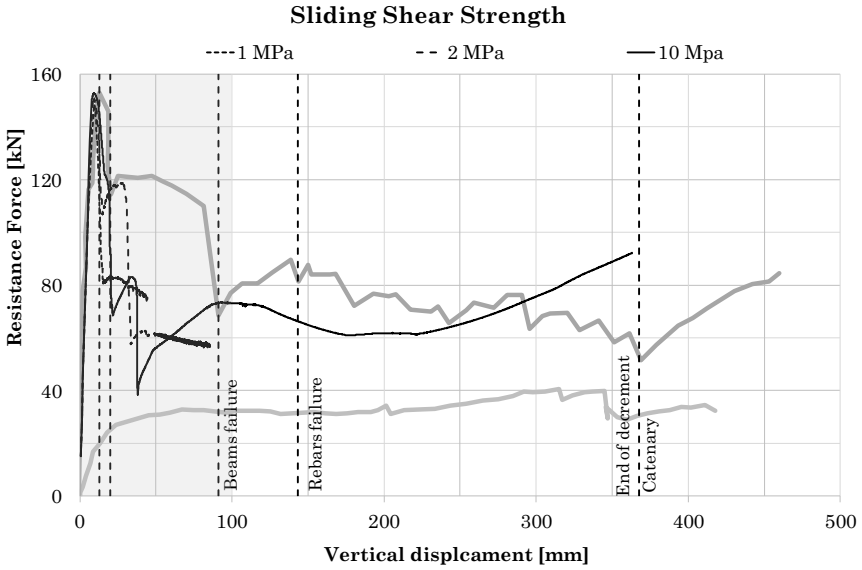

Figure 4.36 Influence of Sliding Ultimate Strength

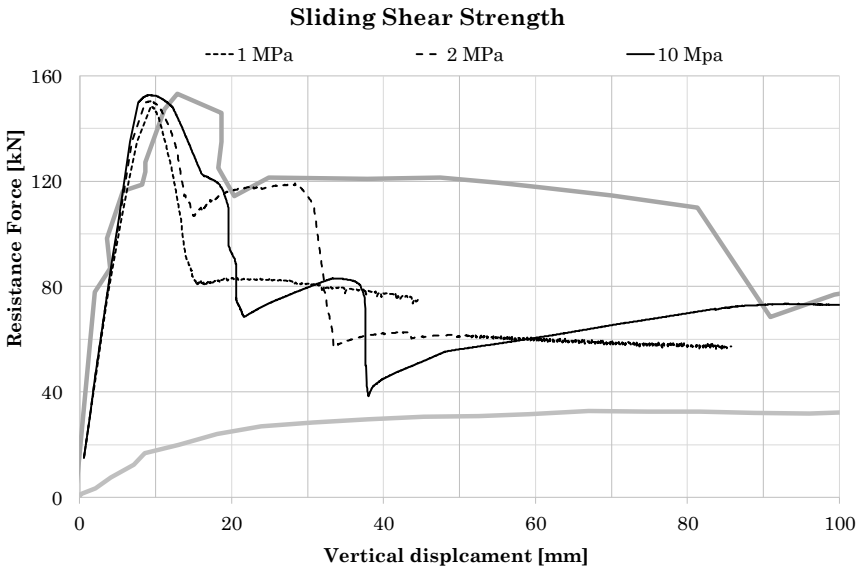

Figure 4.37 Detail of the diagram on the Influence of Sliding Ultimate Strength

- Sliding Elastic Modulus in the masonry panel interfaces (Es)

Lastly, this section considers the influence of the sliding initial elastic modulus. Three values have been considered for evaluating the influence on the global response. Table 4-5 reports the three considered elastic modulus values. The parameter increment reduces the sliding between masonry panel and concrete frames and between contiguous masonry panels.

Table 4-5 Variation of sliding elastic modulus

Es [Mpa]	Es [Mpa]	Es [Mpa]
10	100	200

The Figure 4.38 reports the results in the three analysed cases. Apparently, the sliding elastic modulus does not have influence on the capacity peak value. It is worth noticing that this elastic parameter affects the position of the plastic section, namely plastic hinges (Figure 4.41), and the shear failures for beams. This effect has consequence on the collapse shape as the two pictures in the diagram depict below.

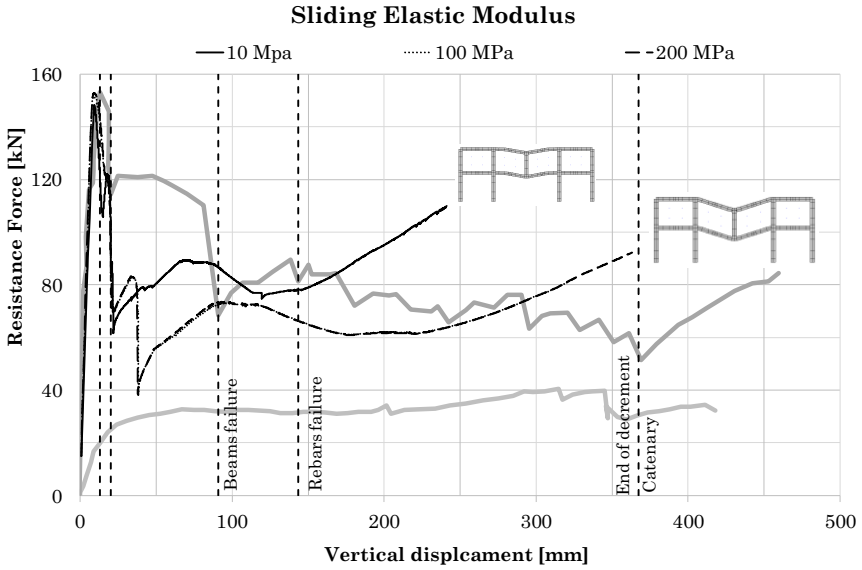

Figure 4.38 Influence of Sliding Elastic Modulus

- Mesh dependence in the infill panel subdivision

The subdivision of the infill panel has been increased from 9 to 35 macroelements for evaluating the mesh dependency (Figure 4.40). The analyses have been performed with three different sliding shear strength values (2 MPa, 10MPa, 200 MPa).

As the Figure 4.39 shows, the peak values have been correctly identified and the results were not influenced by sliding shear strength and infill panel discretization. On the other hand, the infill panel subdivision increased the computational effort and incurred in convergence issues.

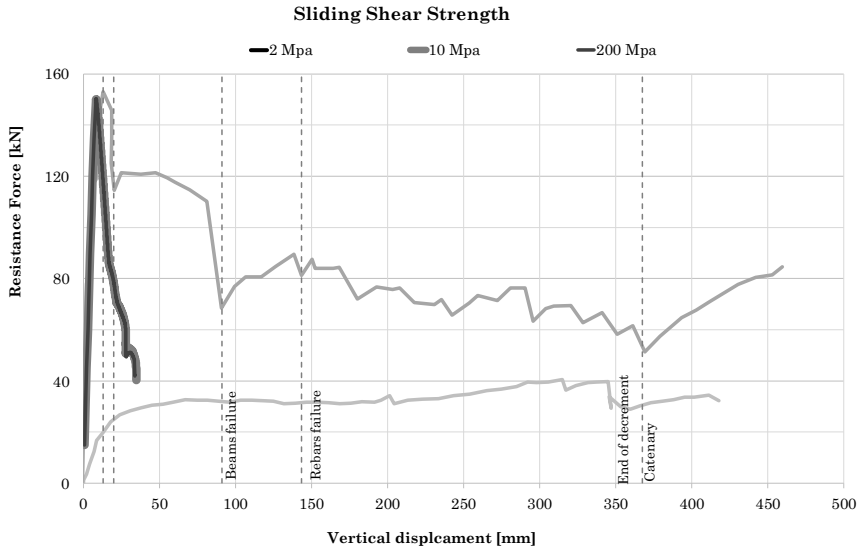

Figure 4.39 Parametric analysis on high subdivided panels

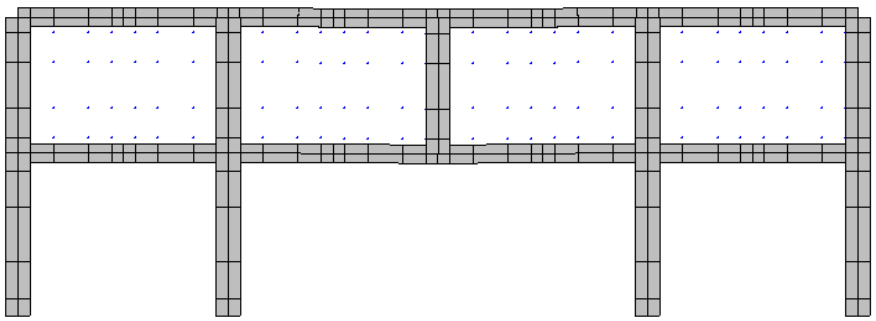

Figure 4.40 Numerical Model with 45 macroelements for each infilled panel

The parametric analysis demonstrated that the proposed numerical model interacts opportunely with the surrounding concrete elements and influence these concrete frames in terms of collapse shape and robustness capacity. The subdivision of each infills in nine sub-macro elements (Figure 4.41) has been considered suitable for the numerical simulation of the experimental test by balancing accuracy and computational demand.

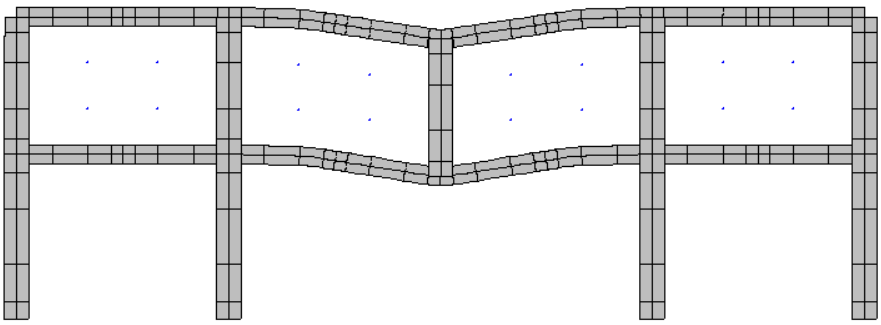

Figure 4.41 Numerical simulation of the full-height infill frame test.

4.5.2 Numerical validation of the implemented macro-element

The present sub-section compares the response of an infill frame model in ADAPTIC that incorporates the proposed macroelement with the identical model implemented in the commercial software 3DMacro [83] in which the macroelement has been originally implemented [65, 81]. The purpose of the subsection has been obtained by investigating two different geometric models. The two models have identical mechanical properties but different geometric ratios:

I. MODEL A: b=5 m; h=3m;
II. MODEL B: b=5 m; h=6m.

The dependency on mesh ratio and panel subdivision of the original macroelement have been already investigated by other authors [82].

Only the masonry mechanical nonlinearity has been taken into account in the two models and an elastic homogeneous frame has been adopted. The beam-column elements have a 30x30 cm square section element. The panel is 25cm thick.

The Table 4-6 summarises the main material properties in which the frame material is defined by the elastic modulus only.

Table 4-6 Materials properties

panel	E	600	MPa
	G	200	MPa
	f_m	2.4	MPa
	τ_0	0.25	MPa
	ρ	~0	N/mm^3
frame	E_{frame}	27386	MPa

Figure 4.42 shows the pushover capacity curves of the Model A. The two lines present a satisfactory agreement up to a lateral displacement of 5mm. The same figure reports the deformed shape of the 3DMacro model. All the macroelements reach the elastic shear limit.

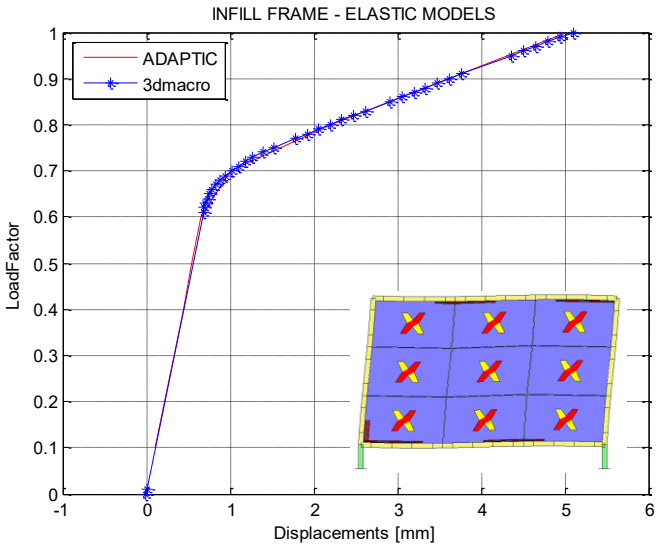

Figure 4.42 (Colour) MODEL A – PushOver Capacity curves

Figure 4.43 depicts the pushover capacity curves of the two models. As the figure shows, a good agreement is still notable in this model up to 25 mm. The satisfactory result demonstrates that the ADAPTIC model is not affected by geometric ratio dependency.

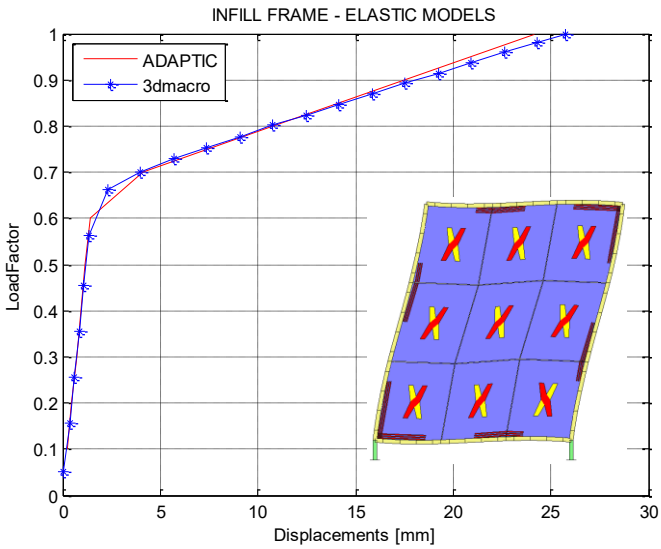

Figure 4.43 (Colour) MODEL B – PushOver Capacity curves.

CHAPTER 5.
SEISMIC VULNERABILITY PARAMETRIC ANALYSES

The Chapter describes the case study and reports code-consistent parametric evaluation of seismic vulnerability of low- and mid-rise reinforced concrete buildings. The case study has been defined according to a simulated design process in collaboration with a research group of the University of Catania [88]. The design process has been based on the study of several examples of existing residential buildings built in Catania between the 60's and 80's of the last century. The structural design is consistent with the Italian structural code that was mandatory in those decades in Italy. In this preliminary evaluation, only pushover analyses have been performed by means of the code 3DMacro, that allows a reliable model of the infilled non-structural elements modelled as plane macro-elements interacting with the surrounding nonlinear frames. Moreover, the design project based on gravity loads only, has allowed a simple identification of a total of nine typical buildings obtained by progressively reducing the number of storeys from the initial ten-storey building until the lower two-storey one. The results have been expressed for different soil conditions according to the Euro-Code spectra provisions and to the Italian 2008 technical code. Each prototype has been fully discussed in terms of collapse scenario and seismic capacity. Aiming at identifying the non-structural elements role all the analyses have been performed with and without the non-structural infills contribution.

5.1 Introduction

The Italian seismic code became mandatory for all the national territory only in 1984, however the main urban expansion in Italy occurred between the 60's and 80's. As a consequence, a great percentage of existing buildings although designed for gravity and wind loadings are highly exposed to earthquake actions Figure 5.1.

The main goal of ANCE Catania project is to deeply investigate the seismic vulnerability of existing buildings not designed to resist to earthquakes and to identify possible retrofitting solutions with particular attention to reinforced concrete structures. To this aim the attention will be focused on a typical building layout, that can be considered representative of many similar buildings built in Catania before the introduction of the seismic code prescriptions.

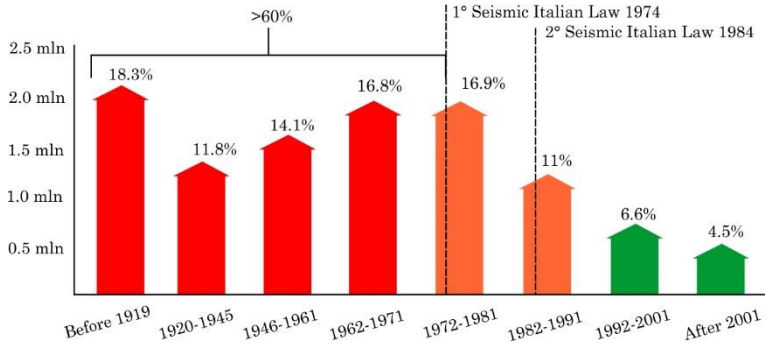

Figure 5.1 (Colour) CRESME 2012 based on ISTAT data in ITALY

In order to identify the prototype structure a survey on several reinforced concrete residential buildings built in Catania between the 60's and 80's has been conducted. Many design drawings of RC structures have been collected and some structural engineers, that were active at that time, have been consulted. Based on the acquired information, the design practice has been recreated in terms mechanical properties of materials, structural detailing, architectural characters and construction strategies.

5.2 The typical building

The collected information from several engineers architects and builders, the available original structural and architectural drawings, the adopted structural design regulation [90, 91] and several in situ inspections allowed to identify the main structural and architectural characteristics of the reinforced concrete buildings built in Catania before the introduction of the seismic code. This survey has been conducted with the synergetic collaboration of the Prof. A. Ghersi research group and the results are summarised in a specific Section of the more general work "ANCE|Catania Project 2016" [88].

, The selected case study is a ten-storey RC framed residential building. The model has a rectangular plan (31.80m x 13.80m) and a symmetry axis with respect to the shorter direction. The columns have a centreline distance of 4.5 meters in both directions. The first storey is 4.30 meter high and all the superior storeys are 3.30 meters high. Four planar RC frames compose the structural layout.

As several buildings built in those decades, a unique structural floor typology has been defined. The hypothesis of "gravity loads only" defines equal Bending Moments and Shear Forces at each floor. A tributary area loads have been used for designing the columns. The cross section optimisation has determinated a decrement of the column cross-sections from the base floor to the top-floor. Table 5-1 reports all the column sections.

The floor system consists in on-way RC ribbed slabs spanning orthogonally to the four frames.

Figure 5.2 shows the plan of the generic floor and depicts the structural plan in which the ribs direction, the concrete columns orientation and the beams types are notable. On the other hand, Figure 5.2.b shows the architectonic plan. The bolder black lines represent the infilled panels that contribute to the structural response of the framed structure because those are placed on the beams and consequently in the frames planes.

The half-turn stairs are longitudinally supported by beams at the outside edges of the landings and are unsupported at the sides. The stairs

slab is 15 cm thick. Figure 5.3 gives a three dimensional representation of the framed structure.

Table 5-1 Columns cross-sections

Storey	1-8-25-32	2-7	3-6	4-5	9-16-17-24	10-15	11-14	12-13	18-23	20-21	19-22	26-31	27-30	28-29
10	30x30	30x30	30x30	30x30	30x30	30x30	30x30	30x30	30x30	30x30	30x30	30x30	30x30	30x30
9	30x30	30x30	30x30	30x30	30x30	30x30	30x30	30x30	30x30	30x30	30x30	30x30	30x30	30x30
8	30x30	30x30	30x40	30x30	30x30	30x30	30x30	30x40	30x40	30x40	30x40	30x40	30x30	30x30
7	30x40	30x40	30x50	30x40	30x40	30x40	30x40	30x50	30x50	30x50	30x50	30x50	30x40	30x40
6	30x50	30x50	30x60	30x50	30x50	30x60	30x50	30x60	30x60	30x60	30x60	30x60	30x50	30x40
5	30x60	30x60	30x70	30x60	30x60	30x70	30x60	30x70	30x70	30x70	30x70	30x70	30x60	30x50
4	30x70	30x70	30x80	30x70	30x70	30x80	30x70	40x80	30x80	30x80	30x80	30x80	30x70	30x60
3	30x80	30x80	40x80	30x80	30x80	40x80	30x80	40x80	40x80	40x80	40x80	40x80	30x80	30x70
2	30x80	40x80	40x80	40x80	40x80	40x80	40x80	40x80	40x80	40x80	40x80	40x80	40x80	30x80
1	40x80	40x80	40x90	40x80	40x80	40x80	40x80	40x90	40x90	40x90	40x90	40x80	40x80	30x80

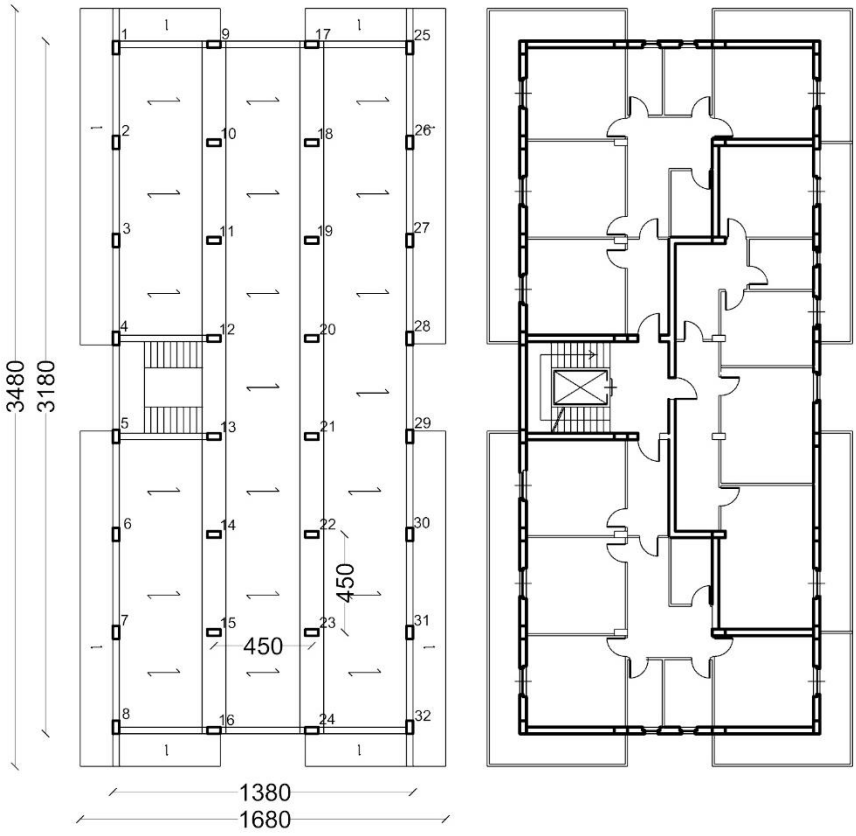

(a) *(b)*

Figure 5.2 Generic architectural (a) and structural (b) plan of the case study.

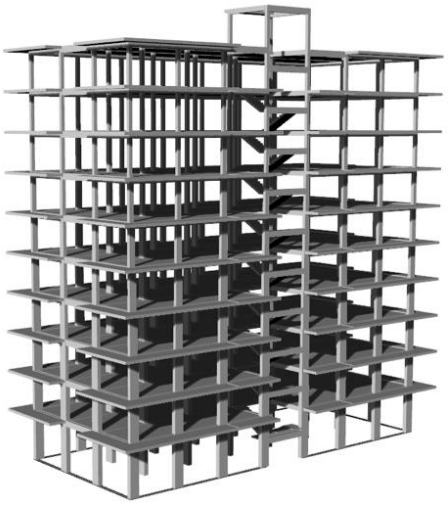

Figure 5.3 A three-dimensional view of the frame structure of the designed typical building.

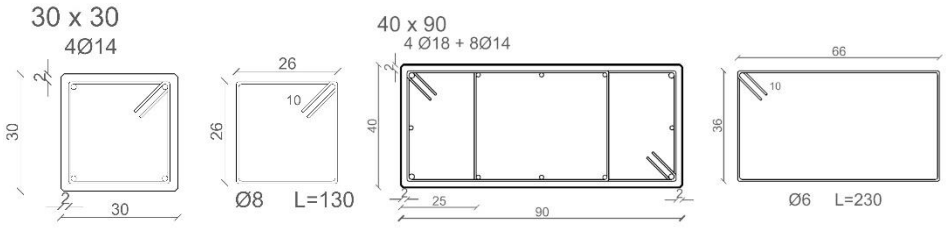

Figure 5.4 Concrete Column cross section and reinforcement layouts (section 30x30 and 40x80)

Figure 5.4 reproduces two generic sections and their internal reinforcement layout.

The concrete beams have been designed only for gravity loads with line loads that represented normal condition of occupancy according to the regulation that was mandatory before the 1981. The reinforcement layout has been based on the several technical drawings and the longitudinal reinforcement have been assumed straight and shaped. The Figure 5.5 shows the external beams in the shorter direction. Additional drawings are reported in APPENDIX IV.

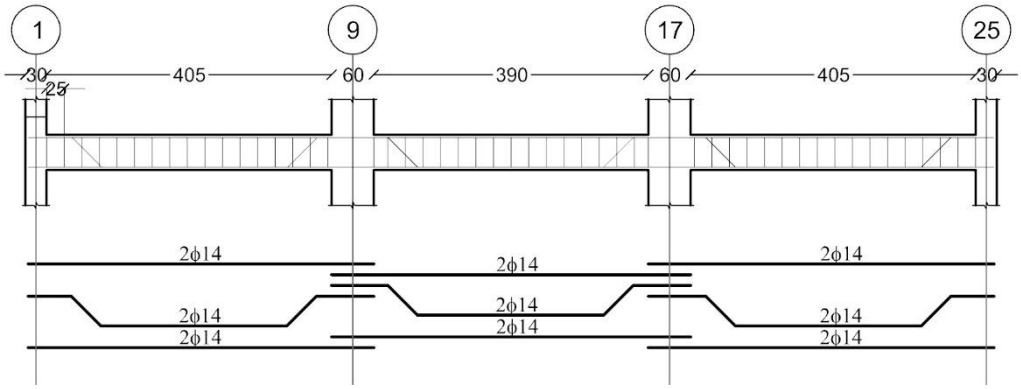

Figure 5.5 Example of reinforcement layout

The mechanical definition of the concrete and steel materials have been based on the habits of that time and supported by the results of structural health monitoring campaigns that were carried out on building in the south east of Sicily where Catania is placed. The Table 5-2and Table 5-3 expose principal mechanical material parameters and their values.

Table 5-2 Characterization of concrete materials

Material property	**cover region**	**core region**
Cylinder Compressive strength (MPa)	20.75	23.25
Young's modulus (MPa)	27386	27386
Strain at maximum strength	2×10^{-3}	2×10^{-3}
Tensile strength in tension	1.04 MPa	1.04 MPa

Table 5-3 Characterization of steel materials

Material property	**Rebars**
Yielding strength (MPa)	375
Young's modulus (MPa)	210000
Strain-hardening ratio	0.01

Two layers of bricks with an interposed air chamber define the infill panel of 30 cm thick. The thickness of the interior brick layer is 8 cm, while the exterior one is 12 cm. This infills configuration was largely diffuse and common in the south of Italy between 60's and 80's. Aiming to evaluate the unreinforced masonry panels contribute only the thicker layer (12cm, exterior) has been taken into account.

The masonry panel characteristics are summarised in Table 5-4 and have been based on the experimental test conducted on an infill frame subjected to cyclic horizontal loads [89].

Table 5-4 Mechanical parameters of masonry walls

Flexural behaviour					Shear behaviour			
E [Mpa]	σ_t [Mpa]	σ_c [Mpa]	g_t [N/mm]	g_c [N/mm]	G [Mpa]	f_{v0} [Mpa]	ϕ	g_s [N/mm]
1200	0.08	0.8	0.02	1.00	600	0.05	0.4	0.10

The Sliding along the mortar joints has been modelled by considering a cohesion c = 0.4 MPa and tangent of friction angle tan(ϕ)=0.7.

5.3 Parametric model

The typical multi-level building has been subjected to incremental static nonlinear analyses for assessing its horizontal capacity with and without the masonry infills contribution. The bare frame model implemented in the software 3DMacro [83] has been compared and calibrated to the high fidelity model implemented in ADAPTIC. The high fidelity ADAPTIC numerical model is discussed in the subsequent CHAPTER 6. The comparison has been performed both in linear and nonlinear context. The linear validation between the two models have been performed in terms of eigen-properties.

Aiming a perfoming a vulnerability assessment for buildings characterised by different number of floors, a set of prototypes characterised by a different number of storeys has been defined. The prototypes have been identified simply by progressively deleting the ground floor. The obtained typical buildings, reported in Figure 5.6, since the result of a design based on vertical loadings, can be considered representative of the existing Catania reinforced concrete frame buildings not designed to resist to earthquake. Figure 5.6 shows the

similarity between the ten-storey and two-storey prototypes and two real buildings built in Catania.

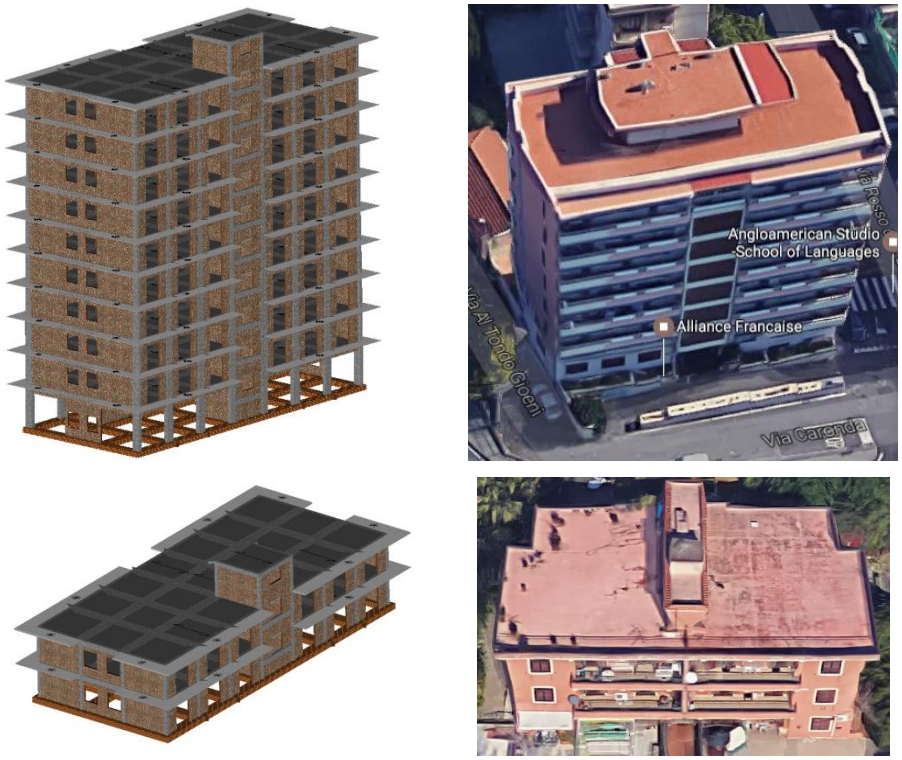

Figure 5.6 (Colour) Similarities between numerical and real buildings

Table 5-5 compares the mode shapes and the corresponding periods of the bare and infill frames models. The left column contains the bare frame ADAPTIC model and the related results, whereas the central column shows the results of the 3DMacro model; the left column reports the modal results of the infill frame structure modelled in 3DMacro. As the Table 5-5 shows, a good agreement has been obtained between the High Fidelity Model (see CHAPTER 6) and the simplified 3DMacro model. The same table depict the influence of the infill panels on the ten-storey building modal response.

Table 5-5 (Colour) Modal calibration of the 3DMacro bare model

ADAPTIC	3DMACRO bare	3DMACRO infill
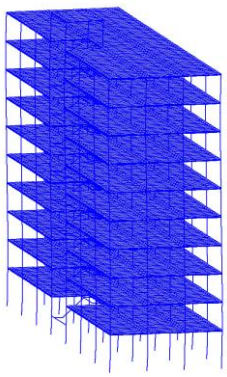	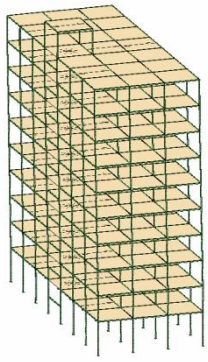	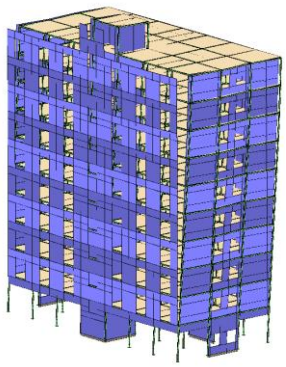
PERIOD (SEC) 2.162	PERIOD (SEC) 2.107	PERIOD (SEC) 1.53
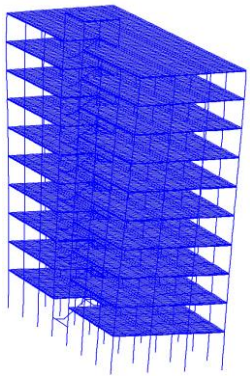	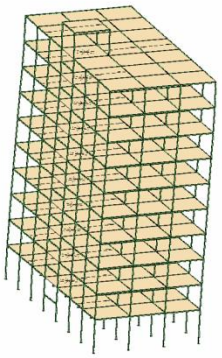	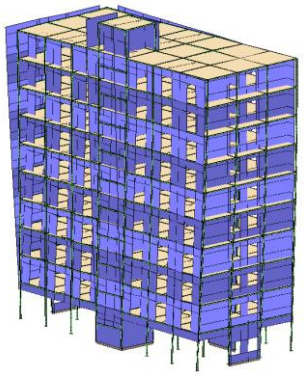
PERIOD (SEC) 1.809	PERIOD (SEC) 1.814	PERIOD (SEC) 1.043
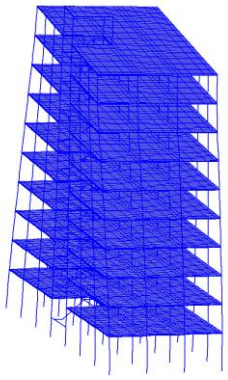	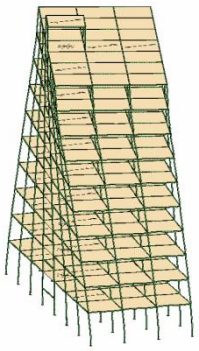	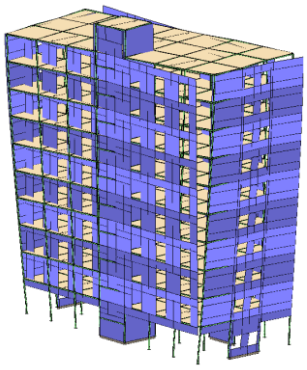
PERIOD (SEC) 1.761	PERIOD (SEC) 1.743	PERIOD (SEC) 0.861

ADAPTIC	3DMACRO bare	3DMACRO infill
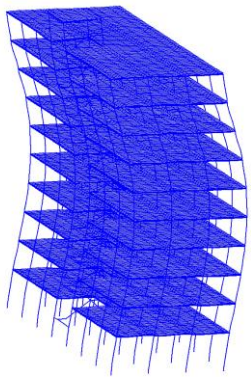	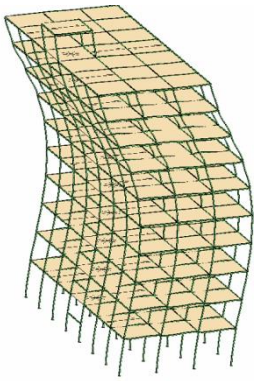	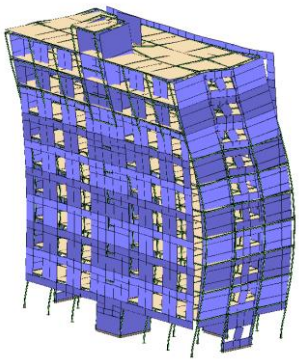
PERIOD (SEC) 0.790	PERIOD (SEC) 0.784	PERIOD (SEC) 0.390
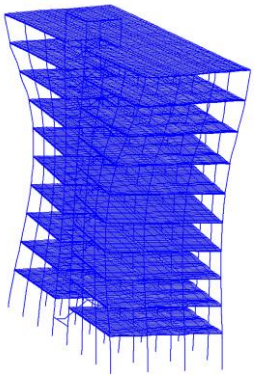	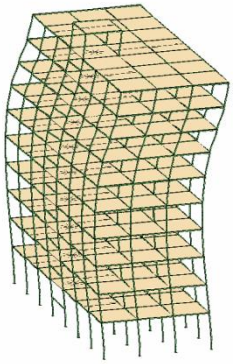	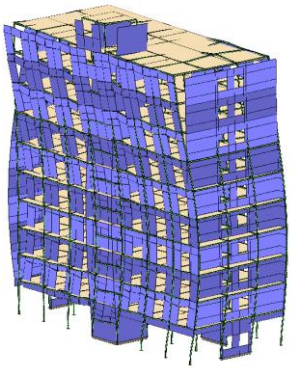
PERIOD (SEC) 0.708	PERIOD (SEC) 0.695	PERIOD (SEC) 0.360
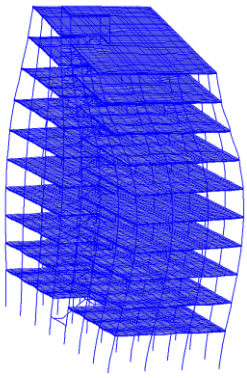	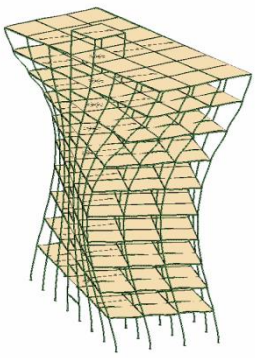	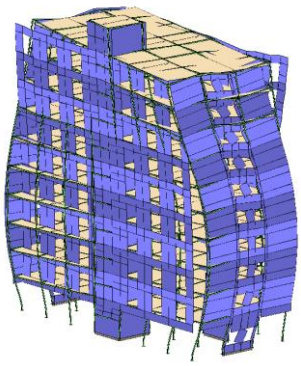
PERIOD (SEC) 0.686	PERIOD (SEC) 0.678	PERIOD (SEC) 0.299

ADAPTIC	3DMACRO bare	3DMACRO infill
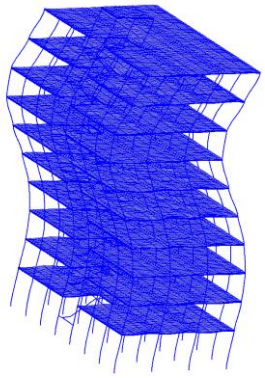	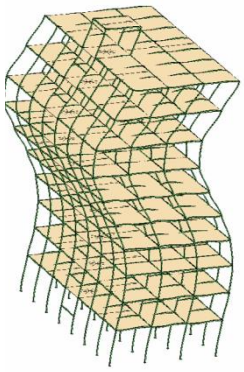	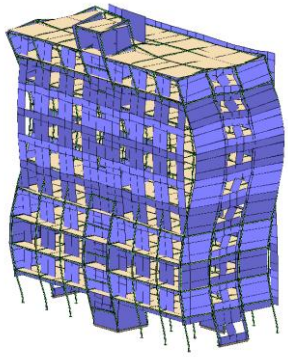
PERIOD (SEC) 0.446	PERIOD (SEC) 0.443	PERIOD (SEC) 0.215
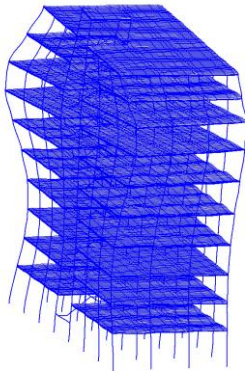	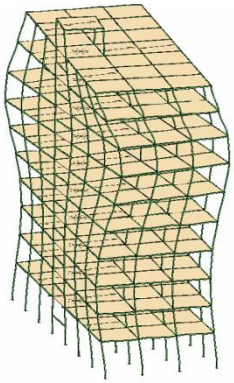	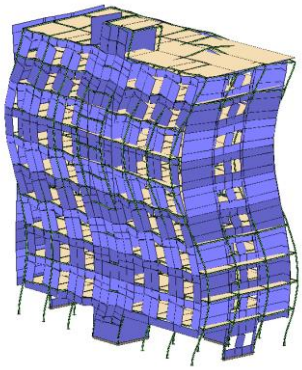
PERIOD (SEC) 0.408	PERIOD (SEC) 0.404	PERIOD (SEC) 0.205
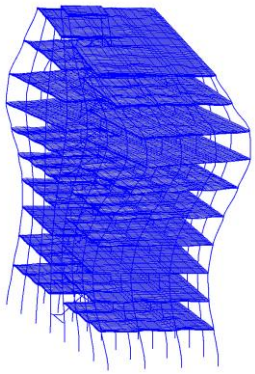	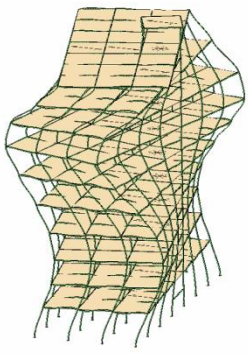	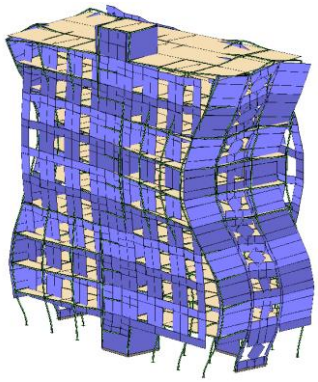
PERIOD (SEC) 0.394	PERIOD (SEC) 0.387	PERIOD (SEC) 0.169

ADAPTIC	3DMACRO bare	3DMACRO infill
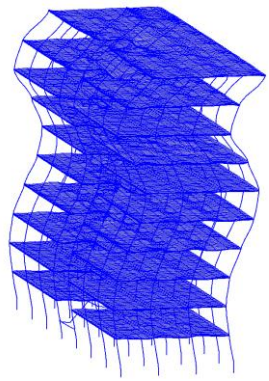	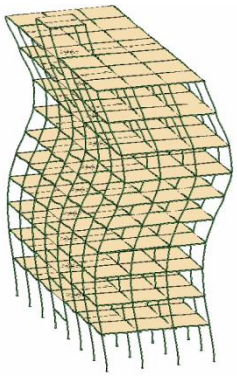	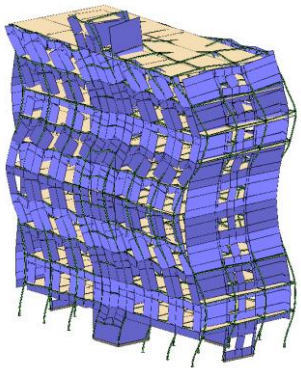
PERIOD (SEC) 0.310	PERIOD (SEC) 0.275	PERIOD (SEC) 0.143

The masonry infilled panels properties have been discussed at the end of the previous Section.

The comparison between the bare frame and the infill frame models have been clearly shows the strong influence of the masonry infills.

Figure 5.7 summarizes the periods of the two structures and adopts the symbolism as follows:

● I Mode ✕ II Mode + III Mode indicate the modal values of the bare frame,

◆ I Mode ■ II Mode ▲ III Mode indicate the modal values of the infill frame.

Furthermore, the dashed line establishes a simplified relationship between the number of floors and an empiric coefficient in agreement with the Italian Seismic Regulation prescription (NTC08 §7.3.5). It is worth noticing that the simplified formula properly matches the eigen-values of the bare frames but underestimates the periods of these existing reinforced concrete frame buildings since totally neglects the contribution of masonry infills, that although realized for architectural needs provide a contribution to the overall stiffness of the structure.

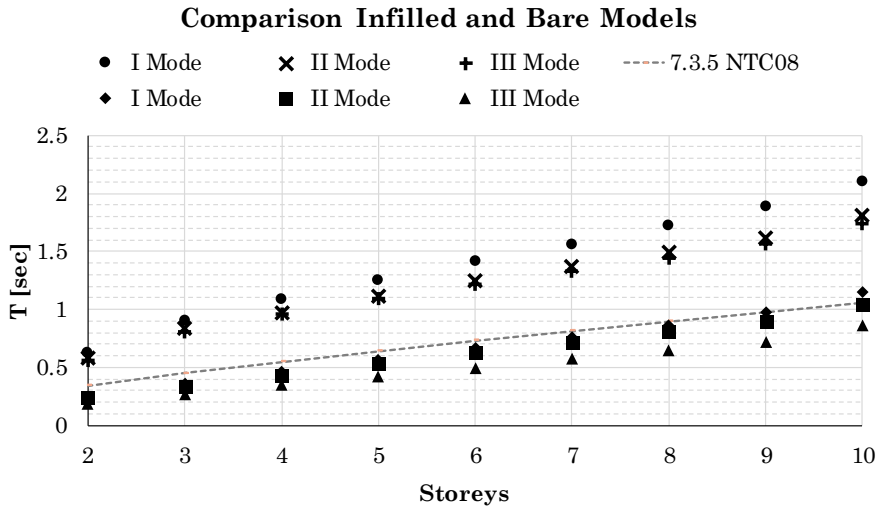

Figure 5.7 Comparison between the modal periods of the two models

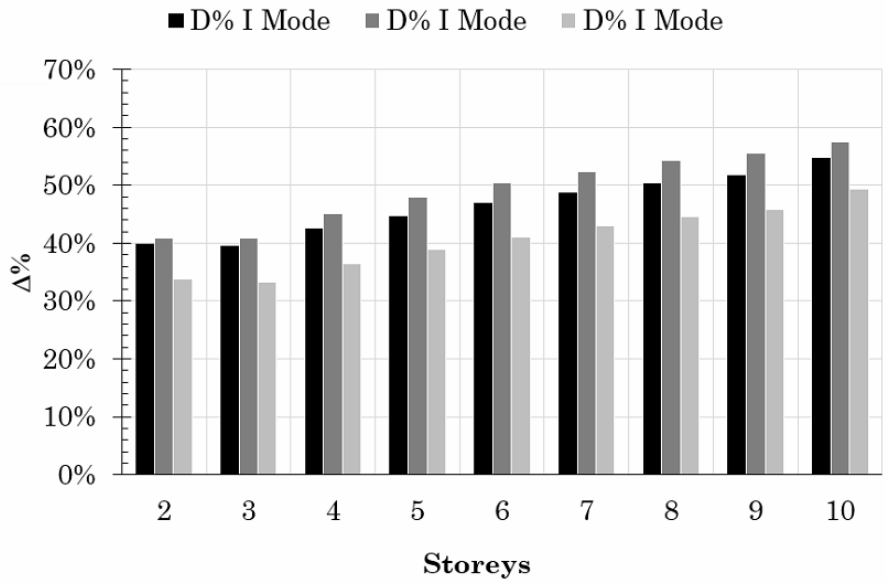

Figure 5.8 Percent Period increment in the early three modes

Figure 5.8 shows the percent increment of the periods that the infilled panels determinate in all the nine prototype for each of the three principal modes.

By comparing the modal periods that have been summarised Figure 5.7 and Figure 5.8, the following considerations can be listed below:

- The modal periods increase almost linearly with the number of floors. The presence of infill panels may mitigate the increment(Figure 5.7);
- The infill contribution appears more pronounced for higher buildings.
- The simplified formula (Italian Seismic Regulation §7.3.5) that provides an estimation of the fundamental period of framed structures is consistent to the bare frame building model as a consequence does not give a satisfactory prediction of the actual building.

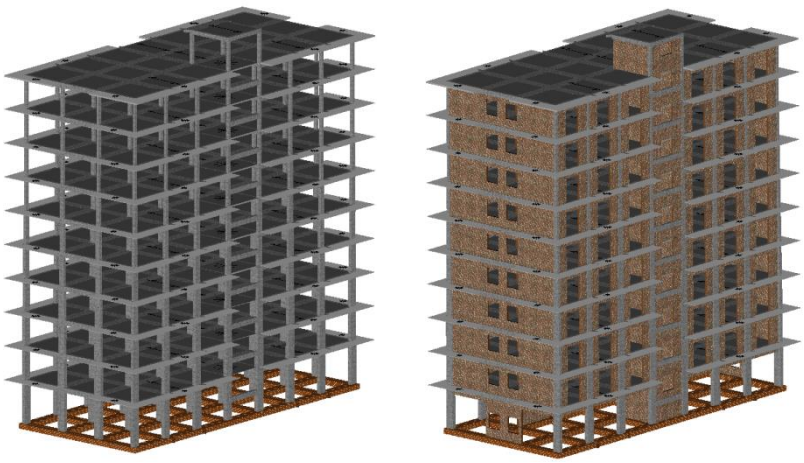

a *b*

Figure 5.9 3DMacro models of the ten storey building a) Bare Frame model b) Infill Frame model

The ten-storey building has been loaded in both the principal directions with two prescribed load distributions, namely the mass proportional and the first fundamental mode proportional loading.

Figure 5.10 and Figure 5.11 show the mass proportional and mode proportional capacity curves, for both the models in the longitudinal and transversal directions. Namely Figure 5.10.a and Figure 5.10.b report the capacity curves along the longer (X) building direction (longitudinal) for the bare and the infill frame structures, respectively. Similarly, Figure 5.10.c and Figure 5.10.d report the capacity curves along the shorter (Y) building direction (transversal). The curves are expressed in terms of

base shear coefficient (Cb) versus top displacement. The base shear coeffiecient has been obtained by dividing the shear base values by the Seismic weight.

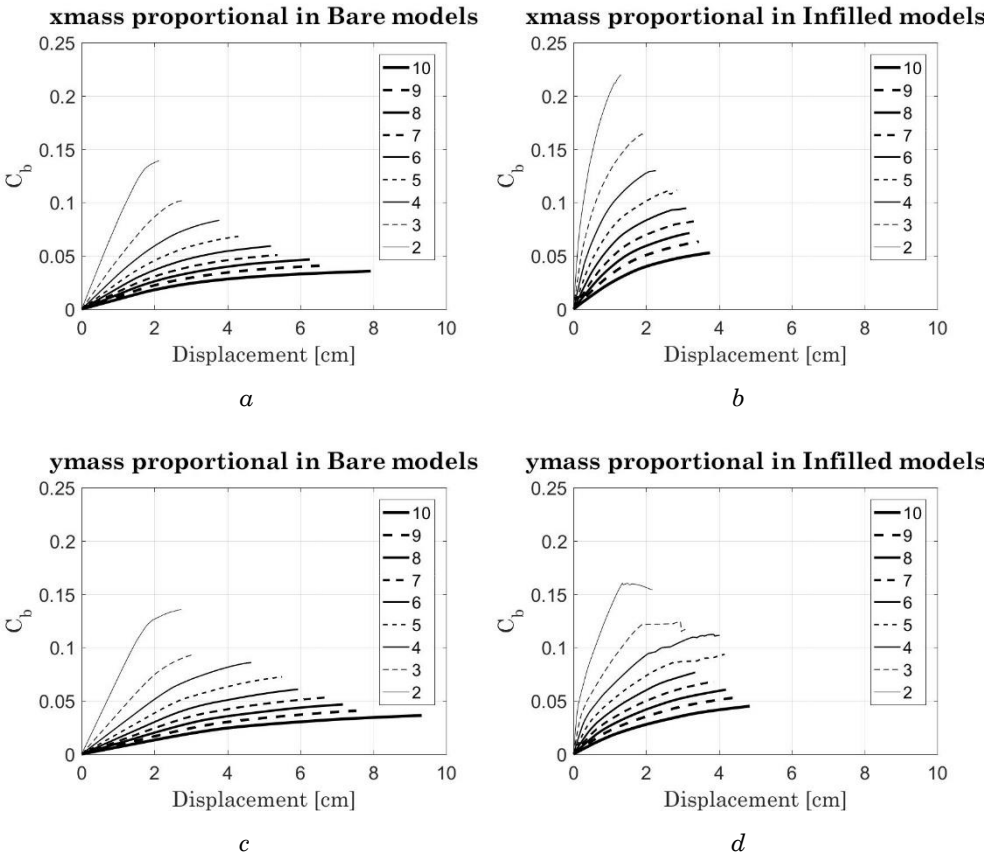

Figure 5.10 Mass proportional capacity curves

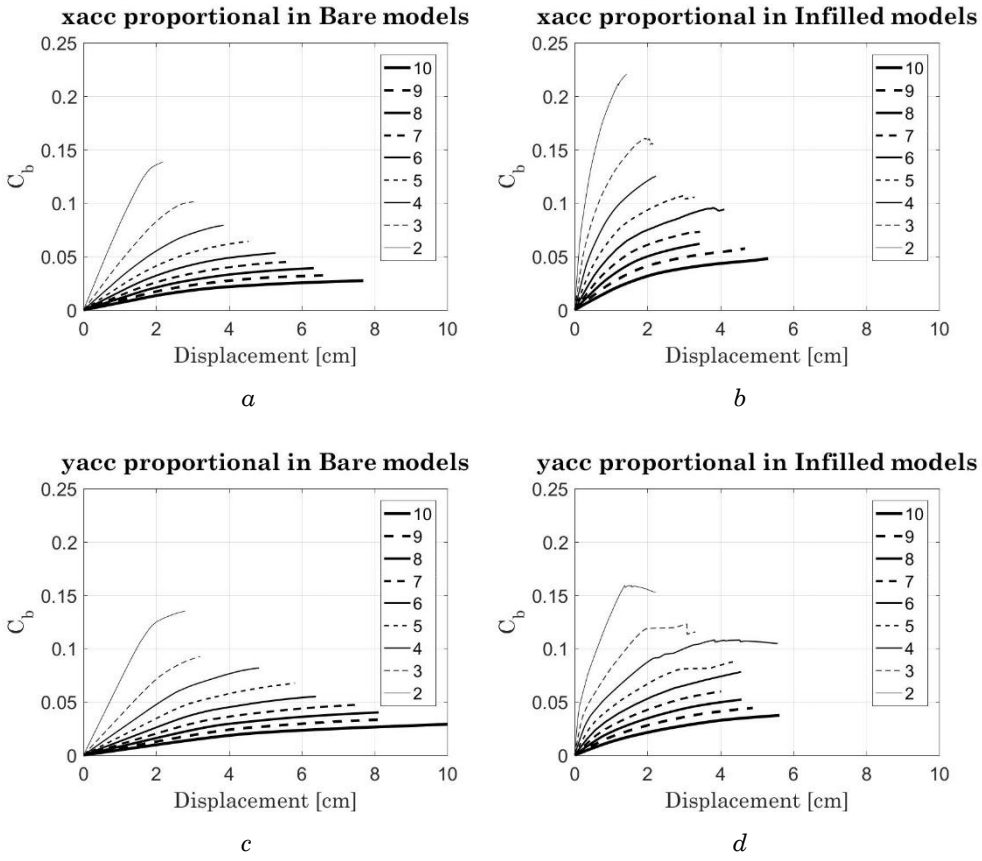

Figure 5.11 Fundamental mode proportional capacity curves

All the curves terminate at the SLV (LD in Eurocode) capacity displacement values. From the observation of the figure clearly emerges how the base shear force capacity varies with the number of floors. Shorter structure are more resistant but characterised by a progressively lower ductility.

As the figures depict, the two load distributions do not correspond to evident global differences. Moreover, the curves reach similar capacity displacements and normalised Cb ratios, for the two load distributions. The panels contribute is more evident in curves that represent the structural response along the X direction. On the other hand, the capacity displacements have been reduced in all four analyses. In detail, the curves terminate when the first plastic hinge in a reinforced concrete element (beam or column) reaches the 75% of the ultimate chord rotation, according to the adopted regulation. The chord rotation capacity and demand for the Italian Seismic Code and Eurocode are fully discussed in APPENDIX I.

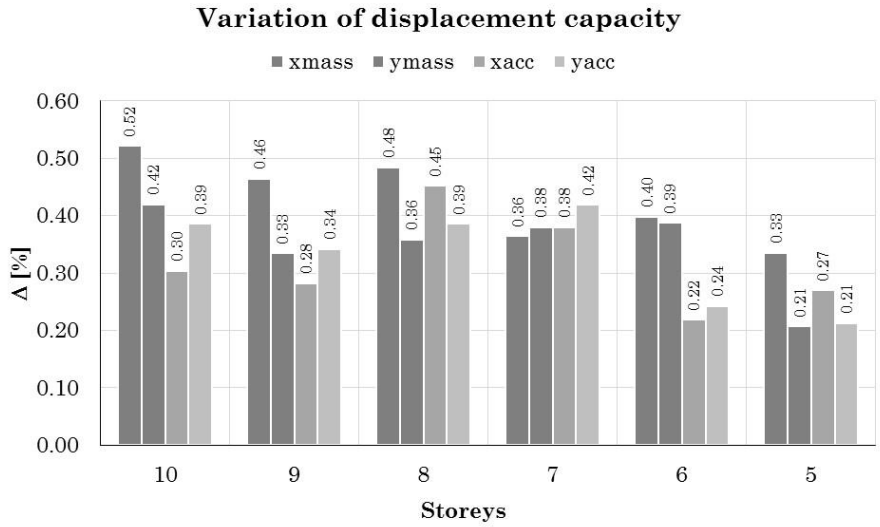

Figure 5.12 Variation of capacity displacement due to infills contribute in mid-rise buildings.

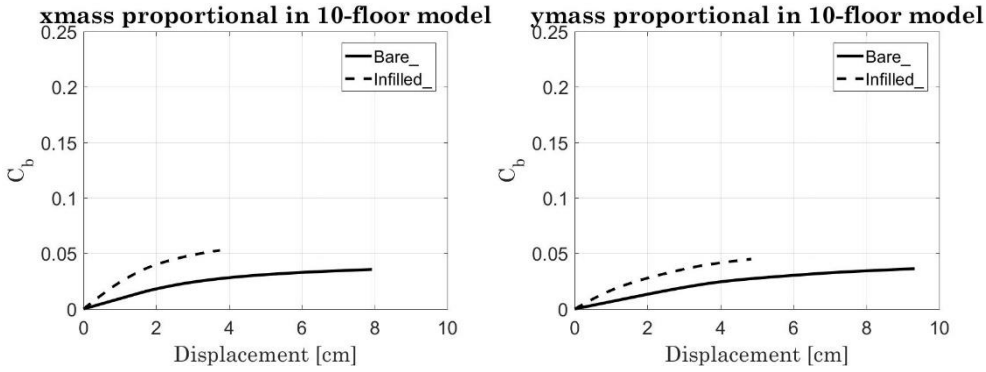

a *b*

Figure 5.13 Ten-storey models capacity curves in a) x and b) y direction for the Mass proportional loads distribution

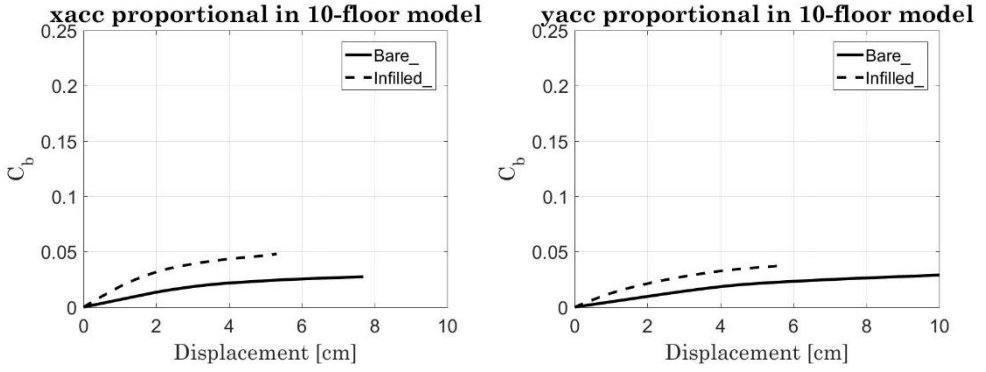

a *b*

Figure 5.14 Ten-storey models capacity curves in a) x and b) y direction for the Fundamental Mode proportional loads distribution

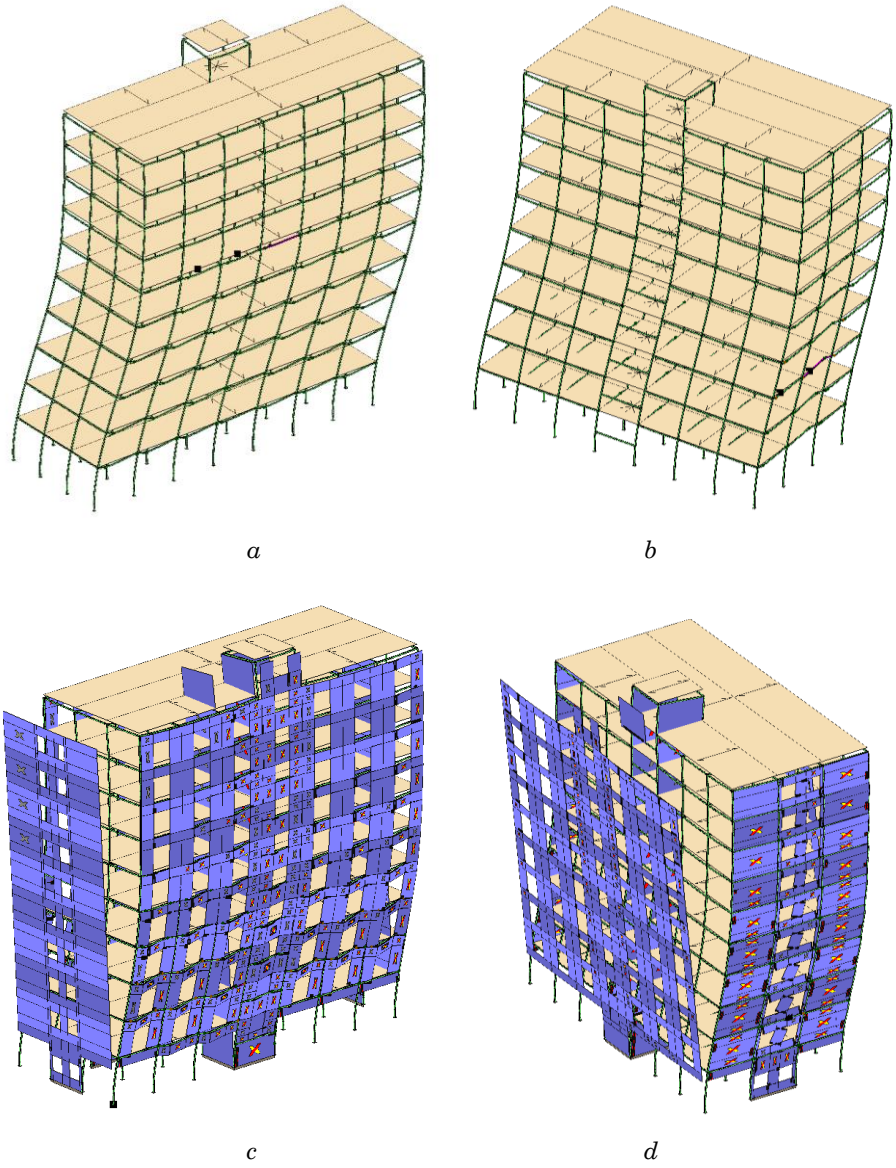

a *b*

c *d*

Figure 5.15 (Colour) Ten-storey models deformed shapes under mass proportional loads distribution: a) x and b) y direction for bare frame model and c) x and d) y direction for infill frame model.

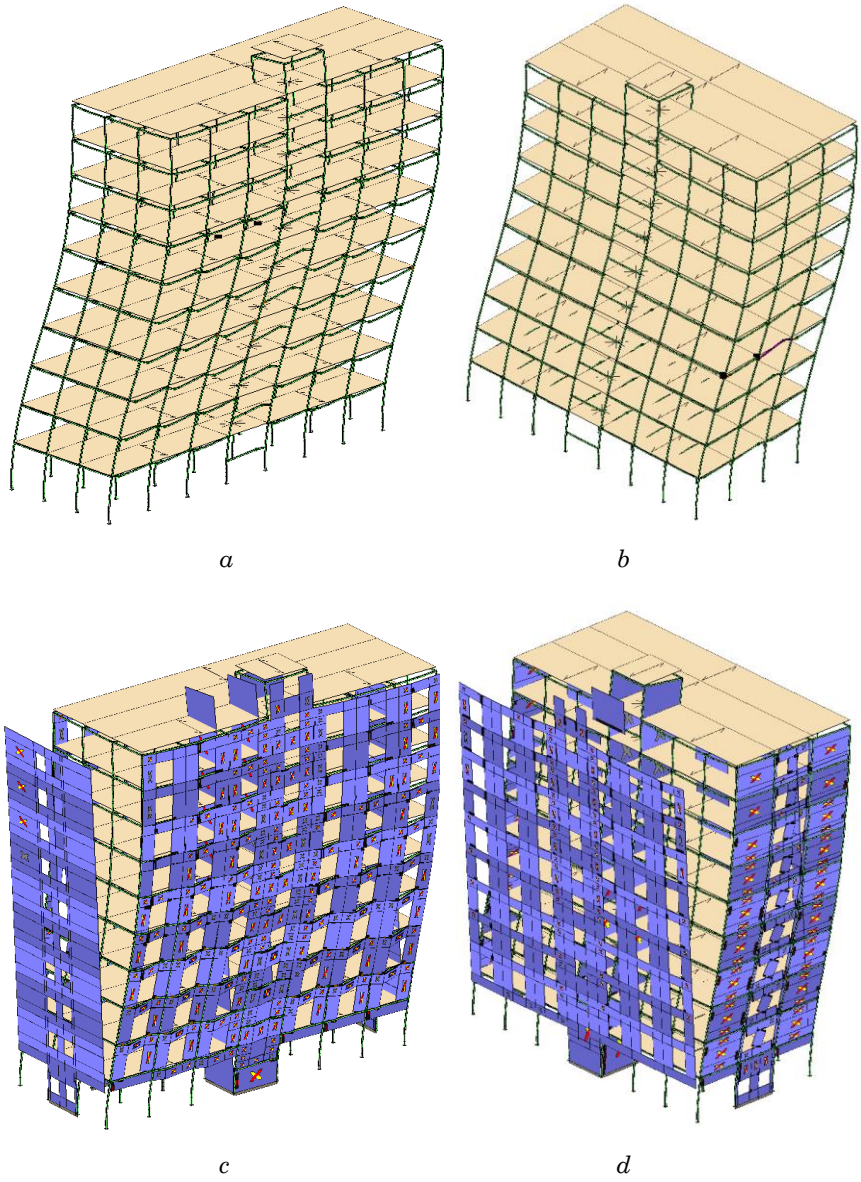

Figure 5.16 (Colour) Ten-storey models deformed shapes under fundamental mode proportional loads distribution: a) x and b) y direction for bare frame model and c) x and d) y direction for infill frame model.

Figure 5.12 considers the displacement capacity variations due to the infilled panels contribution.

For both the loads distributions the collapse mode shapes of the bare and infill ten-storey buildings are strongly influenced by the infilled panels.

Figure 5.15 and Figure 5.16 report the ultimate deformed shapes (Figure 5.13 and Figure 5.14). The figures signed with the letters *a* and *b* represent the collapse behaviour of the bare frame. The absence of infill panels strongly reduces to stiffness of the structure leading to an elongation of the fundamental period and an increased displacement capacity. The bare frame failure has been characterised by a spread distribution of plastic hinges more concentrated at the lower floors (from 1st to 5th). The beam reinforcement layout defines the plastic hinges and their placements as showed in Figure 5.17 in which several plastic hinges are shown along the beams. On the other hand, the infilled frame deformed shape has involved several panels in particular from the 1st to the 4th floors. In this latter case, the plastic hinges positions have been influenced by the infill panels and by the openings.

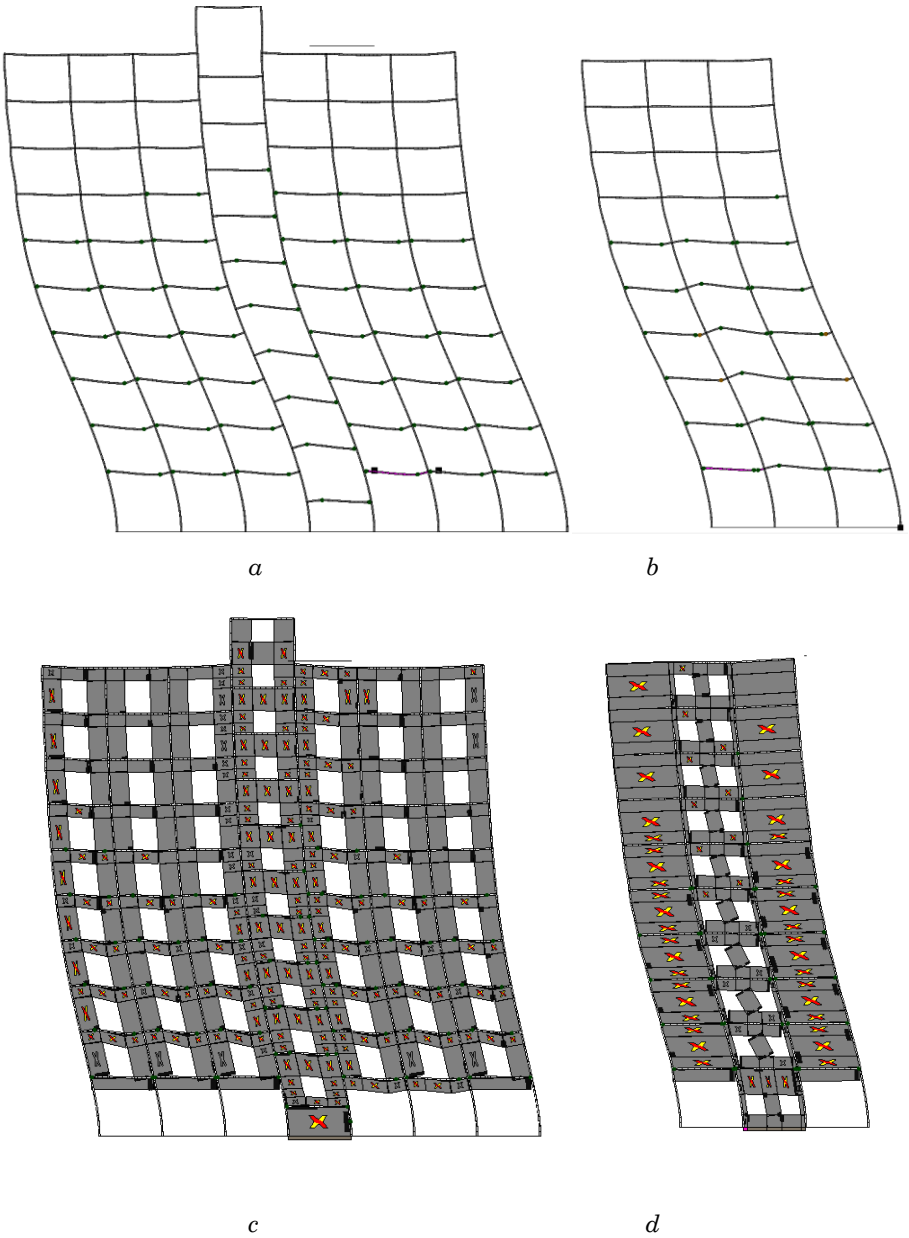

Figure 5.17 (Colour) Ten-storey models deformed shapes: a) x and b) y direction for bare frame model and c) x and d) y direction for infill frame model.

The design process of the building, based on vertical loads only, allowed to define eight additional structures as particular cased of the original ten-storey building. Each model has been obtained by deleting the first storey and applying external base fully fixed constraints. The strategy is allowed by the design hypothesis since each storey column has been designed for resisting to the total vertical loads deriving from upper floors. The lower structure that has been considered is a two-storey building and it is depicted in the following figures. Namely, Figure 5.18.a represents the bare frame and Figure 5.18.b depicts the infill frame, both of them are 3DMacro output schemes.

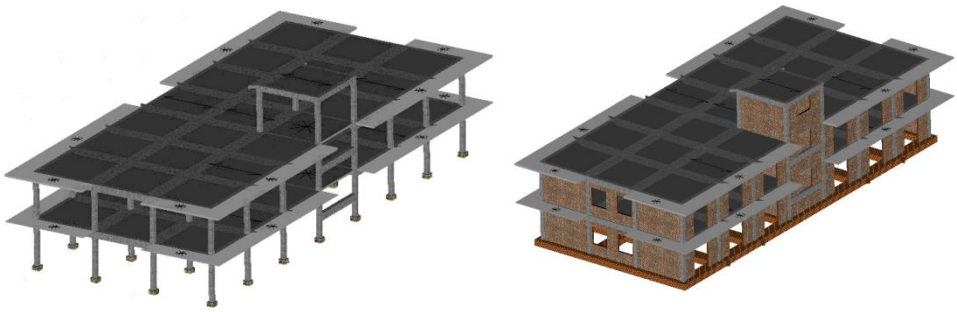

a *b*

Figure 5.18 3DMacro a) Bare and b) Infill two-storey building

Figure 5.20 and Figure 5.21 report the capacity curves for the bare and infilled two-storey frames in the two loads distributions. The curves ends represent the capacity displacement at SLV limit state (Italian Sesmic Code). The curves, reported in Figure 5.20 and Figure 5.21 reach similar values (Normalised Base Shear and Ultimate Displacement) regardless of the load distribution in the two directions. For low-rise buildings, a sensible increment of the ultimate resistance has been detected more than in the mid-rise buildings. The Figure 5.19 shows how the Normalised Base Shear increments in a percentage scale according to the storey number and the pushover analyses. The diagrams demonstrate that the infill frames contribution is more sensible in the longer direction.

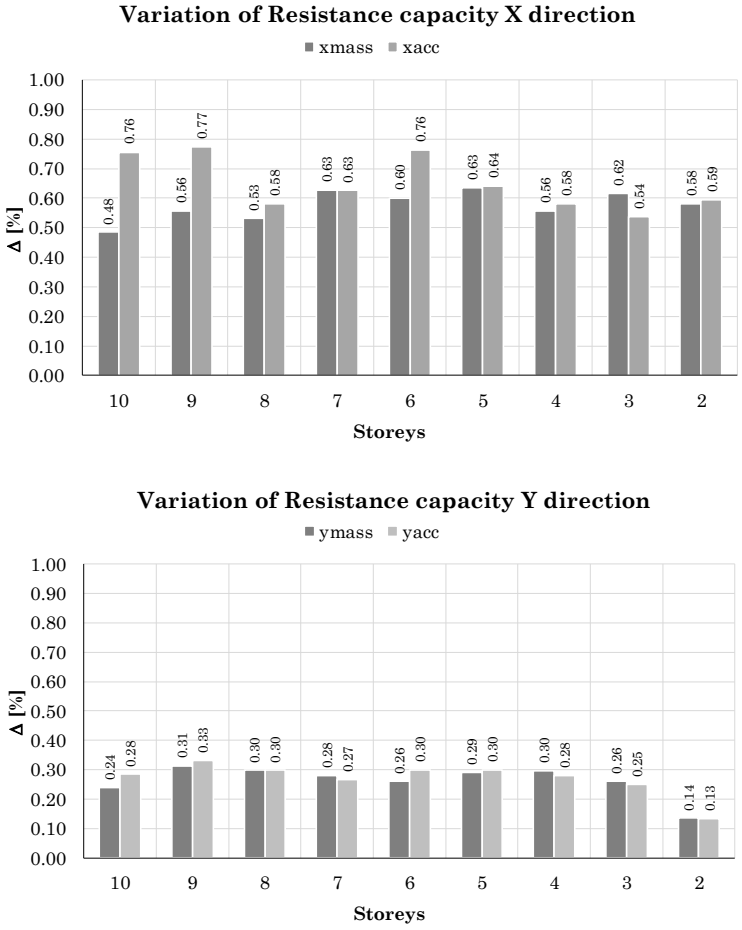

Figure 5.19 Increment of normalised base shear value thanks to infills for the two directions (Soil Category A)

Similarly, Figure 5.22 and Figure 5.23 show the deformed shapes of the two-storey model.

The capacity curves of each model in both directions and load distributions are collected in APPENDIX III.

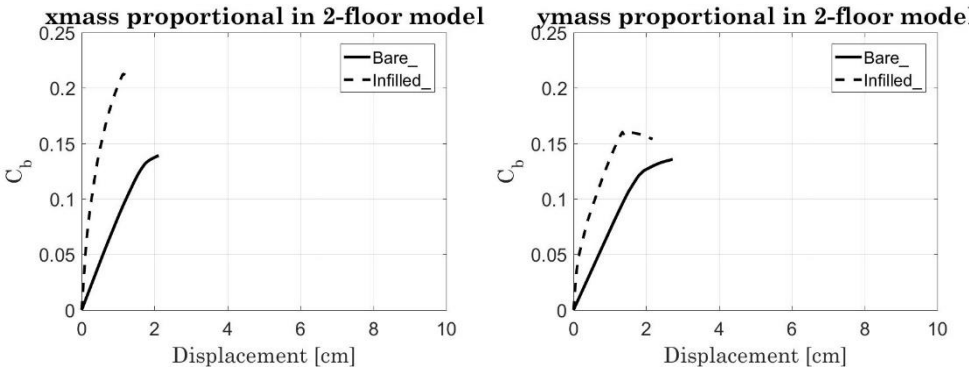

a *b*

Figure 5.20 Two-storey models capacity curves in a) x and b) y direction for the Mass proportional loads distribution

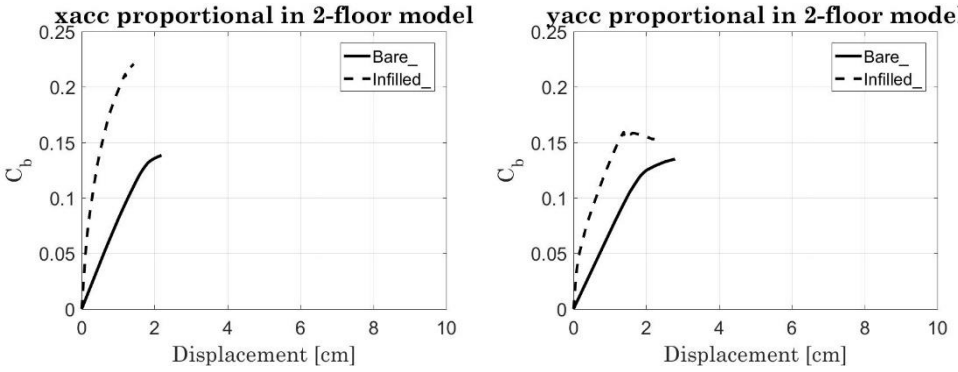

a *b*

Figure 5.21 Two-storey models capacity curves in a) x and b) y direction for the Fundamental Mode proportional loads distribution

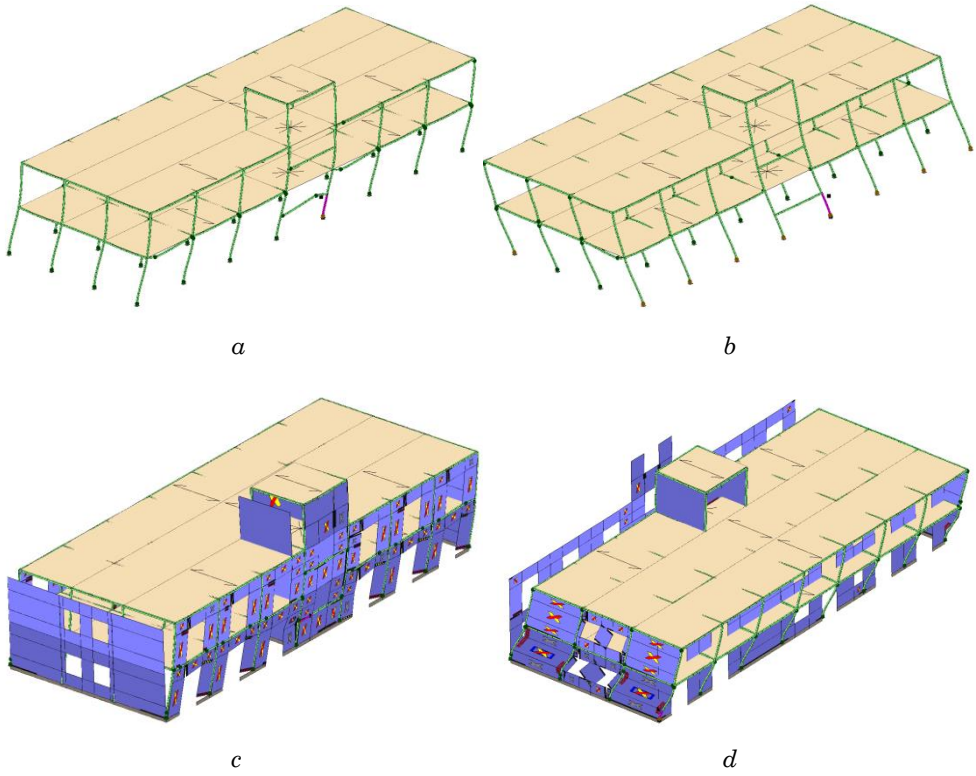

Figure 5.22 (Colour) Two-storey models deformed shapes under mass proportional loads distribution: a) x and b) y direction for bare frame model and c) x and d) y direction for infill frame model.

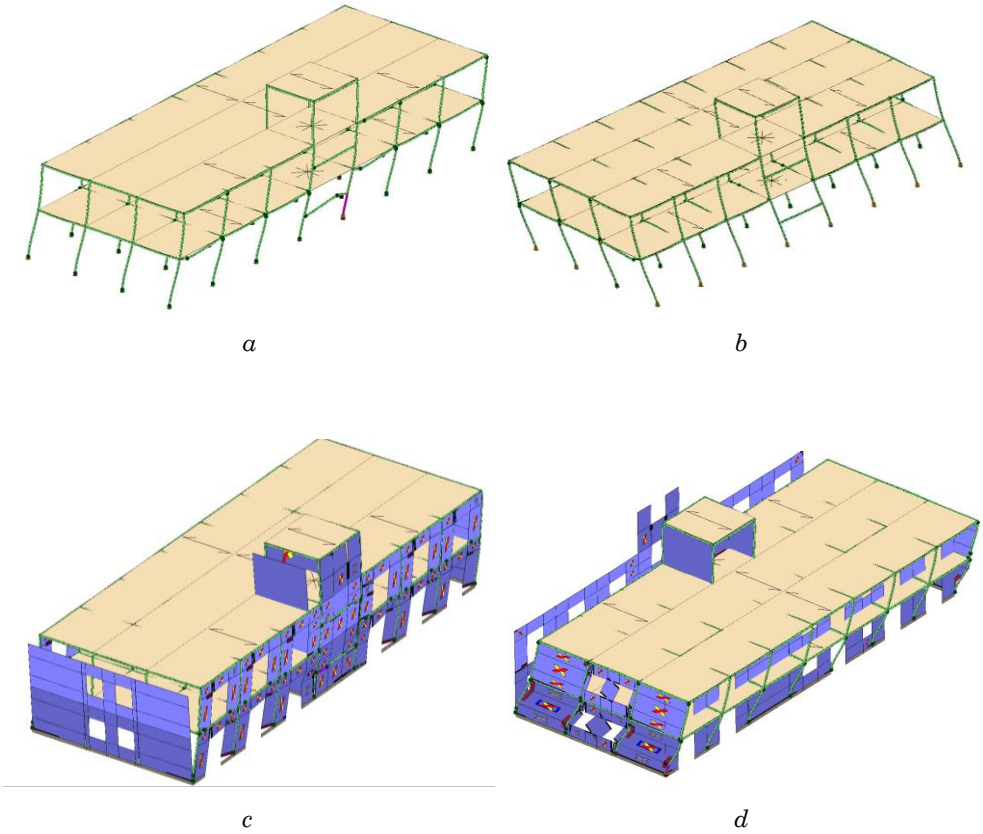

a *b*

c *d*

Figure 5.23 (Colour) Two-storey models deformed shapes under fundamental period proportional loads distribution: a) x and b) y direction for bare frame model and c) x and d) y direction for infill frame model.

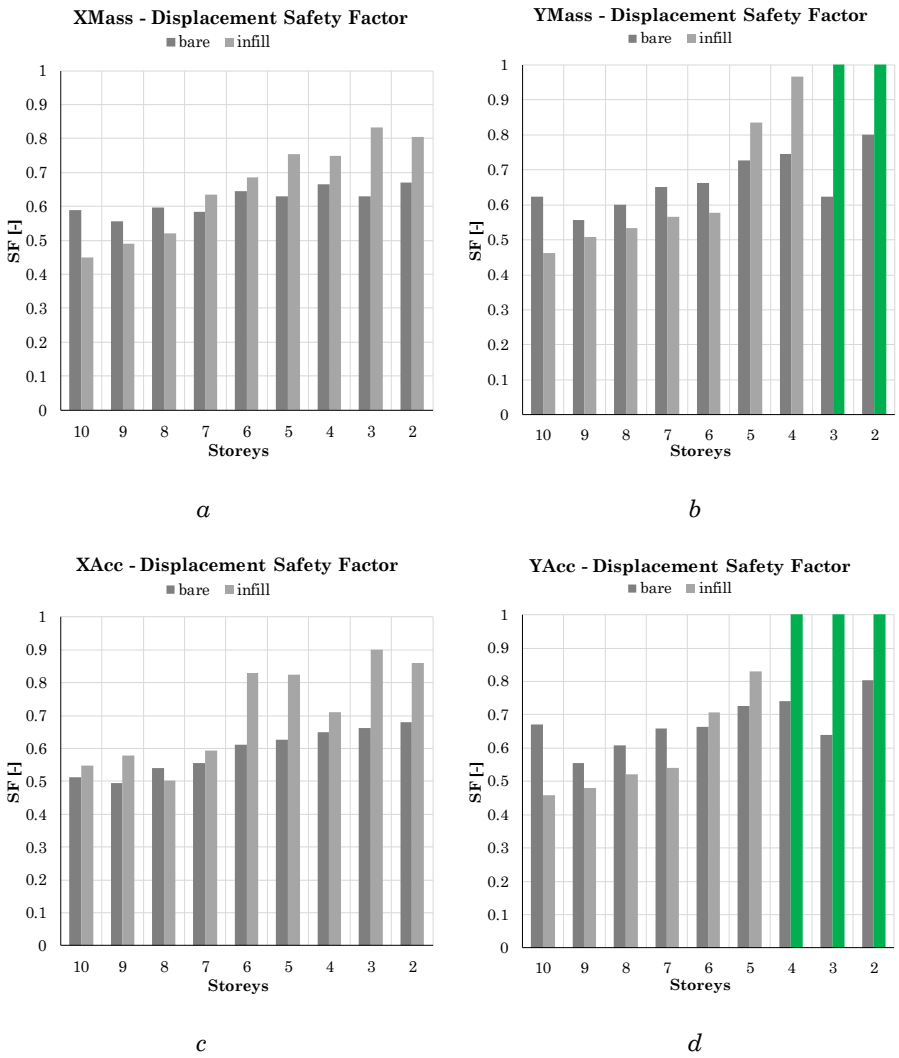

Figure 5.24 Displacement Safety Factors (Soil Category A)

The N2 method [92] has been engaged for defining a reliable safety factor. Figure 5.24 summarizes the safety factors for all the load distributions and directions in Soil Category A. The Safety Factors are reported for two different Soil Category (A and D) in the Figure 5.25. The figures, which aim to compare the safety factor trends in the infill frame and in the bare frame models, depict that the ratios between demand and capacity in terms of displacements have similar trends. It is worth noticing that the safety factors have a decrement in case of infill

frame models. The response is consistent with the masonry panels influence on the frame structures. Furthermore, the panels have a higher influence in the lower buildings and do not affect sensitively mid-rise buildings. On the other hand, the decrement of the same factor in case of bare frame is less evident and almost neglectable in case of Soil Category D.

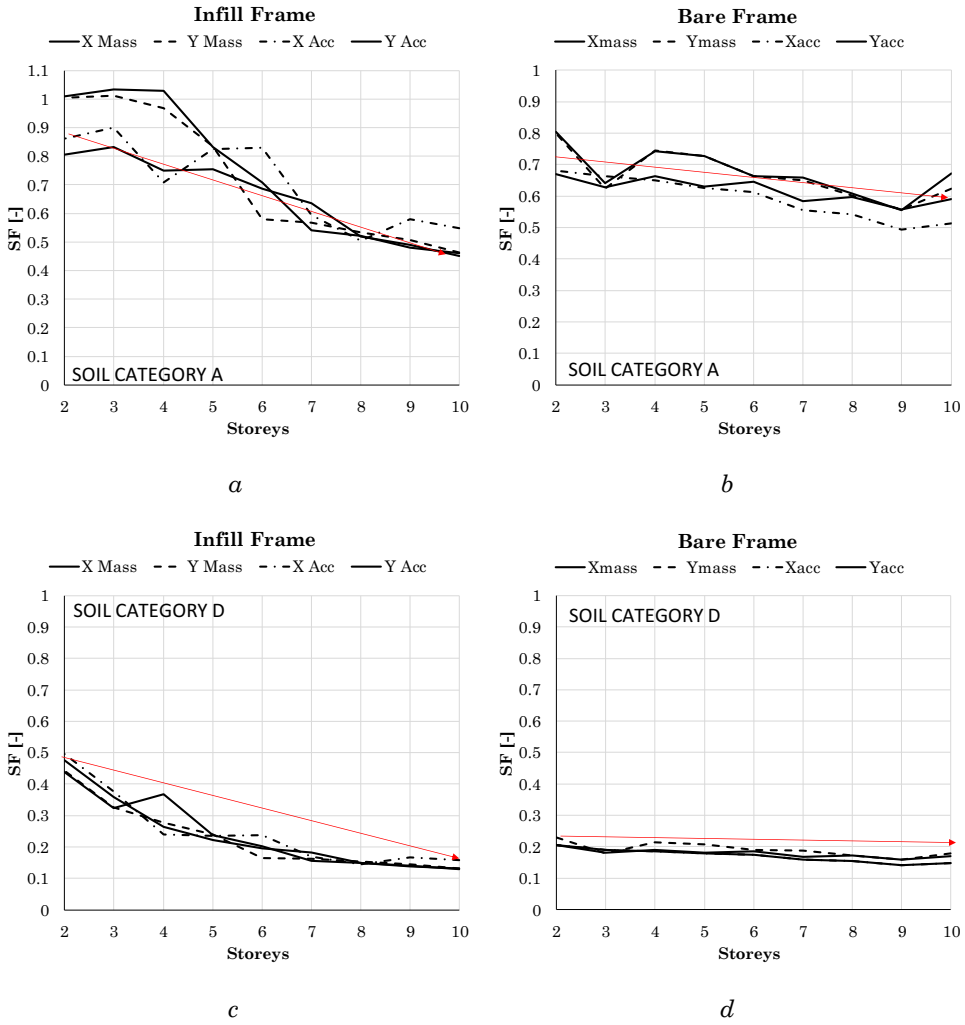

Figure 5.25 (Colour) Trend of the Safety Factors in terms of displacements (Demand/Capacity)

Figure 5.26 shows the trend of the Safety Factors in the two directions as average values of the two load distributions.

The percentage value has been obtained by the following formula:

$$\Delta = \frac{D_{capacity}^{\text{infill frame}}}{D_{capacity}^{\text{bare frame}}} \qquad \textit{Eq. 62}$$

In view of the previous figures, it is worth noticing that the unreinforced masonry panels may determinate a positive effect on the low-rise structure in terms of displacement capacity and, potentially, can preserve the structure from collapse due to seismic loadings. This contribute is evident up to a six- or seven-storey high building. On the other hand, weak infill panels do not supply positive effects in mid-rise buildings.

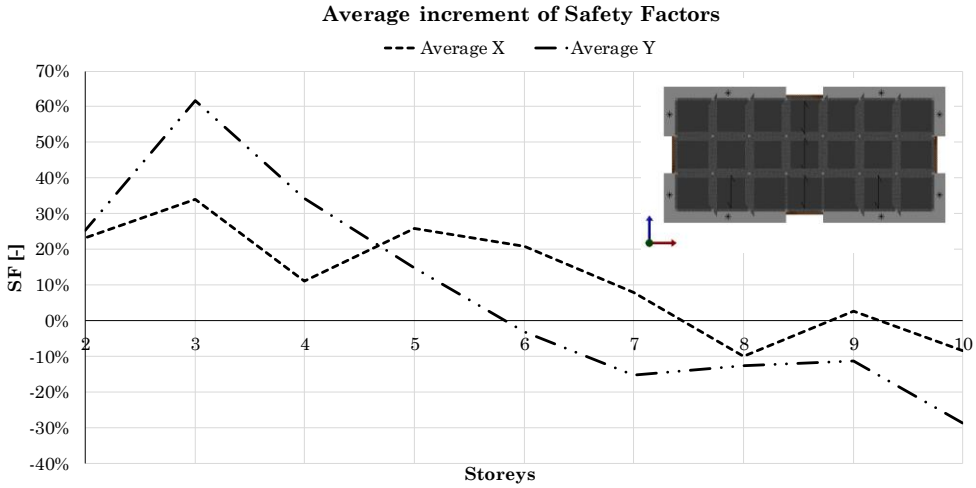

Figure 5.26 Average values of the Safety Factors increments

Thus far, the displacement safety factors has been expressed for different soil category and, consequently, it has been influenced by the soil amplification factor. In view of that, Figure 5.27 and Figure 5.28 summarize the results that has been achieved so far. The results are reported for four different soil categories, namely A,B,C and D, according to the Italian Seismic Code. Lastly, it is still worth noticing

that the ten-storey building is characterised by very poor levels of seismic safety in both the structural models. Inadequate safety level distinguishes the building starting from the Soil Category A, namely in absence soil amplification.

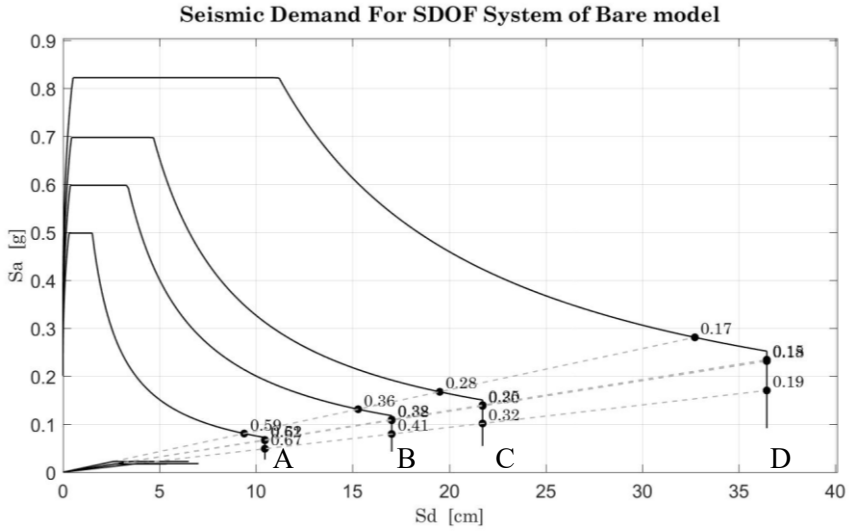

Figure 5.27 Variation of displacement safety factors according to different soil categories.

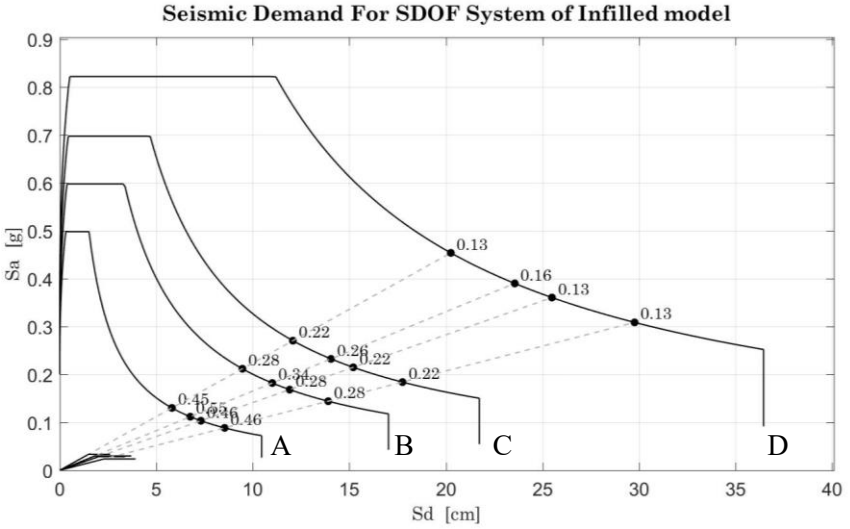

Figure 5.28 Variation of displacement safety factors according to different soil categories.

The results obtained for the considered typical building by varying the number of floor have show that lower structures are characterised by an higher resistance and a lower ductility however they are subjected to a greater seismic demand. In the worst condition of soil (D category) Figure 5.25.d highligths an interisting new results, it seems tha considering the ratio (seismic demand)/(seismic capacity) the vulnerability index of the considered case study, obtained according to nonlinear static analyses, appears to be almost independent on the number of floors and it is close to the very low value of 0.2.

CHAPTER 6.
HIGH FIDELITY ASSESSMENT

This Chapter investigates the seismic vulnerability of the ten-storey case-study building by means of a realistic model implemented in software ADAPTIC. An high fidelity nonlinear large-displacement model of the building accounting for the structural contributions of slab and non-structural masonry infills have been constructed aming at obtaining a reliable structural response of the structure subjected to seismic loads. The macroelement model, which has been described in Chapter 4, has been engaged for modelling the non-structural panels. The nonlinear dynamic response of the building models with and without the contribution of the infilled panels are compared and discussed. The vulnerability assessments have been performed by means of fully nonlinear dynamic analyses that explicitly accounted for material and geometrical nonlinearity.

6.1 Introduction

The seismic performance of the typical multi-storey reinforced concrete (RC) building has been investigated by means of fully nonlinear dynamic simulations on high fidelity 3D models performed in ADAPTIC [59], an advanced finite element code for nonlinear analysis of structures under extreme loading developed by Prof. B. Izzuddin at Imperial College of London. These analyses were part of a research projected that was financed by ANCE|Catania [93, 94]. The author of the present thesis was member of the research group. The realistic 3D model has occurred for establishing the dynamic structural response of the case study, structural deficiencies and elements weaknesses. The structural response of the case study defined the path for identifying the suitable seismic retrofitting strategy. Furthermore, the high-fidelity model has allowed for a high reliable seismic response, the sophisticated model is also able to grasp torsional effects, due to initial damages or structural irregularities due to instabilities or local damage or failures. Moreover, the combined response of the 3D frames, floor slabs, infill panels, retrofitting systems (see CHAPTER 7), and other structural and non-structural components have been accurately modelled allowing for geometric and material nonlinearity. The adoption of realistic nonlinear 3D models in fully dynamic time-history analyses has taken into account potential deterioration in column resistance that may eventually lead to disproportionate collapse. The detailed 3D numerical model has been used in combination with a unique partitioned modelling capability in ADAPTIC that has allowed efficient analysis on High Performance Computing systems [95]. In the following sub-sections, firstly, the main characteristics of the models are presented; then, the results that has been achieved in nonlinear dynamic analyses of the original multi-storey building structure subjected to earthquake loading are illustrated and discussed.

The prototype building has been modelled in ADAPTIC and two different level of sophistication have been analysed aiming to evaluate the staircases contribute to the dynamic structural response. On the other

hand, the high fidelity model has achieved a more accurate evaluation of the dynamic properties.

6.2 Realistic FEM model

Two high fidelity 3D models have been developed in ADAPTIC [63] and used in nonlinear dynamic simulations of the case study building. These include:

- 3D bare frame model (BF) that describes the behaviour of all RC components (e.g. beams, columns and floor system) but it disregards non-structural elements,
- 3D infilled frame model (IF) in which all the structural and non-structural components (e.g. masonry cladding) are explicitly modelled.

Concerning the BF model (Figure 6.2), each RC beams and columns have been discretised in an enough number of 1D elastic-plastic cubic beam-column elements [96] developed according to the distributed plasticity approach, in which the influence of large displacements is considered by using a co-rotational formulation [62]. All the cross-sections have been discretised into an opportune number of monitoring points (Figure 6.1), where strains in concrete and steel reinforcement are determined and then used within specific material relationships to obtain the associated stresses. In this respect, reliable nonlinear material laws for the two materials have been engaged.

The ADAPTIC nonlinear models CON1 and STL1, which have been presented in §3.4, have been embraced for simulating the plastic material response in static and dynamic analyses of RC beam-column elements. These material models have allowed for yielding and strain hardening of steel reinforcement, cracking in tension and crushing in compression of concrete and the specific hysteretic behaviour of the two materials.

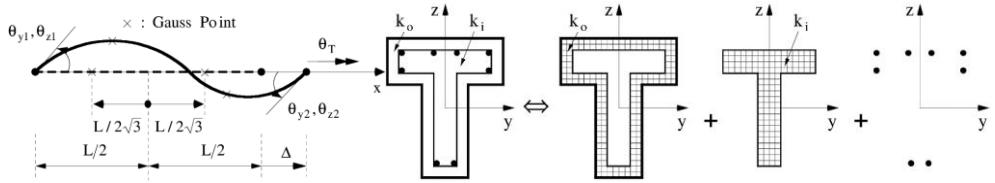

Figure 6.1 Sketch of the Fibre elements with nonlinear material models

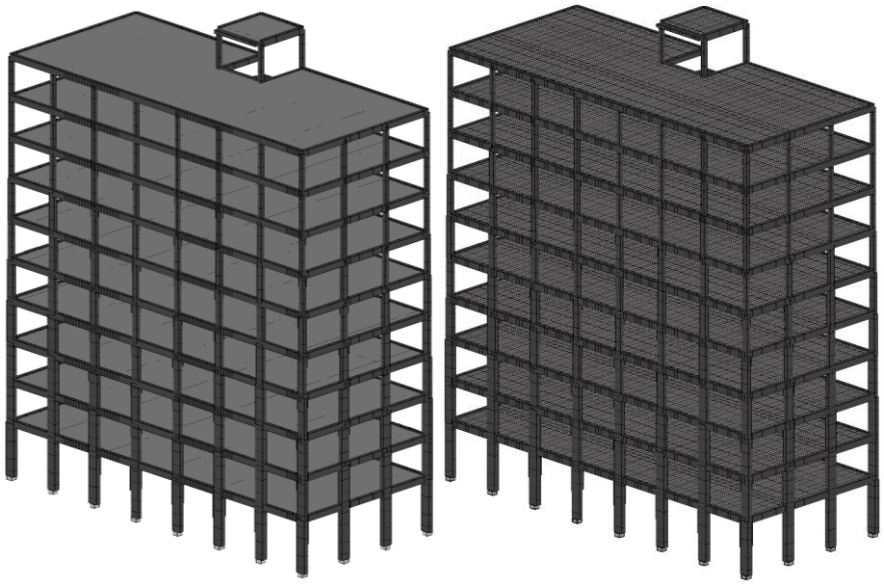

a *b*

Figure 6.2 Bare Frame 3D model in ADAPTIC a) geometric model; b) extruded computational model

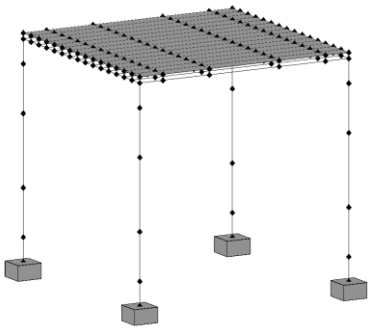

Figure 6.3 Detail of the High Fidelity Model computational model

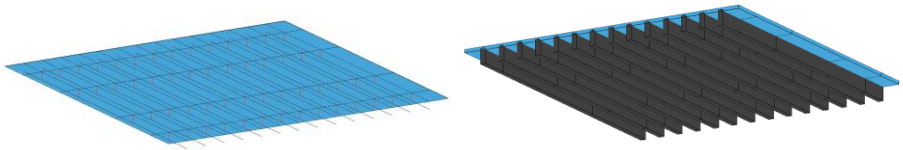

a *b*

Figure 6.4 (Colour) Detail of the one way deck in the High Fidelity Model a) geometric model; b) computational model

The concrete slab and ribs have been modelled accurately. In fact, the floor system is made by one-way RC ribbed slabs spanning in the direction perpendicular to the main frames, as already illustrated in §5.2. Figure 6.3 and Figure 6.4 provide schematic representations of the FE discretisation developed in ADAPTIC for a portion of the floor system in which 1D elastic-plastic beam-column elements have been adopted for modelling reinforced concrete ribs. Each rib has been dividend in five sub-elements and each node has been connected to the concrete 2D slabs by means of a 1D link element (LNKS [63]). The RC slab elements [64, 63] account for material nonlinearity in both concrete and steel reinforcements, for bending and membrane effects and geometric nonlinearity.

Table 6-1 and Table 6-2 report the principal material properties for concrete and steel reinforcement that have been considered in the nonlinear 3D models.

Table 6-1 Concrete materials for the dynamic analysis of the frames

Material property	**cover region**	**core region**
Cylinder Compressive strength (MPa)	20.75	23.25
Young's modulus (MPa)	27386	27386
Strain at maximum strength	2×10^{-3}	2×10^{-3}
Strain at crushing	4×10^{-3}	50×10^{-3}
Tensile strength in tension	1.04 MPa	1.04 MPa

Table 6-2 Steel materials for the dynamic analysis of the frames

Material property	**Rebars**
Yielding strength (MPa)	375
Young's modulus (MPa)	210000
Strain-hardening ratio	0.01

In the infilled frame model (IF) the masonry infill panels have been explicitly modelled and a novel finite macro-element formulation (§4.3) purposely developed and implemented in ADAPTIC has been used (Figure 6.5). The proposed finite element constitutes an original FEM implementation of a discrete macro-element developed at the University of Catania [65, 81, 82] and incorporated in the 3DMacro software [83]. The new ADAPTIC FEM macro-element implementation (MCR4 [63]) has been verified against 3DMacro and experimental results for monotonic and cyclic loading (§4.5).

The material properties in the masonry macro-elements, which represent hollow clay brick-masonry panels of 120 mm thickness, are provided in Table 6-3. Additionally, potential plastic sliding along the mortar joints has been modelled by considering a rigid-plastic Coulomb frictional behavior with cohesion c = 0.4 MPa and friction angle tangent $\tan(\phi)=0.7$.

The softening modulus has been related to the experimental fracture energy according to the Eq. 63.

$$\varepsilon = \frac{2G_f}{f_y l_a} \qquad \textit{Eq. 63}$$

The symbols have the following meanings:

G_f fracture energy;

f_y peak tensile strength;

l_a average dimension of the masonry macro-element.

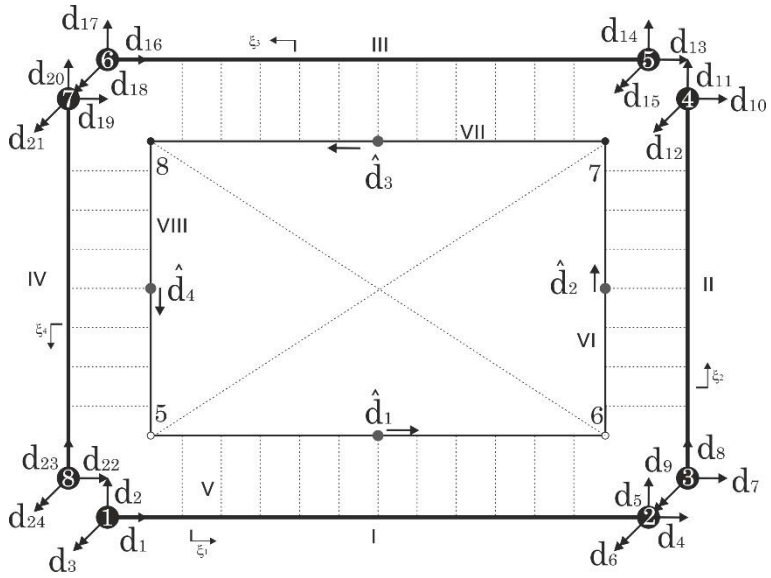

Figure 6.5 Proposed finite macroelement for masonry infill panels

Table 6-3 Steel materials for the dynamic analysis of the frames [89]

Flexural behaviour					**Shear behaviour**			
E [Mpa]	σ_t [Mpa]	σ_c [Mpa]	G_t [N/mm]	G_c [N/mm]	G [Mpa]	f_{v0} [Mpa]	ϕ	G_s [N/mm]
1580	0.1	1	0.02	1	700	0.07	0.58	0.10

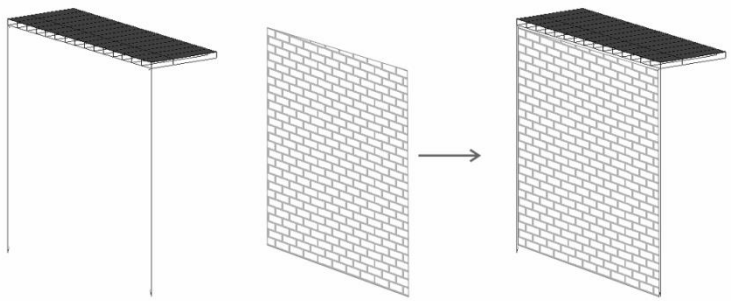

(a) *(b)*

Figure 6.6 Schematic description of the staged construction capability: (a) model for the bare structure, (b) and for the infilled one

Finally, avoiding unrealistic stress distributions in infill masonry panels, a new capability for accounting staged construction has been

developed in ADAPTIC by Prof. B.A. Izzuddin and engaged in the IF model analyses. It has allowed a realistic representation of the non-structural components contribution. More in detail, it guarantees that infill panels do not take dead and imposed loads and that they contribute mainly to withstand seismic actions. Figure 6.6 shows pictorially the staged construction capability; the masonry panels do not provide any contribution in an initial phase under gravity loads but they provide additional resources against horizontal loads.

The high fidelity models, which counts 205.128 degree of freedoms, 37531 frame elements, 15076 slab elements in the IF model, have been coupled with unique partitioned modelling capability in ADAPTIC that allows efficient analysis on High Performance Computing systems for enhancing computational efficiency. Thus, each 3D building model has been divided in 31 partitions and 1 parent file as the Figure 6.7 qualitative illustrates. This capability has increased the computational efficiency and it has reduced the computation effort. Furthermore, the procedure allows adopting a scalable hierarchic distributed memory. Using this enhanced solution strategy, the typical nonlinear dynamic analysis took an average time of 2-3 days, much less than a conventional monolithic model that would have taken several weeks to be solved.

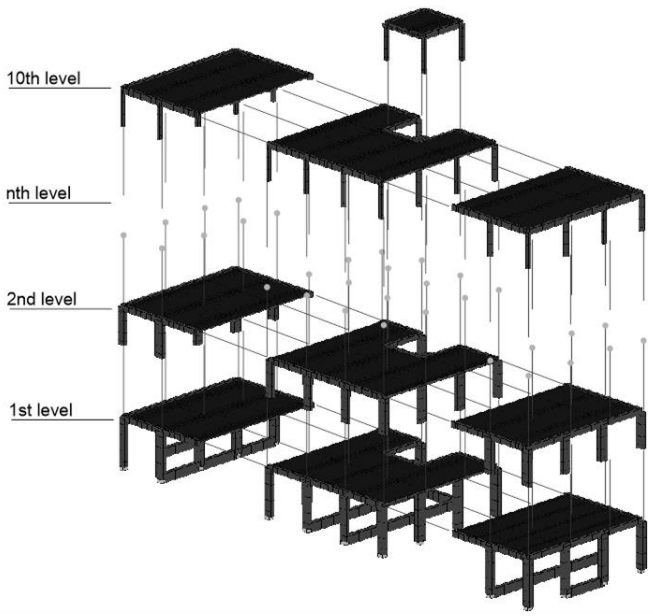

Figure 6.7 Partition strategy with 31 partitions for the analysed building

6.3 Non Linear Dynamic Analyses

Seven nonlinear dynamic time history analyses (NLDA1 to NLDA7), which have considered seven different sets of ground motion acceleration records and that have simultaneously acted along the three spatial directions [97], have been carried out on the high fidelity 3D models. The achieved results have been managed for assessing the typical RC multi-storey building seismic performance. The assessment has been conducted according to the Italian Seismic Code [23, 24]. In particular, the following response characteristics have been analysed:

- horizontal displacements;
- inter-storey drifts;
- ductile mechanisms (chord rotation);
- brittle mechanisms (shear failure).

The horizontal displacements and inter-storey drifts have been considered for evaluating the displacement demands at each storey level and in the whole structure. On the other hand, inter-storey drift capacity can be related to the ultimate chord rotation capacity of the RC columns for each storey.

6.4 Seismic and Robustness Assessment

The global seismic response, determined using the BF model, is illustrated in Figure 6.8, where the deformed shapes at the last step of the analyses are shown. All the colour maps have the same scale. The displacements, except those for 5^{th} and 6^{th} analyses, are magnified 10 times for capturing the ultimate deformations. The average drift values in the two planar directions and the vertical displacements are shown in Figure 6.10. These results suggest that the seismic response of the original building, which neglect the infill panel contribution, is not satisfactory. Large drift values indicate the development of soft storey collapse mechanisms at the top levels (e.g. at seventh and eighth storey).

The results obtained employing the infilled model (Figure 6.9) have showed a minor drift demand at the top floors.

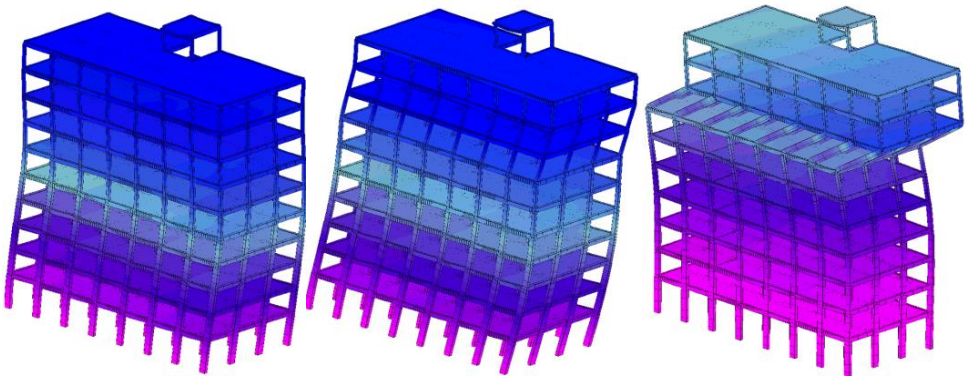

NLDA1 *NLDA2* *NLDA3*

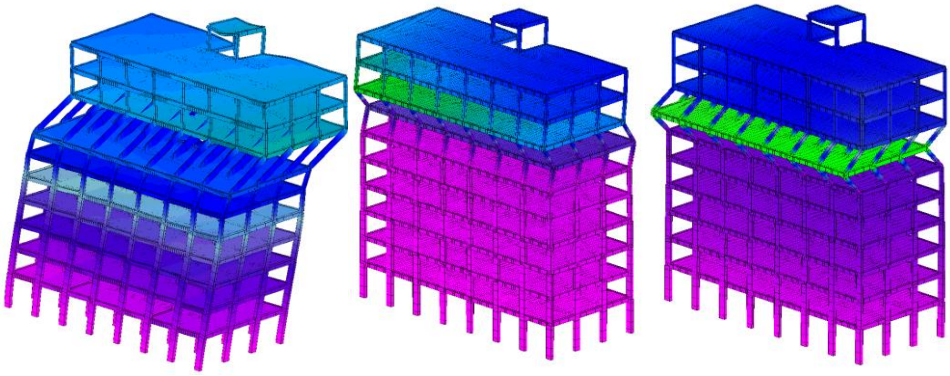

NLDA4 *NLDA5* *NLDA6*

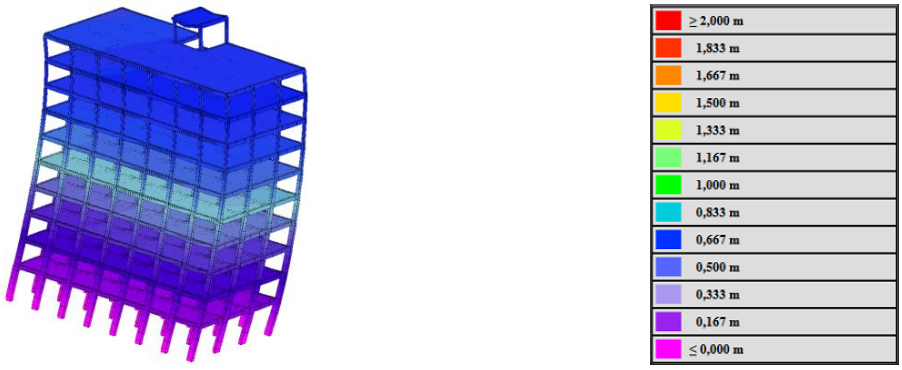

NLDA7

Figure 6.8 Global response of the BF model for the seven accelerograms

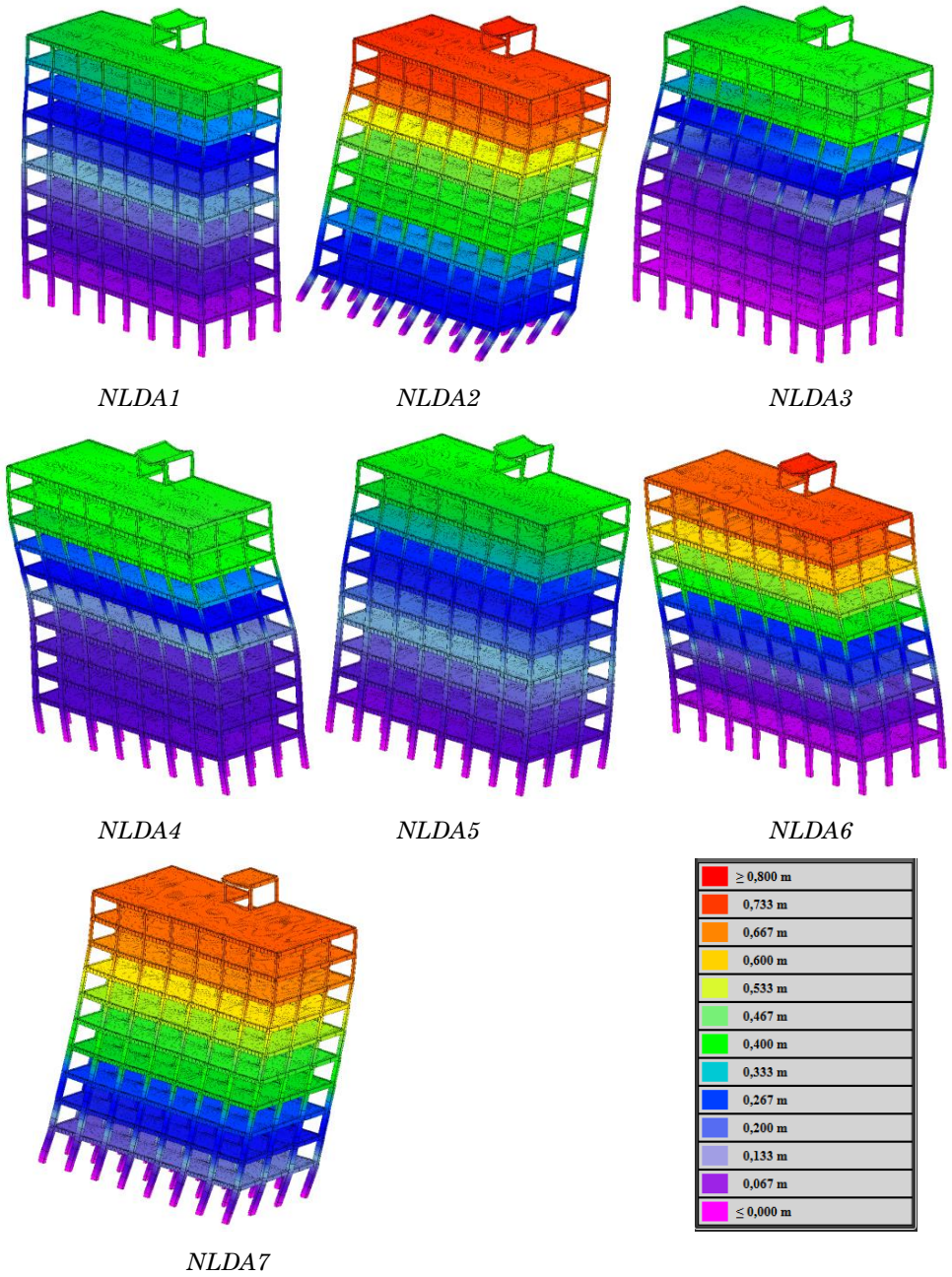

Figure 6.9 Global response of the IF model for the seven accelerograms

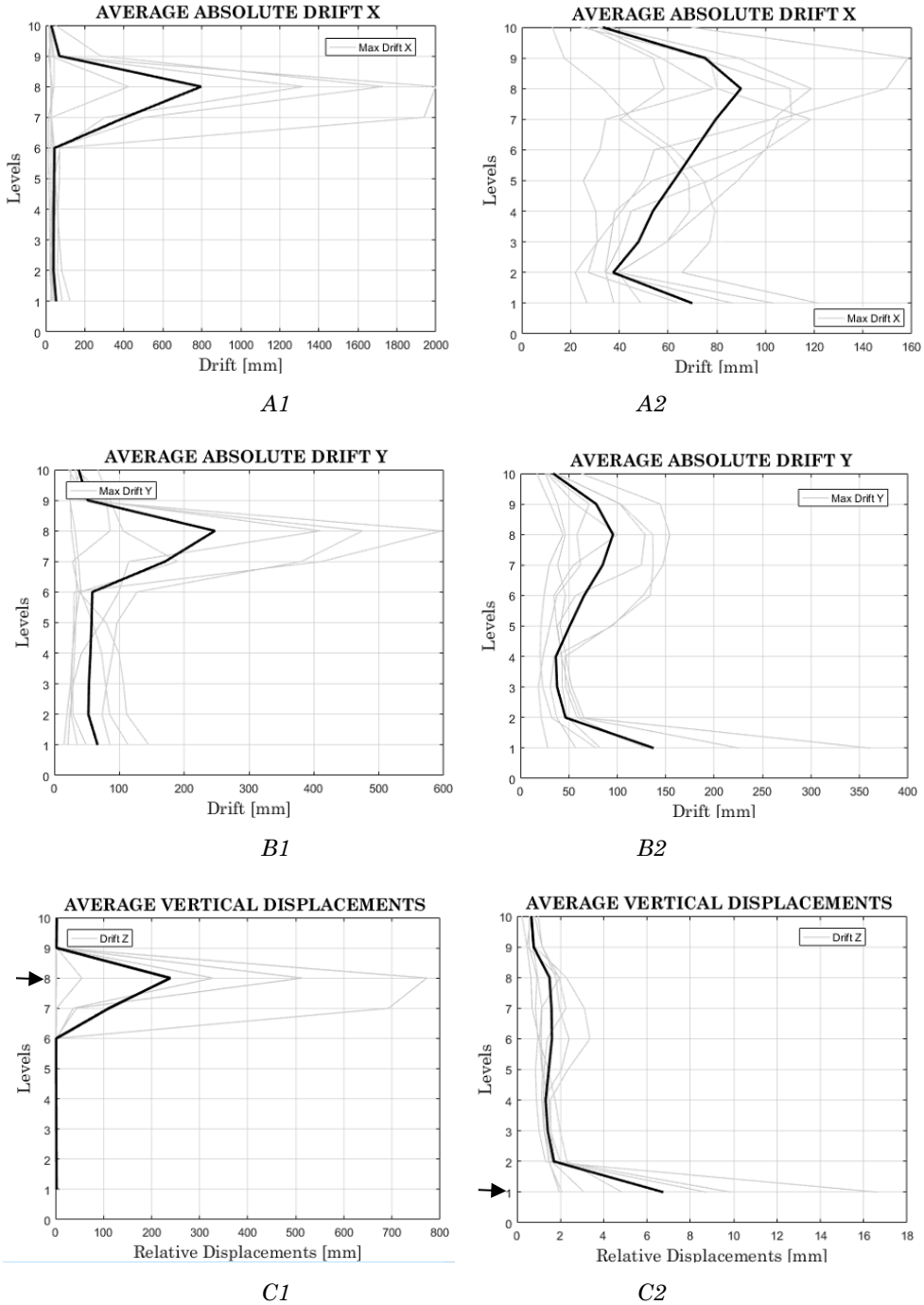

A1 *A2*

B1 *B2*

C1 *C2*

Figure 6.10 Average drift values for the BF (.1) and IF (.2) model in the two planar (a, b) and vertical displacements (c)

Figure 6.10 reports the average maximum drifts in the two planar directions and the vertical displacements. The results have showed that the presence of unreinforced masonry panels has influenced the seismic response of the building structure. In disagreement with the bare frame model in which the drift demand are localised at the eighth floor, the absence of ground floor panels has concentrated the drift demand at the base floor in the infill frame model and a soft first-storey collapse may be expected. At the same time, the analyses on the infilled configuration have underlined less localised but still significant drift demand at the eighth level.

The Figure 6.10.C define the vertical displacements in the bare and infilled cases. As the figure C1 shows, all the analyses have pointed out a localised collapse of the superior floors in disagreement with the figure C2 in which the maximum vertical displacements of the infill frame structure are localised at the ground floor due to the "soft storey" mechanism. The vertical displacement demand depicted in figure C1, demonstrate that the structure is prone to potential progressive collapse due to localised damages. An initial collapse scenario may be considered as the Figure 6.11 reports. It represents the collapse of a concrete reinforced column. The interaction with the staircases has triggered the loss of bearing capacity of the column and the vertical collapse of the superior floors.

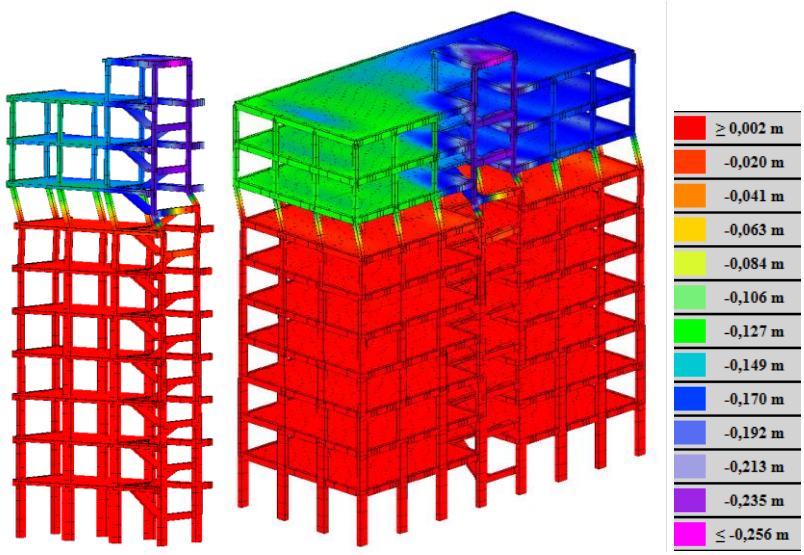

Figure 6.11 (Colour) Detail of the column loss scenario during the NLDA5 analysis.

The Table 6-4 summarises the average absolute drift demands and the vertical displacements.

Table 6-4 Maximum drifts determined by the BF and IF models

Model	Average absolute Drift X [mm]	Average absolute Drift Y [mm]	Average Vertical Displacements [mm]
BF	~800	~230	~210
IF	~90	~170	~8

The ductile behaviour of each structural element has been checked in agreement with code-consistent equations (APPENDIX I) in terms of chord demand and capacity.

The *chord rotation* is defined as the angle between the tangent to the axis at the end and the line that connects this point with the contra-flexure section, placed at the end of the shear span ($Lv = M/V =$ Moment ratio at the end section) as Figure 6.12 shows.

On the other hand, the chord rotation depends from the element drift ratio. Therefore, the chord rotation is the deflection at the end of the shear span with respect to the tangent to the axis at the yielding end divided by the shear span.

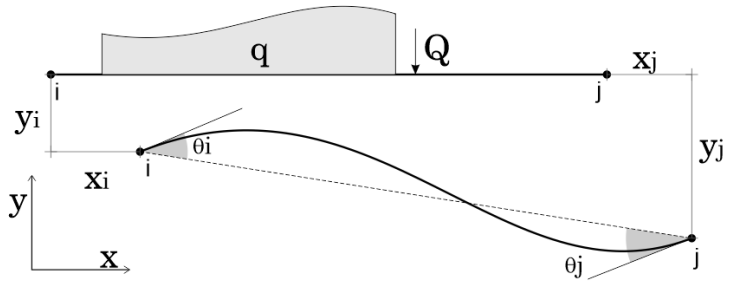

Figure 6.12 General interpretation of the Chord Rotation in Beam/Column Elements

The Italian Seismic Design Code [23, 24] recommends the use of following expression (Eq. 71).

$$\theta_{um} = \frac{1}{\gamma_{el}} 0.016\left(0.3^{\upsilon}\right)\left[\frac{\max\left(0.01;\omega'\right)}{\max\left(0.01;\omega\right)} fc\right]^{0.225}\left(\frac{L_v}{h}\right)^{0.35} 25^{\left(\alpha\rho_{sx}\frac{fyw}{fc}\right)}\left(1.25^{100\rho_d}\right) \qquad \textit{Eq. 64}$$

The Eurocode 8 evaluates the ultimate chord capacity (Limit State Near Collapse (NC)), elastic plus inelastic part, with the following equation Eq. 65:

$$\theta_{um} = \frac{1}{\gamma_{el}} 0.016\left(0.3^{\upsilon}\right)\left[\frac{\max\left(0.01;\omega'\right)}{\max\left(0.01;\omega\right)} fc\right]^{0.225}\left(\min\left(9;\frac{L_v}{h}\right)\right)^{0.35} 25^{\left(\alpha\rho_{sx}\frac{fyw}{fc}\right)}\left(1.25^{100\rho_d}\right)$$

Eq. 65

A more detailed explanation of the two equations is reported in APPENDIX I.

It is worth to noticing that several columns fail due to the displacement demands and shear forces. More specifically, the BF model, which neglects infill panel contribution, develops large chord rotations at the end of the columns that are related to the large inter-storey drifts. On the other hand, the IF model allowing for masonry infill achieves smaller rotations and shear forces in the columns that are induced by the local interaction with the masonry cladding. Both

numerical descriptions clearly indicate local failures in a significant number of RC components under the design ground motion.

The shear checks have been performed in a code-consistent manner. The shear capacity have been evaluated by adapting the formulas for existing reinforced concrete frame structures supposing that the maximum level of confidence and a safety factor equal to 1 that affects the material mechanical properties.

By preliminary consideration on experimental tests, the shear capacity equation suggested by the Italian Seismic Code reduces significantly the ultimate shear capacity of the reinforced concrete elements. Figure 6.13 shows the results of a detailed numerical simulation of an experimental cyclici test on a RC column [98] performed by means of an accurate model of a reinforced concrete column implemented in the software LUSAS [39] . As the graphic depicts, the Italian Seismic Code formula underextimates the ultimate shear capacity. On the other hand, the Eurocode expression better extimates the ultimate shear capacity accounting for a capacity degradation related to the plastic part of the chord rotation demand. Base on this consideration, the shear checks in the present Section have been performed adopting the Eurocode formulation.

Additional details have been reported in APPENDIX II.

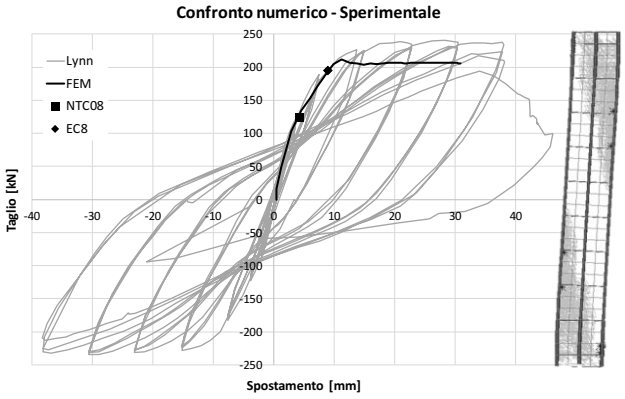

Figure 6.13 Cyclic experimental results [98], numerical simulation and shear capacity assessment in agreement with Eurocode and NTC08.

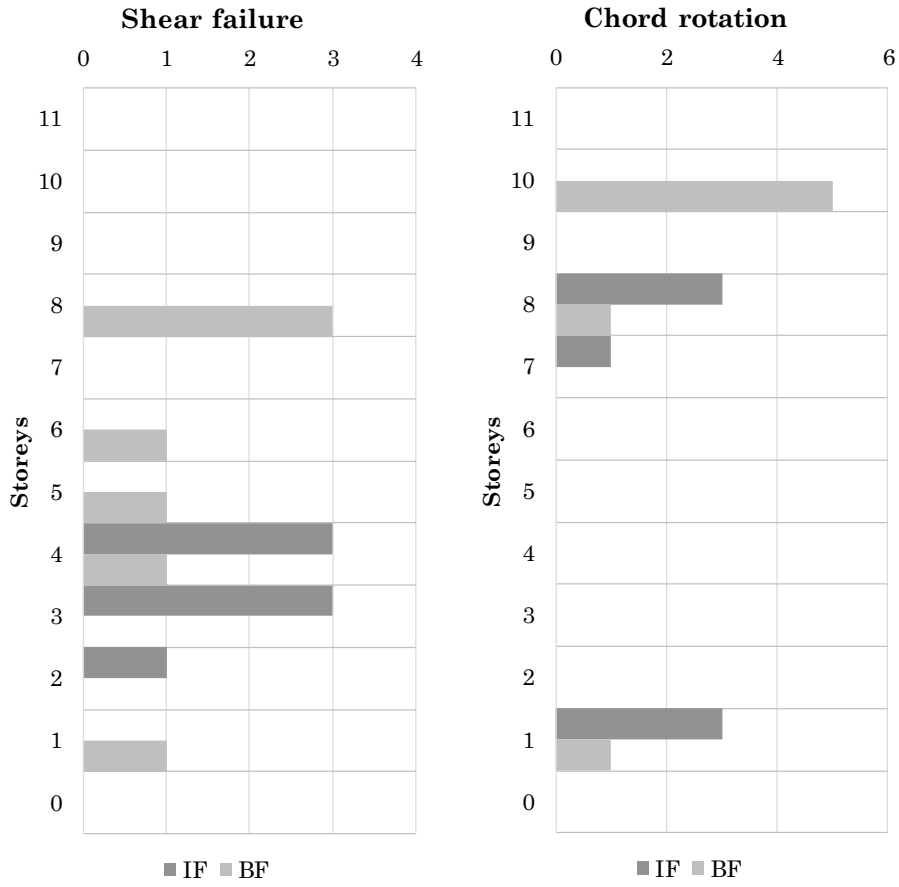

Figure 6.14 Localization of first failures a) Shear failure b) Ultimate chord rotation

The Figure 6.14 depicts the localisation of the initial failures in the BF (bare frame) and IF (infill frame) models. As the figure shows, the shear failures are localised in the initial storeys in case of infill frames and at the upper floors for the bare frame models. On the other hand, the ultimate chord rotation is achieved at the first and eighth storey in case of masonry panels. The absence of the panels determinates the concentration of chord demand at the higher levels and in particular at the tenth storey, showing a significant contribution of the higher modes of vibration.

According to the ductile and fragile code-consistent checks, the following figures report the time history results of all members.

In the following figures, the ratio between Demand and Capacity is represented for each of the investigated element and it is represented for each analysis instants. Each figures report the results for each analysis. Additional information have been reported on the left of each diagrams; the first failed element or the element that has reached the maximum ratio is identified and the related partition is specified.

The figures between Figure 6.15 to Figure 6.21 report the code-consistent check ratios in terms of Shear Demand over Capacity in all the investigated elements of the bare frame model.

The figures between Figure 6.22 to Figure 6.28 report the code-consistent check ratios in terms of Chord Rotation Demand over Capacity. The stream of curves consider the bare frame model.

The figures between Figure 6.29 to Figure 6.35 report the code-consistent check ratios in terms of Shear Demand over Capacity in all the investigated elements of the infill frame model.

The figures between Figure 6.36 to Figure 6.42 report the code-consistent check ratios in terms of Chord Rotation Demand over Capacity. The stream of curves consider the infill frame model.

The figures return the information that have been collected and summarised in Figure 6.14 and that has been already discussed. On the other hand, the figures contribute to identify the variation of demand in all over the checked elements for each analysis.

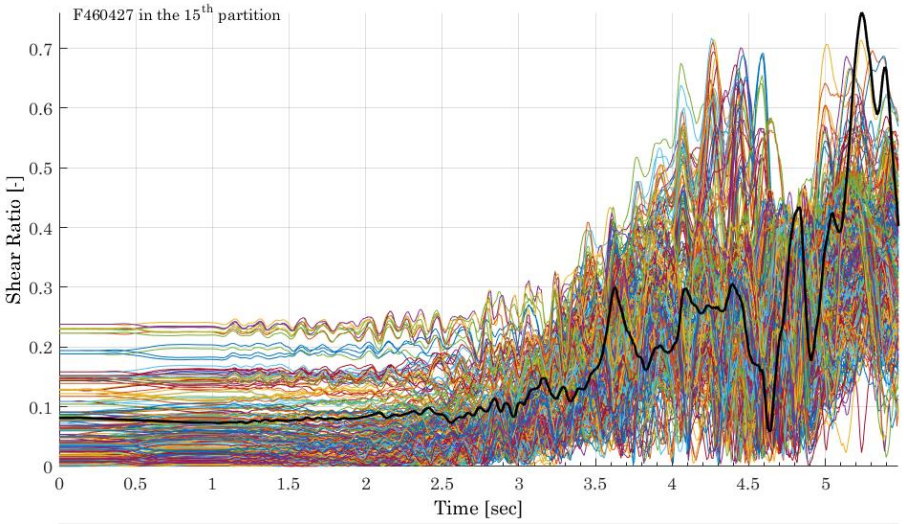

Figure 6.15 (Colour) Shear demand/capacity ratio for the BF model in the NLDA1 analysis.

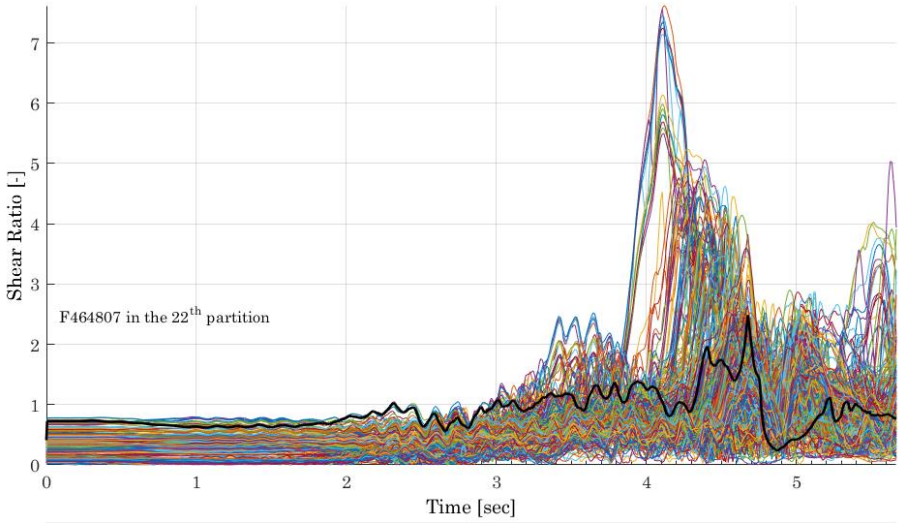

Figure 6.16 (Colour) Shear demand/capacity ratio for the BF model in the NLDA2 analysis.

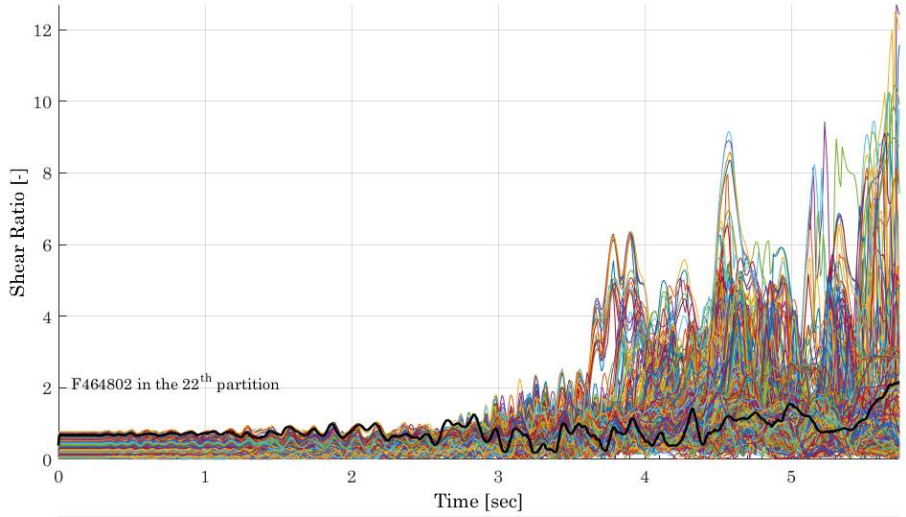

Figure 6.17 (Colour) Shear demand/capacity ratio for the BF model in the NLDA3 analysis.

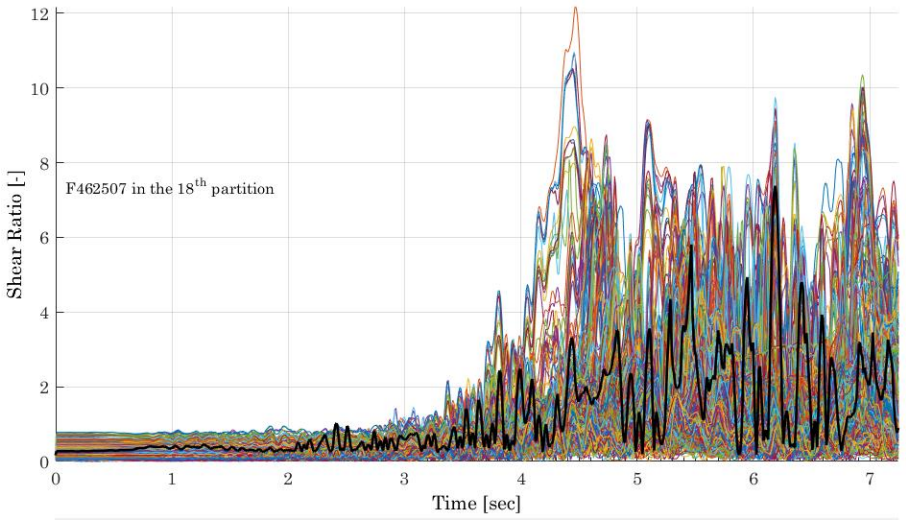

Figure 6.18 (Colour) Shear demand/capacity ratio for the BF model in the NLDA4 analysis.

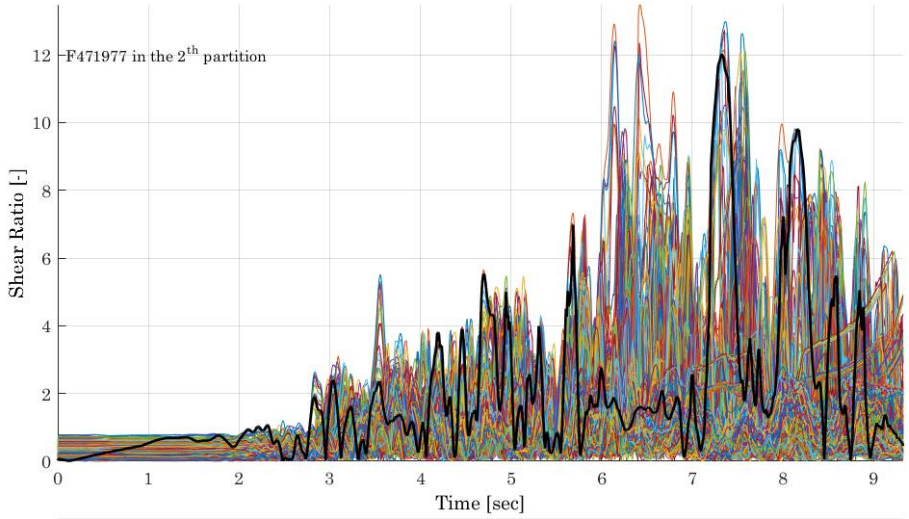

Figure 6.19 (Colour) Shear demand/capacity ratio for the BF model in the NLDA5 analysis.

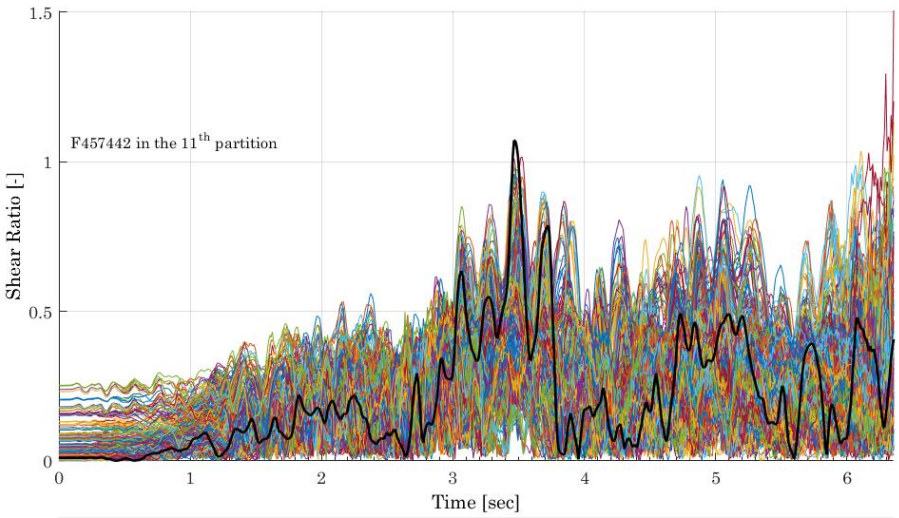

Figure 6.20 (Colour) Shear demand/capacity ratio for the BF model in the NLDA6 analysis.

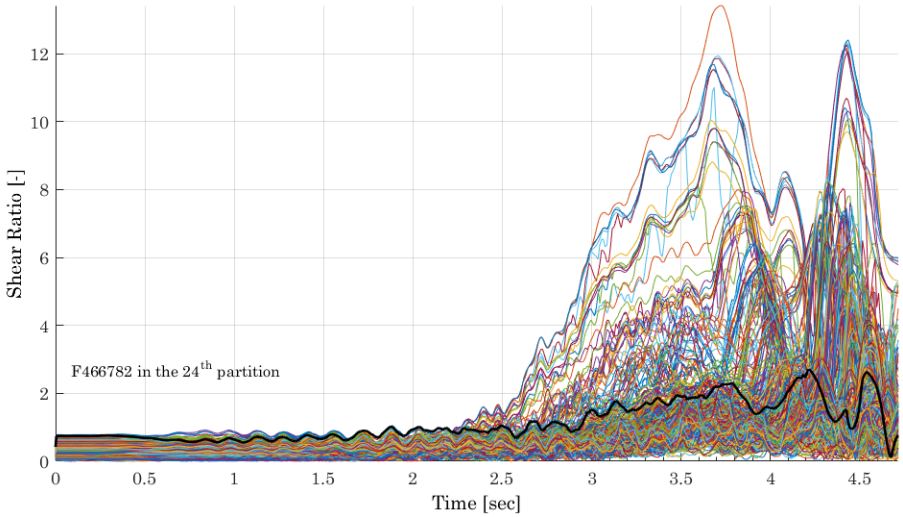

Figure 6.21 (Colour) Shear demand/capacity ratio for the BF model in the NLDA7 analysis.

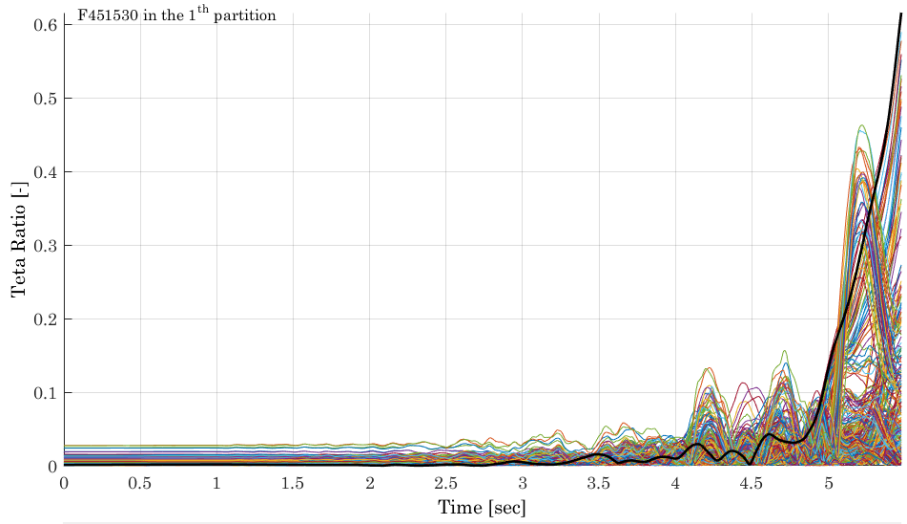

Figure 6.22 (Colour) Chord rotation ratios for the BF model in the NLDA1 analysis.

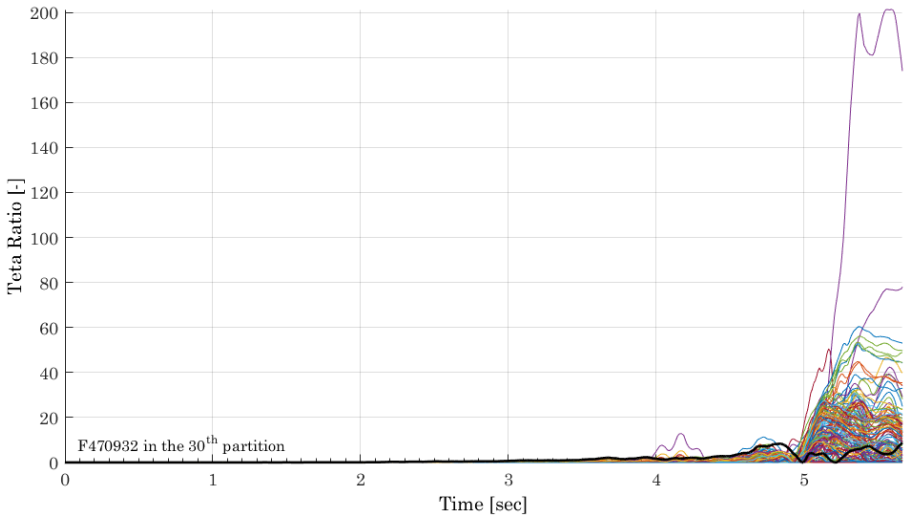

Figure 6.23 (Colour) Chord rotation ratios for the BF model in the NLDA2 analysis.

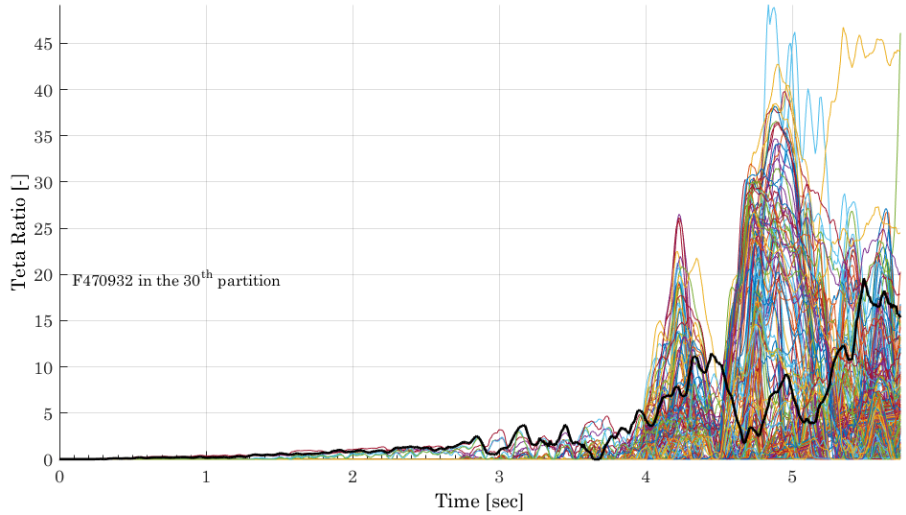

Figure 6.24 (Colour) Chord rotation ratios for the BF model in the NLDA3 analysis.

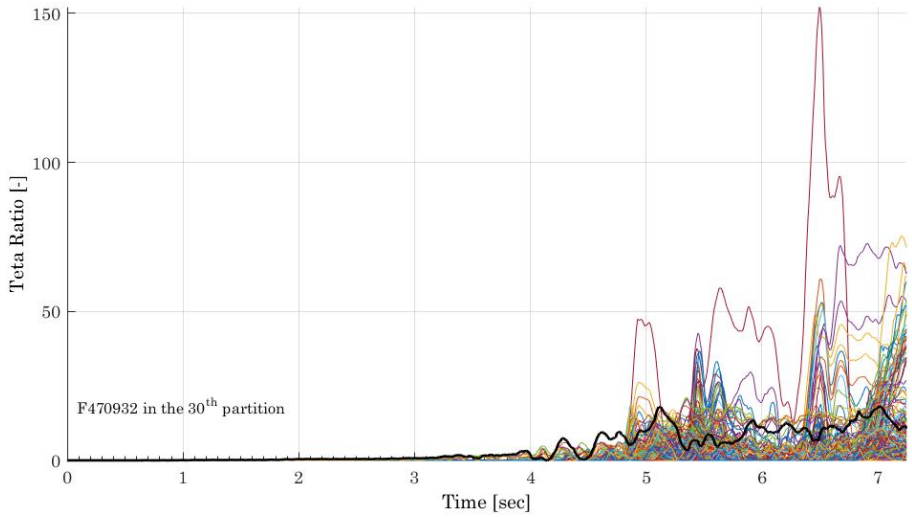

Figure 6.25 (Colour) Chord rotation ratios for the BF model in the NLDA4 analysis.

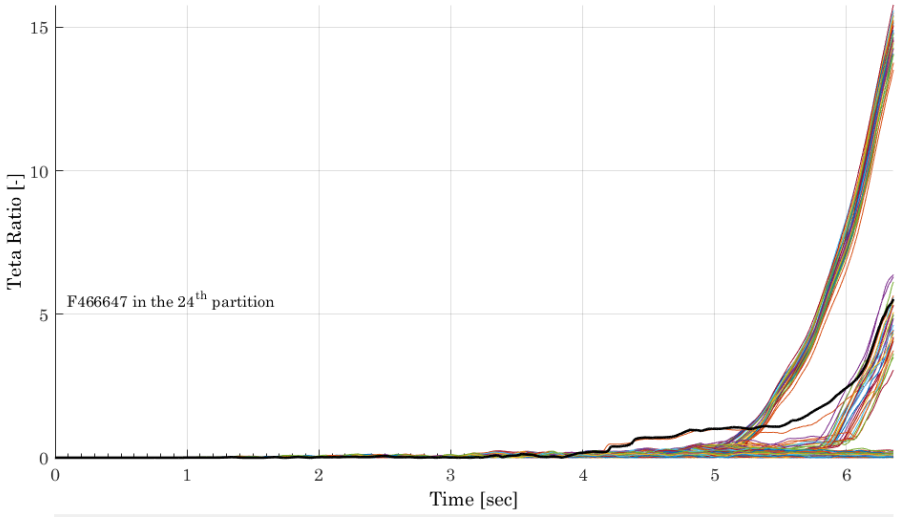

Figure 6.26 (Colour) Chord rotation ratios for the BF model in the NLDA5 analysis.

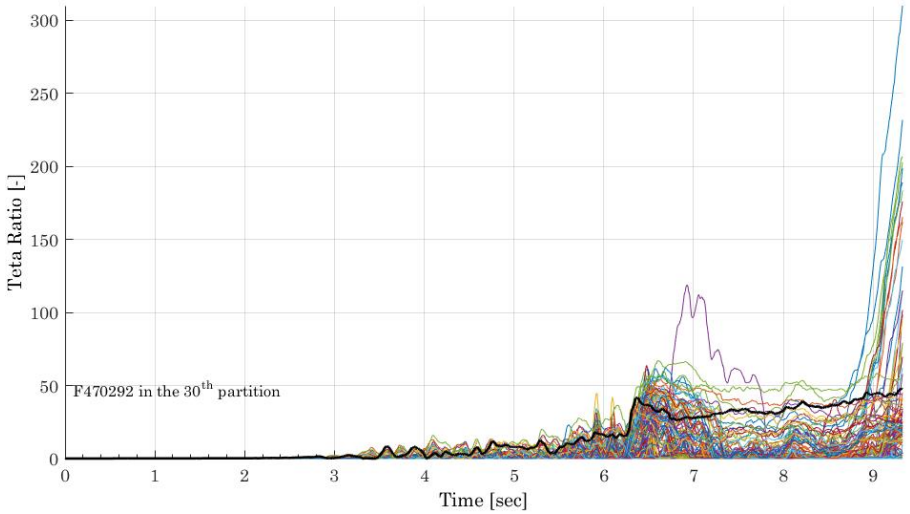

Figure 6.27 (Colour) Chord rotation ratios for the BF model in the NLDA6 analysis.

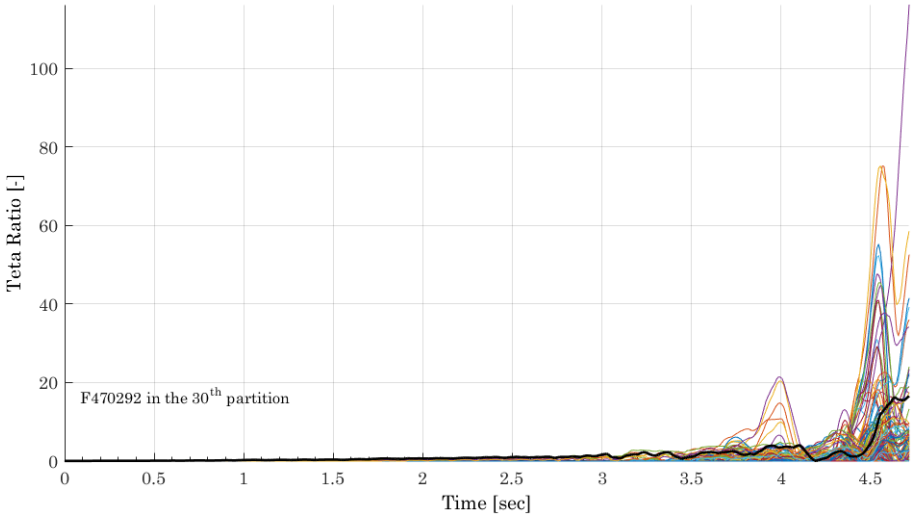

Figure 6.28 (Colour) Chord rotation ratios for the BF model in the NLDA7 analysis.

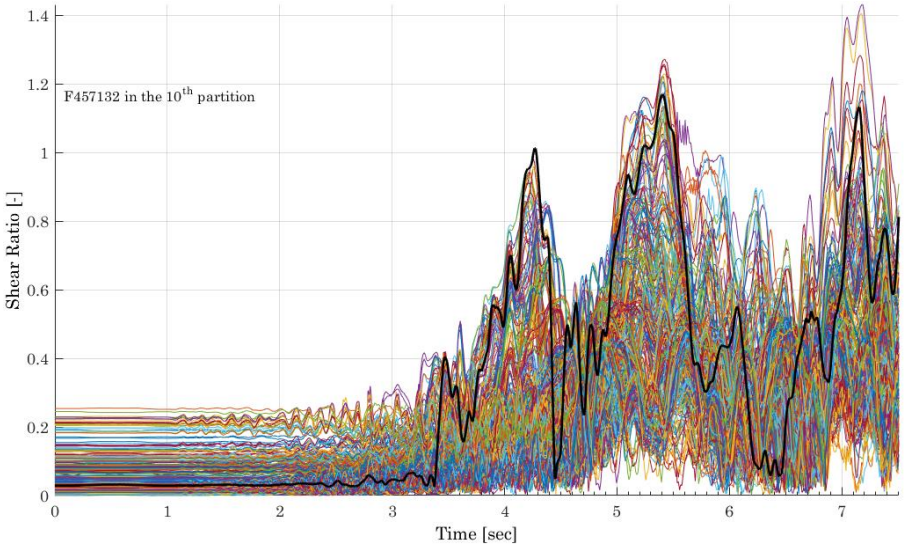

Figure 6.29 (Colour) Shear demand/capacity ratio for the IF model in the NLDA1 analysis.

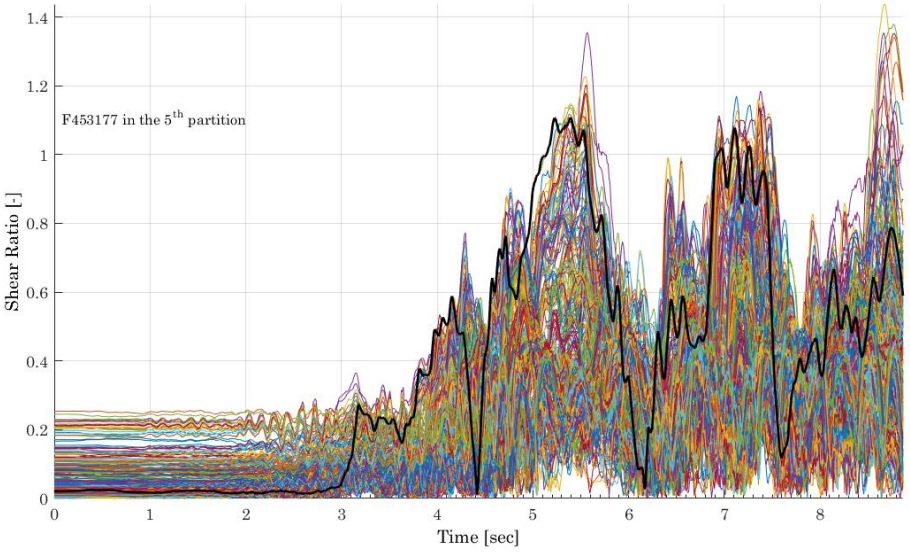

Figure 6.30 (Colour) Shear demand/capacity ratio for the IF model in the NLDA2 analysis.

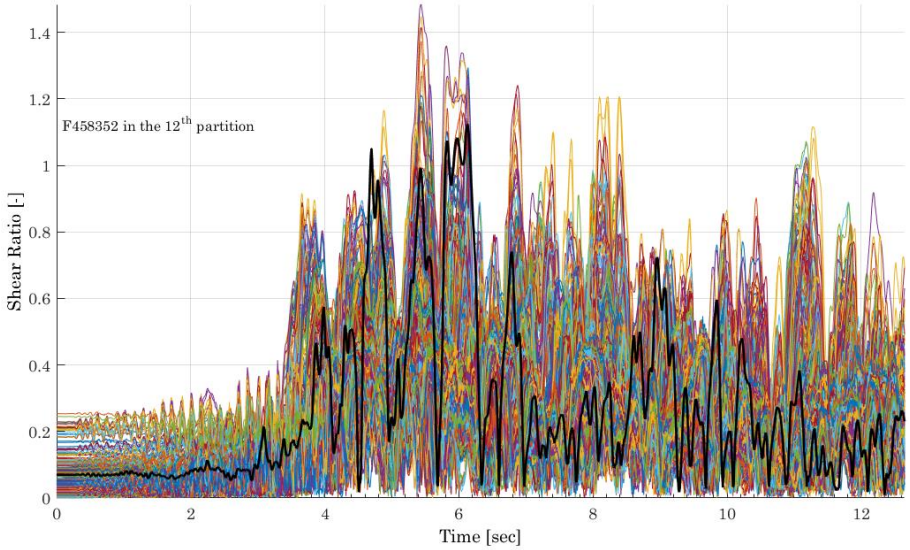

Figure 6.31 (Colour) Shear demand/capacity ratio for the IF model in the NLDA3 analysis.

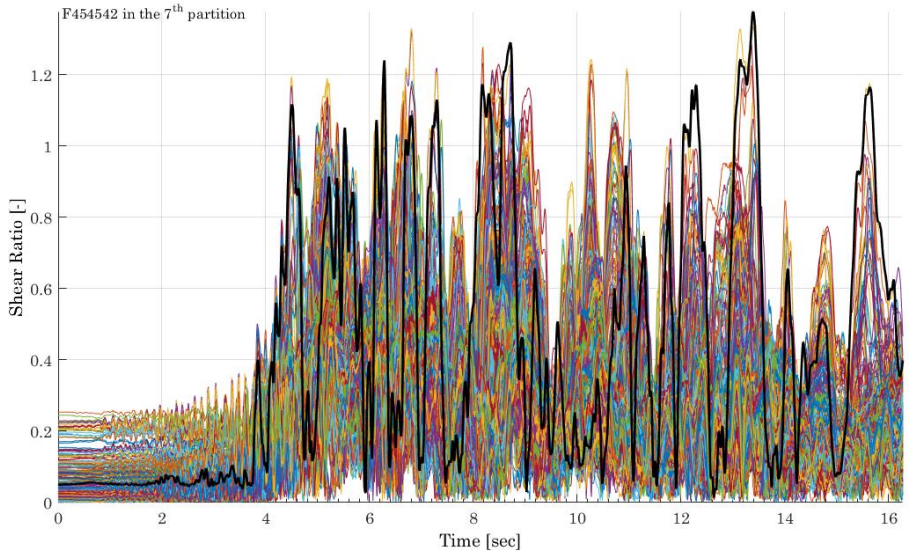

Figure 6.32 (Colour) Shear demand/capacity ratio for the IF model in the NLDA4 analysis.

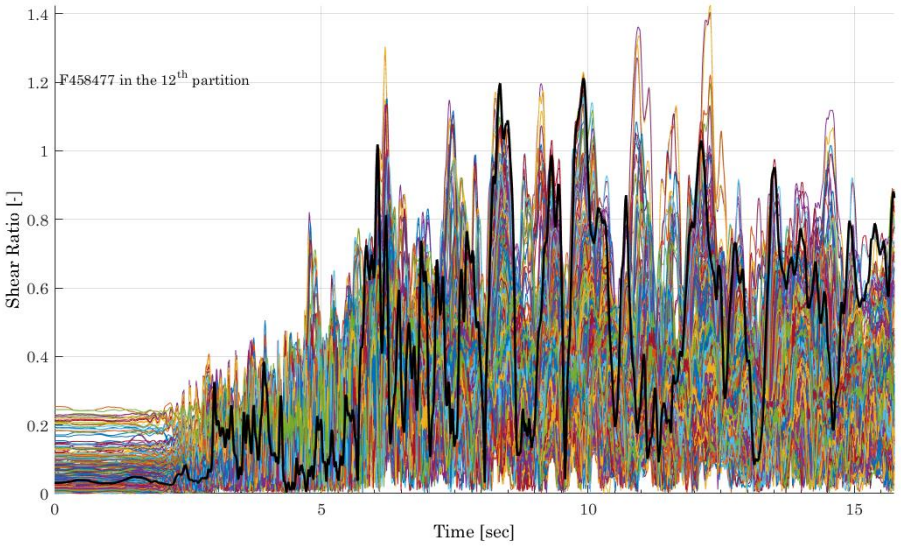

Figure 6.33 (Colour) Shear demand/capacity ratio for the IF model in the NLDA5 analysis.

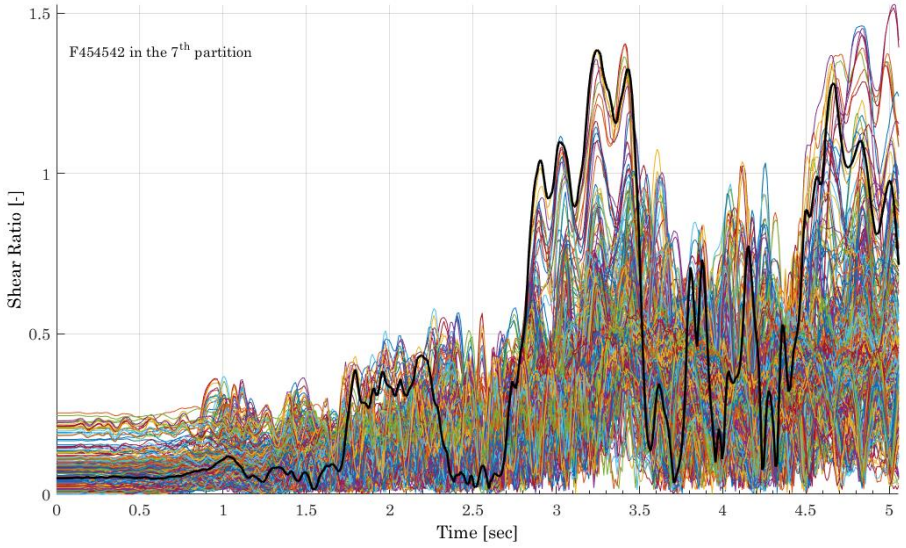

Figure 6.34 (Colour) Shear demand/capacity ratio for the IF model in the NLDA6 analysis.

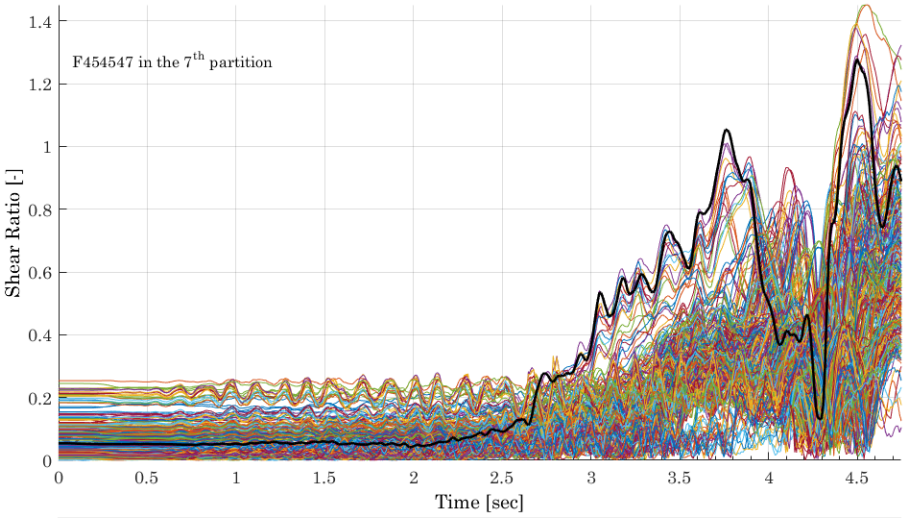

Figure 6.35 (Colour) Shear demand/capacity ratio for the IF model in the NLDA7 analysis.

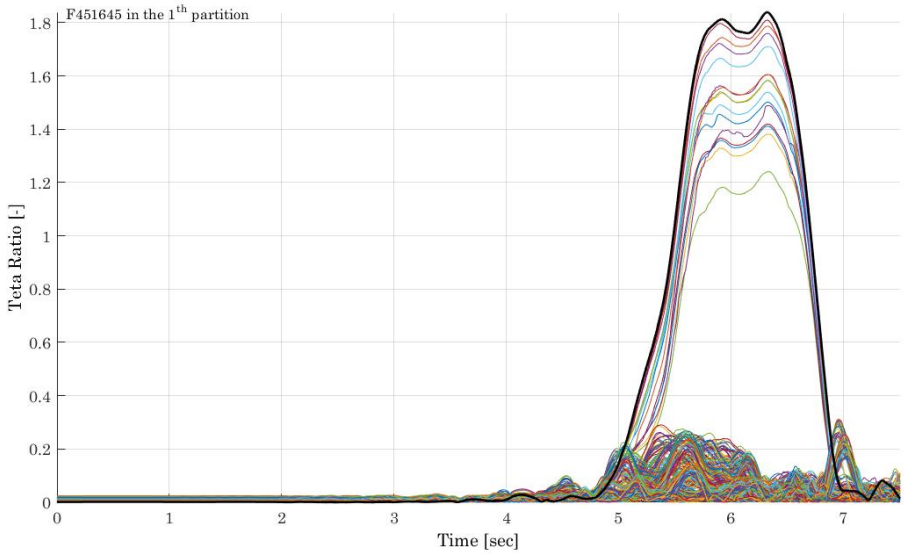

Figure 6.36 (Colour) Chord rotation ratios for the IF model in the NLDA1 analysis.

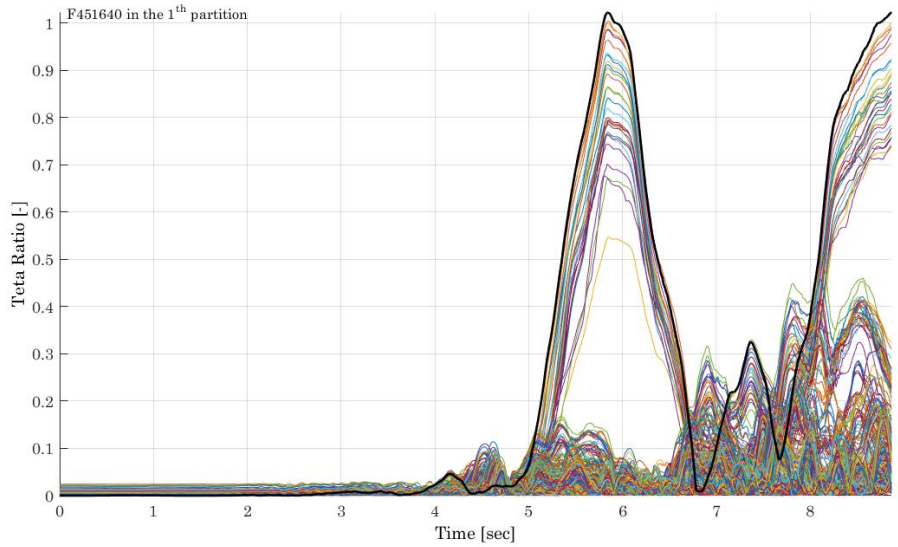

Figure 6.37 (Colour) Chord rotation ratios for the IF model in the NLDA2 analysis.

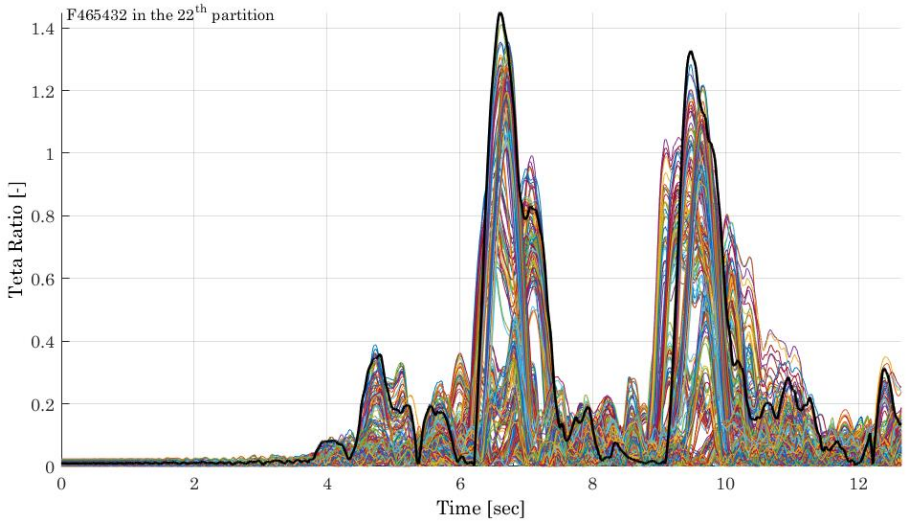

Figure 6.38 (Colour) Chord rotation ratios for the IF model in the NLDA3 analysis.

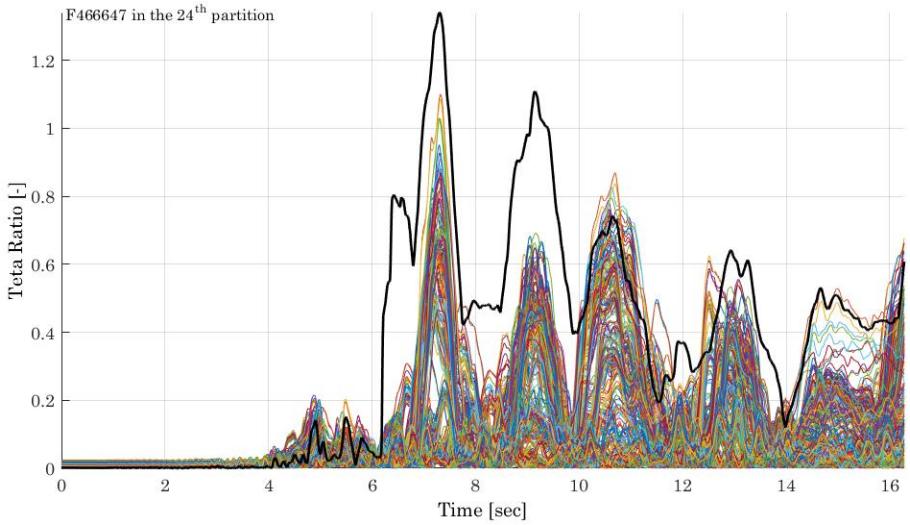

Figure 6.39 (Colour) Chord rotation ratios for the IF model in the NLDA4 analysis.

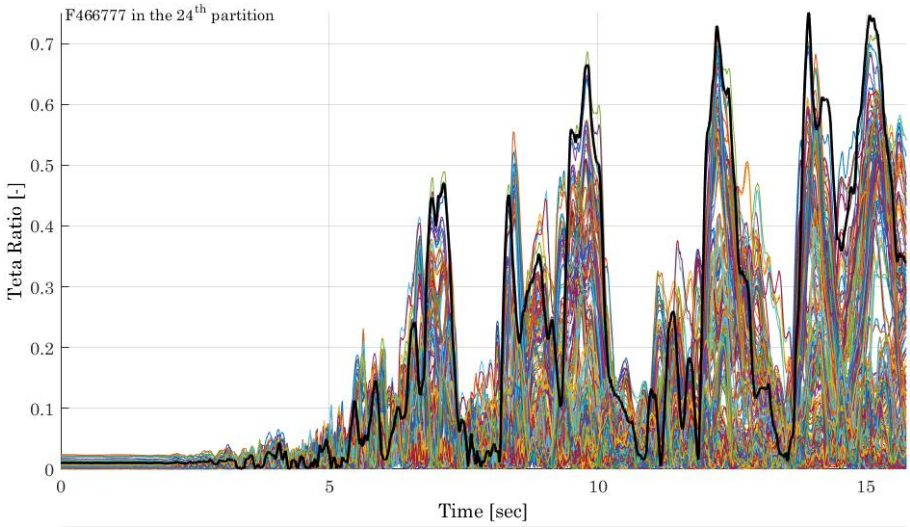

Figure 6.40 (Colour) Chord rotation ratios for the IF model in the NLDA5 analysis.

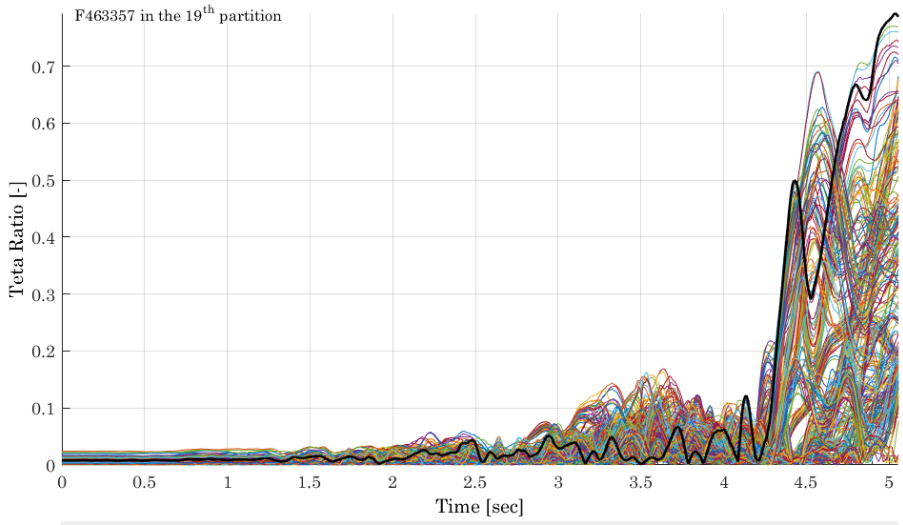

Figure 6.41 (Colour) Chord rotation ratios for the IF model in the NLDA6 analysis.

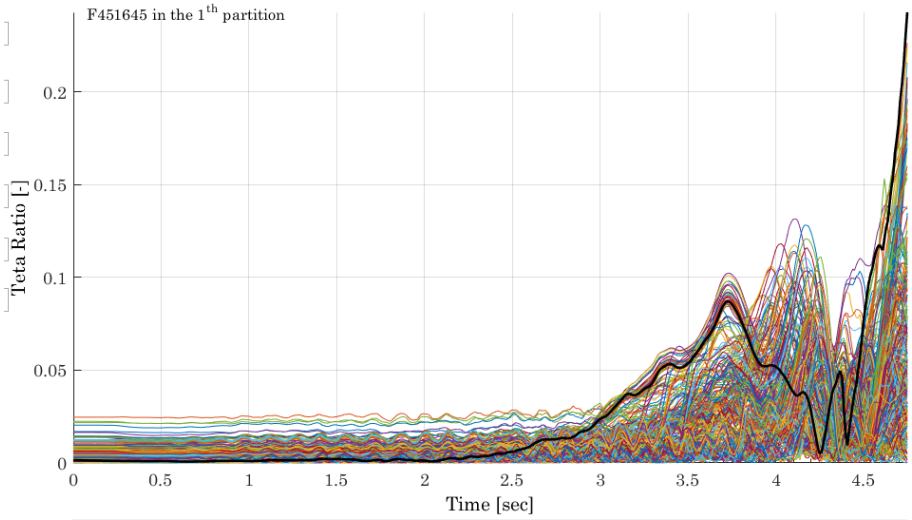

Figure 6.42 (Colour) Chord rotation ratios for the IF model in the NLDA7 analysis.

CHAPTER 7. PROPOSED RETROFITTING STRATEGY

The results obtained in the assessment of the ten-storey RC building have guided the design of the retrofitting solution. After an overview of existing retrofitting methodologies proposed in the literature [99], an innovative solution is proposed. The proposal has been obtained in cooperation with the supervisors of the present study and has been presented in a conference paper [94]. In the design stage several retrofitting solution has been investigated by using the software 3DMacro with implemented code-based checks. The selected strategy consists in an innovative structural perimetral steel skeleton made by a synergetic combination of centred braced frames and eccentric bracing system endowed with dissipative shear links. As an alternative of the proposed solution. The latter strategy takes advantage of the interaction of RC shear walls and dissipative eccentric bracing systems. The proposed solution, based on the innovative Eccentric Bracing System configuration, has been investigated by means of a high fidelity model implemented in the software ADAPTIC.

7.1 Introduction

The identification and calibration of a reliable retrofitting strategy for existing structures is a main topic in the structural engineering research as the Figure 7.1 shows. The figure reports the number of scientific publications in the last 40 years that have been index-linked by the web site Scopus.com [100] under the key words of "Retrofitting" and "Existing building". As the figure demonstrates, the scientific community is strongly interested in this area and the publications have a growing trend.

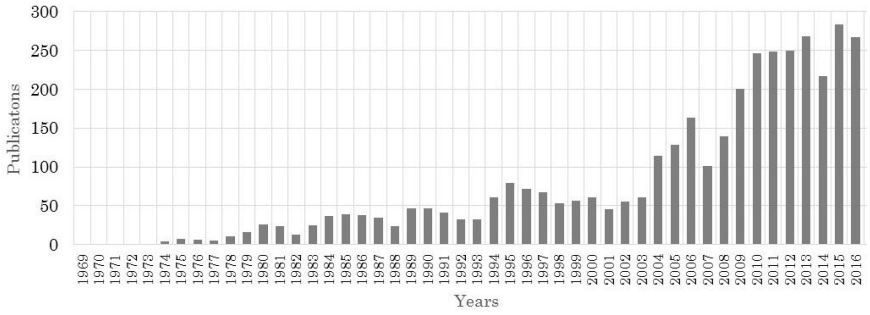

Figure 7.1 Publications on retrofitting strategies of existing structures [100]

All the retrofitting technics have the purpose of mitigating or inhibiting the structural deficiencies that can determinate global or local structural failures. As some author noticed [101], the conventional or advanced seismic retrofitting methodologies can be roughly broken down in two main groups. These groups are definable as Capacity Modification Techniques and Demand Modification Techniques. The first group's purpose is the improvement of one or more seismic parameters that define structural deficiencies. The methodologies increase the Strength, Stiffness or Ductility of the entire structural system by means of local improvements or introduction of additional more performing elements. In these terms, the following retrofitting solution can be pointed out:

- Reinforced Concrete Frames with Masonry Infill
- Beam-Column Joints and Connections
- Column Strengthening

- Bracing
- Masonry Strengthening
- Concrete Walls
- Metal Shear Panels

The second group is defined by retrofitting strategies that are based on the reduction or mitigation of the seismic demand. The decrement may be achieved by means of passive systems such as:

- Seismic Isolation
- Damping systems
- Dissipative systems

On the other hand, an alternative technique follows the so called Weakening Approach as part of the second group. In this case, the seismic response of the structure is modified and the seismic demand is consequently reduced. In this scenario, the seismic demand decreases in critical regions such as shear walls or beam-column joints [102].

From a general point of view, Figure 7.2 summarises the philosophy behind the mentioned approaches.

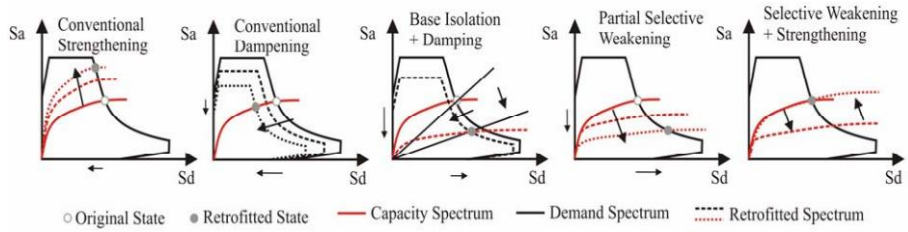

Figure 7.2 (Colour) Acceleration-Displacement Response Spectrum (ADRS) illustration of different retrofit philosophies and strategies a) strengthening b) added damping c) base isolation d) partial SW (weakening only) e) full SW (weakening and further enhancement) [102].

Lastly, hybrid solutions are frequently applied due to the several and simultaneous weaknesses that defines the seismic response of existing framed or infill-framed concrete structures.

In this Section, an innovative peripheral hybrid retrofitting techniques is proposed and discussed in term of seismic efficiency. The results of the original concrete building, discussed at CHAPTER 6, indicated the structural deficiencies and oriented the definition of the retrofitting solution. The retrofitting strategy consists in an innovative structural

steel bracing system made by a synergetic combination of centred braced frames and eccentric bracing systems endowed with dissipative shear links.

7.2 Literature Review

Several seismic upgrading techniques have been presented in literature and usually a synergetic combination of two or more of them may be necessary to achieve the seismic rehabilitation of the reinforced concrete structure, especially in mid- or tall-rise buildings. In the following, few of these numerous techniques are exposed.

Jacketing of existing beams, columns, or joints

As underlined in this thesis, the buildings that were designed before the introduction of national seismic regulations are affected by poor seismic detailing and inadequacy in shear capacity and column ductility. Jacketing existing beams, columns, or joints with new reinforced concrete, steel or fibre wrap overlays can be carried out. Several authors carried out numerical and experimental campaigns on the behaviour of concrete structural elements before and after the Carbon Fiber Reinforced Polymer (CFRP) wrapping.

Steel Bracing

The main advantages of the steel bracing retrofitting technique are the relatively easy design process, the possible compatibility with openings and architectural needs, the lightness of the elements and the advantages in terms of constructions process.

The techniques that modified the structural response are relatively costly and this aspect reduces its application in government or historical buildings [103], but Centred or Eccentric Steel Bracings Systems modify the structural response in seismic or collapse scenarios [104] maintaining the before mentioned advantages and reducing the cost.

Figure 7.3 Steel Braced Frame

Buckling Restrained Braces (BRB)

The buckling restrained braced frames (BRBFs) are one of the newest seismic technologies that have been tested and introduced in the seismic engineering. They have been invented in the 80's and implemented in Japan in 1988 for the first time. The innovative system had the purpose of cover the deficiencies of traditional seismic upgrading systems such as concentric bracing. Although the BRBFs have a similar geometric configuration, their cyclic behaviour is deeply different and regular. The Figure 7.4 compares the cyclic behaviour of a typical concentred brace and a buckling restrained brace [105]. As the figure shows, the step forward of this technology is avoiding buckling phenomena in compression. An internal steel core, an external filled steel tube compose the system. Concrete-like material fills the space between the tube and the brace avoiding buckling issues. For preventing bonding to the concrete, a special coating covers the brace.

The system has several advantages such as:

- Simple hysteretic model defines the cyclic behaviour;
- Special connection systems are not necessary between BRB and frame (concrete of steel);
- Lightness in comparing to shear walls or equivalent conventional concentric system and consequent reduced foundation loads;
- Symmetric tensile-compression behaviour;
- Possibility of replacing after strong earthquakes.

On the other hand, few disadvantages are still in this technology:

- The lack of recentering mechanism;
- Lack of detecting and checking damaged elements methods;
- Dependence of the yielding limit from the geometric and material properties of the steel core.

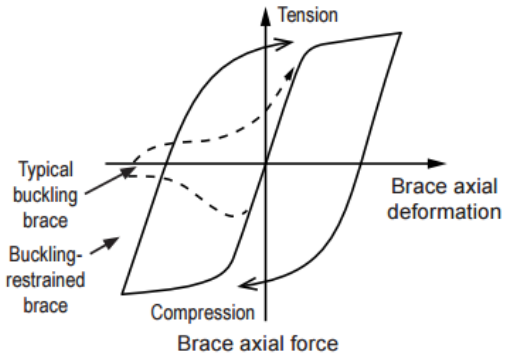

Figure 7.4 Hysteresis plot for buckling-restrained brace and concentric brace [105]

Concrete Shear Walls

Concrete Shear Wall is one of the most common and effective resisting system. The system is part of the lateral force resisting system that carry vertical and horizontal loads. The technique is adopted in structural seismic retrofit increasing the global resistance of the entire structure.

RC walls have been classified, according to Canadian Standard Association, in bearing walls, non-bearing walls, shear walls, flexural shear walls and squat shear walls. A conspicuous percentage of the existing concrete walls in the buildings can be assumed as “moderately slender” according to the height-to-length ratio (aspect ratio) that stays between 1.5 and 3. These aspect ratio values define walls for which the failure mechanism is dominated contemporary by shear and flexure in their principal plane. Aspect ratio less than 1-1.5 defines walls for which the shear mechanism is dominant. Aspect ratio more than 3 defines walls lead by flexural failure mechanisms.

As other authors discussed on the base of experimental evidences [106] the interaction between flexural and shear deformation exists for shear walls with ratio between 3 and 4.

Figure 7.5 Shear wall retrofitting method

Steel Plate Shear Walls (SPSW) and Composite Steel Plate Walls (CSPSW)

Steel plate shear walls (SPW) are an effective resistance system to lateral forces due to earthquakes or wind (in tall buildings). Their use has spread in Japan, United States, Canada and Mexico. The steel plate is welted or bolted to surrounding moment-resisting steel elements. The surrounding horizontal and vertical boundary elements are connected to the surrounding concrete structures.

This technique has similar advantages of the previous mentioned steel bracing methods. It implements the advantages of shear walls but maintains a relatively lightness and an affordable cost of production and implementation in existing buildings. The technique is usually adopted in new structures but few applications in the seismic rehabilitation of reinforced concrete frame structure can be found [107]. Steel shear

panels can be considered as effective strengthening and stiffening devices, whereas the pure aluminium ones are also able to increase significantly the energy dissipation capacity of existing RC framed structures

SPSW have been widely numerically and experimentally investigated and this huge scientific effort led to a sub-classification. Nowadays the SPSW can be subdivided in:

Compact shear panels made by compact steel plates (steel or aluminium) characterised by large hysteretic cycles that defines an excellent energy dissipation capacity and stiffening structural update. They are relatively immune to buckling issues.

Slender shear panels made by thin steel plates. This latter group have a minor weight supply to the structure but it may be heavy affected by buckling problems.

Aiming to avoid elastic and plastic buckling issues, an upgrade of the slender shear plate has been presented by other authors and the Composite Steel Plate Shear Wall (CSPSW) have been introduced. The CSPSW implanted thin concrete plates on both plate sides to control the instability and control the hysteretic behaviour. In this way, the pinching effects due to buckling phenomena can be mitigated.

Figure 7.6 Steel Plate Shear Wall System

Seismic Isolation

An effective seismic upgrading method that changes the seismic demand is the Isolation Systems (IS). Most of them adopt rubber bearings (RBs), namely High Damping Rubber Bearings (HDRBs), or Lead Rubber Bearings (LRBs) or (mainly in Japan) Low Damping Rubber Bearings (LDRBs) in parallel with dampers. On the other hand, the use of more advanced isolation systems are growing. The last systems are based on the dissipative effects due to friction between two convex and concave surfaces and they are named “Friction Pendulum”.

All the mentioned isolation system are based on the reduction of the seismic demand by means of modification of the eigein-properties of the structure leading to consequent substantial elongation of fundamental periods of vibration.

The assumption of these methods is growing, but the use for retrofitting purpose is not always economically and technically affordable. On the other hand, their structural advantages are unneglectable.

7.3 The proposed eccentric bracing system

Several possible retrofitting strategies have been investigated by the simplified model in 3DMacro. The light computational effort together with the built in code-check facilities provided the opportunity to explore different seismic upgrading solutions. The analyses had the aim of define the more reliable methods for the seismic retrofitting of the ten-storey typical building selected as case study.

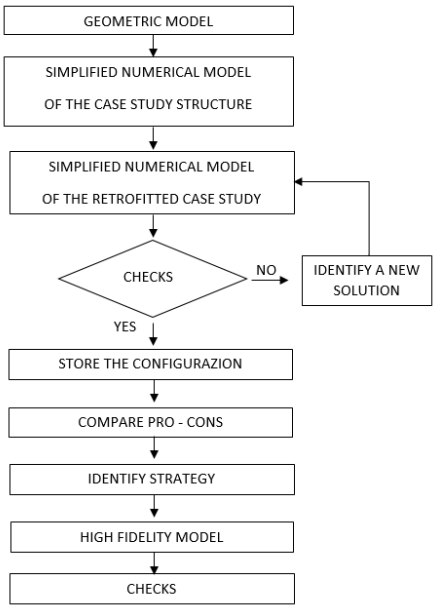

Figure 7.7 Flowchart of the new proposal identification

The Figure 7.7 shows the workflow that has engaged for identifying the proposed solution. The selected strategy accounted for the use of eccentric bracing system endowed with dissipative shear links. The benefits of this system as seismic retrofitting solution has been already discussed in literature [108, 109, 110]. In all of the mentioned research works the use of eccentric bracing system arranged with vertical shear links were discussed and the advantages of the system highlighted. As the authors argued, distributing eccentric bracing systems over the height of the studied building showed a significant contribute in terms of ductile mechanisms under horizontal loads. As other authors already discussed

[111], all of those experiments have been performed on concrete structure with a sufficient ductile and shear capacity. In these conditions, the only parameter that has to be checked is the ultimate link rotation. As matter of facts, the existing reinforced concrete frame structures, not designed to resist earthquakes, are usually characterised by limited chord rotations and shear capacities as highligthed in the previous chapters. These weaknesses may determine premature local failures that can occur before the shear links yielding. Aiming to avoid premature failures that may invalidate the eccentric bracing systems efficiency an adequate design procedure has to be engaged.

Several possible configurations may be adopted for the eccentric bracing systems, such as some authors recently reported [112], as Figure 7.8 shows. A very common configuration is depicted in Figure 7.8d. This latter typology has been frequently engaged in case of seismic upgrading of reinforced concrete frame structure.

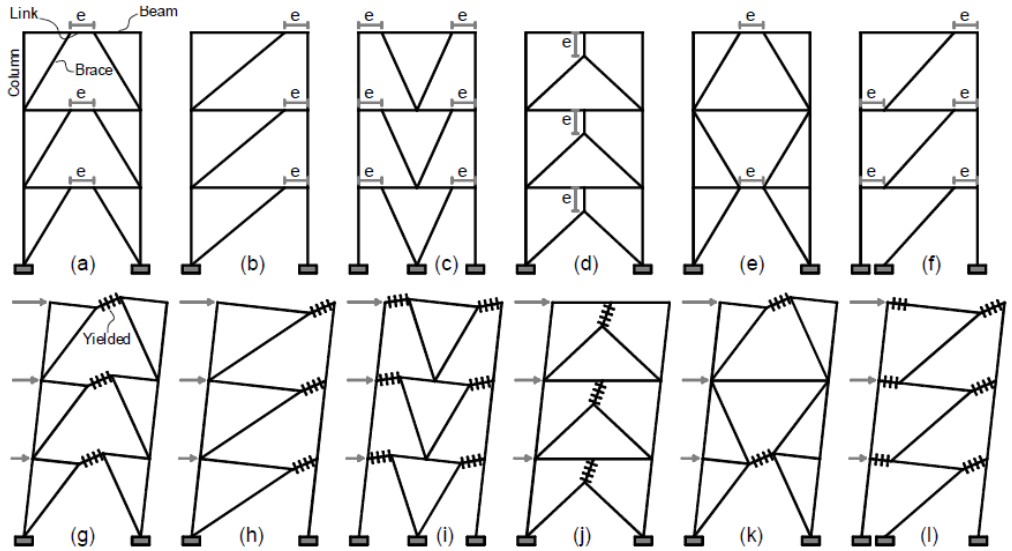

Figure 7.8 Eccentric bracing systems [112].

The use of steel bracing systems for seismic rehabilitation of RC frames offers some advantages such as:

- the ability to accommodate openings;
- minimal added weight to the structure;

- minimum disruption to the function of the building and its occupants.

On the other hand, some of the configuration may determine localised increment of bending moments at least in the existing beams due to the different horizontal displacements and the ends of the vertical links.

Figure 7.9 shows the comparison of generalised stresses in the three different configurations under a generic horizontal concentrated load. The figure compares the bare frame, the Y type eccentric bracing system and the K type proposed for the first time in this research. The images depict, from a qualitative point of view, the axial forces, shear forces and bending moments that the eccentric dispositive determines within the original reinforce concrete frame structure. The schemes do not account for vertical loads effects

The proposed K type configuration maintains the advantages of the Y type. However, differently from the latter, the novel bracing system avoids for localised forces in the existing RC beam..

The A set of figures depicts the axial forces within concrete and steel elements. The configuration here proposed, A3, determines uniform axial forces distributions in the existing reinforced concrete beam differently from the A2 scheme.

The B set of figures shows the shear forces highlighting that the dissipative shear link element is subjected to uniform shear stresses in both the configurations.

Lastly, the C set of figures depicts the influence of the steel braces on the bending moments distribution. The C3 scheme shows the proposed solution does not provide local variations of the bending moments in the existing concrete elements.

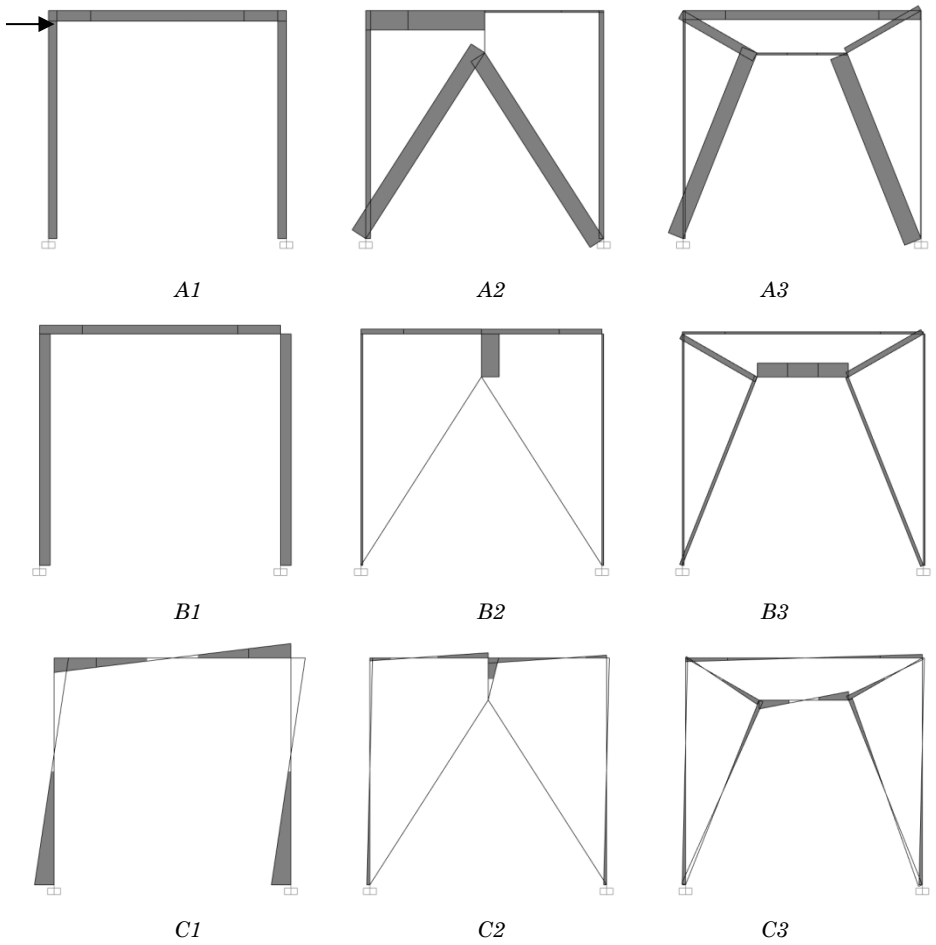

Figure 7.9 Generalised stresses due to a concentrated horizontal load

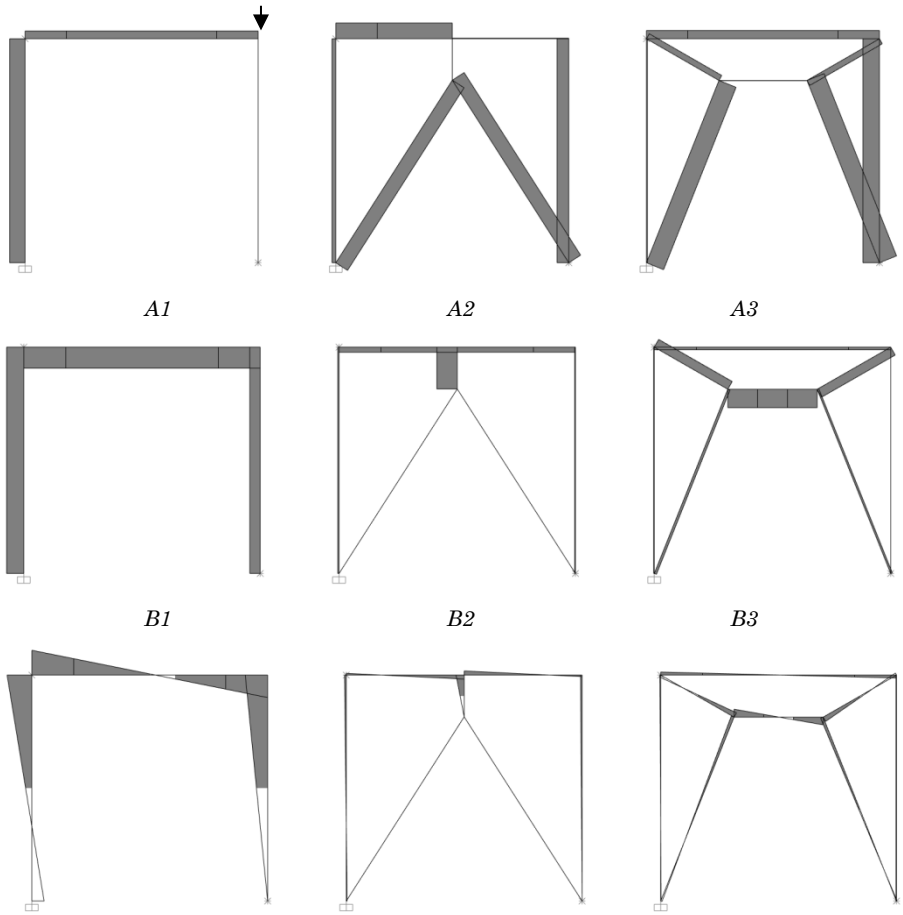

Figure 7.10 Generalised stresses due to a concentred vertical load

The Figure 7.10 reports the previously discussed structural schemes in case of the application of a concentred vertical load in only one column aiming at investigating the retrofitted frame behaviour when subjected to an additional vertical load due to a column loss scenario.

The above reported considerations seem to indicate that the proposed and never adopted K shape configuration may also contribute to improve the robustness of the building. Furthermore, the K proposed shape does not alter the shear forces and bending moment distribution in the existing beam. On the contrary in a column loss scenario, the Y shape configuration may determine the failure of the beam elements due to the increment of bending moments and shear forces unconsistent with the reinforcement details.

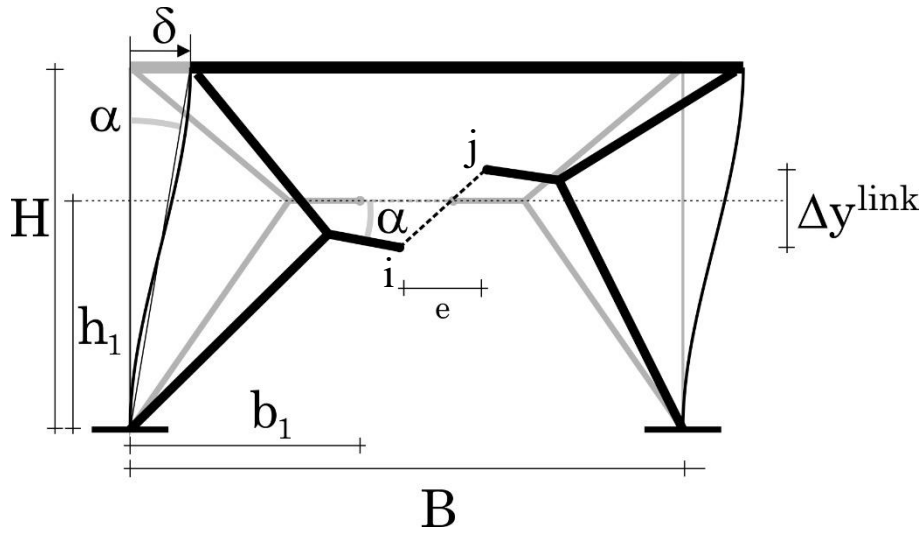

Figure 7.11 Scheme of the proposed Eccentric Bracing System

According to Figure 7.11, making reference to the well-known shear type scheme the initial frame elastic stiffness can be defined as:

$$K_i^f = \sum_{j=1}^{ncolumn} \frac{12 E_c I_{ij}}{h_i} \qquad \textit{Eq. 66}$$

In addition, by assuming that the moment resistant steel elements are sufficiently rigid, the Eccentric Bracing behaviour is governed by the

Shear Link stiffness and the lateral stiffness contribution of the retrofitting system can be expressed as.

$$K_i^K = \sum_{j=1}^{nbay} 2b_1 \tan\left(\frac{\delta}{H}\right)\frac{G_{ij}A_{ij}}{e_{ij}} \approx 2\frac{\delta}{H}\sum_{j=1}^{nbay} b_{1j}\frac{G_{ij}A_{ij}}{e_{ij}} \qquad \textit{Eq. 67}$$

where the involved geometrical parameters are reported in Figure 7.11.

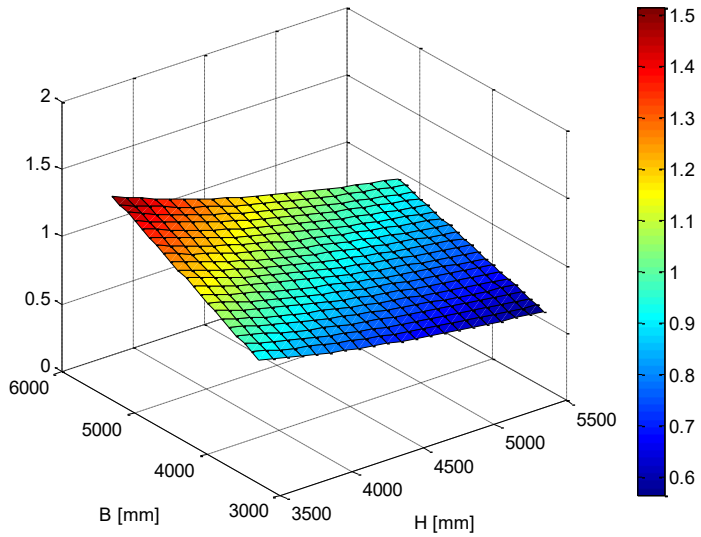

Figure 7.12 Variation of the relative displacements factor

In agreement with the Figure 7.11 and Eq. 67, the generic horizontal displacement δ (namely the storey drift) determinates vertical displacement $\frac{b_1}{H}$ times δ in i and j, being i and j the shear link ends. The relative displacement of the shear link ends is equal to $\frac{2b_1\delta}{H}$, being H the frame height and b_1 the shear link end position, as the Figure 7.11 reports. Differently from the above mentioned Y shape bracing model, for which the shear link ends relative displacement is equal to δ [111], the proposed eccentric bracing system benefits by the factor $\frac{2b_1}{H}$ whose dependence from the frame geometry is depicted in Figure 7.12. Generally, this factor amplifies the prescribed horizontal displacement

δ up to 1.5 times for several existing framed residential buildings for which an average values of H=3.3m and B=4.5m can be assumed. This amplification represents a great advantage of the proposed solution and has a relevant value in the design phase.

In case of existing reinforced concrete framed residential buildings, which are usually affected by poor displacement capacity, the design of the eccentric bracing systems should preserve the damage in the existing reinforced concrete elements by reaching the plastic state for low values of interstorey drifts. As a consequence, the magnification factor guarantees the implementation of stiff shear link sections that are still able to develop their plastic behaviour before the reinforced concrete beams or columns failure.

Lastly, this approach potentially reduces the number of existing elements that have to be seismically upgraded and, consequently, guarantees the retrofitting cost optimization.

The storey initial elastic stiffness of the new system, composed by the original concrete frame and the eccentric bracing elements, can approximately be defined as follows.

$$K_i^{f+K} = K_i^f + K_i^K \qquad \textit{Eq. 68}$$

Basing on that the shear forces on the dissipative shear links are defined by the following expression

$$V_i^{link} = 4\left(\frac{x_i - x_{i-1}}{H}\right)^2 \sum_{j=1}^{nbay} b_j^2 \frac{G_{ij} A_{ij}}{e_{ij}} \qquad \textit{Eq. 69}$$

the axial forces can be neglected

$$N_i^{link} \cong 0 \qquad \textit{Eq. 70}$$

The axial force in the links has been neglected

The proposed geometry is consistent with the definition of short shear link and the bracing cross sections have not been affected by buckling issues.

Figure 7.13 reports the seismic vulnerability of the existing structure. The figure reports the safety factors in terms of displacement demand over capacity for the ten-storey building and the four analyses. The diagrams depict the seismic performance with and without masonry panels. As the figure shows, the amplification factor due to the soil category decreases substantially the safety factors in both the configurations.

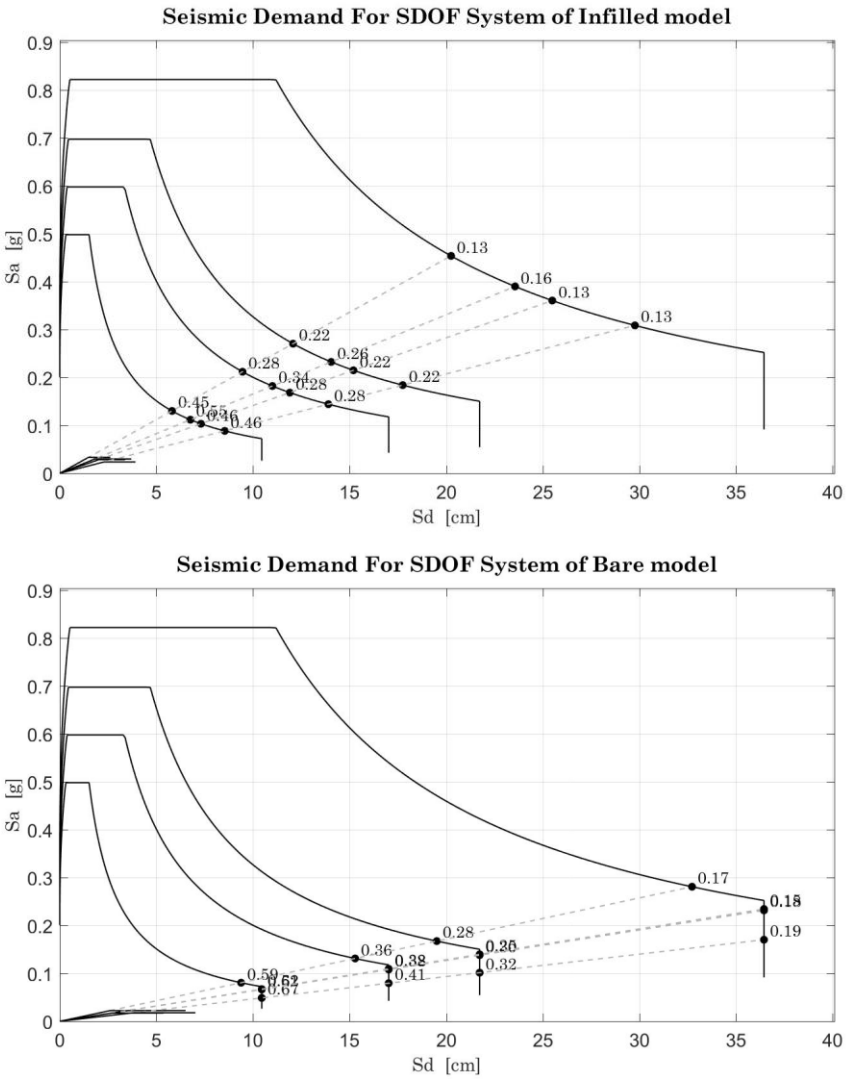

Figure 7.13 Seismic vulnerability of the existing case study with and without infills and for four soil categories.

7.4 The retrofitted case study

The results obtained in the assessment of the RC building have directed the design of the strengthening solution. In the design stage, the software 3DMacro [83] with implemented code-based checks, has been used to explore different retrofitting strategies. Traditional and innovative strengthening systems have been modelled, analysed and compared.

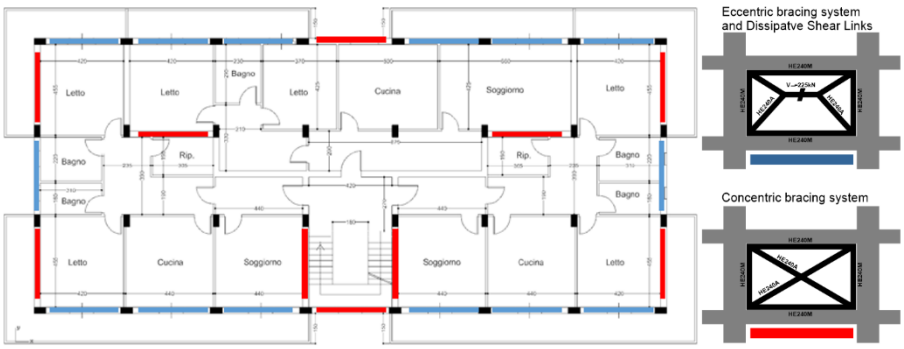

Figure 7.14 Planar scheme of the retrofit systems distribution

The chosen solution considers a set of eccentric steel bracings with dissipative shear links along with traditional concentric steel bracings which are utilised in combination to provide the bare structure with hysteretic energy dissipation capacity and higher lateral stiffness. The K type geometrical layout, adopted for the eccentric steel bracings and introduced in the previous section, has never been proposed before and allows concentrating the damage in the shear link without transferring high shear forces to the existing reinforced concrete beams and without altering the moments distributions as usual in existing proposed geometrical layouts. Significant plastic damage is expected to develop in the shear links that can be easily removed and substituted after a strong earthquake. Figure 7.14 shows the distribution in plan of the strengthening elements, where the red marks indicate the position of the concentric steel bracings and the blue marks the eccentric dissipative bracings.

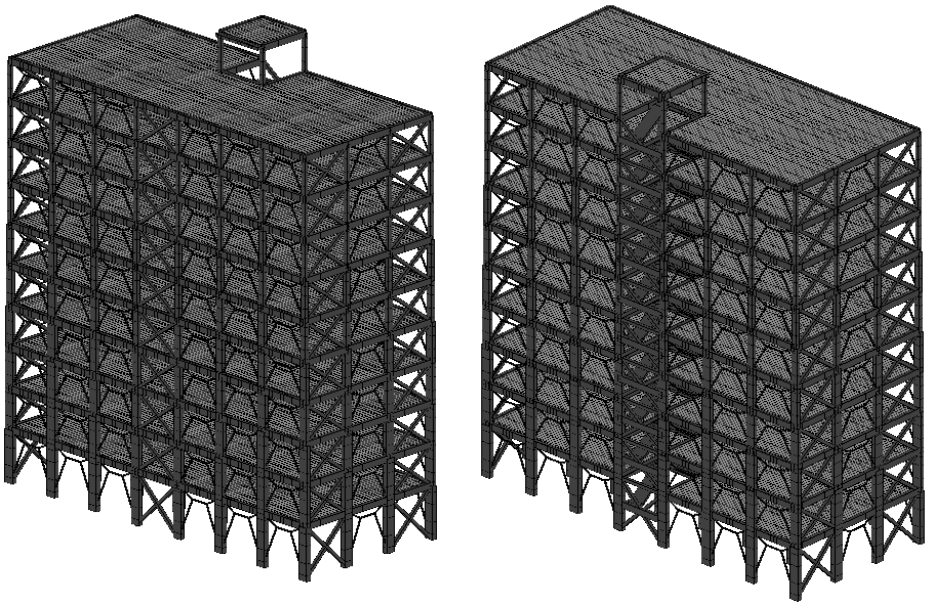

Figure 7.15 Front and back of the retrofitted structure

The strengthening elements span from the foundation level to the roof of the buildings as depicted in Figure 7.15. Nonlinear dynamic simulations have been carried out using the Reinforced Infill Frame model in ADAPTIC.

In the Reinforced Infill Frame model, the steel elements of the strengthening system, encompassing eccentric bracings with dissipative shear links along with traditional concentric bracings, have been modelled using 1D plastic beam-column elements and nonlinear joint elements

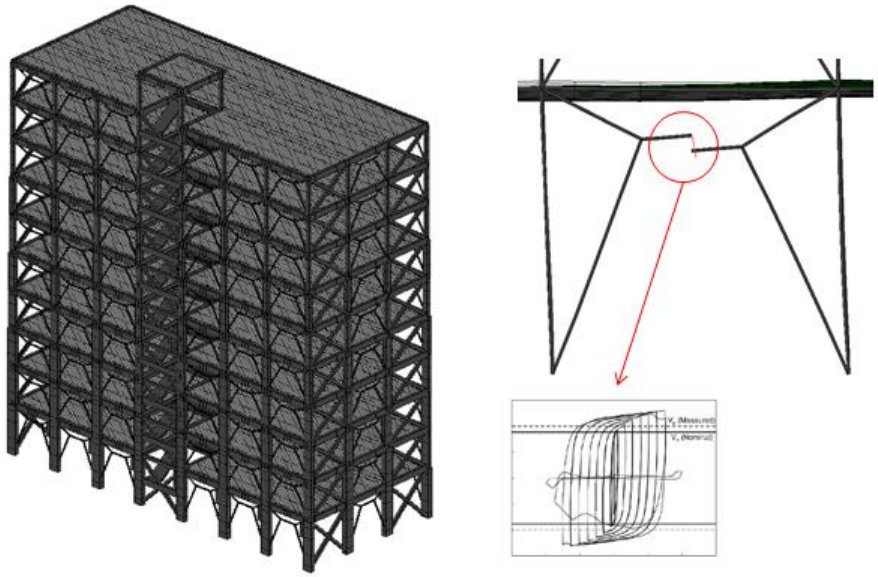

(a) **(b)**

Figure 7.16 (a) 3D ADAPTIC model of the strengthened building, (b) modelling of an eccentric bracing with a dissipative shear link (deformed configuration)

Finally, to avoid unrealistic stress distributions in the steel bracing systems, the staged construction ADAPTIC capability has been engaged in the Reinforced Infill Frame model. The staged construction has ensured that centric and eccentric bracing do not take dead and imposed loads from the original building structure (bare frame) and that they contribute only to resisting seismic horizontal and vertical actions. Figure 6.6 has showed pictorially the concept behind the staged construction capability with regards to the masonry panels, but the identical concept stays behind the retrofitting solution modelling.

The achieved results confirm the effectiveness of the proposed strengthening strategy, as horizontal displacements are significantly reduced limiting damage in the existing RC elements.

Initially. a linear comparison in terms of eigen-values has been performed and reported in Figure 7.17 in terms of modal periods. As the figure depicts, a conspicuous period reduction occurs for the eccentric

bracing contribute (almost 60% and 25% of the original bare structure and infill frame structure, respectively).

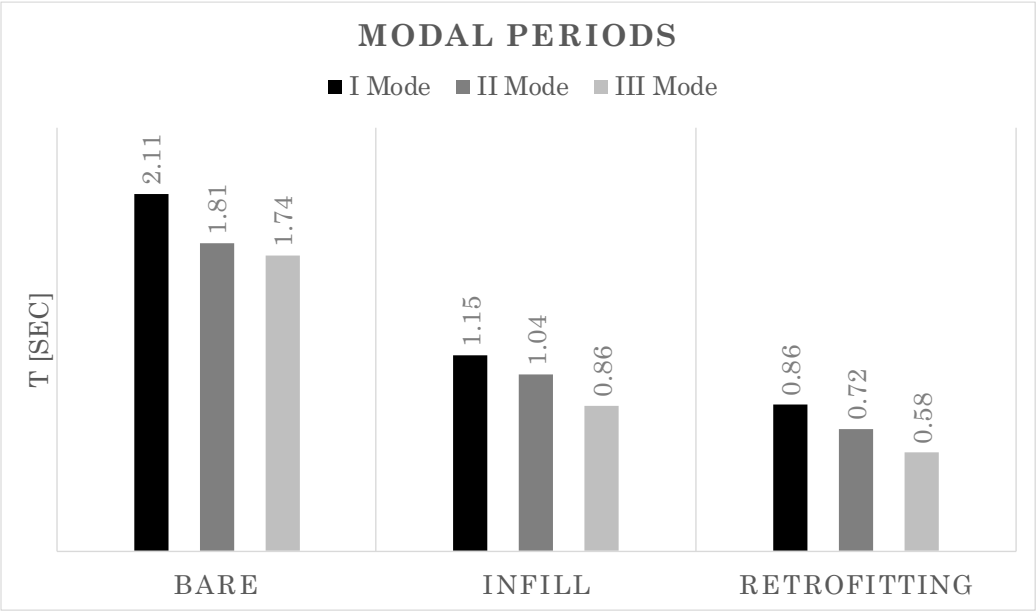

Figure 7.17 Fundamental periods of the bare frame, infilled frame and retrofitted bare frame structures.

Figure 7.18, Figure 7.19 show the deformed shapes and the horizontal displacement profiles of the strengthened building obtained in two nonlinear simulations (e.g. NLDA1 and NLDA 6). Notably, the importance of 3D modelling is clearly evident in Figure 7.19, where a torsional mode is induced due to asymmetric inelastic deformations which cannot be represented using simplified 2D modelling approaches.

It is worth noticing that there is no longer a concentration of deformations at a specific floor level and the distribution of horizontal displacements in the two in plane directions increases monotonically with almost uniform gradient along the height of the building .

The different response of the original structure and of the strengthened building have been compared in Figure 7.20 and Figure 7.21. It is worth pointing out attention on the NLDA6 bare frame deformed shape. The figure exposes an incipient global collapse that has been trigged by a local failure in the not seismically upgraded structure.

The three superior floors collapsed on the lowers and a progressive collapse effect is expected.

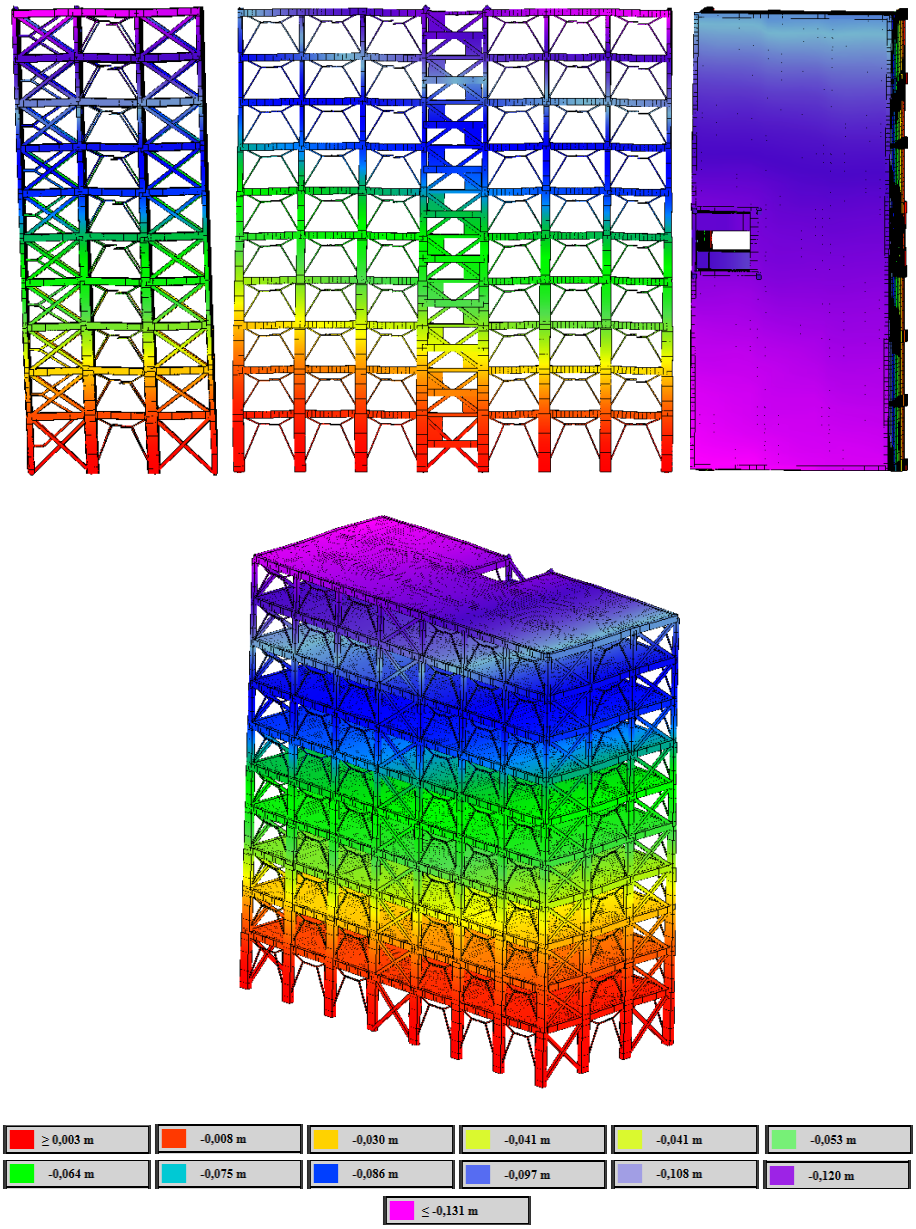

Figure 7.18 (Colour) Deformed shape and Displacements at the last step of the NLDA1 analysis.

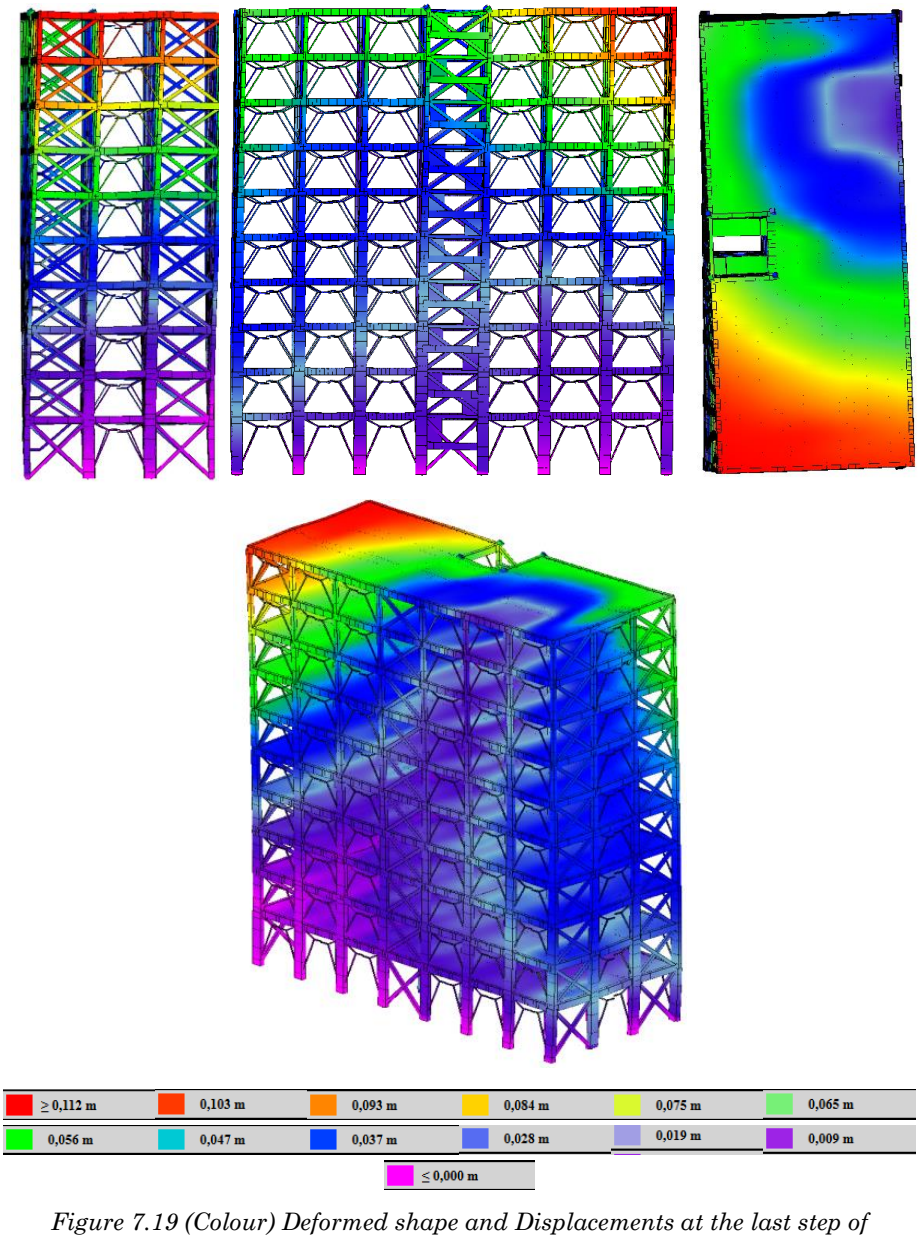

Figure 7.19 (Colour) Deformed shape and Displacements at the last step of the NLDA6 analysis.

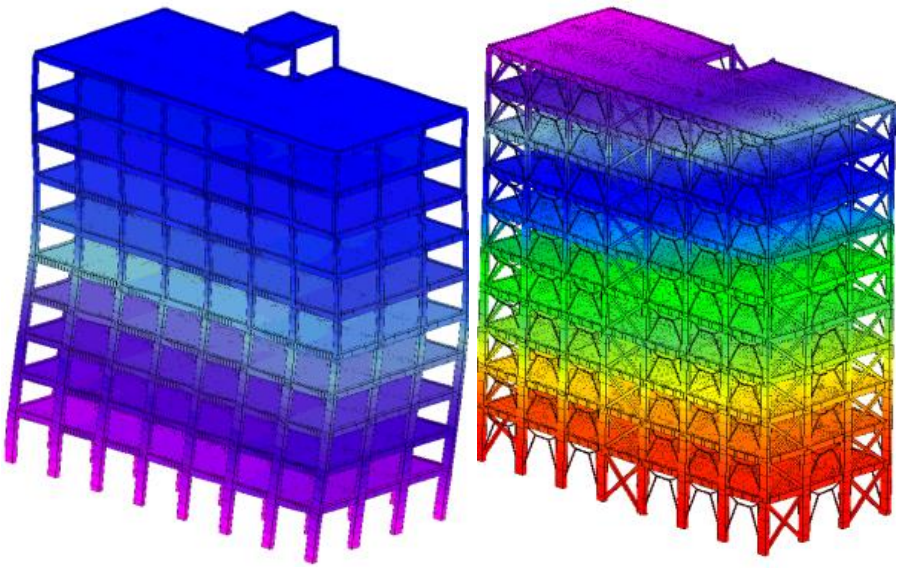

a) *b)*

Figure 7.20 (Colour) Contours of Displacement history of the a) BF models and b) of the RIF models in NLDA1 analysis.

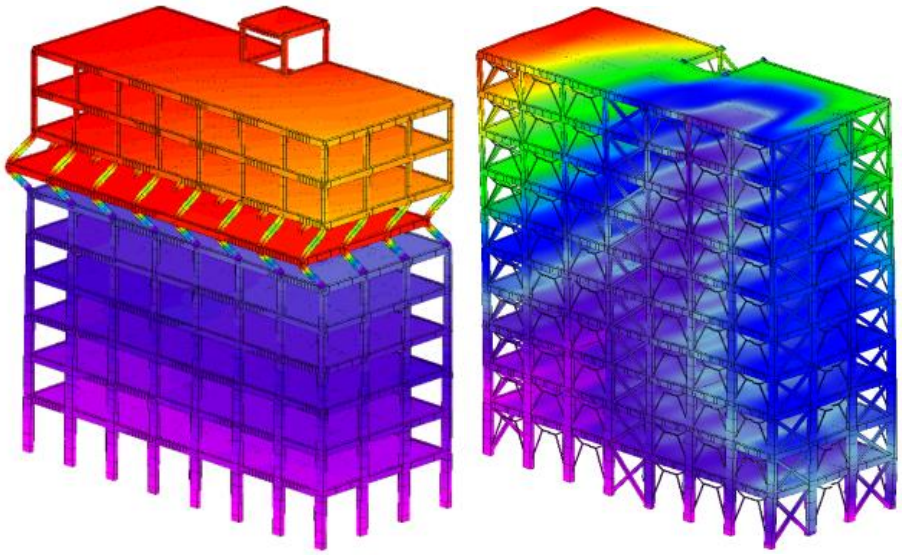

a) *b)*

Figure 7.21 (Colour) Contours of Displacement history of the a) BF models and b) of the RIF models in NLDA6 analysis.

In the Figure 7.22 and Figure 7.23, the horizontal displacements obtained in the simulations for the two structures have been compared. The diagrams expose the displacements achieved in the two configurations during the NLDA1 analysis. The Figure 7.24 and Figure 7.25 report the identical comparison in term of displacements of the models that have been collected in the NLDA6 analysis.

It is important pointing out that the results for the original building depict the response in the early part of the analysis, since, unlike the simulations of the strengthened building, the original building simulations stopped well before the end of the time-history analysis because unrealistically large displacements and local drifts (e.g. 2m drift for NLDA6) which indicating global collapse of the original building.

On the other hand, the results for the strengthened structure refer to the response to the end of the dynamic analysis.

The drift demands have been compared in the Figure 7.26 and Figure 7.28 and in terms of normalised drift demands in the Figure 7.27 and Figure 7.29.

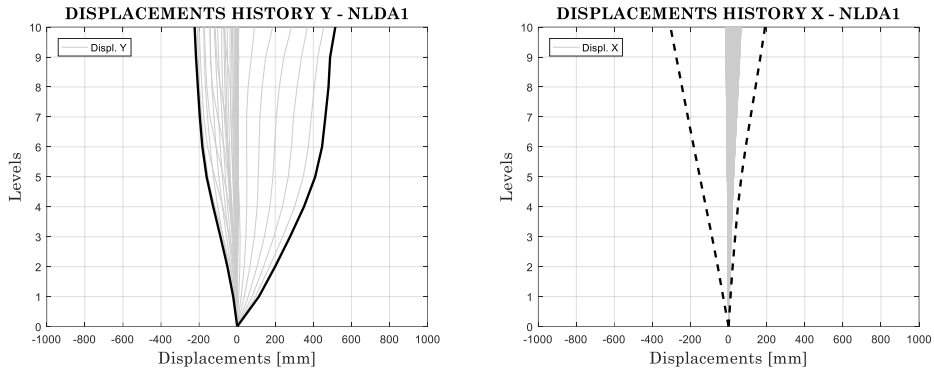

a) *b)*

Figure 7.22 Displacements in Y direction of the a) BF and b) RIF models in NLDA1.

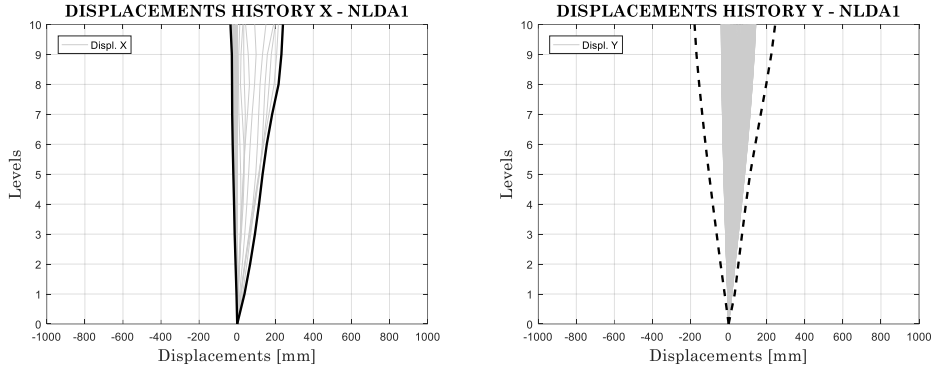

a) *b)*

Figure 7.23 Displacements in X direction of the a) BF and b) RIF models in NLDA1.

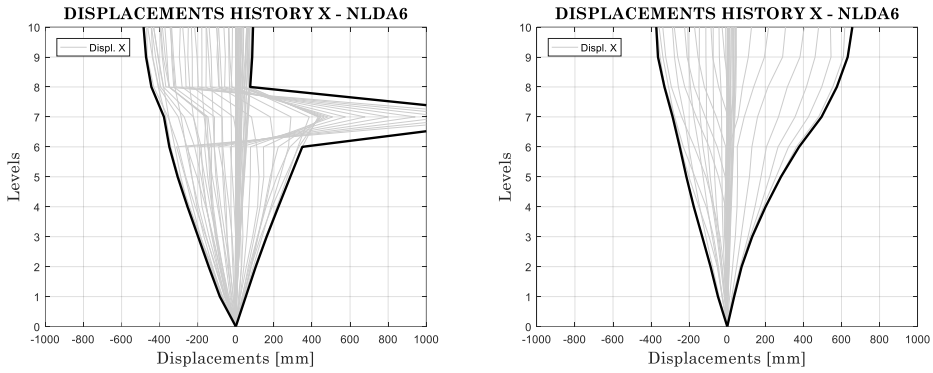

a) *b)*

Figure 7.24 Displacements in X direction of the a) BF and b) RIF models in NLDA6.

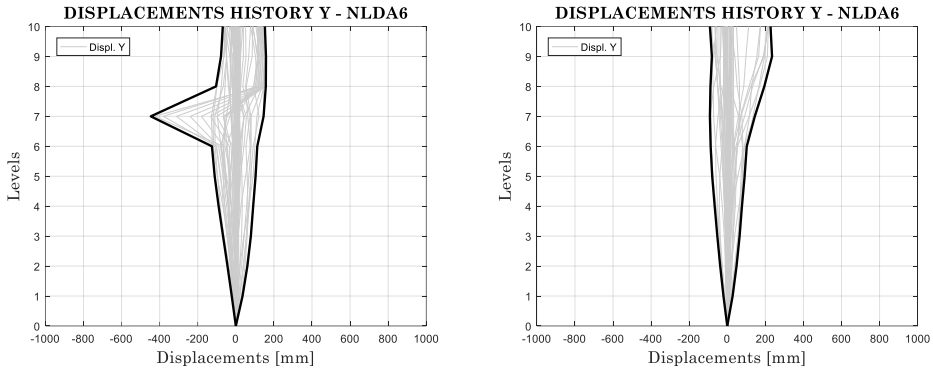

a) *b)*

Figure 7.25 Displacements in Y direction of the a) BF and b) RIF models in NLDA6.

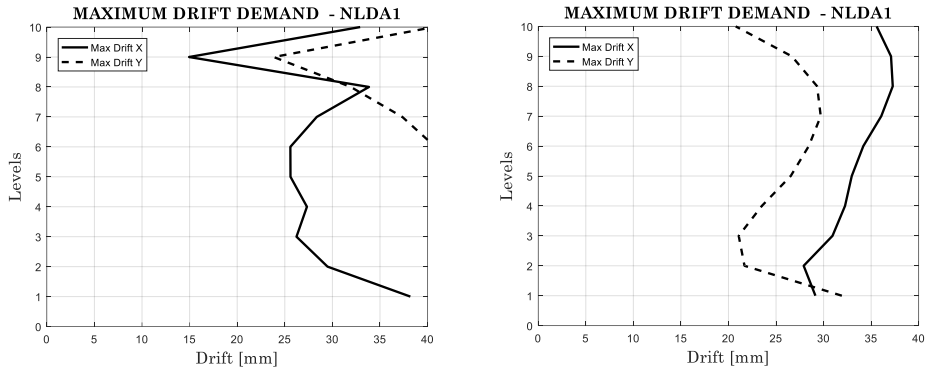

a) *b)*

Figure 7.26 Drift demand of the a) BF and b) RIF models in NLDA1

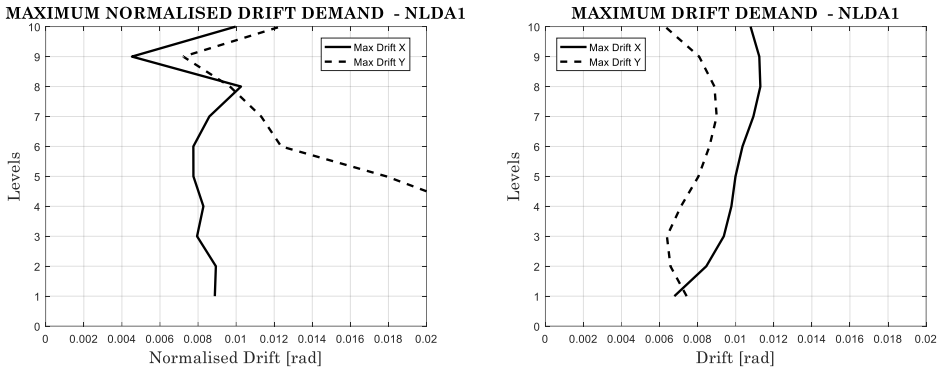

a) *b)*

Figure 7.27 Normalized Drift Demand of the a) BF and b) RIF models in NLDA1

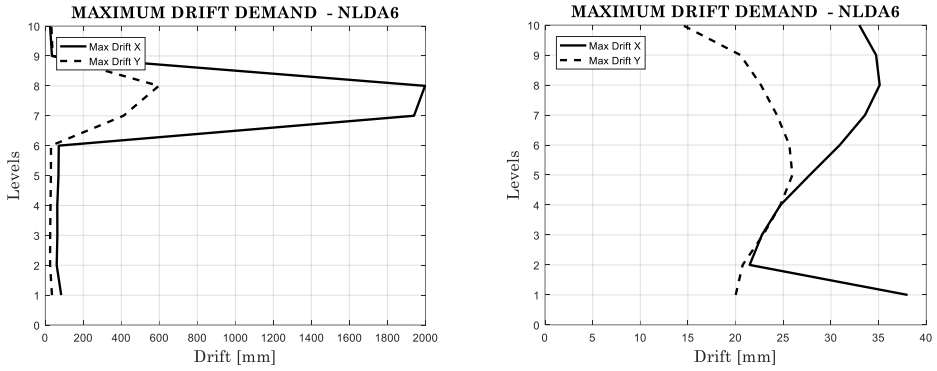

a) *b)*

Figure 7.28 Drift demand of the a) BF and b) RIF models in NLDA6

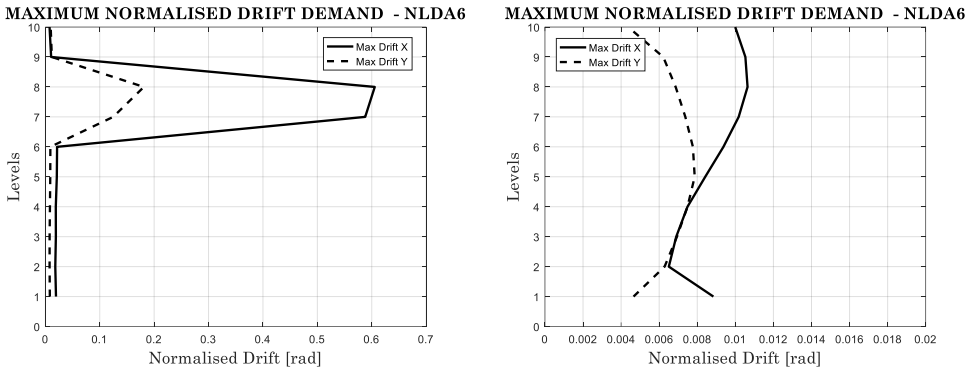

a) *b)*

Figure 7.29 Normalised Drift demand of the a) BF and b) RIF models in NLDA6

The maximum drift values have been reported in Table 7-1 and Table 7-2. It can be seen that the maximum values for the strengthen structure are within acceptable limits, e.g. around 1% maximum drift for the Near Collapse Limit State

Table 7-1 Maxima Drifts Demands

Analysis	IF Model [mm]	RIF Model [mm]
NLDA1	Δ_{max} = ~515	Δ_{max} =~305
NLDA6	Δ_{max} =~2000	Δ_{max} =~280

Table 7-2 Maxima Normalised Drifts Demands

Analysis	IF Model [rad]	RIF Model [rad]
NLDA1	Δ_{max} = ~0.026	Δ_{max} = ~0.011
NLDA6	Δ_{max} = ~0.6	Δ_{max} = ~0.01

This confirms that the proposed strengthening solution has enabled the strengthened building to survive the design earthquakes, also preventing the development of significant damage in the RC columns potentially leading to progressive collapse of the whole structure or a significant portion of it. Even though progressive collapse has been avoided for this strengthened building, the potential of progressive collapse should be an important consideration when it comes to the application of the proposed strengthening measures to other existing buildings.

Local checks for all the RC components (e.g. beams and columns) have been conducted considering local brittle and ductile failure. In particular, the demand chord rotations have been obtained from the results of the nonlinear time-history analyses while the capacity values have been calculated based on the ultimate chord rotation equation proposed by Italian Seismic Code (C8A.6.1 Circolare 2 -02-2009, 617). Figure 7.31 shows the results for all the columns obtained in two different nonlinear dynamic simulations, where it can be observed that

only one column presents a chord rotation ratio (e.g. demand/capacity) larger than 1 indicating the need for limited local strengthening.

Similar results have been obtained in the checks for the brittle mechanisms, where the shear demand/capacity ratios calculated according to a circular interaction domain, as proposed by the Japanese code (AIJ, 1994), were smaller than 1 for all the columns (Figure 7.33). This confirms the effectiveness of the proposed strengthening solutions in protecting the RC building also when subjected to strong earthquakes.

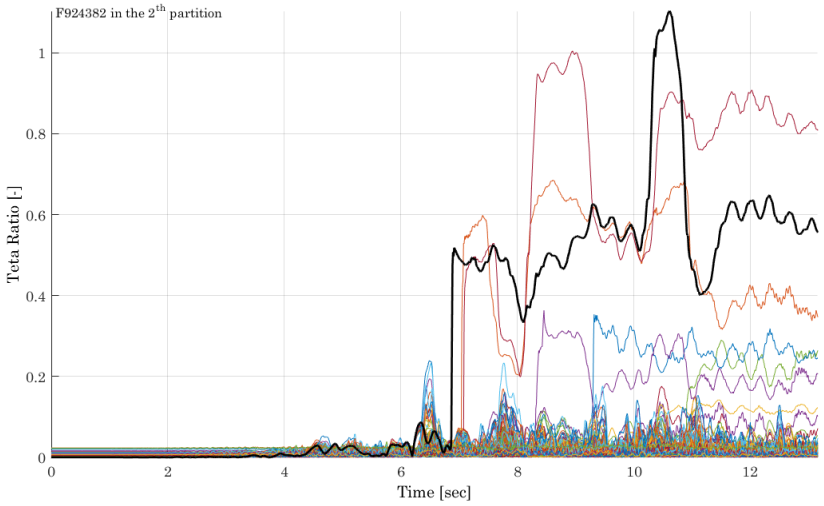

Figure 7.30 Chord rotation ratios of all the concrete columns for NLDA1 analysis

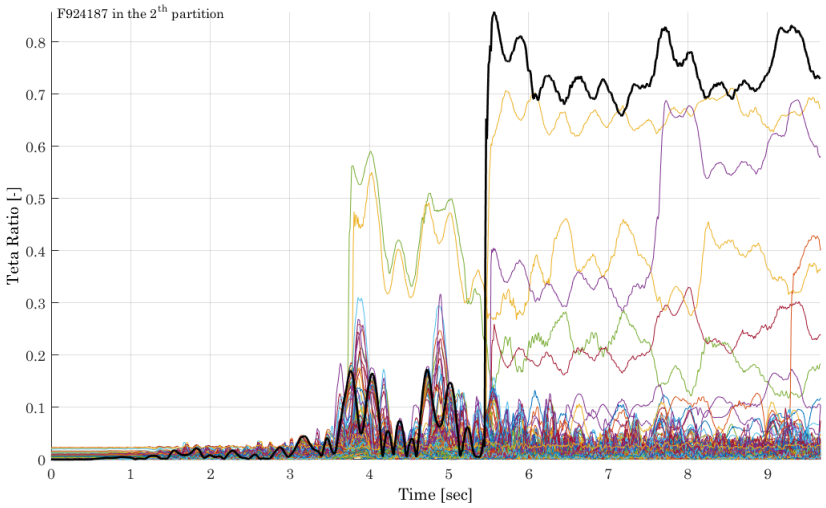

Figure 7.31 Chord rotation ratios of all the concrete columns for NLDA6 analysis

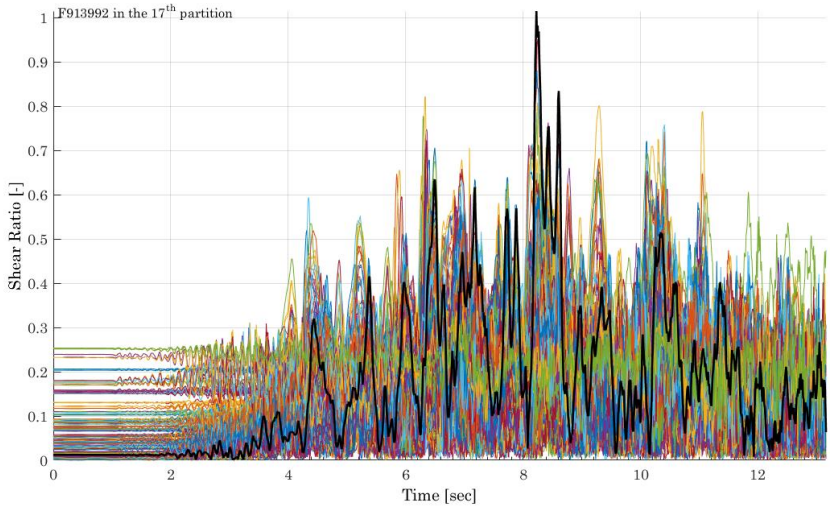

Figure 7.32 Shear demand/capacity ratio of the concrete columns for NLDA1 analysis

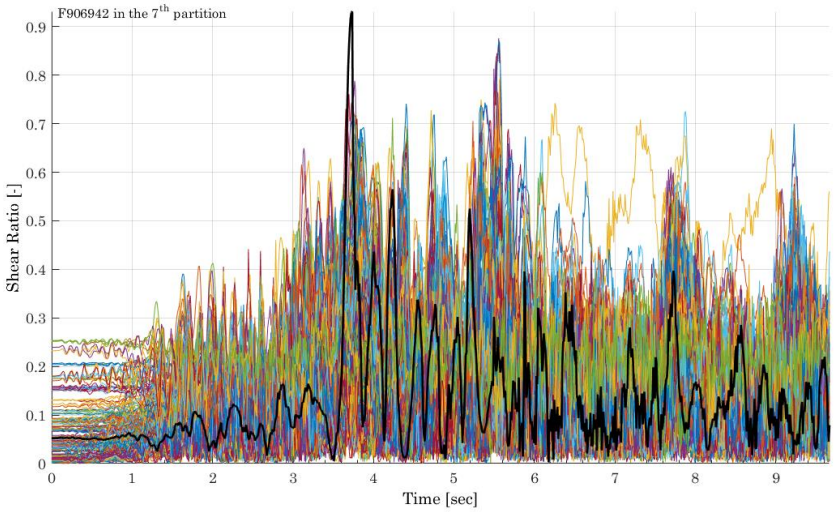

Figure 7.33 Shear demand/capacity ratio of the concrete columns for NLDA6 analysis

CHAPTER 8. CONCLUSIONS

The Section contains the conclusions and a brief summary of the main results and highlights the relevance of the study within the context of retrofitting strategies of mid-rise existing reinforced concrete buildings not designed to resist to earthquake.

8.1 Summary

The contemporary and modern reinforced concrete frame buildings are designed to withstand earthquake loading actions by means of capacity design method. This method, by dividing the structures in dissipative and non-dissipative elements, guarantees structural integrity under earthquake loading. On the other hand, a notable percentage of the entire modern building heritage is composed by existing reinforced concrete buildings that were not designed according to seismic codes and are consequently seismically vulnerable.

This thesis is focused on the seismic vulnerability assessment of existing multi-storey reinforced concrete buildings that were not designed to withstand earthquakes and on the identification of possible retrofitting strategies adoptable for their structural rehabilitation.

A typical ten-storey building has been identified as representative cases study of many similar buildings built in Catania (Sicily, south of ITALY) between the 60's and 80's before the introduction of a national seismic code in 1981. Since the building has been designed with reference to vertical loadings only it allowed the simple identification of further eigth buildings characterised by different number of storeys, from nine to two, but maintaining the same plan layout. Although these buildings have been obtainted by exploring the architectural and structural features of residential building of Catania, the obtained results and conclusions are valuable for many others areas that have been recently recognised as earthquake prone regions.

Aiming at obtaining rigorous results and to validate the standard adopted procedures with those obtained by rigorous detailed simulations, the seismic assessment of the investigated buildings, before and after the proposed retrofitting measures, have been performed. For this purpose, advanced numerical models characterised by different modelling capabilities and computational demands have been implemented.

The seismic vulnerability assessments, consistent to the current European Code prescriptions [113], have been performed by using the research version of the computer code 3DMacro [83] that allows performing nonlinear push-over analyses by considering the important

contribution of the non-structural infill panels. This code has been developed by GruppoSismica, a research team at the University of Catania, and it is based on original macro-element approach [65] originally conceived for Unreinforced Masonry Structures and subsequently extended to infilled frame structures.

The detailed nonlinear analyses have been performed by means of high fidelity models implemented in the advanced nonlinear FEM software ADAPTIC [63] that allows performing full nonlinear static and dynamic analyses accounting explicitly for material and geometric nonlinearity. Moreover, according to a powerful partition modelling strategy and the capabilities of the parallel calculus, ADAPTIC makes possible the implementation of mathematical model of structures with a huge amount of details. The software ADAPTIC has been developed by professor B.A. Izzuddin [63] at Imperial College of London. ADAPTIC allowed also considering the contribution of all the primary and secondary structural elements, their geometry and reinforcement layouts. The interaction between concrete frames and non-structural unreinforced hollow brick masonry infills has been evaluated by means of a FEM *ad hoc* implementation of the planar discrete macro-element, already implemented in 3DMacro [65] within a discrete element framework. The original non-trivial implementation of the discrete macro-element in the FEM code ADAPTIC represents an original contribute of the present thesis. This choice allowed a consistent comparison between all the performed simulations and provided a cross validation between the different adopted modelling approaches.

The large displacements capabilities of the software ADAPTIC has also empowered a new original research investigation that relates the investigation of progressive collapse scenarios due to local failures trigged by low, or moderate, earthquake actions on mid-rise weak reinforced concrete existing structures.

The thesis is divided into seven main chapters.

The first Chapter focuses the seismicity of the east coast of Sicily with major attention at the city of Catania. The problem of the seismic hazard is depicted. Initially, a general vision of the seismic risk in European area

is documented and discussed. Then the aspects of seismic risk in Italy is discussed by recalling the italian main earhquakes in a sort of historical review of the last millennium. After this general review the seismic vulnerability of existing reinforced concrete buildings built in Catania before the introduction of the seismic code is discussed. The unfortunate Catania's geographic position - between the volcano and close to Hyblean-Malta Escarpment - its seismic history and the effects of the evolution of the Italian design regulations on its urbanistic growing is introduced. This introduction contextualizes, from a structural point of view, the residential buildings designed before the 1981 in Catania. The chapted is concluded with the identification of seven sets of accelerograms, based on of scaled natural records. The records and their spatial components have been selected in order to be representative of the seismic input in Catania and compatible to the Italian code design spectra [114]. The records are used in chapter seven for performing accurate non-linear dynamic analyses.

The second Chapter introduce the progressive collapse phenomena and it is preparatory to the investigation of the robustness of existing buildings designed for vertical loads only as possible consequence of moderate earthquake actions. A literature review introduces the topic going through theory and experimental researches and international design codes [33, 31, 29, 23]. The chapter explains the terminologies that are used in the subsequent parts of the thesis, illustrates well-known examples and uses them aiming to describe progressive collapse mechanisms due to typical damage scenarios in frame structures. According to different approaches, the assessment of a structure in a column loss scenario is discussed and different methodologies are described and commented. The *overload factor* [25] and the *simplified dynamic assessment* [26, 27] are assumed as representative of different robustness assessment strategies since a unique assessment procedure does not exist. The *simplified dynamic assessment*, developed by Professor B.A. Izzuddin at the Imperial College of London is accurately described and adopted in the subsequent investigations. The Izzuddin's

assessment method is applicable to sudden column loss [26], failed floor or beam impact over other structural bearing elements [115].

The third Chapter investigates and discusses numerical simulations of an experimental test on progressive collapse of concrete frame structures already reported in literature [46, 44]. Several parametric analyses based on different nonlinear models have been performed with the aim of evaluating the influence of material parameters on the collapse response of typical reinforced concrete frames not designed to withstand earthquakes. Once the numerical model has been correctly calibrated (according to the experimental results), a full-scale multi storey building has been investigated, with reference to column loss scenario, with the aim to obtain further information on the contribution of each structural elements.

In the fourth Chapter an original FEM implementation of a plane-discrete-macro-element is proposed aiming at modelling the non-structural infills in the nonlinear ADAPTIC-FEM models. The macro-model has been implemented in the software ADAPTIC [63] and validated through comparisons with experimental and numerically results, these latter obtained by the use of the software 3DMacro in which the element is implemented under small displacements assumption and according to a discrete-element framework.

The fifth Chapter, firstly, describes the chosen case study, secondly, reports code-consistent parametric evaluation of seismic vulnerability of low- and mid-rise reinforced concrete buildings. The case study has been defined according to a simulated design that was based on the survey of existing residential buildings designed and built in Catania between the 60’s and 80’s and on the design code that the engineers adopted in those decades. In this preliminary evaluation, only push-over analyses have been performed with the computer code 3DMacro that empowers a reliable model of non-structural masonry panels. Starting from the definition and design of the case study ten-storey building, other eight structures have been obtained. All the sub-cases have identical floors since the structural project considered only vertical loads and tributary areas for the column designing. Moreover, the results are expressed for

different soil conditions according to the Italian 2008 technical code. For each considered case a detailed descriptions of the model and of the collapse scenario is reported, aiming at identifying the role of the non-structural elements all the analyses have been performed with and without the contribution of the non-structural infills.

Chapter sixth considers the seismic vulnerability evaluation of the ten storeys case-study by means of a realistic model implemented in ADAPTIC considering the ribbed slabs and the infilled masonry panels contributions. The detailed FEM implementation of the plane macro-element, which is described in the fourth chapter, is adopted to model the non-structural walls. With the aim of evaluating the infill walls contribution, the case study is analysed with and without non-structural panels. The non-linear dynamic response of the two models are compared and discussed underling the unreinforced clay walls contribute. The thorough vulnerability assessments have been performed according to nonlinear dynamic analyses considering both material and geometrical nonlinearities.

The possible retrofitting strategies of the ten-storey building are discussed in Chapter 7. After an overview of existing retrofitting methodologies [99] proposed in the literature, an innovative proposal is presented. The proposal is the results of the research project that has been financed by ANCE|Catania and developed by a research team coordinated by Prof. I.Caliò and Prof. B.Izzuddin [93, 94]. The retrofitting strategy consists in an innovative structural perimetral steel skeleton made by a synergetic combination of centred braced frames and eccentric bracing system endowed with dissipative shear links. The first proposed solution based on the innovative Eccentric Bracing System configuration has been investigated by means of a high fidelity model implemented in the software ADAPTIC

The last Section contains the conclusions and a brief summary of the main results and highlights the relevance of the study within the context of retrofitting strategies of mid-rise existing reinforced concrete buildings not designed to resist to earthquake.

Aspects related to code consistent checks in agreement with the Italian Seismic Code [24, 23] and the Eurocode 8 [113] are reported in Appendix. The equations of chord rotation capacity and shear capacity are discussed. Even though the two design codes have some minor differences in the formulas, they equally prescribe the definition of Demand, Capacity and Checks.

8.1 Some consideration on the achieved results and possible future developments

Catania and its metropolitan area count more than 750000 inhabitants in a territory characterised by high seismic hazard and severe vulnerability of its constructions. These factors make of Catania one of the cities characterised by a very high seismic risk in the world and probably the highest in Italy.

According to several seismological surveys, the maximum magnitude of the expected earthquake in a period of 500 years is 7.4 and the last severe earthquake occurred in 1693. As time goes on, the probability for occurrence of a strong earthquake dramatically increases. Since it is not possible to reduce the probability of occurrence of a seismic event, the only possible action towards mitigation of the seismic risk is to promote strategies for obtaining a significant decrease of the seismic vulnerability of the constructions.

The thesis investigates the seismic vulnerability of existing reinforced concrete buildings built before the introduction of the seismic code and the identification of possible retrofitting strategies with particular reference to medium rise residential buildings.

Different models characterized by different level of accuracy have been used for assessing the seismic capacity of a typical ten-storey building whose structural scheme and architectural features are representative of several others existing structures not designed to withstand seismic loadings. The development of high fidelity models, implemented in the software ADAPTIC, allowed investigating the occurrence of progressive collapse phenomena as consequence of local damage induced by earthquakes. At the same time, the necessity of identifying a suitable retrofitting strategy that accounts for seismic deficiencies along with progressive collapse issues has a huge social impact in those areas that only recently have been catalogued seismically prone.

In this thesis, an extensive investigation of the collapse robustness of existing framed structures has been carried out and the results have been

reported in Chapter 3. The planar models in column loss scenario demonstrate that the existing concrete framed structures that were designed only with gravity, dead and live loads have an inadequate capacity to withstand progressive collapse due to local damage. In this case, the analyses have demonstrated the necessity of accurate beam discretization and the dependency of the structural robustness from the internal beam reinforcement layout. As matter of fact, a sudden change in the reinforcement distribution localizes plastic hinges. This affects the structural robustness and it is frequent in residential building built before 1981. On the other hand, the explicit slab modelling has demonstrated the deep influence of reinforced concrete slab on the progressive collapse. The results demonstrates that mechanical and geometrical nonlinearity, primary and secondary structural reinforced concrete elements have to be explicitly modelled avoiding for inaccurate robustness assessments. The first future extension accounts for establishing the robustness contribute of other recurring concrete slabs typologies. As the achieved results demonstrates, the concrete slab contribute might change the concrete beams collapse behavior and, consequently, the structural robustness of the entire building. In some cases, the reinforced concrete ribbed slab may avoid progressive collapse in existing buildings. Base on that, additional investigations have to be carried out.

A further original contribution of the thesis is constituted by the FEM implementation of a discrete plane macro-element for evaluating the contribution of infill masonry panels on the nonlinear structural response of reinforced concrete buildings. This implementation in the software ADAPTIC allowed the evaluation of the influence of nonstructural infills in high-fidelity models for assessing an accurate evaluation of the structural performance of the typical building selected as case study. The proposed finite (macro) element adopted approach provide a satisfactory simulation of the nonstructural infill panels whose contribution should not be neglected in the structural assessment of the existing buildings. A further extension of the presented work considers future developments of the proposed finite element that can add positive contribute in terms

of reduction of computational effort with a still considerable level of accuracy in high fidelity models and three-dimensional full nonlinear analyses.

The three-dimensional realistic model of the building with and without the retrofitting elements allowed a deeply accurate assessment of the structure when subjected to real accelerograms. The analyses performed in the retrofitted building has allowed to validate an innovative retrofitting strategy, based on eccentric steel bracings endowed with dissipative shear links according to a never adopted geometrical layout possessing several advantages with respect to the proposal already reported in the scientific literature. The high fidelity 3D models of the entire buildings have highlighted the importance of such refined modeling approach that allows a realistic simulation of the nonlinear behavior of the structure in its original configuration and after the proposed retrofitting strategy and is able to account for potential progressive collapse phenomena as a consequence of local damages induced by earthquakes.

Even though the proposed solution can be further investigated and optimized, the obtained results have shown that it can be successfully adopted for reinforced concrete structure not designed to resist to earthquake loadings also in the case of tall buildings for which the retrofitting strategies, based in the modification of the seismic demands, cannot be easily applied.

The structural optimization of the proposed retrofitting solution according to the definition of design criteria can represent an important upgrade of the present research work. The investigation of hybrid solutions based on a synergetic combination between traditional shear wall and the proposed innovative eccentric braced solution represents a further interesting retrofitting strategy that, although partially investigated, has not been reported in the present work but could be the subject of future researches.

CHAPTER 9. BIBLIOGRAPHY

[1] F. Mollaioli and G. M. Verderame, "Caratteristiche degli edifici campione situati nell'area di Catania," *Progetto Catania.*

[2] W. G. CPTI, "Catalogo Parametrico dei Terremoti Italiani (versione 2004, CPTI04): Internet website INGV Sezione di Milano, http://emidius.mi.ingv.it/CPTI/ (last revision 27 May 2004)," 2004.

[3] T. S. Piatanesi A., "A revision of the 1693 eastern Sicily earthquake and tsunami.," *J. Geophys. ,* vol. Res. 103:, p. 2749–2758, 1998.

[4] B. M. S. Azzaro R., "Seismogenic features of SE Sicily and scenario earthquakes for Catania, In The Catania Project: Earthquake damage scenarios for a high risk area in the Mediterranean.," R. Faccioli and V. Pessina (Editors), CNR-GNDT, Roma, 2000.

[5] B. C. Argnani A., "Malta Escarpment fault zone offshore eastern Sicily: Pliocene-Quaternary tectonic evolution based on new multichannel seismic data. Tectonics, 24, Art. No. TC4009, 1-12.," 2005.

[6] M. Gutscher, J. Roger, M. Baptista, J. Miranda and S. Tinti, "Source of the 1693 Catania earthquake and tsunami (southern Italy): new evidence from tsunami modeling of a locked subduction fault plane.," *Geophys. Res. Lett.,* vol. 33, 2006.

[7] G. Lavecchia, F. Ferrarini, R. d. Nardis, F. Visini and M. S. Barbano, "Active thrusting as a possible seismogenic source in Sicily (Southern Italy): Some insights from integrated structural–kinematic and seismological data. „" *Tectonophysics,* Vols. 445(3-4): 1, 2007.

[8] S. D'Amico, R. Azzaro, V. Castelli, A. Mostaccio, L. Scarfì and T. Tuvè, "The historical earthquake catalogue of Mt. Etna volcano (Southern Italy): a long-term dataset to investigate local seismotectonics and seismic hazards," *American Geophysical Union,* 2009.

[9] G. Giarrizzo, "La Siclia dei Terremoti - Lunga durata e dinamiche sociali," in *Atti del Convegno di Studi Università di Catania Facoltà di Lettere e Filosofia ex Monastero dei Benedettini*, Catania , 11-13 dicembre 1995.

[10] R. Azzaro, M. Barbano, A. Moroni and M. Mucciarelli, "The seismic history of Catania," *Journal of Seismology,* vol. 3, p. 235–252, 1999.

[11] M. Barbano and R.Rigano, “Earthquake and Seismic hazard in Southeaster of Sicily,” *Annuali di Geofisica,* 2001.

[12] M. Barbano, R. Azzaro and E. Grasso, “Earthquake damage scenario and seismic hazard of Messina, north-eastern Sicily (Italy) as inferred from historical data,” *Journal of Earthquake Engineering.*

[13] Wikipedia, “https://en.wikipedia.org/wiki/1693_Sicily_earthquake - cite_note-UNESCO-9,” [Online].

[14] G. Oliveto, I. Caliò and A. Greco, “Large displacement behaviour of a structural model with foundation uplift under impulsive and earthquake exitation,” *Earthquake Engineering and Structural Dynamics,* vol. 43, no. 3, pp. 369-393, 2003.

[15] J. J. Bommer and A. B. Acevedo, “The use of real earthquake accelerograms as input to dynamic analysis,” *Journal of Earthquake Engineering,* 2008.

[16] I. Iervollino, C. Galasso and E. Cosenza , “REXEL: computer aided record selection for code-based seismic structural analysis,” *Bull Earthquake Eng,* p. 339–362, 2010.

[17] PEER Pacific Earthquake Engineering Resear Center, “Database, PEER Ground Motion,” [Online]. Available: peer.berkeley.edu/products/strong_ground_motion_db.html.

[18] IRIS-Incorporate Research Institutions Seismology, “IRIS Data Sources,” [Online]. Available: ds.iris.edu/data/sources.htm.

[19] Ingv, “ITACA - Italian Accelerometric Archieve,” [Online]. Available: itaca.mi.ingv.it.

[20] “SIMBAD,” [Online]. Available: wpage.unina.it/iuniervo/SIMBAD_Database_Polimi.pdf.

[21] “ESD The European Strong-Motion Database,” [Online]. Available: www.isesd.hi.is.

[22] F. De Luca, I. Iervolino and E. Cosenza, “Unscaled, scaled, adjusted, and artificial spectral matching accelerograms: displacement- and energy-based assessment,” in *ANIDIS*, Bologna, 2009.

[23] *NTC Normativa tecnica per le costruzionii - DM 14 Gennaio 2008.*

[24] *Circolare C.S.LL.PP. 2 Febbraio 2009.*

[25] K. Khandelwal and S. El-Tawil, “Pushdown resistance as a measure of robustness in progressive collapse analysis,” *Engineering Structures ,* vol. 33 , p. 2653–2661, 2011.

[26] A. B. Izzudin , A. G. Vlassis and A. Y. Elghazouli, “Progressive collapse of multi-storey buildings due to sudden column loss — Part I: Simplified assessment framework,” *Engineering Structures,* vol. 30, pp. 1308-1318, 2008.

[27] B. A. Izzudin, A. G. Vlassis and A. Y. Elghazouli, “"Progressive collapse of multi-storey buildings due to sudden column loss—Part II: Application,” *Engineering Structures,* vol. 30, p. 1424–1438, 2008.

[28] “ Office of the Deputy Prime Minister; The Building Regulamentation 2000. part A, schedule 1: A3. London UK:Disproportionate Collapse 2004”.

[29] UNI, Ed., *Eurocodice 1 Azioni sulle strutture : Part 1-7: Azioni in genere - Azioni eccezionali,* 2006.

[30] Department of Defence, “DoD Minimum Antiterrorism Standards for Buildings,” Unified Facilities Criteria (UFC) 4-010-01.

[31] Department of Defense, “Design of Buildings to Resist Progressive Collapse,” Unified Facilities Criteria (UFC) 4-023-03, 2013.

[32] U. Storessek and M. Haberland, “Progressive Collapse Nomenclature,” *Structures 2009: Don't Mess with Structural Engineers © 2009 ASCE,* 2009.

[33] GSA, General Service Administration, Alternate Path Analysis & Design Guidline for Progressive Collapse Resistance, 2013.

[34] S. Kokot and G. Solomos, “Progressive collapse risk analysis: literature survey, relevant construction standards and guidelines,” JRC , 2012.

[35] C. Pearson and N. Delatte, ““Ronan Point Apartment Tower Collapse and its Effect on Building Codes”,” *Journal of Performance of Constructed Facilities,* 2005.

[36] G. Corley, ““Lessons learned on Improving Resistance of Buildings to Terrorist Attacks.”,” *Journal of Performance of Constructed Facilities,* pp. 68-78, May 2004.

[37] Z. P. Bazant, J.-L. Le, F. R. Greening and D. B. Benson, “What did and did not cause collapse of WTC twin towers in New York,” *Journal of Engineering Mechanics, ASCE,* vol. 134, no. 10, pp. 892-906, 2008.

[38] Z. P. Bazant and M. Verdure, “ (2007). “Mechanics of progressive collapse: Learning from World Trade Center and building demolitions,” *J. Eng. Mech., ASCE,* vol. 133, p. 308–319, 2007.

[39] FEA ltd, LUSAS - Theory Manuals, Lusas Vertion 15.0.

[40] M. Sasami, “Response of a reinforced concrete infilled-frame structure to removal of two adjacent columns,” *Science Direct,* vol. 30, pp. 2478-2491, 2008.

[41] Y. Su, Y. Tian and X. Song, “Progressive Collapse Resistance of Axially-Restrained Frame Beams,” *ACI Structural Journal,* vol. 106, no. 5, pp. 600-607, 2009.

[42] Y. Su, Y. Tian and X. Song, “Progressive Collapse Resistance of Axially-Restrained Frame Beams,” *ACI Structural Journal,* vol. 106, no. 5, pp. 600-607, 2009.

[43] L. Wong, ““Design and Detailing for Catenary Action.”,” 2004.

[44] S. L. Orton, “Development of a CFRP System to Provide Continuity in Existing Reinforced Concrete Buildings Vulnerable to Progressive Collapse,” 2007.

[45] A. Fascetti, S. Kunnath and N. Nisticò, “Robustness evaluation of RC Frame buildings to progressive collapse,” *Engineeering Structures,* vol. 86, pp. 242-249, 2015.

[46] S. M. Stinger, *Evaluation Of Alternative Resistance Mechanisms For Progressive Collapse,* University Of Missouri-Columbia, 2011.

[47] W. Hao, . Z. Anqi, L. Yi and Y. Weiming , “A Review on Progressive Collapse of Building Structures,” *The Open Civil Engineering Journal,* vol. 8, pp. 183-192, 2014.

[48] Q. Kai and B. Li, “Dynamic performance of RC beam-column substructures under the scenario of the loss of a corner column—Experimental results,” *Engineering Structures,* vol. 42, pp. 142-167, 2012.

[49] L. Shaung, S. Shan, Z. Changhai and X. Lili, “Experimental and numerical study on progressive collapse process of RC frames with full-heigh infill walls,” *Engineering Failure Analysis,* vol. 59, pp. 57-68, 2016.

[50] L. Shaung, S. Sidi and X. Lili, “Experimental study on the progressive collapse performance of RC frames with infill walls,” *Engineering Structures,* vol. 111, pp. 80-92, 2016.

[51] W. Tiecheng, C. Qingwei, Z. Hailong and Z. Lei, “Experimental Study on Progressive Collapse Performance of Frame with Specially Shaped Columns Subjected to Middle Column Removal,” *Hindawi Publishing Corporation,* 2015.

[52] H. Lew, Y. Bao, F. Sadek, J. A. Main, S. Pujol and M. A. Sozen, “An Experimental and Computational Study of Reinforced Concrete Assemblies under a Column Removal Scenario,” NIST Technical Note 1720, 2011.

[53] Hyun Jim Kim, “Progressive Collapse Behaviour of Reinforced Concrete Structures with Deficient Details,” Texas, 2006.

[54] H. Huda, S. Hamed and M. Sherif, “Progressive collapse assessment of framed reinforced concrete structures according to UFC guidelines for alternative path method,” *Engineering Structures,* vol. 42, pp. 127-141, 2012.

[55] S. M. Stinger and S. L. Orton, “Experimental Evaluation of Disproportionate Collapse Resistance in Reinforced Concrete Frames,” *Structural Journal,* vol. 110, no. 3, pp. 521-530, 2013.

[56] S. Shan, S. Li, S. Xu and L. Xie, “Experimental study on the progressive collapse performance of RC frames with infill walls,” *Engineering Structures ,* vol. 111, pp. 80-92, 2016.

[57] M. L. Bazan, “Responce of reinfroced concrete elements and structures following loss of load bearing elements,” 2008.

[58] American Concrete Institute, “Building Code Requirements for Reinforced Concrete (318-71),” Detroit, MI., 1971.

[59] B. A. Izzuddin, “Nonlinear dynamic analysis of framed structures,” University of London, Imperial; College, 1991.

[60] D. Kent and R. Park, “Flexural members with confined concrete,” *ASCE Journal of the Structural Division,* vol. 97, no. 7, p. 1969–1990, 1971.

[61] B. D. Scott, R. Park and M. J. N. Priestley, “Stress-strain behavior of concrete confined by overlapping hoops at low and high strain rates.,” *Journal of the American Concrete Institute,* vol. 79, no. 1, pp. 13-27, 1982.

[62] B. Izzuddin, A. Siyam and D. L. Smith, “An efficient beam–column formulation for 3D reinforced concrete frames,” *Computer & Structures,* vol. 80, pp. 659-676, 2002.

[63] B. A. Izzuddin, ADAPTIC User Manual, Department o Civil and Environmental Engineering, Revision Jannuary 2012.

[64] B. Izzuddin, X. Tao and A. Elghazouli, “Realistic Modelling of Composite and R/C Floor Slabs under Extreme Loading – Part I: Analytical Method”,,” *Journal of Structural Engineering,* vol. 130, no. 2, p. 1972–1984, 2004.

[65] I. Caliò, M. Marletta and B. Pantò, “A new discrete element model for the evaluation of the seismic behaviour,” *Engineering Structures,* no. 40, pp. 327-338, 2012.

[66] F. Crisafulli, “Seismic behavior of reinforced concrete structures with Masonry Infills,” *PhD Thesis, Department of Civil Engineering, University of Canterbury,* 1997.

[67] F. J. Crisafulli, A. J. Carr and R. Park, "Analytical modelling of infilled frame structures - A general review," *Bullettin of New Zeland Society for Earthquake Engineering,* vol. 33, no. 1, March 2000.

[68] I. Koutramanos, A. Stravridis, B. P. Shing and K. William, “Numerical modelling of masonry-infilled RC frames subjected to seismic loads,” *Computer and Structures,* no. 89, pp. 1026-1037, 2011.

[69] G. M. CALVI, D. BOLOGNINI and A. PENNA, “SEISMIC PERFORMANCE OF MASONRY-INFILLED R.C. FRAMES: BENEFITS OF SLIGHT REINFORCEMENTS”.

[70] S. V. Polyakov, “On the Interactions Between Masonry Filler Walls and Enclosing Frame When Loaded in the Plane of the Wall,” Moscow, Russia, 1956.

[71] M. Holmes, “Steel frames with Bricwork and concrete infilling.,” in *Proceedings of the Institutionof Civil Engineers*, 1961.

[72] S. B. Strafford, “Lateral stiffness of of infilled frames,” *Proceding of American Society of Civil Engineering, Journal of Structural Division,* vol. 88, no. ST6, pp. 183-199, 1962.

[73] A. P.G., A. S. T., S. D. S. and C. C. Z., "Mathematical Macromodeling of Infilled Frames: State of the Art," *JOURNAL OF STRUCTURAL ENGINEERING ASCE,* 2011.

[74] F. A. E, S. M. A. and G. W. L, "Investigation of the Interaction of Reinforced Frames with Masonry Filler Walls," 1970.

[75] J. Leuchars and J. Scrivener, "Masonry infill panels subjected to cyclic in-plane loading," *Bullettin of New Zeland National Society of Earthquake Engineering,* vol. 9, no. 2, pp. 122-131, 1976.

[76] F. J. Crisafulli and A. J. Carr, "Proposed macro-model for the analysis of infilled frame structures," vol. 40, no. 2, June 2007.

[77] A. Hashemi and K. M. Mosalam, "Seismic Evaluation of Reinforced Concrete Buildings Including Effects of Masonry Infill Walls," *PEER Report 2007/100 Pacific Earthquake Engineering Research Center College of Engineering - University of California, Berkeley,* 2007.

[78] S. Kadysiewski and K. M. Mosalam, "Modeling of Unreinforced Masonry Infill Walls Considering In-Plane and Out-of-Plane Interaction," *PEER Report 2008/102 Pacific Earthquake Engineering Research Center College of Engineering - University of California, Berkeley,* 2009.

[79] M. M. Talaat and K. M. Mosalam , "Computational Modeling of Progressive Collapse in Reinforced Concrete Frame Structures," *PEER Report 2007/10,* 2008.

[80] A. Mohebkhah, A. Tasnimi and H. Moghadam, "A Modified Three Stru (MTS) Model for Masonry-Infilled SteelFrames with Openings," *JSEE,* vol. 9, no. 1, 2007.

[81] I. Caliò and B. Pantò , "A macro-element modelling approach of Infilled Frame Structures," *Computers and Structures,* vol. 143, pp. 91-107, 2014.

[82] B. Pantò, I. Caliò and P. B. Lourenco, "Seismic safety evaluation of reinforced concrete masonry infilled frames using macro modelling approach," *Bull Earthquake Eng,* 2017.

[83] GruppoSismica srl, *3DMacro-Theory manual - Versione 1.11103101.*

[84] F. Xavier, L. Macorini and B. Izzuddin, "Robustness of multistory buildings with masonry infill," *Journal of Performance of Constructed Facilities,* vol. 29, no. 5, 2015.

[85] S. Farazman, B. Izzuddin and D. Cormie, "Influence of Unreinforced Masonry Infill Panels on the Robustness of Multistory Buildings," *Journal of Performance of Constructed Facilities,* vol. 27, no. 6, pp. 673-682, 2013.

[86] F. Xavier, L. Macorini and B. Izzuddin, "Enhanced robustness of multi-storey buildings with unreinforced masonry infill," in *10th International Conference on Shock and Impact Loads on Structures 2013*, Singapore, 2013.

[87] F. B. Xavier, L. Macorini and B. A. Izzuddin, "Mesoscale modeling of masonry structures accounting for brick-mortar interaction.","in *Civil-Comp*, Stirlingshire, Scotland.

[88] I. Caliò, A. Ghersi, M. Edoardo , P. P. Rossi, F. Contrafatto, F. Barbagallo, M. Bosco and G. Occhipinti, "Definition of the pilot building (ANCE|Catania Project 2016)," ANCE | Catania, Catania, 2017.

[89] M. Perreira, "Avaliação do desempenho das envolventes dos edifícios face à acção dos sismos," 2013.

[90] "Italian Ministry of Public Works: Law n. 1086, 5/11/1971, Norme per la disciplina delle opere in conglomerato cementizio normale e precompresso ed a struttura metallica (Regulations for constructions of normal and pre-stressed reinforced concrete and with".

[91] "Italian Ministry of Public Works: Ministry Decree, 22/07/1971, Norme tecniche alle quali devono uniformarsi le costruzioni in conglomerate cementizio armato normale e precompresso ed a struttura metallica (Technical regulations for constructions with reif".

[92] P. Fajfar, "A nonlinear analysis methodo for performance base seismic design".

[93] B. Izzuddin, L. Macorini, I. Caliò and G. Occhipinti, "Assessment and retrofitting of a typical RC building in Catania for seismic action and progressive collapse," ANCE|Catania, Catania, 2017.

[94] G. Occhipinti, B. Izzudin, I. Caliò and L. Macorini, "Realistic 3D nonlinear dynamic analysis of exisitng and retrofitted multi-sorey RC buildings subjected to earthquake loading," in *COMPDYN 2017*, Rhodes, 2017.

[95] G. A. Jokhio and B. A. Izzuddin, "A Dual Super-Element Domain Decomposition Approach for Parallel Nonlinear Finite Element Analysis," *International Journal for Computational Methods in Engineering Science and Mechanics,* vol. 16, no. 3, 2015.

[96] B. Izzuddin and D. Lloyd Smith , "Efficient Nonlinear Analysis of Elasto-Plastic 3D R/C Frames Using Adaptive Techniques," *Computers & Structures,* vol. 78, no. 4, pp. 549-573, 2000.

[97] A. Kadid, D. Yahiaoui and R. Chebili, "Behaviour of reinforced concrete buildings under simultaneous horizontal and vertical ground motions," *ASIAN JOURNAL OF CIVIL ENGINEERING (BUILDING AND HOUSING),* vol. 11, no. 4, pp. 463-476, 2010.

[98] A. Lynn, "Seismic Evaluation of Existing Reinforced Concrete Building Columns," University of California at Berkeley, Berkeley, 1999.

[99] M. Cheung, S. Foo and J. Granadino, "Seismic retrofit of existing buildings: Innovative Alternatives".

[100] "SCOPUS," Scopus® is a registered trademark of Elsevier B.V., [Online]. Available: www.scopus.com.

[101] V. V. Minakshi , A. V. Sandip and K. D. Atul , “Advanced Retrofitting Techniques for RC Building A State of an Art Review,” *International Journal of Current Engineering and Technology ,* vol. 4, no. 2, pp. 579-584, 2014.

[102] W. Kam and S. Pampanin, “Selective weakeinig techniques for retrofit of existing reinfroced concrete structures,” in *The 14th World Conference on Earthquake Engineering* , Beijing, China , 2008.

[103] C. Durucan and M. Dicleli, “Analytical study on seismic retrofitting of reinforced concrete buildings using steel braces with shear link,” *Engineering Structures,* vol. 32, pp. 2995-3010, 2010.

[104] C. T. Sina Kazemzadeh Azad, “A Review of Research on Steel Eccentrically Braced Frames,” *Journal of Constructional Steel Research,* 2017.

[105] A. K. Ryan, A. F. Larry and A. L. Walterio, “Seismic Design of Steel Buckling Restrained Braced Frames - A Guide for Practicing Engineers,” NIST National Institute of Standards and Technology, 2015.

[106] T. T. K. Kolozvari, J. Wallace and K. Orakcal, “Modeling of cyclic shear-flexure interaction in reinforced concrete structural walls,” in *15 WCEE*, Lisboa 2012, 2012.

[107] M. Ismaeil and A. Hassaballa, “Seismic Retrofitting of a RC Building by Adding Steel Plate Shear Walls,” *Journal of Mechanical and Civil Engineering,* vol. 7, no. 2, pp. 49-62, 2013.

[108] A. Ghobarah and H. A. Elfath, “Rehabilitation of a reinforced concrete frame using eccentric steel bracing,” *Engineering Structures,* vol. 23, p. 745–755, 2001.

[109] F. M. Mazzolani, G. D. Corte and M. D'Aniello, “Experimental analysis of steel dissipative bracing systems for seismic upgrading,” *Journal of Civil Engineering and Management,* 2010.

[110] R. Perera, S. Gómez and E. Alarcón, “Experimental and Analytical Study of Masonry Infill Reinforced Concrete Frames Retrofitted with Steel Braces,” *Journal of Structural Engineering ,* 2004.

[111] D. S. Lorenzo, R. Scotta and M. Lazzari, “Optimal design of seismic retrofitting of RC frames with eccentric steel bracing,” *Bull Earthquake Eng,* pp. 613-633, 2015.

[112] A. Sina Kazemzadeh and T. Cem, “A Review of Research on Steel Eccentrically Braced Frames,” *Journal of Constructional Steel Research,* 2017.

[113] “Eurocode 8: Design of structures for earthquake resistance Part 3: Assessment and retrofitting of buildings”.

[114] I. Iervolino, E. Cosenza and C. Galasso, “Spettri, accelerogrammi e le nuove norme tecniche per le costruzioni.”.

[115] A. Vlasses, B. Izzudin, A. Elghazouli and D. Nethercot, "Progressive collapse of multi storey buildings due to failed floor impact," *Engineering Structures,* vol. 31, pp. 1522-1534, 2009.

[116] M. Fardis, Seismic Design, Assessment and Retrofitting of Concrete Buildings Based on EN-Eurocode 8, Springer, 2009.

[117] B. Izzuddin and A. Elnashai, "Adaptive space frame analysis: Part I, a plastic hinge approach," *Proceedings of the Institution of Civil Engineers, Struct Building J,* no. 99, pp. 303-316, 1993.

[118] B. Izzuddin and S. Elnashai, "Adaptive space frame analysis: Part II, a distributed plasticity approach.," *Proceedings of the Institution of Civil Engineers, Struct Building J,* pp. 317-326, 1993.

[119] O. Joh and T. Shibata, "Shear failure of reinforced concrete columns due to biaxial lateral forces," in *World Conference on Earthquake Engineering*.

[120] C. Hansapinyo, K. Maekawa and T. Chaisompho, "Behaviour of Reinforced Concrete Beams Subjected to bi-axial Shear," vol. 58, pp. 321-331, 2003.

[121] Architectural Institute of Japan structural design guidelines for reinforced concrete buildings., Tokyo, Japan.

[122] JSCE: Standard Specification for Design and Construction of Concrete Structures-1986, Partl (Design), 1986.

[123] ACI: Building Code Requirements for Reinforced Concrete and Commentary-AC1318-95, Detroit, 1995.

[124] P. Ren, Y. Li, H. Guan and X. Lu, "Progressive Collapse Resistance of Two Typical High-Rise RC Frame Shear Wall Structures," *Joural of Performance of Constructed Facilities,* vol. 29, no. 3, June 2015.

[125] B. I. Izzuddin and ,. A. Y. Elghazouli, "Failure of Lightly Reinforced Concrete Members under Fire.I: Analytical Modeling," *Journal of Structural Engineering, ASCE,* Jannuary 2004.

CHAPTER 10.
APPENDICES

APPENDIX I. DUCTILE MECHANISMS: CHORD ROTATION CAPACITY

This Appendix compares the chord capacity according to two Seismic Code: Eurocode 8:part3 [113] and Italian NTC08 [23, 24]. The two codes give slightly different formulas for evaluating the ultimate and yield chord capacity.

I. Eurocode-8: part3

The Eurocode 8 recommends evaluating the ultimate chord capacity (Limit State Near Collapse (NC)), by the following formula:

$$\theta_{um} = \frac{1}{\gamma_{el}} 0.016\left(0.3^{\upsilon}\right)\left[\frac{\max\left(0.01;\omega'\right)}{\max\left(0.01;\omega\right)} fc\right]^{0.225}\left(\min\left(9;\frac{L_v}{h}\right)\right)^{0.35} 25^{\left(\alpha\rho_{sx}\frac{fyw}{fc}\right)}\left(1.25^{100\rho_d}\right)$$

Eq. 71

In which

γ_{el} is a safety factor; it is equal to 1.5 for primary seismic elements and 1 for secondary seismic elements.

$\nu = \frac{N}{bhf_c}$ in which b is the width of the compressed zone and N is the axial force on the element. The axial force is assumed positive for compression stresses.

h is the depth of cross section according to the plan in which the rotation is evaluated.

L_V=M/V is the ratio Moment over Shear at the end of the section, also defined as "Shear Span".

ω is the mechanical reinforcement ratio of the tension longitudinal reinforcements.

ω' is the mechanical reinforcement ration of the compression longitudinal reinforcements.

f_c, f_{yw} and f_{yl} are the concrete compressive strength (MPa), the stirrup yield strength (MPa) and the longitudinal steel yield strength (MPa), respectively. Strength values should be the mean values appropriately divided by the confidence factor accounting for the level of knowledge attained.

$\rho_{sx} = A_{sx}/b_w s_h$ is the ratio of transverse steel parallel to the direction x of loading (s_h is the stirrup spacing).

ρ_d is the steel ratio of diagonal reinforcement (if any), in each diagonal direction.

α is the *confinement effectiveness* factor that may be taken equal to the following expression:

$$\alpha = \max\left\{1;\left(1-\frac{s_h}{2b_0}\right)\left(1-\frac{s_h}{2h_0}\right)\left(1-\frac{\sum b_i^2}{6h_0b_0}\right)\right\} \qquad \textit{Eq. 72}$$

The *confinement effectiveness* factor should always be positive value and not less than 1.

b_o and h_o are the dimensions of confined core to the centreline of the hoop as shown in Figure 10.1.

b_i is the centreline spacing of longitudinal bars (indexed by i) laterally retrained by a stirrup corner or a cross-tie along the perimeter of the cross section hoop as shown in Figure 10.1.

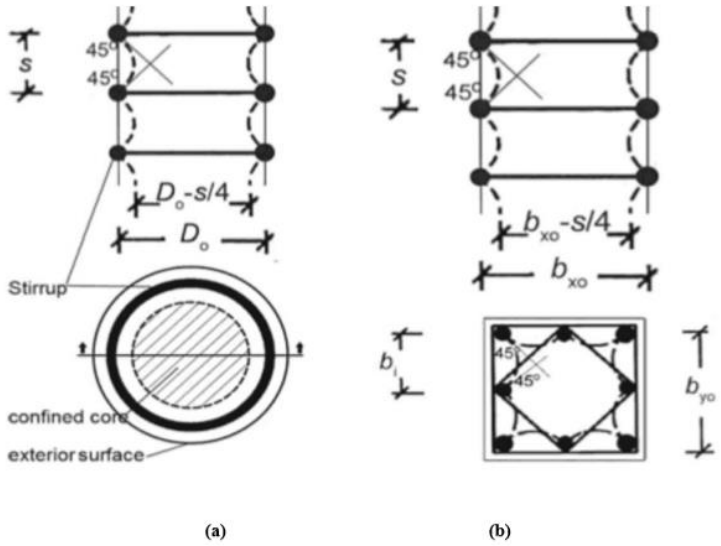

Figure 10.1 Confined and unconfined parts over the cross-section and along member with (a) circular section and circular hoops; or (b) square section and multiple ties [116].

If cold-worked brittle steel is used, the factor 1.6 divides the total chord rotation capacity.

As before mentioned, the formula Eq. 71 defines the value of ultimate chord capacity as sum of the elastic and plastic part. The value of the

plastic part of the chord rotation capacity of concrete members under cyclic loading may be calculated from the following expression:

$$\theta_{um}^{pl} = \theta_{um} - \theta_y = \frac{1}{\gamma_{el}} 0.0145\left(0.25^{\upsilon}\right)\left[\frac{\max\left(0.01;\omega'\right)}{\max\left(0.01;\omega\right)}\right]^{0.3} f_c^{0.2}\left(\min\left(9;\frac{L_v}{h}\right)\right)^{0.35} 25^{\left(\alpha\rho_{sx}\frac{fyw}{fc}\right)}\left(1.275^{100\rho_d}\right)$$

Eq. 73

Where the θ_y is the chord rotation at yield and it may be calculated by the Eq. 78 or Eq. 79.

γ_{el} is a factor equal to 1.8 for primary seismic elements and to 1.0 for secondary seismic ones.

If cold-worked brittle steel is used, the value 2 divides the plastic part of the chord rotation capacity.

In members without detailing for earthquake resistance, the Eq. 71 and Eq. 73 are divided by 1.2

The Eq. 73 can be applied to members with deformed (high bond) longitudinal bars without lapping near the end region where yielding is expected. If deformed longitudinal bars have straight lapped ends starting at the end section of the member, as is often the case in columns and walls with lap-splicing starting at floor level, expressions Eq. 71 and Eq. 73 should be applied with the value of the compression reinforcement ratio, ω' doubled over the value applying outside the lap splice. Moreover, if the lap length l_0 is less than $l_{0u,min}$, the plastic part of the chord rotation capacity given in Eq. 73 should be multiplied by $l_0/l_{0u.min}$. While the value of the chord rotation at yielding, θ_y, added to it for obtaining the total chord rotation capacity, should account for the effect of the lapping as in the later explained.

$$l_{ou,\min} = d_{bL} f_{yL} / [(1.05 + 14.5\alpha_l \rho_{sx} f_{yw} / f_c)\sqrt{f_c}] \qquad \textit{Eq. 74}$$

being:

d_{bL} is the diameter of the lapped bars

f_{yL} is the mean value of the yield strength of the lapped bars (MPa) multiplied for the corresponding confidence factor

$$\alpha_l = \left(1 - \frac{s_h}{2b_0}\right)\left(1 - \frac{s_h}{2h_0}\right)\frac{n_{restr}}{n_{tot}} \qquad \textit{Eq. 75}$$

Being n_{restr} the number of lapped longitudinal bars laterally restrained by a stirrup corner or a cross-tie and n_{tot} is the total number of lapped longitudinal bars along the cross-section perimeter.

In members with smooth longitudinal bars without lapping in the vicinity of the end region, where yielding is expected, the total chord rotation capacity may be taken equal to the value calculated in accordance with Eq. 71 and multiplied by 0.8.

The plastic part of the chord rotation capacity may be assumed equal to the value that is calculated in accordance with Eq. 73 and multiplied by 0,75 . In case of existing structures a reduction factor l.2 accounts for the lack of detailing for earthquake resistance. If the longitudinal bars are lapped starting at the end section of the member and their ends are provided with standard hooks and a lap length l_0 of at least $15d_{bL}$, the chord rotation capacity of the member may be calculated as follows.

The shear span L_V is reduced by the lap length l_0 as the ultimate condition is controlled by the region right after the end of the lap.

The total chord rotation capacity may be taken equal to the value calculated before (Eq. 71) and multiplied by $0.019\left(10 + min\left(40, \frac{l_0}{d_{bL}}\right)\right)$.

The plastic part may be calculate as before suggested (Eq. 73) and multiplied by $0.019\left(min\left(40, \frac{l_0}{d_{bL}}\right)\right)$.

The Eurocode suggests an alternative expression for evaluating the ultimate chord rotation capacity:

$$\theta_{um} = \frac{1}{\gamma_{el}}\left(\theta_y + \left(\phi_u - \phi_y\right)L_{pl}\left(1 - \frac{0.5L_{pl}}{Lv}\right)\right) \qquad \textit{Eq. 76}$$

Being:

ϕ_u is the ultimate curvature at the end section,

ϕ_y is the yield curvature at the end section.

For members with detailing for earthquake resistance and without lapping of longitudinal bars approximately to the section where yielding is expected, L_{pl} may be calculated as follows:

$$L_{pl} = 0.1L_V + 0.17h + 0.24\frac{d_{bL}f_y}{\sqrt{f_c}} \qquad \textit{Eq. 77}$$

The plastic hinge length depends on the strength and deformation capacity of concrete enhancement due to confinement.

The Eurocode indicates additional consideration for structures with seismic detailing that are not part of the aim of this thesis.

The chord rotation capacity that corresponds to *Significant Damage* SD may be assumed to be 3/4 of the ultimate chord rotation.

The capacity for the Limit State of *Damage Limitation* (DL) is the yielding bending moment under the design value of the axial load.

The chord rotation capacity at yielding θy is:

$$\theta_y = \underbrace{\phi_y \frac{L_v + a_v z}{3}}_{\textit{flexural contribute}} + \underbrace{0.0014\left(1+1.5\frac{h}{L_v}\right)}_{\textit{shear deformation contribute}} + \underbrace{\frac{\varepsilon_y}{d-d'}\frac{d_{bL}f_y}{6\sqrt{f_c}}}_{\textit{anchorage slip contribute}} \qquad \textit{Eq. 78}$$

Or from the alternative (and equivalent) expression

$$\theta_y = \underbrace{\phi_y \frac{L_v + a_v z}{3}}_{\textit{flexural contribute}} + \underbrace{0.0014\left(1+1.5\frac{h}{L_v}\right)}_{\textit{shear deformation contribute}} + \underbrace{\phi_y \frac{d_{bL}f_y}{8\sqrt{f_c}}}_{\textit{anchorage slip contribute}} \qquad \textit{Eq. 79}$$

$a_v z$ is the tension shift of the bending moment diagram;

z length of internal level arm

a_v is assumed equal to 1 if shear cracking is expected to precede flexural yielding at the end section

ε_y is equal to f_y/E_s,

d and d' are the depths to the tension and compression reinforcement, respectively,

d_{bL} is the mean diameter of the tension reinforcement.

The Eq. 78 and Eq. 79 contain three term that take into account three different contributes. Moreover, the first term accounts for the flexural contribution, the second term represents the contribution of shear deformation and the third considers the anchorage slip of bars.

II. Italian NTC08

The Italian Seismic Design Code [23, 24] recommends the use of an expression that appears to be similar to the suggested one in Eurocode [113] (Eq. 71).

$$\theta_{um} = \frac{1}{\gamma_{el}} 0.016 \left(0.3^{\upsilon}\right) \left[\frac{\max\left(0.01;\omega'\right)}{\max\left(0.01;\omega\right)} fc\right]^{0.225} \left(\frac{L_v}{h}\right)^{0.35} 25^{\left(\alpha\rho_{sx}\frac{fyw}{fc}\right)} \left(1.25^{100\rho_d}\right)$$

Eq. 80

Where all the symbols have the identical meanings of the before described symbols in the Eurocode formula.

The value of the mentioned ultimate chord rotation has to be multiplied by 0.85 in case of members without detailing for earthquake resistance (it was 0.833 in the Eurocode).

Consistently with the stirrups typologies the NTC imposes to assume α equal to zero (Eq. 76) if the bending angle of the hooks is not enough (minus than 135°).

In agreement with the Eurocode, the NTC imposes a reduction of the chord capacity in case of lapping near the section in which the plastic hinge is expected. In case of deformed longitudinal reinforcement bars, the Eq. 80 has to be multiplied by

$$\underbrace{0.25 \cdot \min\left(40, \frac{l_0}{d_{bL}}\right)}_{lapping} \cdot \underbrace{0.85}_{defincencies}$$

Eq. 81

The last term has to be considered only in case of absence of seismic details.

In case of smooth longitudinal reinforcement bars, the Eq. 80 has to be multiplied by

$$\underbrace{0.02 \cdot \left[10 + \min\left(40, \frac{l_0}{d_{bL}} \right) \right]}_{lapping} \cdot \underset{defincencies}{0.85} \qquad \textit{Eq. 82}$$

The last term has to be considered only in case of absence of seismic details.

Consistently with the Eurocode, the NTC suggests an alternative expression for evaluating the ultimate chord rotation capacity:

$$\theta_{um} = \frac{1}{\gamma_{el}} \left(\theta_y + \left(\phi_u - \phi_y \right) L_{pl} \left(1 - \frac{0.5 L_{pl}}{Lv} \right) \right) \qquad \textit{Eq. 83}$$

Where:

ϕ_u is the ultimate curvature at the end section,

ϕ_y is the yield curvature at the end section.

The L_{pl} expression in the Italian Seismic Code is identical to the Eq. 77, but without any restriction.

III. Ductile Mechanisms: Chord Rotation Demand

This section convers the explanation of the methodology that has been adopted to evaluate the chord demand by ADAPTIC. The column/beam element is a 3D beam-column elastic-plastic cubic formulation, based on fibre discretization, and it has been engaged in this research for modelling the elastic-plastic response of RC beams and columns. The material nonlinearity has been explicitly considered according to the spread plasticity method [62]. The geometric nonlinearity is take into account by means of a co-rotational approach [117, 118].

The cubic formulation assumes cubic shape functions for the transverse displacements v(x) and w(x). Figure 10.2 illustrates the local

degree of freedoms of the elastic-plastic cubic formulation that employs a constant centroid axial strain criterion with the six associated local freedoms θ_{y1}, θ_{z1}, θ_{y2}, θ_{z2}, Δ, θ_T. Thus, the generalised strain consists of centroid axial strain, rate of twist, and curvature strains about the two principal axes. The Figure 10.2 shows the strains corresponding to one sub-element. In the 3D framed building each column and beam are subdivided in not less than 6 and 10 sub-elements, respectively. These are reasonable discretization that can accurately capture the deformations of the RC beams and columns.

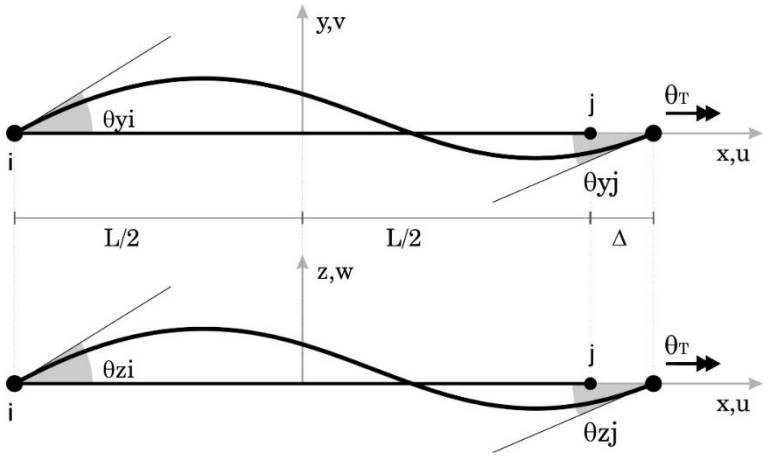

Figure 10.2 Local dof of 3D elastic-plastic cubic beam [62]

The beam and column chord rotation demand is the resultant of the three rotational components listed below:

a) The rotation due to the flexural curvatures along the two principal axes denoted as θ_{y1}, θ_{z1}, θ_{y2}, θ_{z2} for the two element ends as shown in Figure 10.2.

b) The rotational component in columns due to the relative horizontal displacement of the two ends of the first sub-element, θ_2. This component has the same meaning in the beams and in this case is the most significant rotational component in a horizontal element especially during a column loss scenario as the Figure 10.3 shows. The same component on the opposite element end is marked by the accent.

c) The rotation due to the horizontal lateral displacement at the two ends of the column (drift ratio) and due to the vertical displacement at the two ends of the beam, θ_3. This rotational component is not significant in beams where it is defined as the relative vertical displacement at the beam ends divided by the geometric element length.

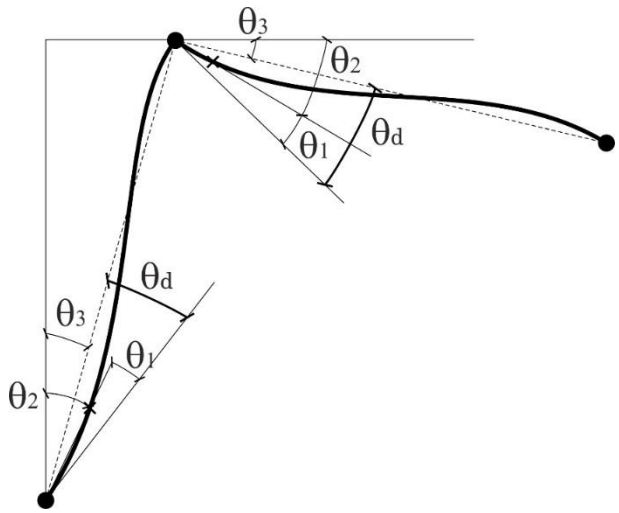

Figure 10.3 Chord Rotation components

IV. Biaxial Bending

Three-dimensional structures are subjects to biaxial loading and the demand rotation is the resultant of the uniaxial rotations along the two principal axes. A circular interaction is a reasonable approximation for the biaxial chord rotation [116]. The Eq. 84 depicts the relationship between chord demand and capacity along the two principal axes. The Eurocode indicates to consider the biaxial interaction in a circular dominium. On the other hand, the Italian Seismic Code does not give any specific indication on the contemporaneity of chord components on both the principal axes. Due to this difference, the circular dominium suggested by the Eurocode has been adopted in this thesis.

$$\sqrt{\left(\frac{\theta_{uy,\mathrm{D}}}{\theta_{uy,C}}\right)^2+\left(\frac{\theta_{uz,\mathrm{D}}}{\theta_{uz,C}}\right)^2}\leq 1 \qquad \textit{Eq. 84}$$

In which, y and z are the principal axes and D is the Demand and C the Capacity.

APPENDIX II. BRITTLE MECHANISMS: SHEAR CAPACITY

This Appendix describes the model that the Eurocode 8:part3 [113] and Italian NTC08 [23, 24] consider for evaluating the shear capacity of existing concrete frame elements. Concrete beams and columns are evaluated in terms of brittle mechanism, namely failure mechanism that are characterised by extrimely low ductility level. The shear ultimate capacity does not have identical model in the two selected codes.

I. Eurocode 8

The European code defines the Shear Capacity, V_R, as a resistance that decreases with the plastic part of ductility demand, expressed in terms of ductility factor of the transverse deflection of the shear span or of the chord rotation at member end, $\mu_\Delta^{pl} = \mu_\Delta\text{-l}$. For this purpose μ_Δ^{pl} may be calculated as the ratio of the plastic part of the chord rotation, θ, normalized to the chord rotation at yielding, θy. The value of θy is calculate as described in the APPENDIX I.

The Shear Capacity is sum of three different contributes:

$$V_R = V_N + V_C + V_W \qquad \textit{Eq. 85}$$

being

V_N shear capacity contribute of the axial compression forces

V_C shear capacity contribute of the concrete strut

V_W shear capacity contribute of the reinforcement elements

$$V_R = \frac{1}{\gamma_{el}}\left[\frac{h-x}{2L_V}\min\left(N;0.55A_c f_c\right)+\left(1-0.05\min\left(5;\mu_\Delta^{pl}\right)\right)\cdot\ldots\right.$$
$$\left.\left[0.16\max\left(0.5;100\rho_{tot}\right)\left(1-0.16\min\left(5;\frac{L_V}{h}\right)\right)A_c\sqrt{f_c}+Vw\right]\right] \qquad \textit{Eq. 86}$$

V_W represents the transverse reinforcement contribute and, in case of rectangular section, is equal to:

$$V_W = \rho_W \cdot b_W \cdot z \cdot f_{yW} \qquad \textit{Eq. 87}$$

The symbols of the Eq. 86 and Eq. 87 are explained below:

γ_{el} is equal to 1.15 for primary seismic elements and 1.0 for secondary seismic elements,

h is the depth of cross-section,

x is the compression zone depth,

N is the compressive axial force (positive, taken as being zero tension),

L_V is the ratio moment/shear at the end section,

A_c is the cross-section area, taken as being equal to $b_w d$ for a cross-section with a rectangular web of width (thickness) b_w and structural depth d,

f_c is the concrete compressive strength; for primary seismic element it has to be further divided by the partial factor for concrete in accordance with EN 1998-1: 2004, 5.2.4,

ρ_{tot} is the total longitudinal reinforcement ratio,

ρ_w is the transverse reinforcement ratio,

z is the length of the internal lever arm,

f_{yw} is the yield stress of the transverse reinforcement as defined for expression Eq. 71; for primary seismic elements should be further divided by the partial factor for steel in accordance with EN 1998-1: 2004, 5.2.4;

Lastly, if the shear span ratio, Lv/h, at the end section with the maximum of the two end moments is less or equal to 2.0, V_R should not be assumed greater than the value corresponding to failure due to web crushing along the diagonal of the column after flexural yielding.

$V_{R,max}$, in a cyclic loading is assumed as Eq. 88 shows(with units: MN and meters):

$$V_{R\max} = \frac{4/7 \cdot \left(1 - 0.02 \cdot \min\left(5; \mu_{\Delta}^{pl}\right)\right)}{\gamma_{el}} \cdot \left(1 + 1.35 \frac{N}{A_c f_c}\right) \cdot \ldots$$
$$\left(1 + 0.45 \cdot \left(100 \rho_{tot}\right)\right) \cdot \sqrt{\min\left(40; f_c\right)} \cdot b_W \cdot z \cdot \sin\left(2\delta\right)$$

Eq. 88

In the seismic assessment, the minimum value of the two expressions Eq. 86 and Eq. 88 has to be adopted.

II. Italian Seismic Code

The Italian Seismic Code defines the Shear Capacity V_R of existing concrete beam/column elements as the minor value between the Shear Capacity of the concrete strut and the Shear Capacity of the steel tie.

In case of stirrups, the stirrups contribute is defined with the expression:

$$V_{Rsd} = 0.9 \cdot d \cdot \frac{A_{SW}}{s} \cdot f_{yd} \cdot \left(\mathrm{c}tg\alpha + ctg\theta \right) \cdot \sin\alpha \qquad \textit{Eq. 89}$$

The concrete contribute is evaluated by the expression:

$$V_{Rcd} = 0.9 \cdot d \cdot b_W \cdot \alpha_c \cdot f'_{cd} \cdot \frac{ctg\alpha + ctg\theta}{1 + ctg^2\theta} \qquad \textit{Eq. 90}$$

The Ultimate Shear Capacity is defined as

$$V_{Rcd} = \min\left(V_{Rsd}, V_{Rcd} \right) \qquad \textit{Eq. 91}$$

Where:

d is the depth of cross-section;

b_W is the minimum width of cross-section;

$\sigma_{cp}=N_{Ed}/A_c$ is the average compression stress of cross-section ($\leq$0.2fcd);

A_{SW} is the transversal steel area;

s is the stirrups spacing;

α is the angle between the shear reinforcements and the element axis;

θ is the angle between the concrete strut and the element axis and it has the limits of

$$0 \leq ctg\theta \leq 2.5 \qquad \textit{Eq. 92}$$

f'_{cd} reduced compression ultimate strength f'cd=0.5f_{cd},

α_c coefficient that accounts for the compression state contribute within the cross-section. It is defined as follows:

$$\alpha_c = \begin{cases} 1 & if \quad \sigma_{cp} \le 0\,(tension) \\ 1+\sigma_{cp}/f_{cd} & if \quad 0 \le \sigma_{cp} < 0.25 f_{cd} \\ 1.25 & if \quad 0.25 f_{cd} \le \sigma_{cp} < 0.5 f_{cd} \\ 2.5\cdot\left(1-\sigma_{cp}/f_{cd}\right) & if \quad 0.5 f_{cd} \le \sigma_{cp} < f_{cd} \end{cases}$$

Eq. 93

Lastly, the regulation limits V_{Rcd} in case of existing concrete structure. It imposes that the concrete strut contribute has not to exceed the value calculated without stirrups contribute. This value is defined by the expression:

$$V_{Rd} = \left\{ \frac{0.18\cdot k\cdot\left(100\cdot\rho_l\cdot f_{ck}\right)^{1/3}}{\gamma_c} + 0.15\cdot\sigma_{cp} \right\}\cdot b_W\cdot d \ge \left(v_{\min} + 0.15\cdot\sigma_{cp}\right)\cdot b_W\cdot d$$

Eq. 94

Where

$k=1+(200/d)^{1/2}\le 2$;

$v_{min}=0.035k^{3/2}f_{ck}^{1/2}$;

$\rho_l=A_{sl}/(b_W d)$ is the longitudinal reinforcement geometric ratio.

III. Biaxial Shear

In a three-dimensional analysis, the concrete frame elements are subjected to biaxial loadings. Consequently, the shear demand in a 3D element is the resultant of the demand in two principal directions. Even if the concrete beams are prevalently subjected to vertical shear demand under vertical loads, this assumption may be not true in case of seismic actions. Due to that, the contemporary presence of shear forces in two directions has to be considered. Even if some experimental tests conducted on concrete elements under biaxial shear forces [119, 120] found some differences between the code circular resistance dominium and the experimental results, international regulations suggest adopting circular or elliptical interaction dominia. The so far described seismic regulations do not specify the biaxial shear capacity dominium of rectangular elements. Consequently, the mentioned circular resistance dominium (Eq. 95) has been adopted in agreement with other international codes, such as AIJ [121], JSCE [122] and ACI [123].

$$\sqrt{\left(\frac{V_{y,\mathrm{D}}}{V_{y,C}}\right)^2+\left(\frac{V_{z,\mathrm{D}}}{V_{z,C}}\right)^2}\le 1 \qquad \textit{Eq. 95}$$

APPENDIX III.
PARAMETRIC MODELS

The Appendix reports all the capacity curves of each model for all the directions and the load distributions.

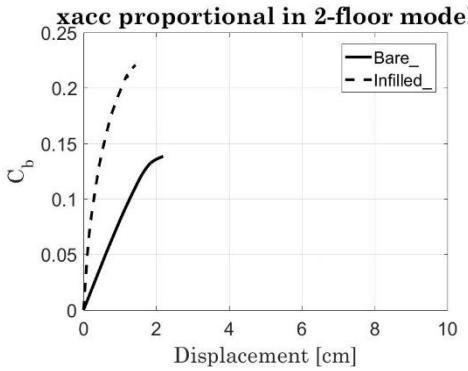
xacc proportional in 2-floor model
Bare_
Infilled_
C_b
Displacement [cm]

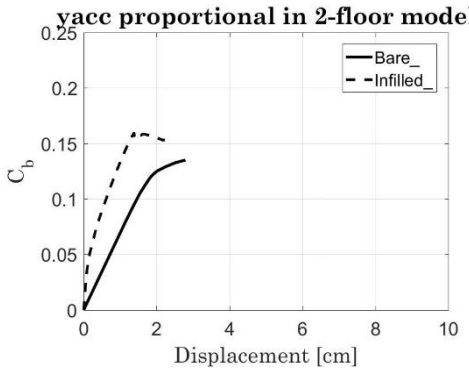
yacc proportional in 2-floor model
Bare_
Infilled_
C_b
Displacement [cm]

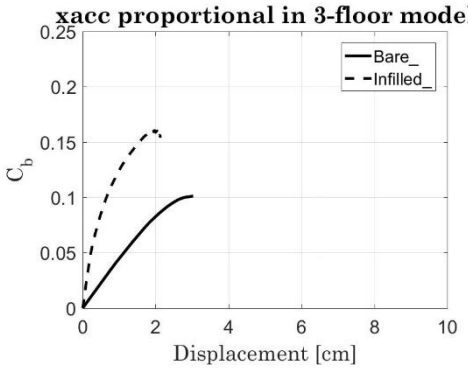
xacc proportional in 3-floor model
Bare_
Infilled_
C_b
Displacement [cm]

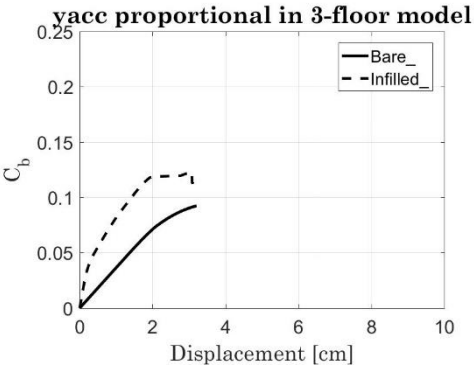
yacc proportional in 3-floor model
Bare_
Infilled_
C_b
Displacement [cm]

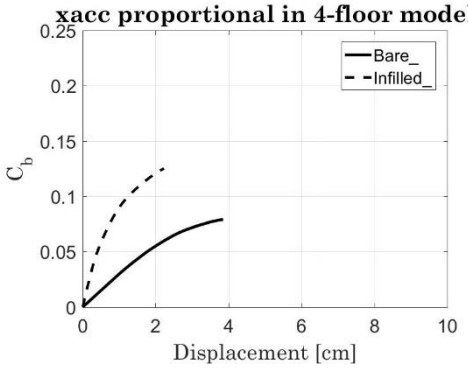
xacc proportional in 4-floor model
Bare_
Infilled_
C_b
Displacement [cm]

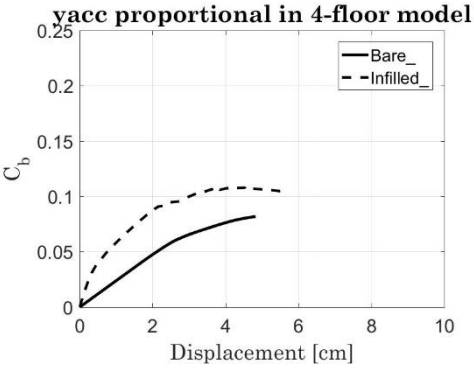
yacc proportional in 4-floor model
Bare_
Infilled_
C_b
Displacement [cm]

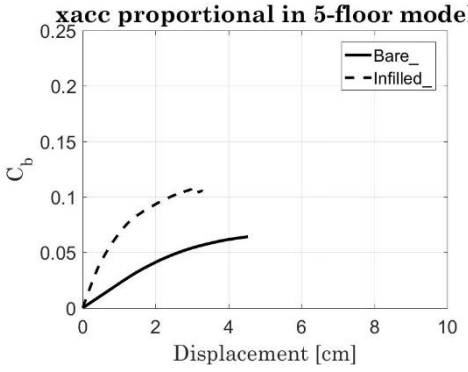
xacc proportional in 5-floor model
Bare_
Infilled_
C_b
Displacement [cm]

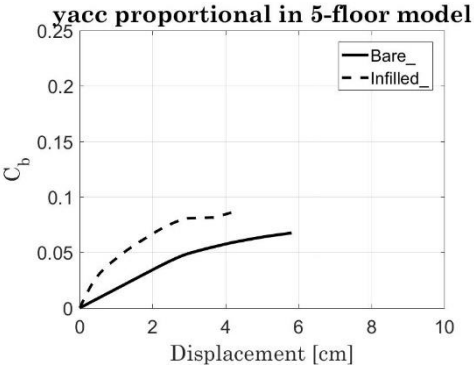
yacc proportional in 5-floor model
Bare_
Infilled_
C_b
Displacement [cm]

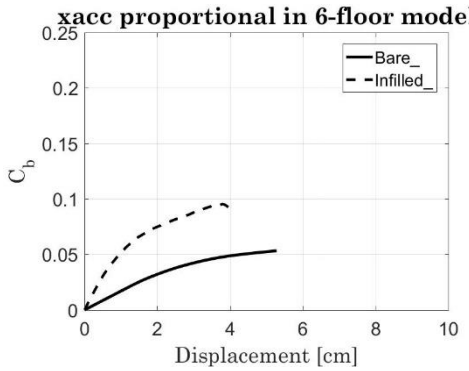
xacc proportional in 6-floor model
Bare_
Infilled_
C_b
Displacement [cm]

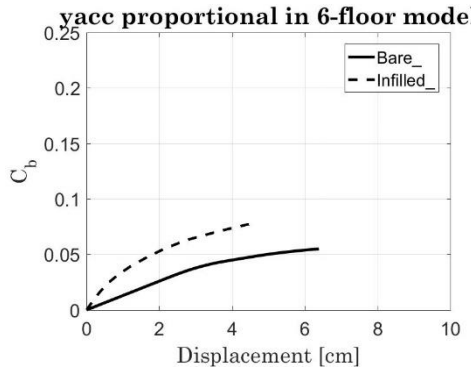
yacc proportional in 6-floor model
Bare_
Infilled_
C_b
Displacement [cm]

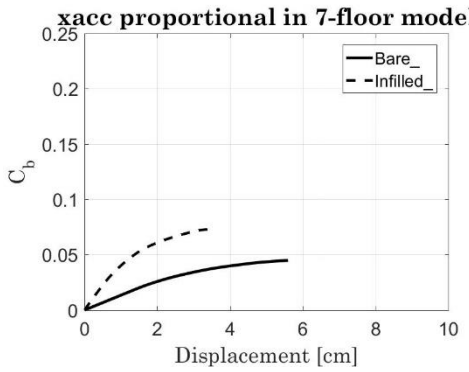
xacc proportional in 7-floor model
Bare_
Infilled_
C_b
Displacement [cm]

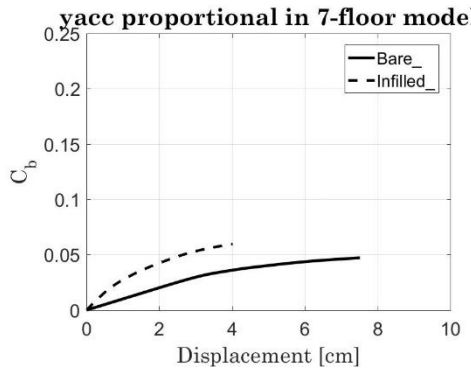
yacc proportional in 7-floor model
Bare_
Infilled_
C_b
Displacement [cm]

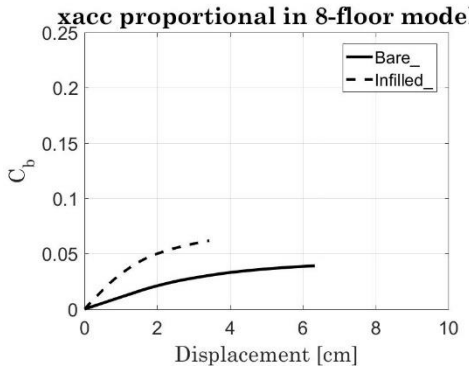
xacc proportional in 8-floor model
Bare_
Infilled_
C_b
Displacement [cm]

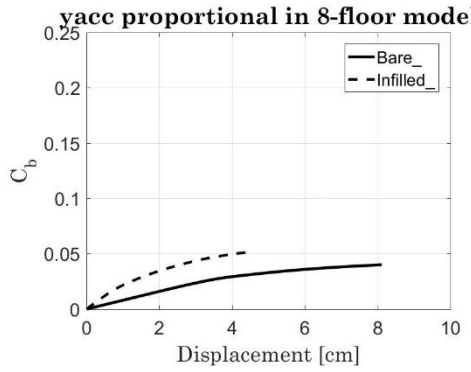
yacc proportional in 8-floor model
Bare_
Infilled_
C_b
Displacement [cm]

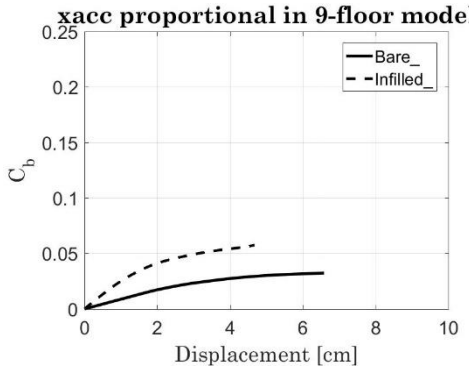
xacc proportional in 9-floor model
Bare_
Infilled_
C_b
Displacement [cm]

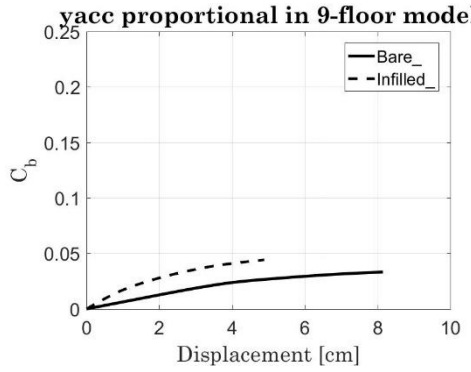
yacc proportional in 9-floor model
Bare_
Infilled_
C_b
Displacement [cm]

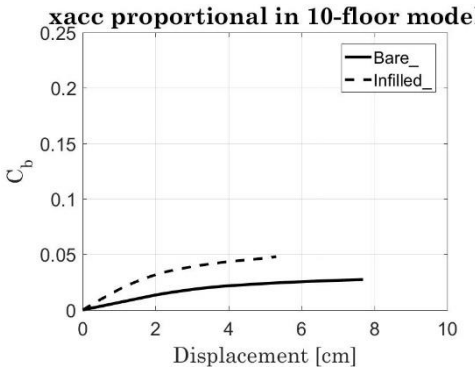
xacc proportional in 10-floor model
Bare_
Infilled_
C_b
Displacement [cm]
0.25
0.2
0.15
0.1
0.05
0
0
2
4
6
8
10

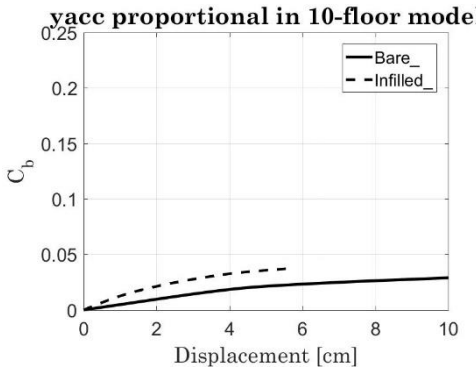
yacc proportional in 10-floor model
Bare_
Infilled_
C_b
Displacement [cm]
0.25
0.2
0.15
0.1
0.05
0
0
2
4
6
8
10

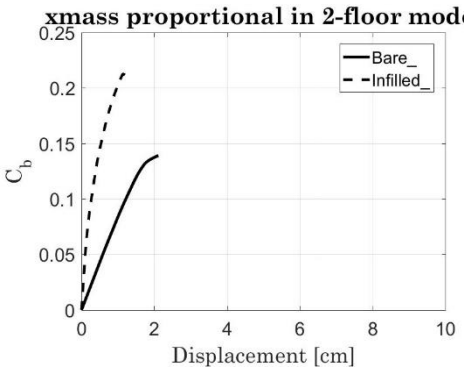
xmass proportional in 2-floor model
Bare_
Infilled_
C_b
Displacement [cm]

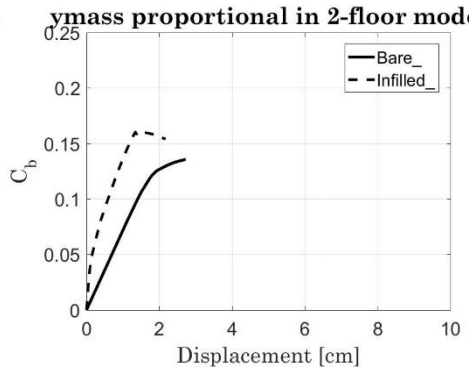
ymass proportional in 2-floor model
Bare_
Infilled_
C_b
Displacement [cm]

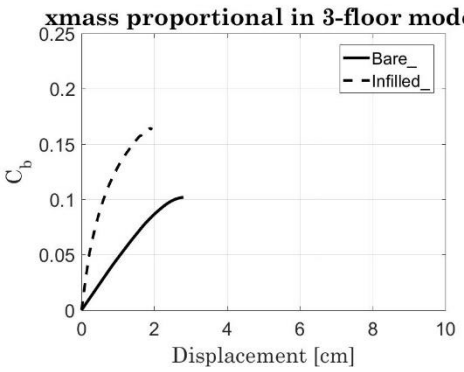
xmass proportional in 3-floor model
Bare_
Infilled_
C_b
Displacement [cm]

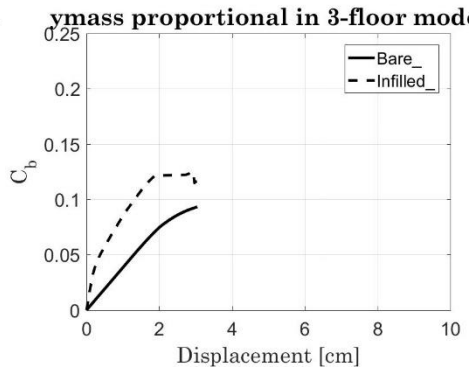
ymass proportional in 3-floor model
Bare_
Infilled_
C_b
Displacement [cm]

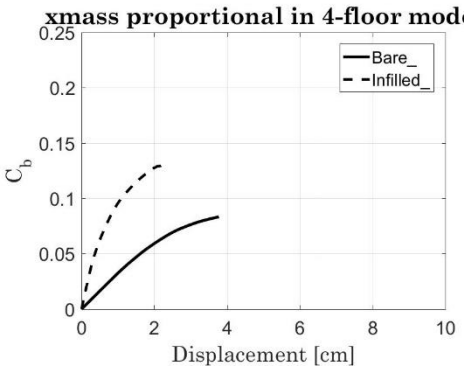
xmass proportional in 4-floor model
Bare_
Infilled_
C_b
Displacement [cm]

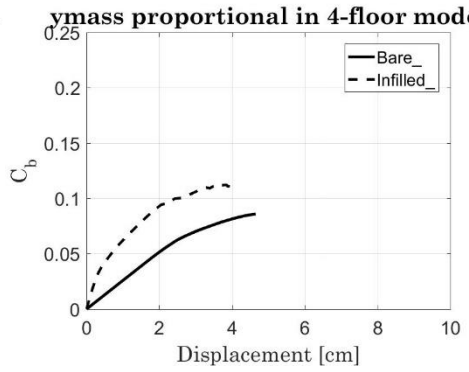
ymass proportional in 4-floor model
Bare_
Infilled_
C_b
Displacement [cm]

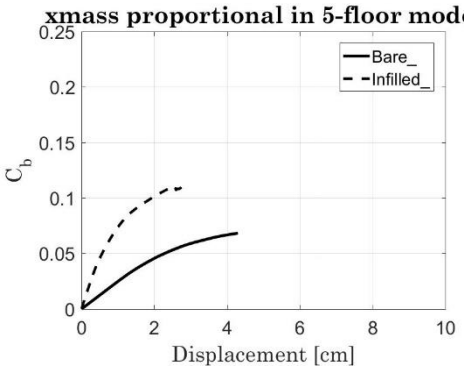
xmass proportional in 5-floor model
Bare_
Infilled_
C_b
Displacement [cm]

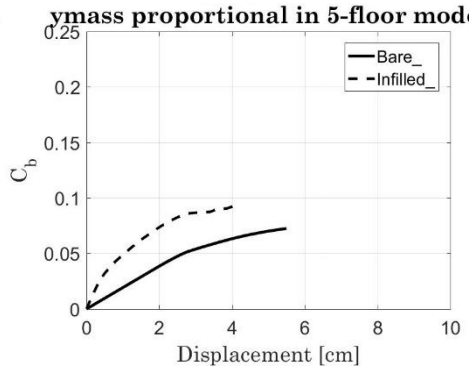
ymass proportional in 5-floor model
Bare_
Infilled_
C_b
Displacement [cm]

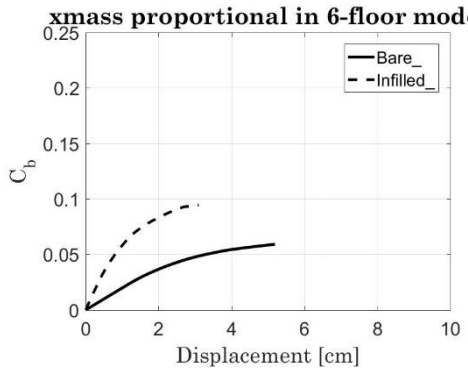
xmass proportional in 6-floor model
Bare_
Infilled_
C_b
Displacement [cm]

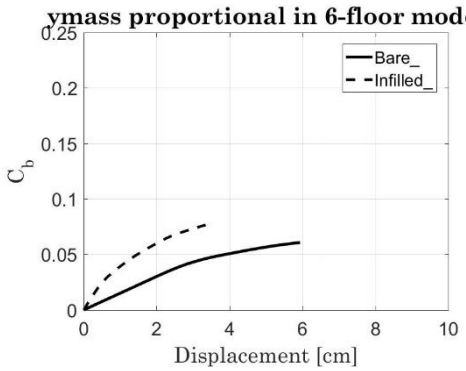
ymass proportional in 6-floor model
Bare_
Infilled_
C_b
Displacement [cm]

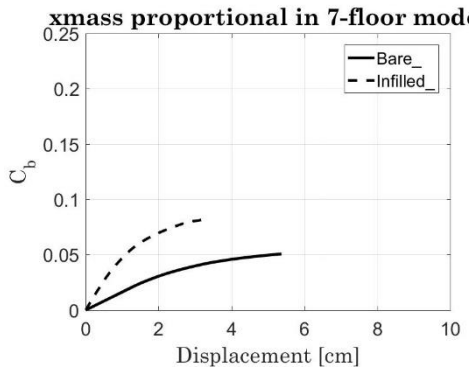
xmass proportional in 7-floor model
Bare_
Infilled_
C_b
Displacement [cm]

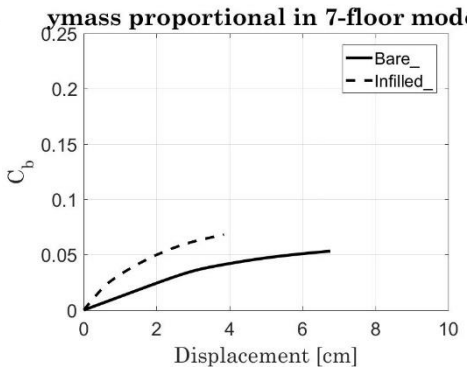
ymass proportional in 7-floor model
Bare_
Infilled_
C_b
Displacement [cm]

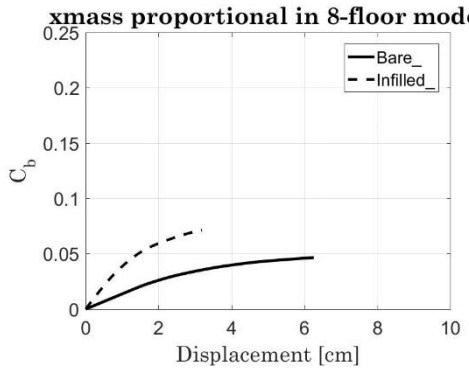
xmass proportional in 8-floor model
Bare_
Infilled_
C_b
Displacement [cm]

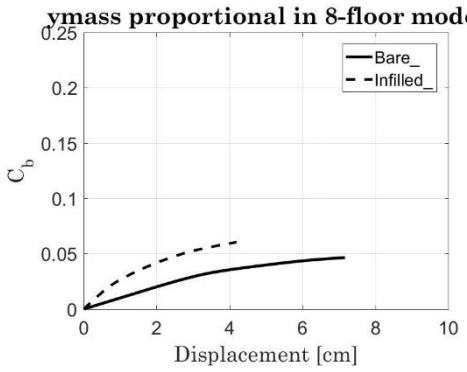
ymass proportional in 8-floor model
Bare_
Infilled_
C_b
Displacement [cm]

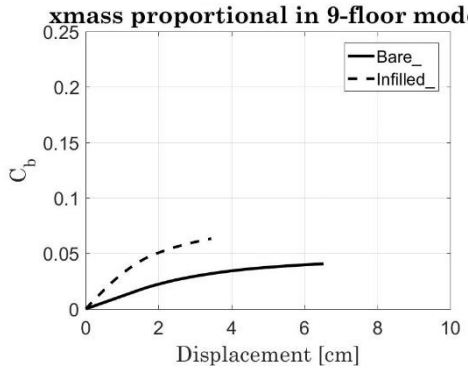
xmass proportional in 9-floor model
Bare_
Infilled_
C_b
Displacement [cm]

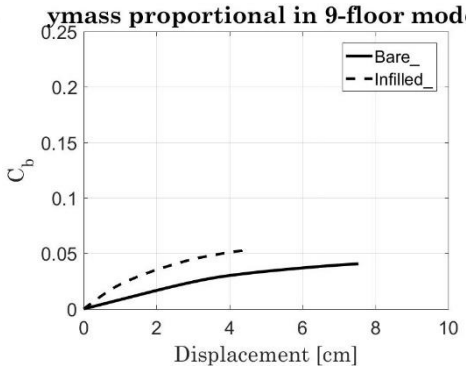
ymass proportional in 9-floor model
Bare_
Infilled_
C_b
Displacement [cm]

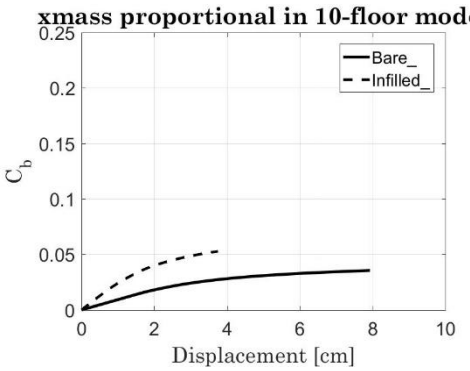
xmass proportional in 10-floor model
Bare_
Infilled_
C_b
Displacement [cm]
0
0.05
0.1
0.15
0.2
0.25
0
2
4
6
8
10

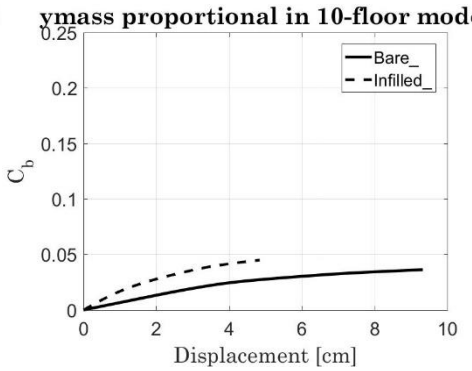
ymass proportional in 10-floor model
Bare_
Infilled_
C_b
Displacement [cm]
0
0.05
0.1
0.15
0.2
0.25
0
2
4
6
8
10

APPENDIX IV. TECHNICAL DRAWINGS

The Appendix collects all the technical drawings that define the case study structures.

The case study and the technical drawings have been developed in collaboration with a research team of the University of Catania [88]

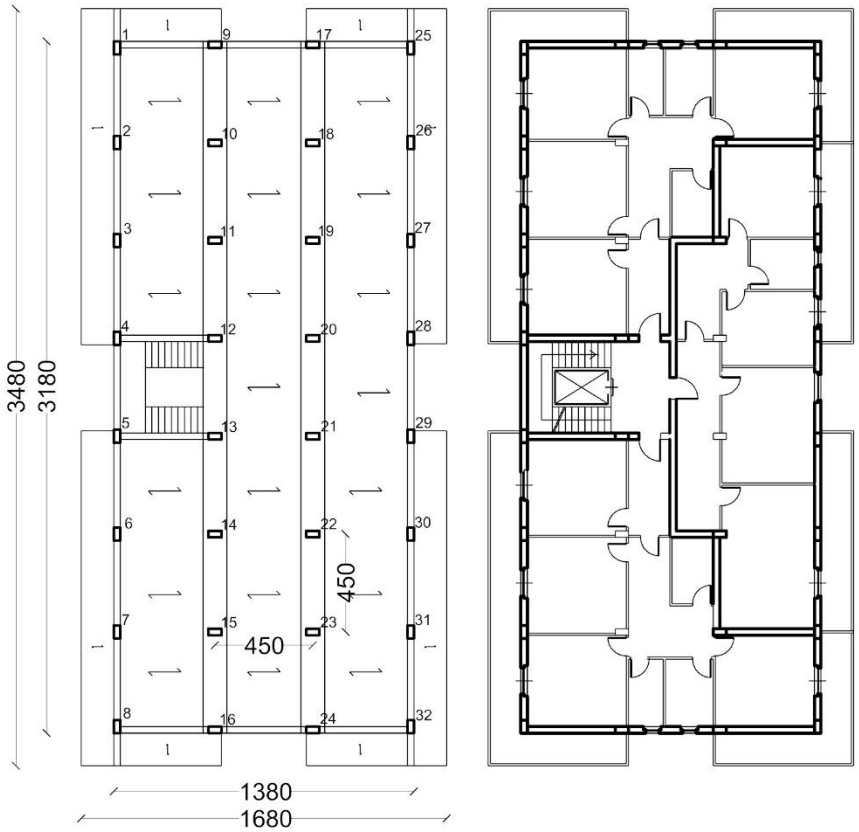

a *b*

Figure 10.4 Generic architectural (a) and structural (b) plan of the case study.

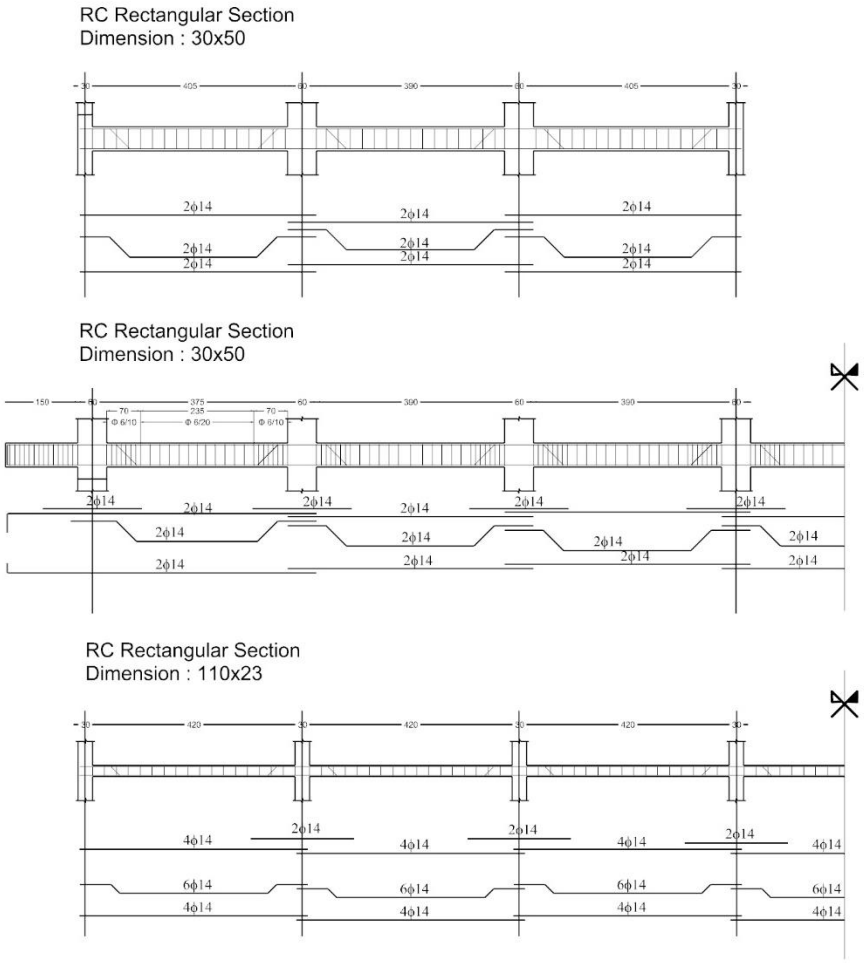

Figure 10.5 RC Beams.

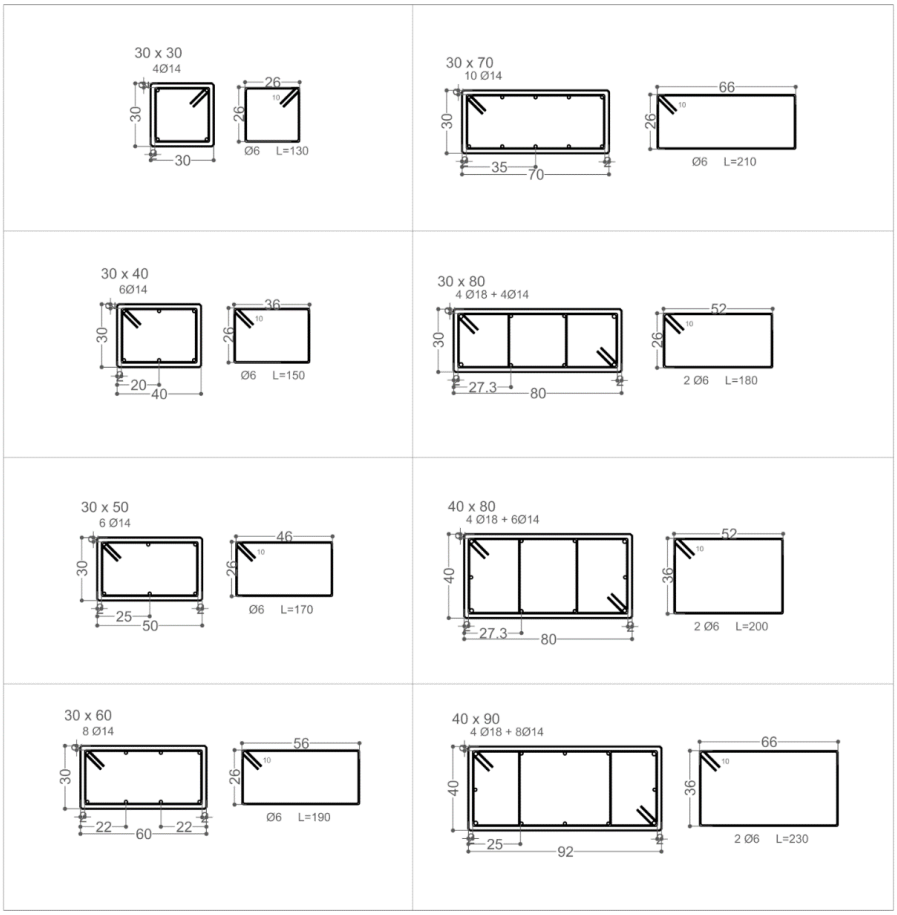

Figure 10.6 RC Columns Cross-Sections.